SYMPOSIUM ON FUEL CELLS
PRESENTED BEFORE THE DIVISION OF PETROLEUM CHEMISTRY
AMERICAN CHEMICAL SOCIETY
CHICAGO MEETING, September 3-8, 1961

ADVANCES IN FUEL CELL TECHNOLGY

By

Anthony M. Moos
Leesona Corporation

One-hundred twenty years after Sir William Grove, the father of the fuel cell, demonstrated that fuel cells using gaseous fuels were possible, a Symposium on Fuel Cells was organized and held by the Gas and Fuel Chemistry Division of the American Chemical Society at the 136th National Meeting in September, 1959. The papers presented at that Symposium were collected and published by Professor George Young in June, 1960. This book represents the first authoritative source of information on these revolutionary energy conversion devices.

In the spring of 1960, a technical and economic analysis of developments and opportunities in electrochemical fuel cells under the title, "Fuel Cells - Power for the Future", was published by Research Associates, a group of graduate students at the Graduate School of Business Administration of Harvard University. This book is an optimistic, but excellent, reference source on the economic potential of fuel cells.

Periodically, since 1959, the U. S. Army Research Office has reviewed the status of fuel cells with emphasis on the military developments.

Fuel cells and their progress to date can be best measured and placed in historical perspective when compared to other technical developments. Quoting from the Congressional Record of 1875, eighty-six years ago:

"A new source of power, which burns a distillate of kerosene called gasoline, has been produced by a Boston engineer. Instead of burning the fuel under a boiler, it is exploded inside the cylinder of an engine. This so-called internal combustion engine may be used under certain conditions to supplement steam engines. Experiments are under way to use an engine to propel a vehicle.

"This discovery begins a new era in the history of civilization. It may some day prove to be more revolutionary in the development of human society than the invention of the wheel, the use of metals, or the steam engine. Never in history has society been confronted with a power so full of potential danger and at the same time so full of promise for the future of man and for the peace of the world.

"The dangers are obvious. Stores of gasoline in the hands of the people, interested primarily in profit, would constitute a fire and explosive hazard of the first rank. Horseless carriages propelled by gasoline engines might attain speeds of 14 or even 20 miles per hour. The menace to our people of vehicles of this type hurtling through our streets and along our roads and poisoning the atmosphere would call for prompt legislative action even if the military and economic implications were not so overwhelming. The Secretary of War has testified before us and has pointed out the destructive effects of the use of such vehicles in battle. Furthermore, our supplies of petroleum, from which gasoline can be extracted only in limited quantities, make it imperative that the defense forces should have first call on the limited supply. Furthermore, the cost of producing it is far beyond the financial capacity of private industry, yet the safety of the nation demands that an adequate supply should be produced. In addition, the development of this new power may displace the use of horses, which would wreck our agriculture.

". . . the discovery with which we are dealing involves forces of a nature too dangerous to fit into any of our usual concepts."

These remarks made over 80 years ago are familiar to us involved in fuel cells: the new fuels, their hazards and cost, the military interest, the mobile application, the promise for the future, the present danger, and the probable impact on society.

In attempting to place the 1961 state-of-the-art of fuel cell research, development and technology in perspective, we might go back five years.

In 1956, exploratory work on fuel cells was only being carried out at a few places around the world.

In England, Francis T. Bacon, the dedicated pioneer was working for the Electrical Research Association on the high pressure hydrogen oxygen Bacon System.

In Germany, Professor Justi, the brilliant physicist and inventor, had started to fabricate and test the first Raney nickel D. S. K. metal defect electrodes.

In Russia, Davtyan; in England, Chambers; in Holland, Ketelaar; and Gorin in the United States, were investigating high temperature carbonaceous fuel cells using fused salt electrolytes. In the United States, five years ago, only a few companies were actively engaged in fuel cell research--Consolidation Coal, National Carbon, General Electric, Leesona, and Aerojet.

A modest military program had been started by the United States Navy and the United States Army Signal Corps.

Since that time, in 1961, the fuel cell world-wide effort has grown expoentially. In the United States, over 50 companies are known to be actively engaged.

As an example, more than 40 firms are sponsoring a cooperative fuel cell research program at the Battelle Memorial Institute and represent the chemical, oil, transportation, public utilities, automotive, aircraft, electronics, engine and power plant industries. The fundamental research being carried out at Battelle supplements government and private industry projects. In 1961, government expenditures in fuel cells for military and space application will exceed 4 million dollars. Under government sponsorship, at government installations, universities, non-profit organizations and industry fundamental electrochemical phenomena are being studied, new concepts for space applications are being evaluated, and power plants and engines are being fabricated and tested.

In the United Kingdom, Chambers and Bacon are working under sponsorship of the National Research Development Corporation. The Central Electric Generating Board has a substantial fuel cell program evaluating fuel cells for central power station applications and a number of private companies are studying fuel cell systems, such as, Shell, British-Petroleum, Hawker-Siddley and Chloride.

In Holland, Broers is investigating high temperature systems under T. N. O. 's sponsorship.

In Germany, fuel cell development is carried out by a number of private concerns, such as, Ruhrchemie, A. F. A., Siemens, A. E. G. and at a number of technical institutes, such as, Braunschweig under the direction of Professor Justi, and at Bonn and Munster Universities.

The French government started two years ago a comprehensive fuel cell program and excellent work is being done at the French Petroleum Institute and at French Center of Electrical Research, a number of private companies, such as, St. Gobain, Picheney, Compagnie Sans Fils, and Compagnie Generale D'Electricite are also doing pioneer work in this field. It is known that the Indian government, the Commonwealth of Australia and Japanese public and private interests have fuel cell research programs. Little is known of the Russian and Chinese fuel cell projects.

In the last two years, we have seen the revival and mushrooming of fuel cell research and development throughout the world. What progress has been made?

In 1961, two years after the Fuel Cell Symposium held by the Gas and Fuel Division at the 136th National Meeting of the A. C. S., a hydrogen-oxygen fuel cell system can be purchased from a number of U. S. manufacturers. These engines or power plants range from hundreds of watts to kilowatts and will operate thousands of hours with negligible maintenance at energy efficiencies of the order of 60%.

The U. S. government is testing fuel cells for use in submarines, as secondary power sources for satellites and space vehicles and for ground power generation. These systems are believed to use hydrogen and oxygen as feed gases and operate at temperatures ranging from 20°C. to 200°C. The impetus of military funding has also resulted in the investigation of more exotic and novel systems: biological, regenerative, use of high energy fuels, etc. In 1961, there is a substantial military fuel cell market in the U. S. A.

Substantial progress has taken place in the development of high temperature systems. This type of fuel cell operating on cheap fuels, such as, natural gas, propane, kerosene and air is now being system engineered and tested at the multikilowatt level. Some of the endurance, corrosion, reliability materials and cost problems which plagued the courageous pioneers in 1959 and limited the system utility have been solved. A number of commercial applications exist for this type of ground power supply operating at fuel efficiency of 50% or higher.

At the 1959 Symposium, no mention was made of low temperature fuel cells using medium cost fuels such as hydrazine, ammonia, methanol, ethylene oxide, ethylene glycol or methylamines. Significant results here and abroad have been achieved in the utilization of these fuels using air as an oxidant. This type of fuel cell is economically sound in a number of applications, ranging from industrial storage battery replacement to vehicular power. I believe that in 1962, this type of engine will be commercially available in the United States or overseas.

Handling, storage, logistic and economic problems limit the utility of fuel cells using oxygen at the cathode. Significant progress has been made in 1960 and 1961 as a result of fundamental work on the oxygen electrode. A better understanding of fuel cell electrode reaction mechanisms and structural requirements has resulted in the development of useful practical air electrodes operating in a variety of electrolytes over a wide range of temperatures.

The large acceptance of fuel cells hinges on the use of a cheap and readily available fuel, such as, natural gas, propane or methane in moderate temperatures and pressures fuel cells using air as an oxidant. Significant progress has been achieved towards this goal by a number of organizations such as Esso Research and the French Petroleum Institute. Further progress is dependent on continued basic and fundamental research in electrode reactions and kinetics and surface catalysis leading to a better understanding of the rate determining processes.

The practical and commercial criteria for a fuel cell power plant can be readily defined as a function of intended application: high efficiency, low capital cost, minimum upkeep, long life, etc. Some of these criteria are met by existing already engineered systems.

Energy efficiency in a fuel cell power plant is independent of size. The impact of this concept will not be fully felt in the United States, United Kingdom or Western Europe, but might well create a technical revolution in the under-developed countries of the world. These countries need electrical power and do not have the time or the capital to build large power plants and create distribution networks. Small fuel cell power stations will help our friends and neighbors living in the under-developed countries.

The growth of fuel cell technology will be felt in many areas and affect many industries. As an example, in the PAU region of France, deposits of Bauxite and fields of natural gas are contiguous; in Venezuela, iron ore and oil fields. The marriage of natural resources together with the fuel cell will certainly create new economic and industrial climates.

The petroleum industry and natural gas industry might be profoundly changed with the coming of age of fuel cell power plants in stationary or mobile applications. These might range from shifts in production methods to reduced fuel requirements in the U. S. A. where the natural gas pipelines sometime parallel and in other cases supplement the electrical power grid competition between these public utilities might result in profound changes in local economies.

The increase in research, development engineering that has taken place since our last symposium two years ago assures us that fuel cells will become successful and competitive electrical power sources in a variety of applications within the next few years.

Quoting again from the 1875 Congressional Records,

"Never in history has society been confronted with a power so full of potential danger and at the same time so full of promise for the future of man and the peace of the world."

SYMPOSIUM ON FUEL CELLS
PRESENTED BEFORE THE DIVISION OF PETROLEUM CHEMISTRY
AMERICAN CHEMICAL SOCIETY
CHICAGO MEETING, September 3-8, 1961

HIGH-TEMPERATURE METHANE FUEL CELLS

By

E. B. Shultz, Jr., K. S. Vorres*, L. G. Marianowski and H. R. Linden
Institute of Gas Technology, Chicago 16, Illinois

INTRODUCTION

If it were feasible to utilize methane in fuel cells, the development of small power packs for dwellings would be an attractive venture. In many areas of the United States, the cost to the residential consumer of a unit of energy in the form of natural gas (methane) is only one-sixth to one-eighth as much as a unit of energy in the form of electricity. (2, 15) This basic cost advantage would seem to be large enough to offset the unavoidably higher costs of generating electricity in a multiplicity of small installations.

Direct electrochemical oxidation of methane does not appear practical at this time, because of low reactivity in all types of fuel cells. However, it is possible to use it "directly" in a high-temperature fuel cell in the presence of steam. Reforming is presumed to occur on the anode surface, with the observed current due primarily to electrochemical oxidation of intermediate hydrogen. (8, 9)

As an alternative, a hydrogen-rich stream can be produced from methane in external apparatus by such gas conversion processes as catalytic steam reforming or partial oxidation, supplemented by carbon monoxide shift if necessary. If caustic electrolytes were to be employed, the effluent could then be fed to a hydrox fuel cell after carbon oxide removal. The removal step would be unnecessary if hydrox cells were selected that carry the charge through the electrolyte via hydrogen ions. In principle, cation exchange cells could be employed, although insensitivity of the catalysts to carbon oxides would have to be established. Recent data on phosphoric acid cells indicate that they may also be considered, although they have received relatively little attention thus far. (14)

Because catalytic steam reforming and partial oxidation of natural gas are widely practiced, and cation exchange cells have been brought to an advanced stage of development, a power pack based on indirect utilization of methane should be technically feasible. However, it seems likely that this approach may be uneconomic because of high investment costs of ion exchange cells (1) and gas conversion and purification equipment.

The technical feasibility of utilizing methane and steam in high-temperature cells has not been thoroughly established in previous studies which were directed primarily to the use of hydrogen and town-gas. (8-11) Considerable improvement in performance of high-temperature methane cells should be achievable. This would not be as likely for the gas conversion processes and low-temperature cells of the indirect approach, which have received far more attention.

PREVIOUS STUDIES OF HIGH-TEMPERATURE FUEL CELLS

Almost all of the recent work on high-temperature cells has involved molten carbonate electrolytes. Hydrogen, carbon monoxide and propane have been the principal fuels, and a few tests with methane have been reported. (8-11) The technology includes: 1) molten electrolyte held in porous sintered magnesia matrices, (8, 9, 11, 16, 17, 23) 2) plastic ("pasty") mixtures of molten electrolyte and inert filler (10, 11), and 3) free molten electrolyte. (11-13) In practical cells, powder electrodes and single-porosity sintered electrodes have been used with the first two electrolyte-retention methods, (8-11, 16, 17, 23) and dual-porosity sintered electrodes with the last. (11, 12)

Nickel has been the principal anode material. (8-10, 12, 13, 16, 17, 23) Silver (8-10 (8-10, 12, 13), silverized ZnO (11), and lithiated NiO (16, 17, 23) were shown to be

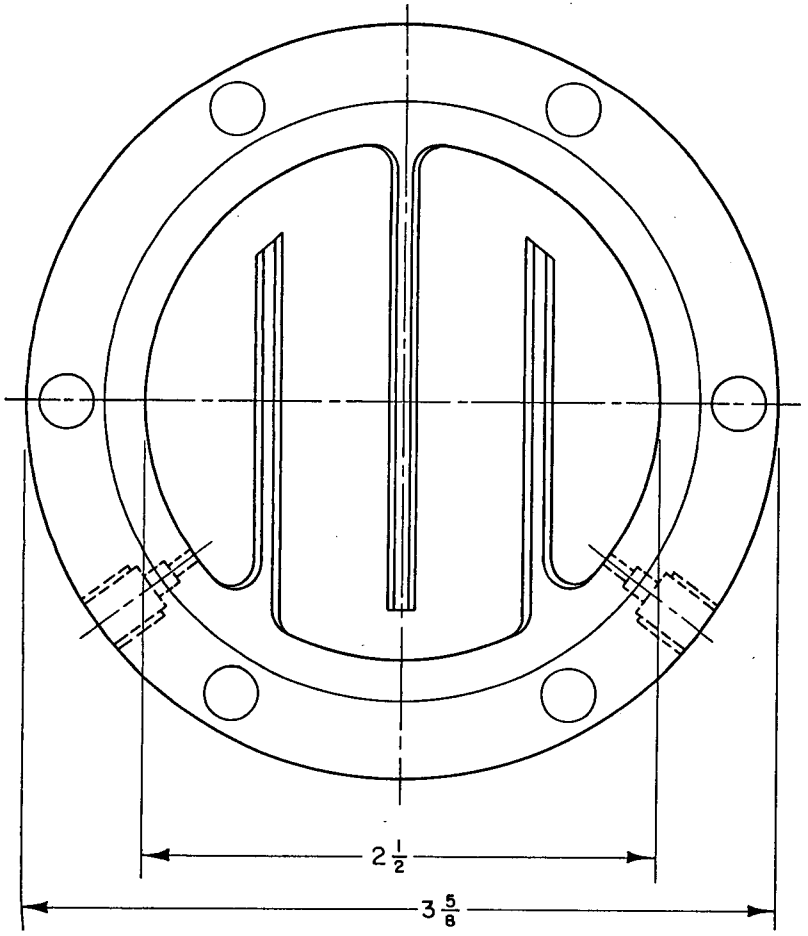

Figure 1. Fuel cell flanges were constructed with fingers to provide contacting pressure and distribute gas over electrode surfaces.

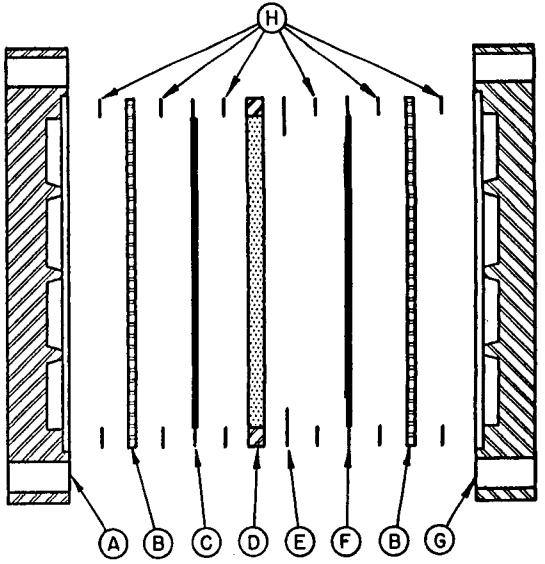

A ANODE FLANGE
B PERFORATED PLATE, 2-3/4" OD x 1/32" THICK
C POROUS NICKEL ANODE (CLEVITE), COINED ON BOTH SIDES, 2-3/4" OD x 50 MIL THICK
D STEEL RETAINING RING FOR PLASTIC ELECTROLYTE, 2-3/4" OD x 2-1/2" ID x 1/8" THICK
E MICA SEPARATOR, 2-3/4" OD x 2-1/4" ID
F POROUS SILVER CATHODE (CLEVITE), COINED ON BOTH SIDES, 2-3/4" OD x 50 MIL THICK
G CATHODE FLANGE
H SILVER GASKET, 2-3/4" OD x 2-1/2" ID x 0.01" THICK

Figure 2. These components were used in high-temperature fuel cell tests with molten carbonate electrolytes

effective cathode materials. With hydrogen-oxygen cells, little or no polarization has been reported for both anodes and cathodes at operating temperatures above the range 500o-600°C. (9, 13).

High-temperature fuel cell studies have also been conducted with solid oxides as electrolytes, by Baur. (3, 4) The most interesting of numerous oxide mixtures tested empriically were "Nernst-mass" (85 mole % ZrO_2-15 mole % Y_2O_3), and a mixture of 1 part CeO_2, 3 parts WO_3 and 2 parts clay. Baur's efforts were not successful from a practical viewpoint. Carbon was the fuel, which is much less reactive than conventional fluid fuels. Electrolytes were formed into thick-walled thimbles, and fuel cells were constructed in the form of crucibles. No attempt was made to build cells with practical shapes or thicknesses. Further, oxides of polyvalent elements such as cerium were studied, which may exhibit semiconductivity at fuel cell operating temperatures, and cause cell short-circuiting. In recent years, some interest in solid oxide electrolytes has been noted (5), but the concepts have not yet been demonstrated with gaseous fuels in practical cells, as has been done in the case of molten carbonate electrolytes.

In the present work, the effects of methane flow rate were studied in leak-tight cells at 650° and 750°C. Comparisons of molten carbonate cells were made, using: 1) plastic mixtures of carbonates and powdered magnesia, and 2) porous sintered magnesia matrices impregnated with molten carbonates. Some preliminary results of a study of the effects of temperature from 750° to 850°C. have been published. (25)

CARBONATE ELECTROLYTES

Experimental

Disk-shaped fuel cells were constructed with pressure fingers, to give good contacting and gas distribution (Fig. 1). The components for plastic electrolyte tests and the silver gasket sealing technique are shown in Fig. 2. Details of the construction have been published. (25)

Porous sintered nickel and silver electrodes were fabricated with embedded metal gauzes for strength. The adaptation of nickel-cadmium battery plaque techniques to high-temperature fuel cell operation was carried out by the Clevite Corporation.

Plastic electrolytes were prepared from -325 mesh, high-purity (99.0%) crystalline magnesium oxide and the equimolar eutectic $NaLiCO_3$. Mixtures of the powders were cold-pressed in steel retaining rings shown in Fig. 2, and heated to just above the melting point of the eutectic. After cooling, the disks were ground flush with the retaining ring. Electrolyte flaws were common, and could be readily patched by applying additional mixed powders and reheating.

Cell short-circuiting through the metal retaining ring was prevented by use of a thin ring of mica which performed satisfactorily in short tests. Over extended periods this would not be feasible due to loss of water from the mica, so experiments with steel retaining rings flame-sprayed with insulating ceramics have been initiated with good results.

Magnesia matrices were prepared initially by a method used by previous investigators. (23) Improvements which essentially eliminated warpage were made with the aid of the Ceramics Research Division of Armour Research Foundation. Disks were impregnated with molten $NaLiCO_3$, cooled, and ground to measure 0.118 ± 0.003 inches thick at a number of points. The cell assembly and sealing technique was identical to that shown in Fig. 2, except that the impregnated disk replaced the retaining ring, plastic electrolyte and mica.

The sealing method was successful in eliminating peripheral leakage of gases. The plastic electrolyte technique eliminated cross-leakage of oxidant and fuel also, as demonstrated by inclusion of helium and argon tracers in the feed streams, and mass-spectrometric analysis of the exit gas streams. In cells with ceramic matrices, it was not possible to prevent cross-leakage completely.

Fuel and oxidant were fed as mixed gases supplied by the Matheson Company in cylinders. A small amount of carbon dioxide was included in the fuel to insure against electrolyte decomposition, and the stoichiometric CO_2/O_2 feed ratio for carbonate ion formation was used in the oxidant stream. Typical analyses of the gases were:

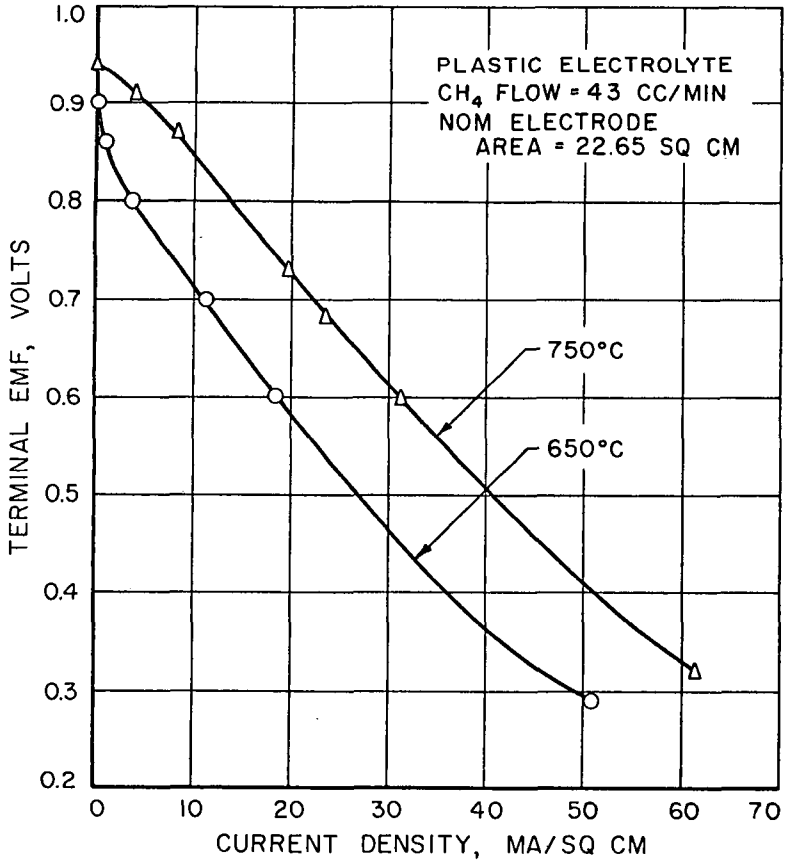

Figure 3. With steam-methane feed gas, better results were obtained at 750° than at 650° C, but performance level was still of practical interest at 650° C

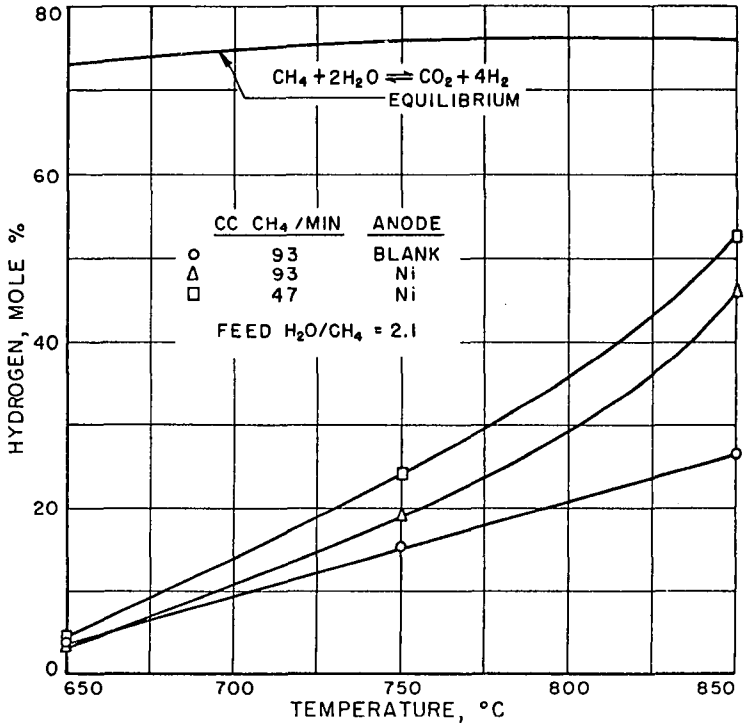

Figure 5. Porous sintered nickel anodes, prepared by commercial methods for nickel-cadmium battery service, were shown to have catalytic steam reforming activity at methane fuel cell operating temperatures

Mole %	Fuel Stream	Oxidant Stream
CH_4	92.0	--
C_2H_6	0.3	--
Higher Hydrocarbons	0.6	--
CO_2	4.7	65.1
H_2	0.3	--
O_2	--	33.3
N_2	0.5	--
A	--	1.6
He	1.6	--
Total	100.0	100.0

Steam was generated in an electrically heated tee filled with wire packing, and fed through a hypodermic tube. The fuel stream was passed through the heated tee to pick up the steam, before being conducted to the fuel cell. A gas-fired furnace was used to heat the fuel cells.

The flow of water and all gas streams was measured by calibrated rotameters. Water was condensed from the anode exit gas, and the stream was dried by passage over Drierite before flow measurement. Reported gas volumes are in cubic centimeters, dry, at 0°C. and one atmosphere.

Temperatures were sensed by a chromel-alumel thermocouple embedded in one flange of the cell. All tests were conducted at atmospheric pressure.

Cell polarization data were obtained upon stabilization of performance after application of load. A constant-load test showed no perceptible drift in performance with time for 10 to 20 hours. During this period, terminal voltage and current could be measured with good reproducibility.

Feed and exit gas analyses were carried out with a Consolidated Engineering Company Model 21-103 mass spectrometer. X-ray tests of electrode and electrolyte materials were performed on selected specimens with a General Electric X-ray diffractometer.

In all methane tests, the cell was brought to temperature with hydrogen flowing over the anode, and a one-hour hydrogen treatment at 650°C. was given, before the methane-steam mixture was introduced. Also, during the approach to operating temperature, the oxidant mixture was passed continuously over the cathode.

Effects of Variables

Figure 3 shows typical cell polarization curves for 33 mole % methane - 67 mole % steam at 650° and 750°C., using plastic electrolyte. Performance at 650°C. was at a higher level than expected from published observations on the lack of reactivity of methane below about 700°C. (10)

With electrolyte in magnesia matrices, no effect of methane flow rate was observed from 23 to 93 cc/min (Fig. 4). A decrease to 9.3 cc/min resulted in a decline in performance above about 15 ma/sq cm; at this current density, the flow rate corresponds to about eleven times the stoichiometric requirement. At the highest current density obtained at 9.3 cc/min (44.2 ma/sq cm), the flow rate is about four times the stoichiometric.

Figure 4 also compares the performance electrolyte mixture, with the more conventional magnesia matrix. A substantial improvement was obtained with the plastic electrolyte, amounting to about 40% more current at 0.5 volts, and higher percentage increases at higher voltages.

A significant amount of electrolyte penetrated the electrodes during guel cell tests. For example, carbonate analysis of a typical used magnesia matrix indicated that about 24% of the initial charge of electrolyte had been lost. To see if this was due to seepage into the electrodes, or due to decomposition of the carbonates, the matrix was also analyzed for sodium and lithium. The observed carbonate content agreed well with the value based on the assumption that all sodium and lithium was present as carbonate. Further, analysis of the electrodes indicated presence of roughly the amount of carbonate lost from the matrix.

In one test, the consequences of loss of methane flow were explored. Steam flow was maintained, and methane was replaced by carbon dioxide; performance dropped almost immediately. After 1-1/2 hours, short-circuit values of only 0.06

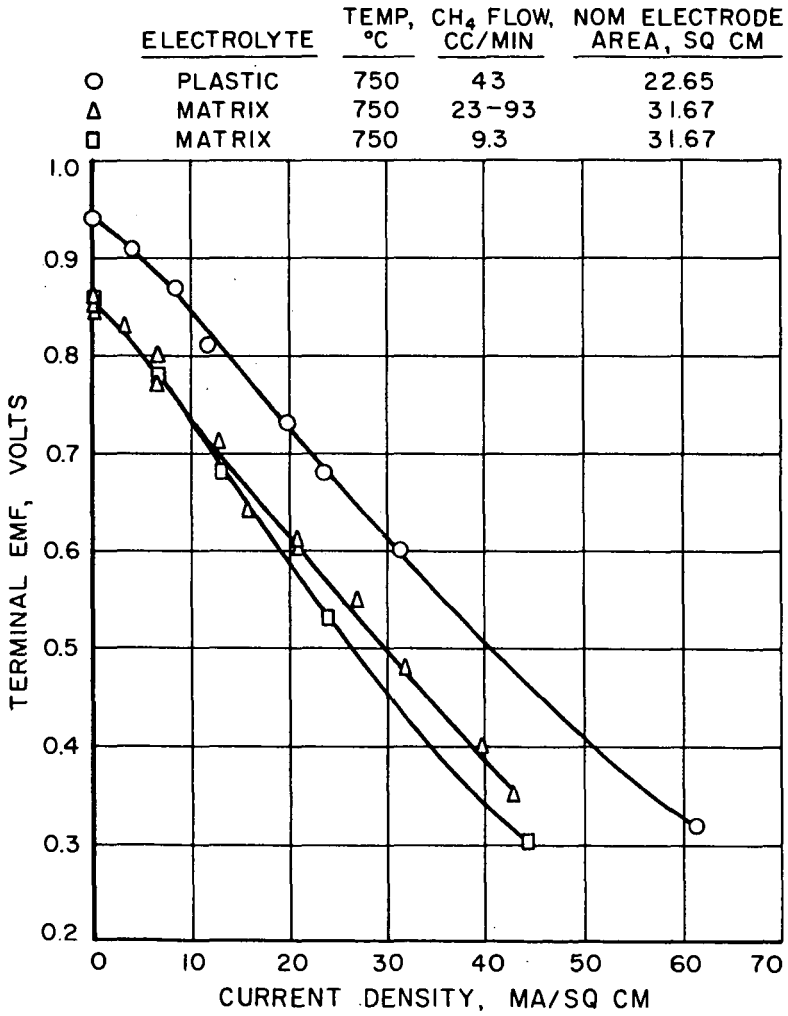

Figure 4. Plastic electrolyte mixtures of magnesia and molten carbonate showed superior performance, as compared to carbonate held in sintered matrices. Little effect of flow rate was noted below about 15 ma/sq cm current density

volts and 5.7 ma/sq cm were obtained. Hydrogen was then fed for two hours, but performance was not restored. Examination of the cell after the run indicated that most of the electrolyte had been lost from the matrix, and that the perforated disk supporting the anode had been partially fused in place by heat. X-ray studies of the anode showed strong lines for nickel oxide, as well as $NaLiCO_3$ and nickel; normally no lines for nickel oxide are found. Thus, it appears that sudden loss of methane flow can permit rapid oxidation of the anode, localized overheating, and expulsion of electrolyte.

Catalytic Reforming Tests with Anodes

Porous sintered nickel anodes cut from battery plaques manufactured by Clevite Corporation for nickel-cadmium batteries, were tested for steam reforming and CO shift activity at temperatures from 650° to 850°C. Runs were conducted using fuel cell flanges, but with the electrolyte and cathode replaced by a steel plate.

Methane flow rates of 47 and 93 cc/min (1.5 and 2.9 cc/min-sq cm electrode) were studied, with a steam to methane molar feed ratio of 2.15. Flow per unit area may be compared with industrial steam reforming practice for methane; for wide-packed, 1/2-inch spheres of supported nickel catalyst, a value of about 3 cc/min-sq cm catalyst surface gives good conversion at 750° to 850°C.

The results shown in Figure 5 indicate low activity at 650°C., increasing significantly with temperature. The decrease in flow rate from 47 to 93 cc/min led to some increase in conversion, at each temperature studied. In additional tests (not shown) significantly higher catalytic activities were often achieved by prolonged pretreatment with hydrogen at 650°C. before the methane-steam mixture was introduced. Only a one-hour treatment was used in the tests of Figure 5.

In one 750°C. reforming test at 100 cc/min (not shown), no steam was fed, and the methane feed stream was dried by passage through two dry ice-acetone condensers in series. Considerable carbon formation occurred. After five hours, the anode was swollen, very friable, and contained 52.3 wt. % carbon by combustion train analysis. Nickel content was 47.8 wt. % by dimethylglyoxime precipitation.

X-ray examination showed graphite and nickel, but no carbides. Gas samples taken after one and four hours at temperature contained 20.0 and 31.0 mole % hydrogen, respectively, indicating substantial activity for methane cracking without the presence of steam.

OXIDE ELECTROLYTES

Although molten carbonate electrolytes are useful, they may eventually be replaced by electrolytes which will avoid some or all of the inherent disadvantages of carbonates. Molten carbonates require a finite partial pressure of carbon dioxide at both anode and cathode, to prevent decomposition. Also, carbon dioxide must be included in the oxidant feed gas in near-stoichiometric quantities for the generation of carbonate ions. Further, carbonates are corrosive, have low viscosities and are difficult to retain over long operating periods.

Porous sintered magnesia matrices are commonly used to contain molten carbonates, and a substantial thickness is required to give adequate mechanical strength to the matrix. The presence of the matrix leads to ionic conductivities at least an order of magnitude lower than those for the same thickness of free fused salt. (10) It is difficult to impregnate all pores of sintered matrices, and cross-leakage of gases between anode and cathode rooms is usual. (9) Further, in vertical configurations, electrolyte flows within the matrix due to gravity, tending to open pores, increasing cross-leakage and the non-electrochemical reaction of fuel and oxidant. If free electrolyte is used, electrode flooding can occur unless expensive dual-porosity electrodes are employed.

For these reasons, a solid oxide electrolyte was sought to transport oxygen in the form of oxide ions. An approach to the following ideal properties was desired:

1. Oxide ion transference number of unity.
2. Rapid migration of oxide ions, since current density is directly proportional to rate of oxide ion migration.
3. Chemical stability in the presence of reducing gases or oxygen at temperatures as high as about 1000°C.

4. Physical stability, with no shrinkage, creeping or warping in service.
5. Impermeability to gases.

The migration of oxygen ions through many solid oxide electrolytes can be described by Fick's law of diffusion, with the diffusion coefficient represented as an Arrhenius function of temperature. (21) High permeation rates are favored by increases in temperature and concentration gradient. The highest concentration difference that can be realized will be fixed by the concentration of oxygen on the cathode surface, and an oxygen concentration of zero at the anode. If this obtains, then permeation rate can only be increased by increases in temperature or decreases in electrolyte thickness, for a given electrolyte.

Previous attempts to use solid oxide electrolytes in fuel cells (3, 4) resulted in permeabilities too low for practical interest, largely due to excessive electrolyte thickness. At that time, the diffusion mechanism of oxygen ion migration in solid oxides had not yet been clarified.

Theory of Ionic Conduction in Oxides

Oxygen may migrate via interstices, or via oxygen ion vacancies in the crystal lattice. Relative sizes of the atoms or ions, and the type of crystal structure, control the mode of diffusion. In fluorides having the fluorite structure, Seith has noted that the anion is the only species to migrate. (24) The similarity in radius between fluoride and oxide ions suggests oxide ion diffusion only, in fluorite-type oxides. Kingery has demonstrated this for $Zr_{0.85}Ca_{0.15}O_{1.85}$, by means of heavy oxygen exchange experiments, and electrolytic conductivity measurements. (21)

Because of the difference in valence, each calcium atom combines with only one oxygen atom instead of the two held by zirconium. The fluorite structure may be preserved with a given stoichiometry, by creation of oxygen ion vacancies, or addition of interstitial cations; density measurements indicate that the former prevails. Therefore, Kingery concluded an oxygen ion vacancy mechanism accounted for the conduction in $Zr_{0.85}Ca_{0.15}O_{1.85}$, and postulated that conductivity increases proportionately to the concentration of oxygen ion vacancies, at low concentration levels. (21)

A number of materials can generate vacancies in the lattice. This can occur, for instance, when cations of valence less than four replace zirconium randomly in the fluorite lattice. The term "mixing oxide" is used to denote additions of this type, and examples are the oxides of calcium, magnesium, yttrium, scandium, lanthanum and other rare earths. In this instance, zirconia may be termed the "host" oxide; other hosts are the oxides of hafnium, thorium, uranium, and rare earths such as cerium, praseodymium and terbium. However, the tetravalent rare earths and uranium may become semiconductive at high temperatures. Also, there is evidence that thorium systems show electronic conductivity, perhaps due to impurities; under the same conditions, ZrO_2-CaO solid solutions were not semiconductive. (22)

Conductivity Studies on Solid Oxides

Conductivity measurements for $Zr_{0.85}Ca_{0.15}O_{1.85}$ have been published. (18, 21, 26) Since current is carried only by oxygen ions, oxygen permeation values can be converted to current density values. For example, to obtain 100 ma/sq cm, temperatures from 700° to 1000°C., and electrolyte thicknesses from one to 10 microns are indicated, assuming that all lattice vacancies are filled at the cathode-electrolyte interface, and empty at the anode-electrolyte interface. Limitations in electrode performance, or in electrode-electrolyte contacting would lead to lower performance levels, of course.

Trombe and Foex (26) studied the conductivity of the zirconia-calcia system, as a function of composition at 1000°C. In contradiction to Kingery's postulation, the maximum conductivity (about 250 $ohm^{-1}cm^{-1}$) was found at about 15 mole % calcia, at the phase boundary between monoclinic zirconia saturated with calcia, and the fluorite-type solid solution with the minimum amount of calcia. The decrease in conductivity in the fluorite region from 15 to 33 mole % calcia was attributed to ordering in the lattice. The conductivity of several solid solutions in the thoria-yttria and thoria-lanthana systems have also been measured, and values of practical interest to fuel cell applications recorded. (19, 20)

Fabrication of Thin Films of Oxides

To obtain current densities of significance, thin films are essential. A number of useful techniques are being evaluated for this purpose: flame spraying (6), electron beam vaporization, and solution ceramics. (7) Preparation of thin wafers by conventional pressing, and optical grinding and polishing methods, does not appear adequate.

The application of sufficiently thin (about one micron) and even coatings of $Zr_{0.85}Ca_{0.15}O_{1.85}$ on porous sintered metal electrodes was carried out for the Institute by the Alloyd Corporation. The technique involves impingement of a beam of high-energy electrons on a target of oxide, vaporization of the oxide, and condensation of the vapors on a cool substrate. In these tests, the films were porous and not sufficiently adherent. Some changes in composition during vaporization were found by X-ray examination, but the fluorite structure was preserved.

Flame spraying may have more promise, and is presently being investigated for the Institute by the Ceramics Research Division of Armour Research Foundation. In this approach, fine particles of oxide are entrained in the oxygen stream of an oxy-acetylene or oxy-hydrogen flame, and molten or semi-molten particles are directed against a substrate. Porosity may be overcome by applying suitable impregnants, or by densifying the flame-sprayed wafer. Porous layers of metal electrode materials may then be applied to either or both sides of the wafer, also by flame-spraying, to give intimate electrode-electrolyte contact and excellent adherence. In a variation of this method, the oxide powder is fed into the gas used to stabilize the arc of a plasma jet.

Preliminary fuel cell tests of wafers of $Zr_{0.85}Ca_{0.15}O_{1.85}$ prepared by flame-spraying, with and without flame-sprayed electrodes, have given encouraging results. By flame-spraying, electrolyte films cannot yet be prepared as thin as by electron beam vaporization. Indications are that it may be possible to reduce thinkness sufficiently to obtain practical current densities, in accordance with the predictions based on published conductivity measurements.

UTILIZATION CONCEPTS

A natural gas power pack for home installation would provide for the addition of steam to the gas feed, and in the case of carbonate electrolytes, the addition of flue gas as a source of carbon dioxide to the air feed. Waste gas from the cells would be underfired to compensate for normal heat losses. Waste heat could be utilized in several conventional applicance functions in the home.

The high operating temperature of methane fuel cells is not compatible with the on-off, low load factor character of home utilization of electricity. Storage batteries could be used to raise the load factor so the high-temperature fuel cells could operate essentially continuously. Thus, investment in a large pack of fuel cells capable of meeting peak electrical loads would be unnecessary.

CONCLUSIONS

With methane-steam feed at low flow rates, it is possible to obtain current densities of practical interest, using plastic electrolyte mixtures of $NaLiCO_3$ and powdered magnesia in flat cells having porous sintered nickel anodes and porous sintered silver cathodes. Electrode fabrication techniques of commercial nickel-cadmium battery practice are adaptable to high-temperature fuel cell service, and steam-reforming tests of commercial sintered nickel anodes indicate considerable catalytic activity for methane conversion to hydrogen.

Substantially higher performance levels can be achieved with plastic electrolyte, than with electrolyte held in porous ceramic matrices. Further, cross-leakage of gases between anode and cathode rooms can be eliminated with plastic electrolyte, but is difficult to eliminate with the ceramic matrix technique. Peripheral leakage in flat-disk cells can be avoided by use of coined electrodes and silver gaskets, and steel retaining rings for plastic electrolytes.

In principle, development of solid oxide cells would be desirable, because of the inherent limitations of molten carbonates. It is proposed that a number of solid state reaction products with the fluorite structure should be useful as replacements for carbonates, in high-temperature fuel cells. Thin films are necessary, and promising results have been obtained with flame-sprayed films of oxides, with and without flame-sprayed nickel electrodes.

ACKNOWLEDGMENT

Thanks are due to N. W. Hamilton, S. D. Novak and P. C. Cunningham for assistance in data collection and equipment construction.

LITERATURE CITED

(1) Adams, D. R., et al., "Fuel Cells: Power for the Future." Cambridge, Mass.: Fuel Cell Research Associates, 1960.

(2) American Gas Association, "Gas Facts, 1959". New York: The Association, 1960.

(3) Baur, E., and Preis, H., Zeit. Elektrochem. 43, 727-32 (1937).

(4) Baur, E., and Preis, H., Zeit. Elektrochem. 44, 695-98 (1938).

(5) Betts, A. L., and McCollum, P. A., "Unconventional Electrical Power Sources," Parts I and II, PB 131218 and PB 131411. Washington, D. C., Office of Technical Services, 1954-55.

(6) Bradstreet, S. W., (to Armour Research Foundation), U. S. Patent 2,904,449 (Sept. 15, 1959).

(7) Bradstreet, S. W., and Griffith, J. S., The Frontier (Armour Research Foundation, Chicago), pp. 24-26, Vol. 17, No. 4, 1954.

(8) Broers, G. H. J., Ph. D. Dissertation, University of Amsterdam, 1958.

(9) Broers, G. H. J., and Ketelaar, J. A. A., "High-Temperature Fuel Cells", in Young, G. J., ed., "Fuel Cells", 78-93. New York: Reinhold, 1960.

(10) Broers, G. H. J., and Schenke, M., "High Temperature Galvanic Fuel Cells", (Final Report). A. S. T. I. A. AD No. 234 912. Frankfort, U. S. Army Procurement Center, January, 1960.

(11) Chambers, H. H., and Tantram, A. D. S., "Carbonaceous Fuel Cells", in Young, G. J., ed., "Fuel Cells", 94-108, New York: Reinhold, 1960.

(12) DeZubay, E. A., "High Temperature Fuel Cells", Unpublished paper presented at Society of Automotive Engineers, Aeronautic Meeting, New York, April, 1960.

(13) Douglas, D. L., "Molten Alkali Carbonate Cells with Gas-Diffusion Electrodes", in Young, G. J., ed., "Fuel Cells", 129-49. New York: Reinhold, 1960.

(14) Elmore, G. V., and Tanner, H. A., "Intermediate Temperature Fuel Cells", Unpublished paper presented at Electrochemical Society Meeting, Chicago, Ill., May, 1960.

(15) Federal Power Commission, "Typical Residential Electric Bills - Cities of 2,500 Population and More". Washington, D. C.: Federal Power Commission, 1960.

(16) Gorin, E., and Recht, H. L., Chem. Eng. Progr. 55, 51-58 (1959) August.

(17) Gorin, E., and Recht, H. L., "Nature of the Electrode Processes in Fuel Gas Cells", in Young, G. J., ed., "Fuel Cells", 109-128. New York: Reinhold, 1960.

(18) Hund, F., Z. physik. Chem. 199, 142-51 (1952).

(19) Hund, F., Z. anorg. u. allgem. Chem. 274, 105-113 (1953).

(20) Hund, F., and Mezger, R., Z. physik. Chem. 201, 268-77 (1952).

(21) Kingery, W. D., et al., J. Am. Ceram. Soc. 42, 393-98 (1959).

(22) Kiukkola, K., and Wagner, C., J. Electrochem. Soc. 104, 379-86 (1957).

(23) Recht, H., and Gorin, E., "Conversion of Carbonaceous Fuels to Electrical Energy," Quarterly Reports 1-17, Contract No. DA-36-039, Signal Corps Supply Agency, Ft. Monmouth, N. J., 1954-58.

(24) Seith, W., Z. Elektrochem. 42, 635-54 (1936).

(25) Shultz, E. B., Jr., Marianowski, L. G., Linden, H. R., and Vorres, K. S., Am. Gas J. 188, 24-32 (1961) May.

(26) Trombe, F., and Foex, M., Compt. Rend. 236, 1783-5 (1953).

SYMPOSIUM ON FUEL CELLS
PRESENTED BEFORE THE DIVISION OF PETROLEUM CHEMISTRY
AMERICAN CHEMICAL SOCIETY
CHICAGO MEETING, September 3-8, 1961

RECENT DEVELOPMENTS IN HIGH-TEMPERATURE CELL RESEARCH IN THE NETHERLANDS

By

G. H. J. Broers and M. Schenke

I. INTRODUCTION

Research on high-temperature fuel cells have been carried out in the Netherlands since 1950 by the Central Technical Institute of the Organization for Industrial Research T. N. O. Up till 1955, similar research has been done by Scholte and co-workers at the "Staatsmijnen" research laboratory at Geleen, partly in close cooperation with T. N. O. Results of the latter work have not been published, but they were fairly similar to those of T. N. O. An extensive survey, up till 1958, of the investigations by the Central Technical Institute has been given in a thesis (1) by one of the present authors. Some additional communications (2, 3, 4) on the same work were published in 1960.

During the period 1950-1958, laboratory cells were developed showing fairly good electric performances at 500°-750°C. on H_2-H_2O, CO-CO_2, CH_4 steam and similar gas mixtures, over quite long periods (viz. up to 6 months).

The small disk-shaped cells (about 5 cm dia.) had a sintered MgO-molten carbonate "semi-solid" electrolyte, sandwiched between two thin metal powder electrodes. The MgO ceramic carrier of 40-50% porosity provided the mechanical strength and simultaneously immobilized the liquid carbonate phase.

The major weakness of the cells was their insufficient electrolyte gas-tightness, caused by small cracks and gradually increasing numbers of open pores in the refractory MgO body. Although gas-tightness is an obvious and essential demand for any practical cell, it is very difficult to realize this completely with the mentioned electrolyte body. Nevertheless, it was felt that this problem must be solved before it will be possible to construct larger sized cells of real practical sense.

At our present state of knowledge, only molten carbonate electrolytes appear to be useful for high-temperature cells, this in connection with the necessary chemical stability against the cell reactants and their products, and the required low specific resistance. (The practical application of solid oxygen ion conductors in the range of 500°-800°C. seems very difficult.)(5) Therefore, our research with the electrolytes mentioned was continued from 1959 onwards. The use of refractory porous MgO electrolyte carriers involves a number of disadvantages:

1. MgO can be sintered only at fairly high temperatures (1300°C.) and sintering promoters may be applied only when they do not react with the carbonate melt to be impregnated afterwards.

2. Increasing, e. g., the diameter of ceramic disks, leads inevitably to increased fragility since their thickness must remain small (say less than 1 cm).

3. The rigid ceramic bodies, after impregnation with the melt, must pass twice the "dangerous" temperature region of the liquid-to-solid (and reverse) transition of the melt, namely upon cooling for assembling the cells and upon heating for operation. It was found that in the case of a ternary (Li-Na-K) carbonate mixture, the relative volume change at the melting point was more than 5%, so the formation of at least a few stress cracks in the MgO support seems very hard to avoid.

4. Although MgO is chemically inert against carbonate melts, it is slightly soluble in them. This was verified by qualitative tests. Recently, Janz and Lorenz (6) made similar observations. Owing to the dynamic character of the solid-solute equilibrium, it seems unlikely that the ceramic MgO structure will remain unaltered in the long run. Moreover, there might be a direct O^{2-} ion exchange between CO_3^{2-} and the MgO lattice ions. Some experiments with highly sintered porous MgO tubes*, exposed to

*Manufactured by "Degussa", Frankfurt a. m., Germany. ("Sintermagnesit Mg 24").

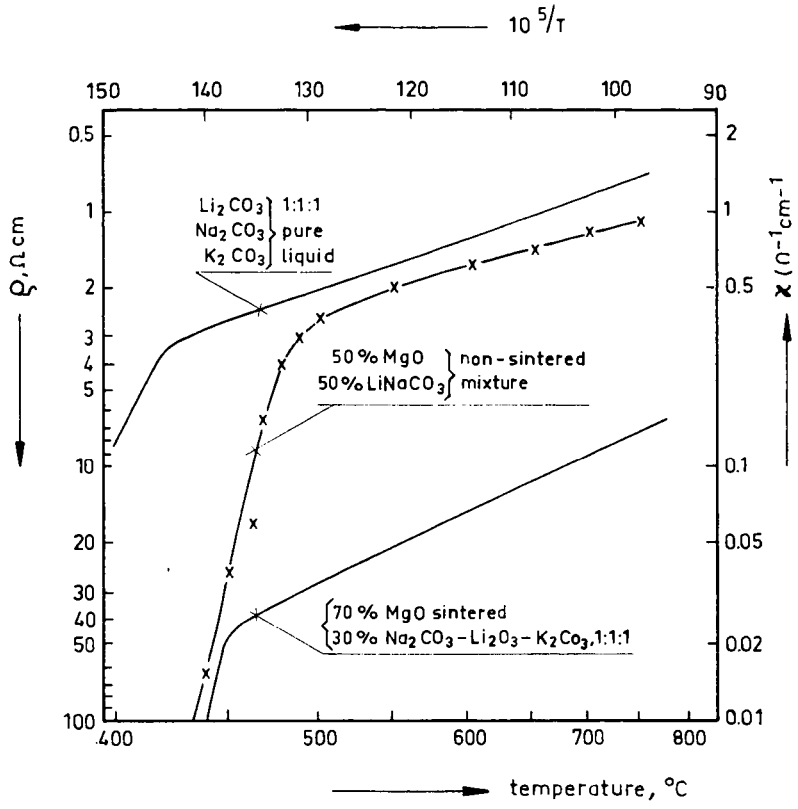

Fig. 1 Specific resistance (conductivity of liquid-paste-and sintered matrix electrolytes

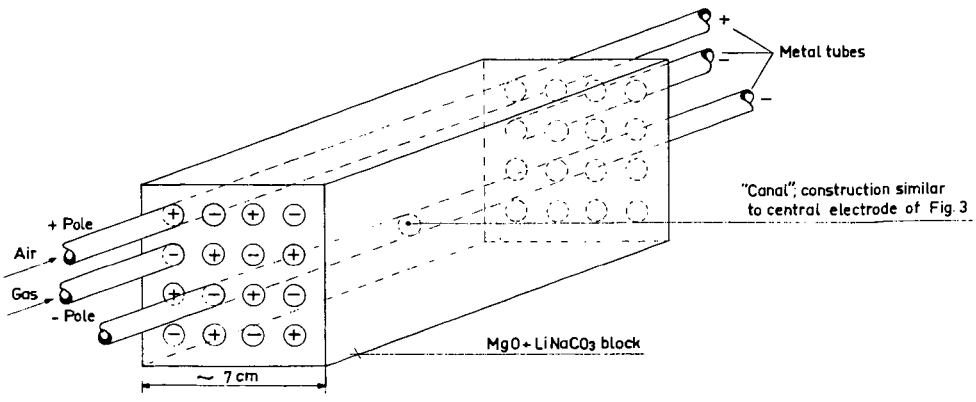

Fig. 2 Canal cell (schematically)

$LiNaCO_3$ melts at 700°C. for some weeks, indeed revealed a slow but steady disintegration of the ceramic structure. (Powdered MgO could be washed out of the pores.)

On the basis of these arguments, further experiments with refractory carriers were abandoned.

An obvious and technically sound approach towards complete gas-tightness is the direct use of liquid carbonates, e.g., as applied by Chambers and Tantram (7) and by Douglas. (8)

However, in that case the mechanical strength of the cell must be found completely in the electrode construction. A system of "double porosity electrodes", sintered onto backing plates, seems necessary to avoid pore flooding and gasbubble formation. Apart from the question whether or not these systems will withstand the prolongued exposure to the carbonate melt, the price of such highly refined units might be a serious drawback for electricity generation for non-specialized purposes on large scale.

II. PASTE ELECTROLYTES

In our opinion, it seems worthwhile to study a third alternative, i.e., the application of paste electrolytes which possibly combine the advantages of electrolyte immobilization and some mechanical strength with the avoidance of the ceramic body problems. The obvious method is to prepare pasty mixtures of an inert carrier powder (for which MgO serves well) and molten carbonates. (The approach is not a new one. Already Baur (9) applied similar mixtures as electrolytic bridges. Greger (10), too, mentioned their possible use. The idea, however, does not seem to have been worked out in detail.)

Preliminary experiments revealed that pellets (cold-pressed) from fine MgO powder and $LiNaCO_3$ (m.p. 510°C.) mixtures did not show any plastic deformation after 16 hours of heating at 700°C., even when their carbonate content was as high as 50% by weight.

In a further test the relation was studied between the MgO particle size range and the "maximal" amount of $LiNaCO_3$ that could be mixed with the MgO powders, without the mentioned deformation under their own weight. Observations were made with pellets of 1.3 cm dia. and 1.5 cm thickness, cold-pressed from different relative amounts of MgO and carbonate. The pellets were first baked during 24 hours at 700°C., whereafter their shape was observed. Then they were baked another 24 hours at 850°C. It was found that all pellets that did not deform at 700°C., neither did so at 850°C. This means that the viscosity of $LiNaCO_3$ melt bears no detectable influence upon the consistency of the substance. The results of this test are given in Table 1. Strong deformation (nearly liquid flow) is indicated by +++, less stronger by ++, just detectable by +, no observable by -. The MgO particle size ranges were obtained by wind sieving a milled sample of highly sintered "Degussa" magnesite.

The very fine power of the 0.05 - 0.1 micron fraction was a usual commercial product ("MgO levissimum", Messrs. Brocades, Amsterdam). The particle size in this case was measured by electron microscopic photographs.

TABLE I
DEFORMATION OF $LiNaCO_3$ - MgO PELLETS UNDER OWN WEIGHT AFTER 24 HOURS OF HEATING AT 700°C. AND SUBSEQUENT 24 HOURS OF HEATING AT 850°C.
PELLET SIZES: 1.3 cm dia., 1.5 cm thickness

Particle size range MgO in microns	Weight % $LiNaCO_3$			
	20	30	40	50
0.05 - 0.1 (levissimum)	-	-	-	-
< 1 Degussa	-	-	-	+
1 - 3 "	-	-	-	+++
3 - 10 "	-	-	-	+++
10 - 25 "	-	-	+	+++
24 - 40 "	-	-	++	+++
30 - 100 "	-	-	+++	+++

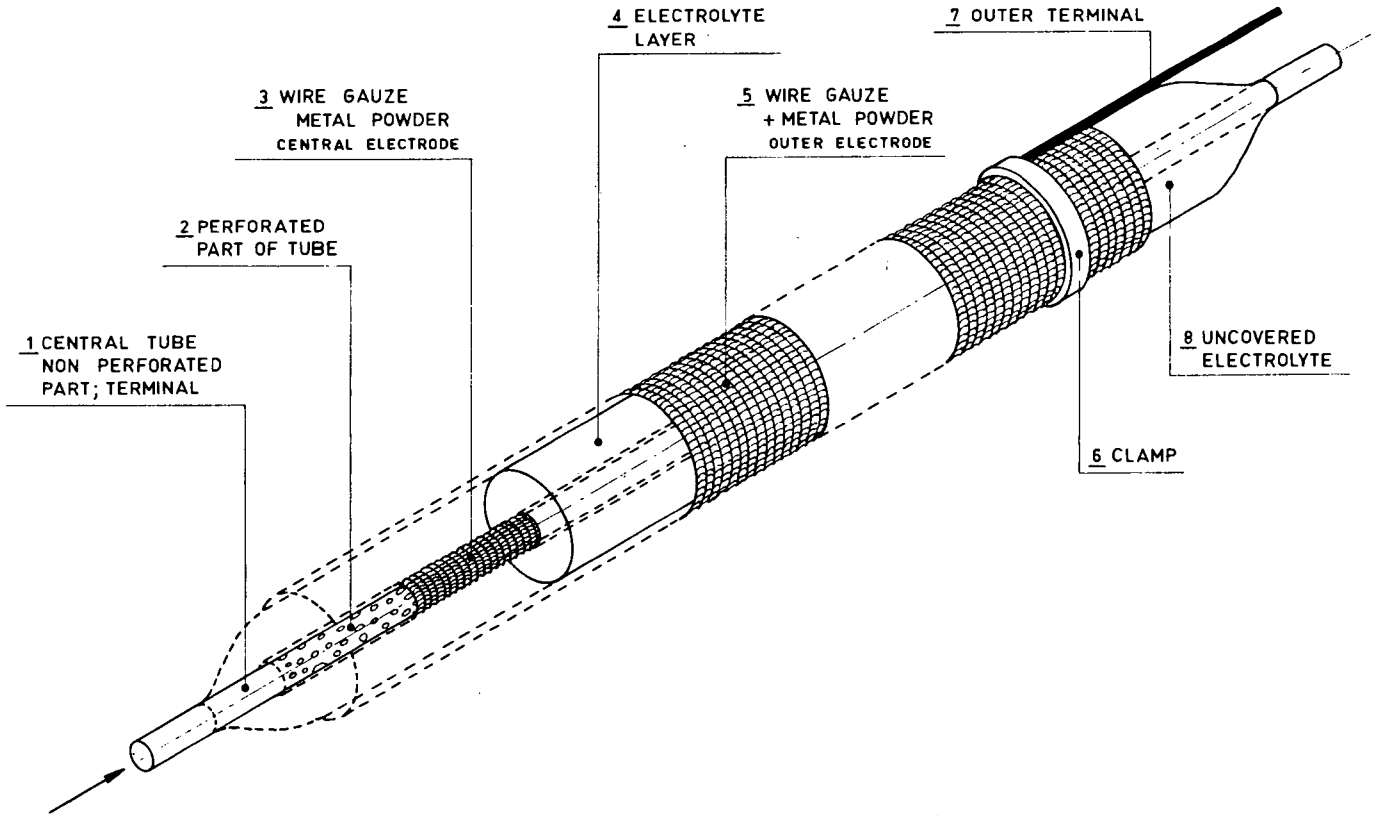

FIG. 3 EXAMPLE OF TUBE CELL CONSTRUCTION

The electrolyte paste is moulded around 2 and 3

Clearly, the finest powder is able to absorb the largest quantity of melt without plastic flow of the mixture. From the electrochemical standpoint, the use of fine powder is also favourable. First, the specific resistance of the mixtures with large melt contents will be low, and, second, the capillary forces retaining the melt inside the oxide matrix will be greatest in case the pores between the oxide particles are narrowest. The danger of electrode "drowning" thus becomes smaller in this case, and electrodes with correspondingly narrower pores might be used, yielding greater three phase zones.

So far, the "levissimum" powder has been used in further work. The great majority of the experiments was done with mixtures of this powder and carbonates in weight ratios ranging from 46/54 to 53/47.

By experiments of different kind, the following results and data were found.

1. $LiNaC0_3$ (m. p. 510°C.) may be substituted by lower melting combinations, such as equal parts of Li, Na and K carbonate (m. p. 390°C.), without observable change in mechanic deformability. Above the eutectic melting point, the substance is a stiff, white paste.

2. Cold-pressed and subsequently baked sheets of this paste are gas-tight at 700°C. under an excess gas pressure of 10 cm water column; layer thickness 0.2 cm, exposed area 1 cm^2.

3. The specific conductivity of the paste is roughly 50%-70% of the pure liquid phase specific conductance (measured with 1000 c. p. s. alternating current). Fig. 1 shows a comparison of conductance vs. temperature curves of

a. a pure carbonate melt,
b. a 50 Mg0/50 $LiNaC0_3$ paste, and
c. a ceramic Mg0 frame impregnated with carbonate melt.

Although the absolute accuracy is probably not better than 20%, the superiority of the paste electrolyte is obvious.

4. The paste can be moulded into any shape. Different techniques can be applied. They include simple "hand"-moulding the hot substance by means of cooled metallic stamps or rolls (to which the paste does not stick), cold hydraulic pressing and subsequent baking, hot-pressing in chemically resistant moulds under relatively small pressures (5-15 kg/cm^2) and flame-spraying upon porous metallic layers such as wire gauzes impregnated with metal powders, perforated sheets and tubes and other electrode structures.

5. The internal porosity of the moulded substances in the cold state is small. It depends on the technique used. Representative figures are:

Hand-moulding: 8%
Cold-pressing* + baking: 14%
Hot-pressing: 3%
Flame-spraying: 8%.

*Hydraulically pressed at 1250 kg/cm^2.

6. No high-purity Mg0 is needed if proper precautions are taken during the preparation stages. The latter comprises:

a. mixing the components;
b. heating the mixture at 600°-700°C. as a first homogenizing step;
c. grinding the loosely sintered product;
d. a second heating, preferably in a $C0_2$ atmosphere, over a sufficiently long period as to allow completion of all chemical reactions of the fused carbonates with any impurity still present ($C0_2$ evolution must have stopped);
e. when needed, a second grinding step of the now much denser product.

At stage e. and from thereon, take up of fresh impurities should be avoided.

7. The plastic flow under own weight of larger sized bodies is surprisingly small. A hot-pressed block of 5 x 5 x 14 cm, weighing about 0.9 kg, was placed vertically upon a stainless steel support and heated in air at 700°C. during a 39 days' period (eutectic m. p. of the carbonates 390°C.). After this period, the length decrease was 0.1 cm or 0.7%. The weight decrease was 6.7 g or 0.75% (the steel support showing some chemical attack). The other dimensions of the block were found to be unchanged.

These results demonstrate the fairly favourable prospects for practical application of the paste electrolyte in high-temperature cells.

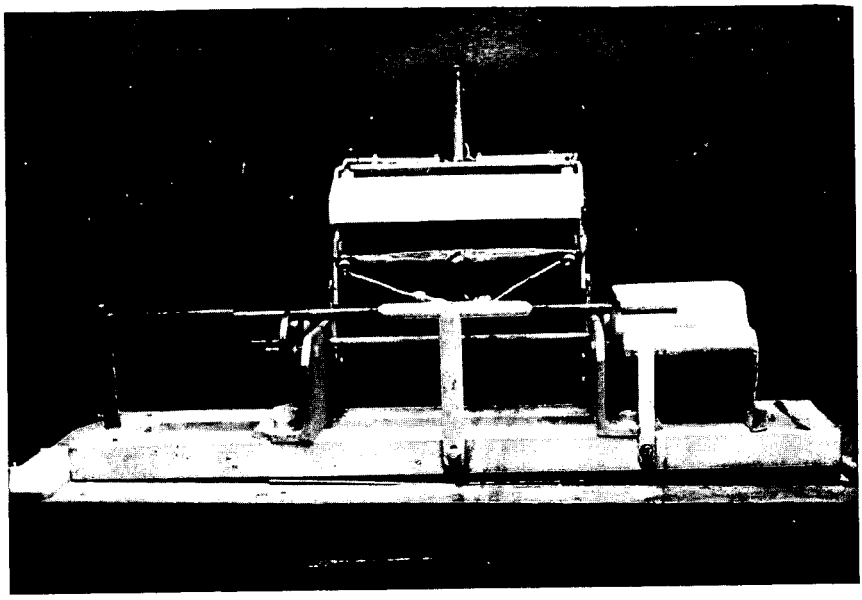

Fig. 4 Installation for hot moulding of tube cell electrolytes. Heating elements and surface nivellation roll mounted in hinging support.

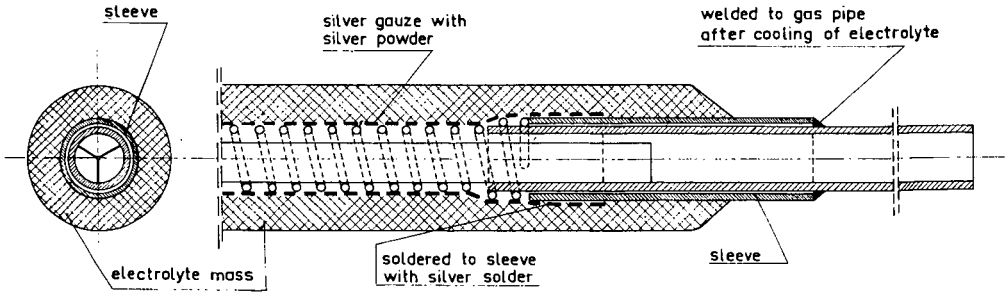

Fig. 5 Modified tube cell construction, allowing free contraction of the electrolyte upon cooling

III. SURVEY ON RESULTS WITH COMPLETE CELLS

A. Constructions

The "flexibility" of the paste electrolyte allows the construction of cells in various shapes. Whereas in the usual solid matrix arrangements an electrolyte disk is enclosed between gas spaces, (11) a reversal of this principle can be realized with relative ease, for instance when blocks can be manufactured in which canals are drilled out. The general concept of such a "canal cell" is shown in Fig. 2. It has been proposed already by Baur et al. (9) The advantage of the model is that no gasket materials (other than the paste itself) are needed. (To our knowledge, carbonate-resistant non-metallic gaskets are not known.) Of course, modified versions are thinkable, such as, for instance, mutually perpendicularly crossing air and fuel gas canals or a parallel arrangement of narrow rectangular cavities. In the latter case the model approaches a stack of disk cells in electric parallel connection.

Another model conceivable is the "tube cell", as shown in Fig. 3. In this case, the electrolyte is moulded around a central porous electrode and covered in turn by an outer electrode. Several of these cells may be placed in one single fuel gas (air) space, while air (fuel gas) is fed into the central electrodes. Again, no gasket materials in contact with the electrolyte are needed.

So far the majority of the experiments have been taken with single tube cells. No special attention has been directed towards the preparation of highly active electrode materials, the factor cell stability being considered as more important than the factor output in this stage of the research. Silver powder, embedded between the meshes of silver gauze, was used as air electrode in all experiments (based upon its excellent performance found in earlier research). Iron and nickel powders (or mixtures), obtained by reduction of the corresponding oxides, were used as fuel gas electrodes. No high-purity metals have been applied. In great lines, preparation and procedures with regard to the electrodes were similar to those described earlier. *

The tube cell construction is evident from Fig. 3. Moulding of the electrolyte paste around the central core (perforated tube + wire gauze with impregnated metal powder) can be performed in different ways. Simple hand-moulding by a procedure not unlike that of a glass-blower, namely alternate heating, addition of fresh material and surface nivellation with a cold metal sheet, was found quite effective in the hands of a skilled technician. ** Flame-spraying the electrolyte powder directly onto the automatically rotating core, with surface nivellation by means of a cold aluminum roll, is a second possibility. It was found, however, that inhomogeneities were caused by the wind sieving action of the flame upon the powder constituents.

At present the electrolyte powder is sprinkeled directly from a container onto the rotating core, which is heated by radiating elements. Surface nivellation again takes place on a cooled, freely rotatable aluminum roll. The present apparatus is pictured in Fig. 4. Some other methods, requiring less skill, are under study.

The only critical stage in the process is cooling the electrolyte body to ambient temperature. Because of the relatively larger thermal contraction of the electrolyte with respect to the perforated central tube of Fig. 3, the former is liable to occasional cracking.

A satisfactory solution to this problem is the spiral and sleeve construction shown in Fig. 5. The spiral is (slidingly) wound around the y-shaped support and connected to the sleeves. It carries the wire gauze - metal powder. The inlet tube fits rigidly around the y-support, but moves freely inside the sleeve. Free contraction of the cooling electrolyte is now possible by the flexibility in the length direction. In the cold state the sleeve is welded to the inlet.

The outer electrode may be constructed by wrapping a wire gauze "ribbon" in spiral turns around the electrolyte. Adjacent turns are spot-welded and the (slightly wetted) metal powder is pressed between the meshes afterwards.

For experiments the cell is enclosed in a long quartz tube, forming the outer gas space. The greater part is heated in a furnace, while the cold extremities are closed by rubber stoppers, allowing the gas-tight passage of the central pipe ends and other necessary objects (thermocouple, outer terminal, etc.). All experiments were carried out at atmospheric pressure.

*Compare, e.g., Ref. 1, p. 254, or Ref. 3, p. 83.

**The aid of Mr. J. Roele, technician of the Laboratory for Electrochemistry of the University of Amsterdam is greatly appreciated by the authors.

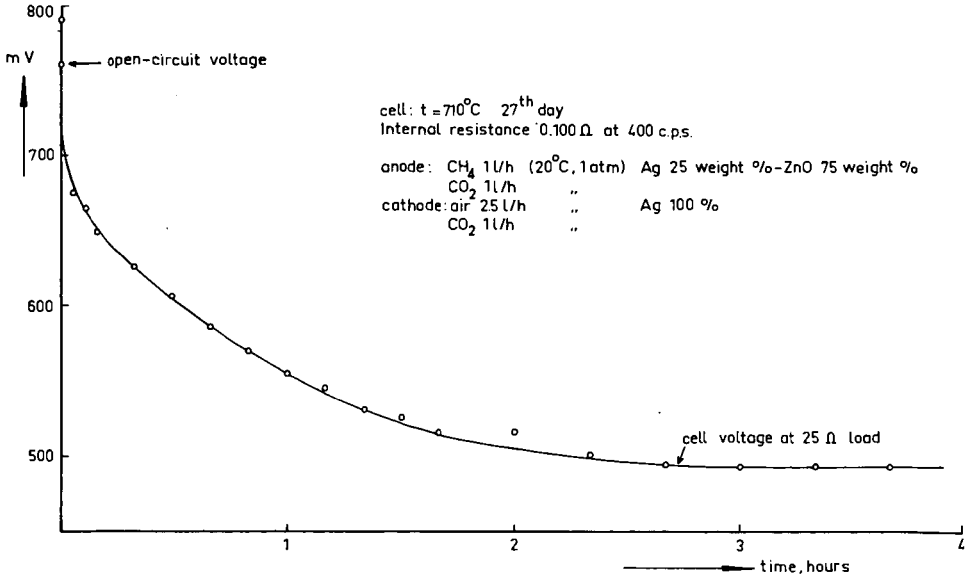

Fig. 6 . Slowness of the d.c. polarization processes

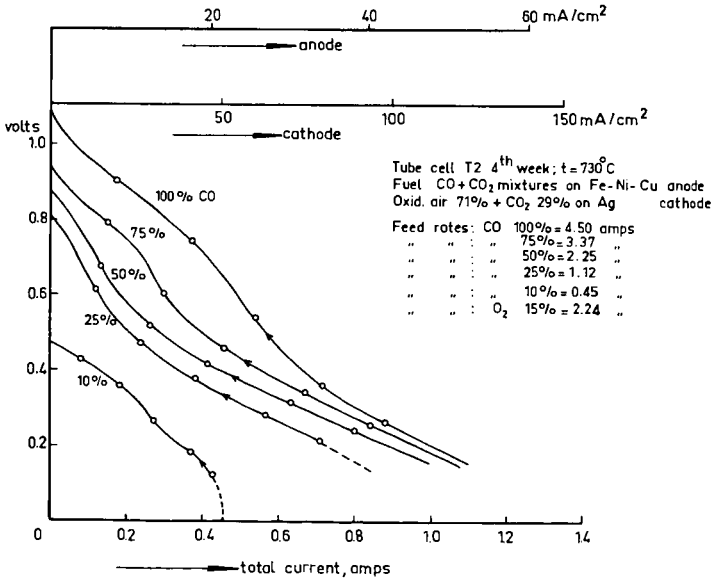

Fig. 7 Results with $CO-CO_2$ mixtures at 730°C
In the 10% mixture, complete conversion is reached in one pass.

B. Experiments with Leak-Tight Cells

It was soon observed that the leak-tightness of these cells was considerably better than that of the formerly used ceramic disk cells. In some cases no leaks could be detected at all, even after two months of operation. (In fact, the maintenance of gas-tightness of the outer space was sometimes found to be more difficult than that of the paste.) Therefore, experiments could be undertaken which it was senseless to do with leaking cells.

1. Fuel gases (CO, CH_3OH, H_2) could be "locked up" in the anode room at constant pressure and stationary temperature,* by means of a soap bubble membrane present in a calibrated tube connected to the gas outlet. It was found that in short duration tests the fuel gas volume increased at a rate directly proportional to the current drawn (within a few percents). There was a similar decrease in the cathode space, too, air + CO_2 being the oxidant. On open circuit, there was no volume changes. The rate of change was found to correspond with the theoretical figures in the case of air + CO_2 and CO + CO_2. With hydrogen and methanol vapour the practical figures were smaller than those calculated, but this effect is probably due to condensation of H_2O in the cold ends of the cell. Obviously Faraday's law is obeyed.

2. In similar experiments of longer duration (approximately one hour) it could be shown that the discharge capacity of an iron-nickel-copper powder anode was definitely larger than the charge stored in the locked-up quantity of gaseous fuel. First, a continuous stream of gas was passed over the anode. Then this supply was stopped and current drawn (at constant load) from the cell till a low cut-off voltage (0.2 volt) was reached. The voltage vs. time curves were recorded. They did not show any pronounced breaks, pointing to changes in the anodic reactions during discharge. The quantity of gaseous fuel could be calculated from the volume and the temperature distribution in the anode space (1 equivalent gas = 1 Faraday ≡ 26.8 Ah). Some typical data found are:

a. CH_3OH 10 vol.% + CO_2 90 vol.% at 550°C.
(1 mole CH_3OH = 6 Faradays);
charge withdrawn from cell: 0.275 Ah;
charge in gaseous fuel 0.01 Ah; ratio: 27.5:1.

b. CH_4 50 vol.% + CO_2 50 vol.% at 730°C.
(1 mole CH_4 = 8 Faradays);
charge withdrawn from cell: 0.57 Ah;
charge in gaseous fuel 0.45 Ah; ratio 1.26:1.

It is clear that either a chemisorbed phase is present, or that the metal powder is gradually oxidized. In the methanol case chemisorption of hydrogen is highly probable, whereas in the CH_4 case probably much less hydrogen is adsorbed. The significance of these experiments is that they prove that the "foregoing history" of electrodes may have a great influence upon their performance in later experiments, unless care is taken that really steady states are observed. Polarization curves measured under non-steady conditions are meaningless as a measure of cell performance. In some cases several hours are required before such a state is reached, as Fig. 6 may show.

3. In a steady state experiment CO_2 transport through the electrolyte was studied. The now commonly accepted overall electrode reactions for a carbonate electrolyte are:

cathode : $1/2\ O_2 + CO_2 + 2e^- \longrightarrow CO_3^{--}$ (1)

anode : CO_3^{--} + fuel $\longrightarrow$ oxidation product + CO_2 + $2e^-$ (2)

These reactions were verified in a gas-tight cell with slightly wet H_2 as fuel and air + CO_2 as oxidants. The anodic products were led through $CaCl_2$ and soda lime tubes during one hour. The results are given in Table 2.

Since the water gas shift reaction:

$$CO_2 + H_2 \rightleftarrows CO + H_2O \qquad (3)$$

will have practically no influence upon the composition of the anodic outlet (in the colder parts of the cell being in favour of CO_2 + H_2), the more than 90% "yields" of CO_2 and H_2O can be seen as a direct proof of reactions (1) and (2). To our knowledge such a proof has not been given earlier.

4. In earlier work** it was found that the open circuit voltage of cells operating on CO + CO_2 mixtures was very sensitive to oxygen leakage from the cathode. Thermodynamically calculated values are never reached in that case. Table 3 shows that very

*Temperature gradients could not be avoided. Before the experiments the gas spaces were flushed with similar gas mixtures.

**Compare Ref. 3, p. 90.

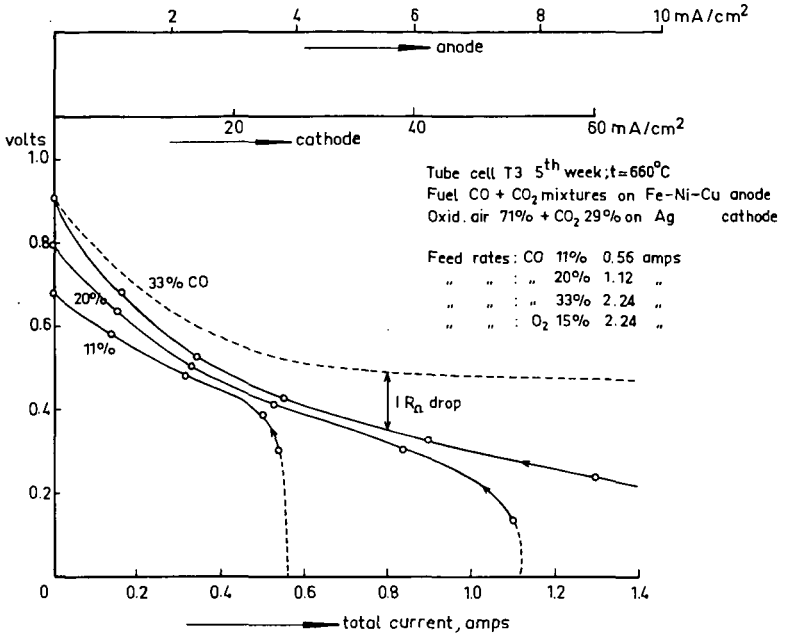

Fig.8 $CO + CO_2$ mixtures at 660°C
In the 11% and 20% mixtures, complete conversion is reached.
Effect of ohmic drop shown in upper curve.

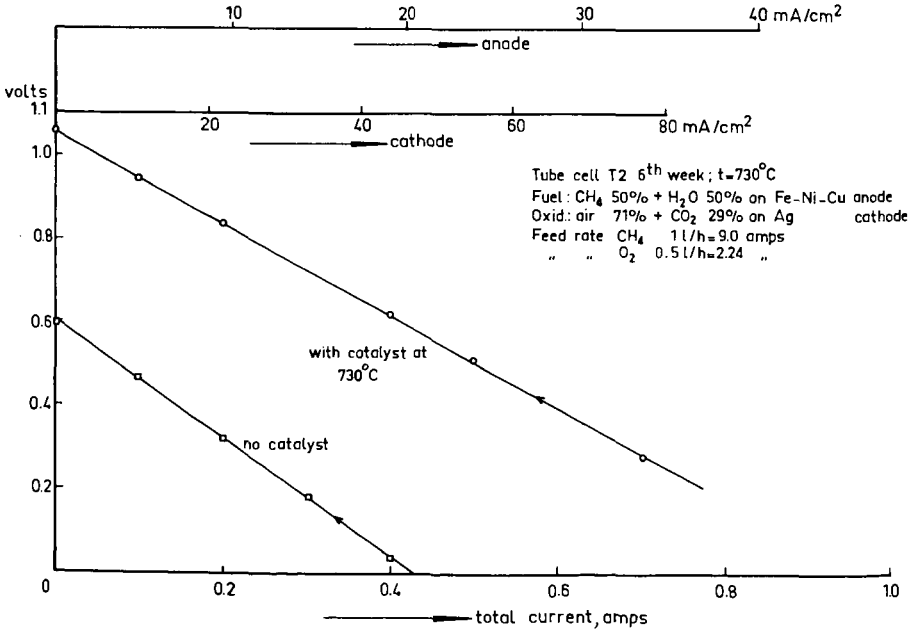

Fig. 9 Influence of nickel catalyst upon CH_4-steam equilibrium and resulting cell performance.

good agreement is found in absence of leakage. Before the o. c. v. measurement the cell was discharged for some time.

TABLE 2
STEADY STATE CO_2 TRANSFER THROUGH A CARBONATE ELECTROLYTE AT 600°C.

Cell current at constant voltage : 0.332 A = 12.36 milli equivalents/hour			
Anode	H_2 feed rate : 70.3 meq/h	anodic H_2O collected	: 12.90 meq/h
	H_2O " " : 1.60 "	" H_2O in feed	: 1.60 "
Cathode	O_2 " " : 83.2 "	" H_2O by discharge	: 11.30 meq/h = 92% "yield"
	CO_2 " " : 83.2 "	" CO_2 collected	: 11.90 meq/h = 96% "yield"
H_2 galvanically converted for 18%; O_2 for 15%.			

TABLE 3
THEORETICAL AND PRACTICAL CELL OPEN CIRCUIT VOLTAGES ON C0 + CO_2 MIXTURES AT 710°C.

CATHODIC GAS : air: 71.4 vol.% (O_2: 15.0 vol.%) CO_2: 28.6 vol.%

NERNST EQUATION : $E_{th.} = E_o + \frac{RT}{2F} \ln\left[p^{\frac{1}{2}}(O_2)_c \; p(CO_2)_c \; p(CO)_a / p^2(CO_2)_a\right]$;

$E_{o_{th.}}$ (710°C) = 1.020 V

ANODE : Ag + ZnO; CATHODE : Ag

Volume % CO (CO_2 = balance)	E calc.d. mV	E obs. mV	day of experiment
50	932	932	19th
25	885	881	9th
10	837	820	20th

C. Performance Data

Some steady state, total polarization curves (characteristics) are given in Figs. 7-10. The feed rates of fuel and oxygen (air used as oxidant) are expressed in amperes, for convenient comparison with the current drawn from the cell. The comparison with the current drawn from the cell. The compositions of the gas feeds are in volume percents; the feed rate of air - CO_2 was held constant (O_2 to CO_2 ratio 1:2). The inner electrodes were used as cathodes. Figs. 7 and 8 show results with C0 - CO_2 mixtures in two cells of different anode geometry but with similar electrodes. It was found that this "similarity" of anodes usually gave far from identical results, in connection with the still primitive ways of contacting the powder metals with the outer electrolyte surfaces and the ill defined character of the metal particles. From the figures it can be seen that:

1. Anodic current densities are widely different, while cathodic ones are of the same order of magnitude.

2. At C0 contents less than 20% the galvanic combustion can be virtually completed in one pass (at low c. d. in Fig. 8, but at >20 mA/cm^2 in Fig. 7). Obviously,

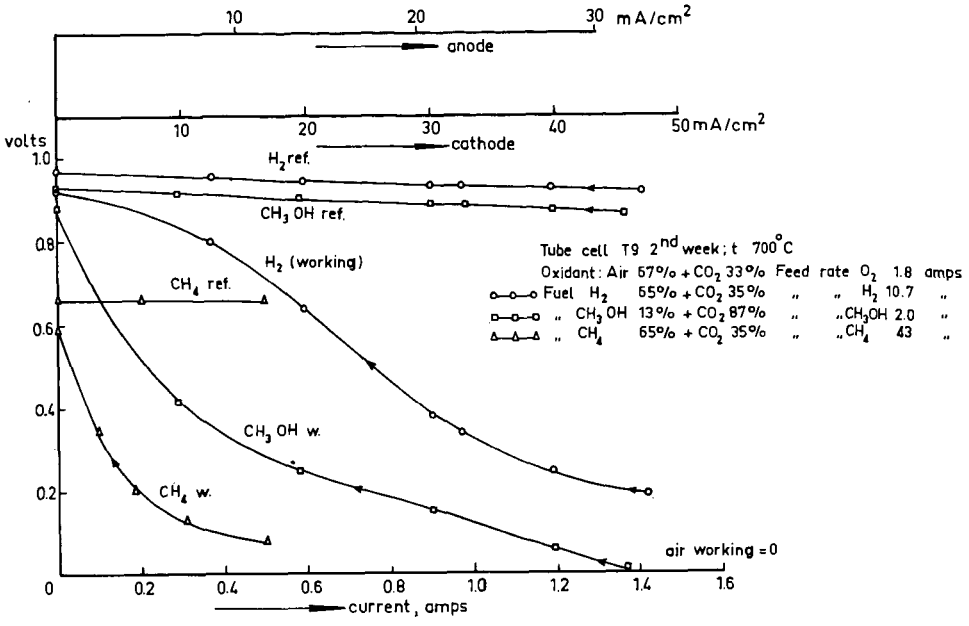

Fig. 10 Characteristics and electrode polarization on different fuels. Anode: "flaked nickel" cathode: silver The cathode does not polarize at 4% final O_2 content.

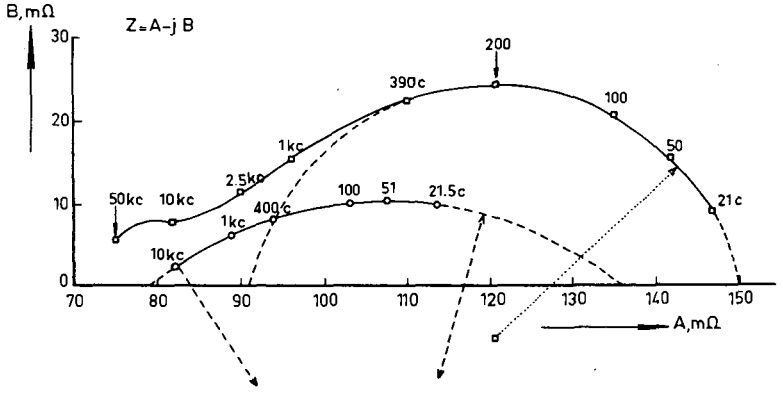

Fig. 11 Real vs. imaginary (Argand) diagrams of cell impedance Z = A - jB
Commercial dry cell at 20°C
Fuel cell at 700°C, on petroleum ether - CO_2 mixture. (no d.c. polarization)

the polarization caused by gaseous diffusion is extremely small, otherwise the observed limiting currents would have been smaller than those prescirbed by the feed rate.

3. In the case of Fig. 7 there has been some leakage, which is evident from the fact that the open circuit voltages on low CO contents are definitely too low.

4. Polarization (to be ascribed to the anodes) is obvious, since the slopes of the curves correspond with effective resistances of 0.20 - 0.75 ohm, while the a.c. resistances at 1000 c.p.s. were less than 0.20 ohm (compare "ohmic drop" at the upper curve of Fig. 8). Fig. 9 shows results with a 50 - 50 vol.% CH_4-steam mixture, fed directly into the cell (lower characteristic) and passed first over a nickel-on-magnesite "reforming catalyst" at 730°C., respectively. Since the conversion percentage of the fuel remains below 10% at the maximal current (0.7 amp), most probably only hydrogen and CO have been galvanically oxidized in the catalyst experiment. Although the improvement is striking, it should be stressed that in practical batteries the necessary heat for the CH_4 conversion must be supplied by the battery itself, and not by external heat sources as in usual laboratory experiments.

(With higher hydrocarbons complete misinterpretation of characteristics may be caused by neglection of feed rate data, as is obviously the case in a fairly recent Russian publication. (12) The high temperature of the cell furnace will cause appreciable thermal dissociation into hydrogen and unsaturated compounds. From propane, for instance, 45 vol.% of H_2 can be formed at 700°C., which means that for a 1 amp current a feed rate as small as 0.55 l/h (20°C., 1 atm) is needed to run the cell on hydrogen only. For complete combustion only 45 ml/h of propane would be required.)

Fig. 10 pictures results obtained with a cell in which the anode was divided into two halves, about equal in area. One part served as reference electrode. The metal powder used in this case was "flaked nickel"*, particle size < 44 microns. The cathode (central electrode) was, as usual, silver powder. In the figure the potential of the cathode is taken as zero. Since the outer (anodic) space showed some leakage not through the electrolyte), fuel supply rates had to be taken larger than usual. Clearly, only the anode is responsible for the polarization observed in all the presented figures. At a cell current of 1.4 amp (47 mA/cm^2 cathodic) the 0_2 from the feed is converted for 78% and the final oxygen content is 4 vol.% without any significant polarization. The very poor performance of CH_4 (without extra catalysts) is obvious.

D. Canal Cells

A restricted number of experiments was made with this type. The cell performance depends greatly upon the quality of the electrolyte blocks and the proper insertion of canals and electrodes. Pore- and crack-free blocks are still difficult to prepare, though hot-pressing techniques have been used with some success. Blocks of 5 x 5 x 15 cm could be formed under 16 kg/cm^2, with a volume porosity of 2.5% - 5% in the cold state.

Contamination pick-up after the second preheating stage of the electrolyte material (cf. Sect. I) must be avoided, otherwise CO_2 bubbles are formed upon heating in the pressing mould. The cooling stage, especially the solidification temperature range, is quite critical with regard to crack formation. Canals can be drilled by cold tooling, but this procedure is unattractive in connection with the great hardness of the cold substance. Their formation in the hot state is under study. Cold, thin-walled metal tubes can be used to "cut out" canals in the hot substance if they are quickly inserted and withdrawn again. The insertion of electrodes in the canals also needs further study.

Experiments at 700°C., with a few, yet primitive models, in which some of the seven canals served as reference anodes and cathodes have learned that:

1. Polarization, apart from "ohmic drop", is completely due to the nickel powder (H_2) anodes used so far. Ohmic drops in the electrolyte are small: less than 80 mV at 50 mA/cm^2.

2. The silver powder (air + CO_2) cathodes remain unpolarized up to the point where the 0_2 turnover is virtually in balance with the feed rate; that means, where the 0_2 depletion is complete (verified at 50 to 100 mA/cm^2). These facts are in full accordance with the tube cell results of Fig. 10.

3. The establishment of good electric contact between anode and electrolyte is of major importance for the power output. In this respect the cathodic contact seems to have less influence in the present apparent current density range (at least within certain limits).

*Manufactured by "Larsen Industries, Inc.", Murray, Utah, U.S.A. (at presnet: United Techn. Industries).

4. The use of powder metal anodes with micropores (say < 0.2 micron) leads to occasional flooding.

5. The shape of electrolyte blocks, used in two week experiments, remains unchanged.

E. Conclusions and Further Outlooks

It can be concluded that the use of paste electrolytes yields a significant improvement in the construction of permanently gas-tight cells. The consistency of the paste is such that the mechanical strength of the construction need not be borne by the electrodes only, as in liquid electrolyte cells. When the substance is crack-free in the initial (cold) state, it remains so during operation for at least 2-1/2 months, this period being the longest so far, during which single cells were tested. Chemical analyses of tube cell electrolytes, held in vertical position during two months, have revealed that no significant separation occurs of MgO and carbonates. (Differences in MgO content of 0.5% were observed between upper, middle and lower sections of a 20 cm tube.)

The silver powder cathodes of usually less than 0.1 mm thickness are almost ideal air electrodes, both in electric performance and long-run behaviour. The nature of this phenomenon is not yet understood completely.

Clearly, the fuel gas electrodes are the bottlenecks in further developments, although a perfectioning of electrolyte moulding techniques is also an important technological problem.

The study of anodic reaction mechanisms was taken up when sufficiently stable cells could be produced. A start has been made with a. c. measurements of electrode impedances as a function of frequency, in the range 20 c to 50 kc, by means of a modified Kelvin bridge technique. (This method enables an accurate determination of the very small impedances involved; magnitude less than 0.10 ohm.) A strong dependence upon frequency, gas composition and d. c. polarization was found in many cases. The interpretation of the results, which may proceed along general lines given by Euler and Dehmelt, (13) Euler (14) and Vetter (15), is fairly involved because of the ill defined state of the porous structures used so far. There is evidence of a slow (non-gaseous) diffusion process, probably coupled with a heterogeneous chemical reaction as being rate determining.

An example is given in Fig. 11, where the real components A of the cell impedance A-jB is plotted against the imaginary B, with the frequency as parameter (Nyquist or Argand diagram). For comparison similar results are given, obtained with a commercial dry cell. In both cases there is evidence of a circular plot, which in the case of the dry cell can be largely explained by the parallel combination of a constant double layer capacity and a constant resistance associated with a slow electrochemical exchange reaction at the zinc electrode. (13) In the fuel cell case (the center of the circle being situated much lower) the equivalent circuit seems to be composed of a "Warburg impedance" (which is caused by diffusion) in parallel with a constant resistance, presumably also related to exchange processes. It should be said, however, that plots of various course have been found with different cells, even when the anodes were "similar".

Therefore, another approach has been made recently, in which the behaviour of better defined anode materials will be studied.

The impedance behaviour of the present silver cathodes escapes detection with the bridge; presumably the reactions are too fast to be followed in the mentioned frequency range.

ACKNOWLEDGMENTS

The authors would like to thank the U. S. Army Procurement Center at Frankfurt a. M., Germany, for the financial support since 1959, and in particular Lt. Colonel G. Metcalfe and Dr. B. R. Stein for their help in providing transportation facilities and for their personal interest.

They thank their T. N. O. colleagues of the C. T. I. for their enthusiastic efforts in the technological development of the work.

They also want to express their gratitude towards the director of C. T. I., Dr. J. Hamaker, and Ir. A. H. de Haas van Dorsser for their advice and permission to publish this material.

Finally, the authors' grateful acknowledgments are due to Prof. Dr. J. A. A. Ketelaar and Mr. J. Roele of Amsterdam University for their invaluable help and advice from the beginning of this work.

LITERATURE CITED

(1) Broers, G. H. J., High Temperature Galvanic Fuel Cells, Ph. D. thesis, Municipal University of Amsterdam 1958.

(2) Broers, G. H. J., and Ketelaar, J. A. A., Ind. & Eng. Chem. 52, (1960), 303.

(3) Broers, G. H. J., and Ketelaar, J. A. A., Fuel Cells, pp. 78-93, G. J. Young, editor, Reinhold Publ. Corp., New York 1960.

(4) Broers, G. H. J., Dechema Monographien Band 38, 277-303, Frankfurt a. M., 1960.

(5) Reference 1, p. 150.

(6) Janz, G. J., and Lorenz, M. R., Techn. Report No. 10, p. 4, August, 1960, ONR contr. Nonr. 591-10, Rensselaer Polytechn. Inst., Troy, New York.

(7) Chambers, H. H., and Tantram, A. D. S., Reference 3, p. 99.

(8) Douglas, D. L., Reference 3, p. 129.

(9) Baur, E., Treadwell, W. D., and Trümpler, G., Z. Elektrochem. 27 (1921), 204.

(10) Greger, H., German Patent 570,600 (1933).

(11) Reference 3, p. 84.

(12) Daniel-Bek, V. S., Mints, M. Z., Sysoeva, V. V., and Tikhonova, M. V., Zhur. Priklad. Khim. 32 (1959), 649-655.

(13) Euler, J., and Dehmelt, K., Z. Elektrochem. 61 (1957), 1200.

(14) Euler, J., Electrochim. Acta 3 (1960), 134.

(15) Vetter, K. J., Elektrochemische Kinetik, Chapters 2 and 3, Springer-Verlag, Berlin 1961.

SYMPOSIUM ON FUEL CELLS
PRESENTED BEFORE THE DIVISION OF PETROLEUM CHEMISTRY
AMERICAN CHEMICAL SOCIETY
CHICAGO MEETING, September 3-8, 1961

AN OUTLINE OF THE ECONOMICS OF A DOMESTIC FUEL CELL SYSTEM

By

C. G. von Fredersdorff
Institute of Gas Technology, Chicago 16, Illinois

INTRODUCTION

A methane fuel cell power pack would be an attractive domestic application if the savings in fuel cost of natural gas over purchased electricity were sufficient to pay out the investment within a reasonable time or at least within the expected life of the system. Other requirements for the fuel cell system are, of course, reliability and adaptability of this type of power in the home.

This economic study is directed toward the high-temperature molten-carbonate-electrolyte type fuel cell which is under experimental investigation at the Institute of Gas Technology. This cell is capable of utilizing methane in the presence of steam at 650 to 850°C. or higher. The cell mechanism apparently involves in situ reforming of methane at the anode, followed by electrochemical oxidation of the reformate by carbonate ions. Several experimental constants relating to polarization and effective resistivity are taken from results of Shultz, et al. (2) on the molten-carbonate cell. This analysis is equally applicable to other fuel cell types for which electrode area and polarization data are available.

Because of the steep voltage-current characteristic of molten-carbonate cells, it appears unlikely that the power can be utilized under the normal variations of the domestic load without extreme voltage regulation. This would entail a substantial loss in fuel cell efficiency. Since domestic appliance load factors are usually 15 to 20%, this means the fuel cell power pack would be under low load or idling for long periods and under heavy load for short periods. The fuel cell efficiency would be further reduced by virtue of the standby heat required to maintain the operating temperature during the idling periods.

As a consequence, an electrical storage system seems to be indicated. If lead-acid storage batteries are interposed downstream of the power pack, a fairly constant voltage to load could be maintained; for periods of heavy loads several auxiliary 2-volt storage cells could be arranged to switch automatically into the circuit to maintain voltage regulation within prescribed limits. The storage system would allow reduction of the power pack capacity by a factor of 4 or 5 by virtue of nearly continuous fuel cell operation, say at a load factor of 90%, in charging the storage batteries.

The domestic system is visualized as comprising the power pack; means for recovering waste heat from the pack for water heating or other use; the storage batteries, equipped with a current limiting voltage regulator to limit the charging rate, and one or more dc inverter units to supply services requiring 60 cycle alternating current. Since inversion of dc to ac involves loss of efficiency, it would be advantageous from this standpoint to utilize dc power directly for the purely resistive loads and the ac power for resistive-inductive-capacitative loads. It is not clear, however, that the advantage of inverting only part of the load to ac would outweigh the disadvantage of needing a double wiring system.

The dc inverter might comprise: 1) motor-alternator set, 2) a multiplicity of small-capacity germanium transistorized units for individually operating radio, television, small motors and 3) preferably a several-kilowatt solid state device based on the silicon controlled rectifier (SCR). (3) With specialized frequency regulation, the SCR inverter can be sufficiently accurate to operate electric clocks. With wave form filtering, these units should be satisfactory for powering hi-fi equipment.

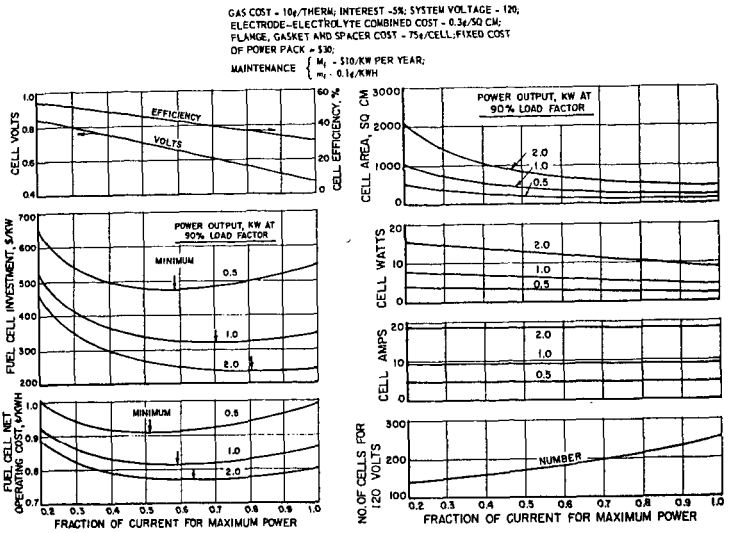

Figure 1. Effect of current density and fuel cell capacity upon cost factors and operating characteristics is demonstrated for the case where the fuel cell load factor is held at 90%, and 90% of the waste heat is credited at fuel value

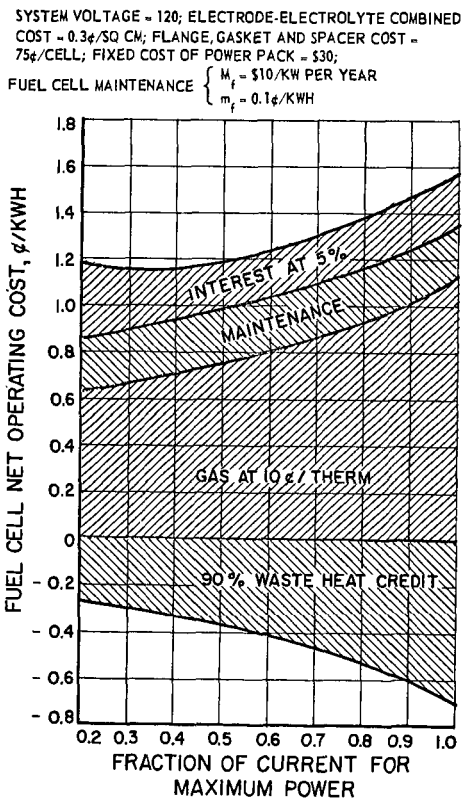

Figure 2. Fuel cell operating costs can fall within economic limits by maintaining an average load factor of 90% at 1 kw average power output

CAPITAL AND OPERATING COST RELATIONS OF POWER PACK

In this section methods of computing the estimated costs of only the fuel cell power pack are considered. This is followed in the next section by estimation of payout time of the power pack-waste heat recovery-storage battery-dc to ac inverter system. Some preliminary relations of cell performance are given here because these bear directly upon the costs.

Cell Performance

If i represents external current density, amps/sq cm; A the electrical path area per cell, sq cm; I = iA, the total external current, then the cell terminal voltage V is expressed by:

$$V = E^{o}_{act} - E_c - E_a - Ir_i \qquad (1)$$

where E_c and E_a are the concentration polarization and activation polarization in volts, respectively, for which Austin (1) gives typical theoretical relations.

E^{o}_{act} is the actual open circuit voltage that would obtain under the concentration and temperature conditions if all polarization effects were absent. It is not necessarily equal to the experimental open circuit voltage.

r_i is the cell ohmic resistance comprising the contributions of resistivities of electrolyte, anode and cathode, and contact resistances of anode and cathode to electrolyte and to external circuitry.

For the range of current densities of interest, 10 to 40 milliamps/sq cm, the sum of the polarizations can be represented to a good approximation as a straight line: $E_c + E_a = a_p + b_p I/A$ where a_p and b_p are empirical polarization constants. If we represent $b_p/A = \beta_p r_i$ and the external load resistance $r_L = mr_i$, so that $I = V/mr_i$, then the external power, p in watts/cell, may be written:

$$p = \frac{mr_i (E^{o}_{act} - a_p)^2}{\left[(m + 1 + \beta_p) r_i\right]^2} \qquad (2)$$

For fixed thicknesses of electrodes and electrolyte, r_i is inversely proportional to electrical path area A. Thus, Ar_i is practically independent of cell areas for constant temperature and constant contact resistivities. From the above definition, β_p is also a constant, and we get a direct proportion for scaling up to different cell areas:

$$(1 + \beta_p) Ar_i = \text{constant} = \left[(1 + \beta_p) Ar_i\right]_{exp} \qquad (3)$$

This makes:

$$(1 + \beta_p) r_i = r_{eff} A_{exp}/A = R_{eff}/A \qquad (4)$$

where r_{eff} is the experimental value of $(1 + \beta_p) r_i$, which is given by the negative slope of the linearized portion of the voltage-current density curve divided by the experimental cell area, i.e. $-\Delta V/\Delta i A_{exp}$. A particular set of data, (2) upon which part of the present study is based, for a plastic form of carbonate electrolyte between nickel and silver electrodes with 33 mole % methane-67 mole % steam at 750°C., gave $r_{eff} = 0.468$ ohms, making $R_{eff} = 10.62$ ohm-cm^2 for the reported 22.65 cm^2 cell.

In equation 2, the quantity $(E^{o}_{act} - a_p)$ represents the intercept obtained by extending to zero current density the linearized portion of the cell voltage curve. This value was 0.94 volt for the above plastic carbonate cell. Also in this equation, the external power reaches a maximum at the optimum resistance ratio $m^* = 1 + \beta_p$, for which the corresponding maximum current I* becomes:

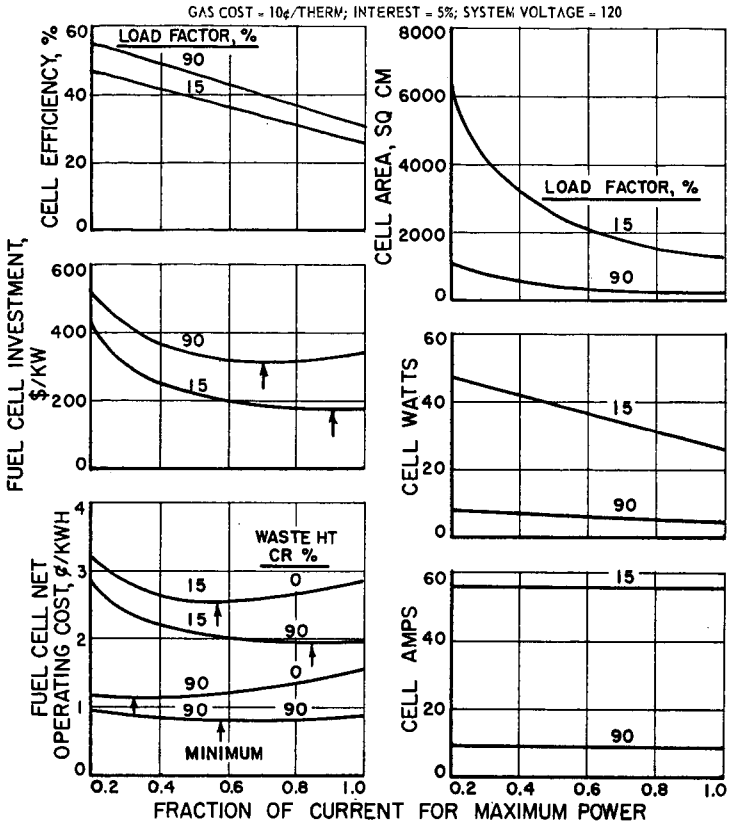

Figure 3. Load factor and waste heat credit contribute a significant effect to cost factors of a fuel cell of 1 kw average power output

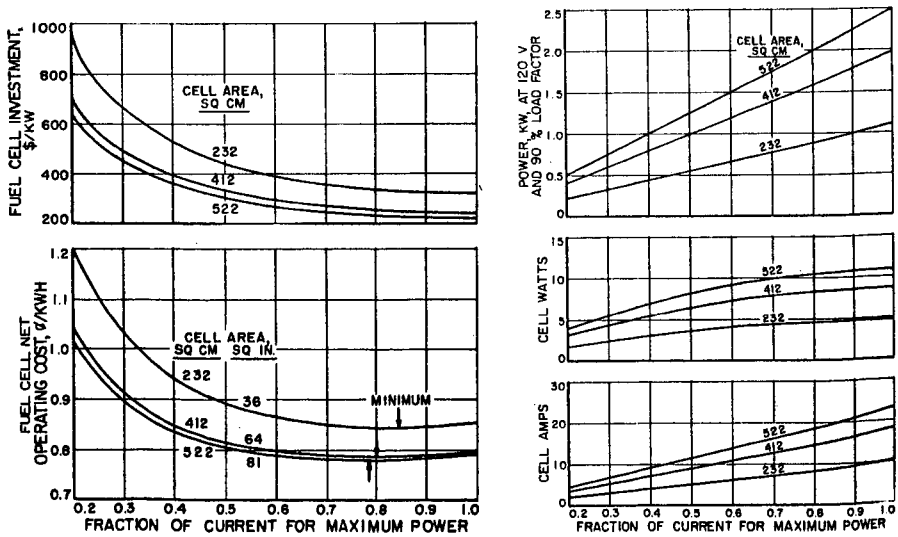

Figure 4. Effect of current density and cell area upon cost factors and operating characteristics is demonstrated for a power pack maintained at 90% load factor and credited with 90% of the waste heat

$$I^* = (E^o - a_p)A/2R_{eff} \tag{5}$$

For purposes of calculations, it is convenient to represent the actual external current I as a fraction x of the current for maximum power, $I = xI^*$. We may then write Equation 2 in the form:

$$p = (E^o_{act} - a_p)^2(2 - x)Ax/4R_{eff} \tag{6}$$

The load resistance is expressed as:

$$r_L = mr_i = R_{eff}(2 - x)/Ax \tag{7}$$

and the cell voltage for the linearized portion of the polarization curve becomes:

$$V = (E^o_{act} - a_p)(2 - x)/2 \tag{8}$$

Costs

In setting up the fuel cell costs, we choose that the total output voltage of the power pack shall be fixed at V_t volts. Then the number of cells in series, N_C, is given by:

$$N_C = V_t/V = 2V_t/\left[(E^o_{act} - a_p)(2 - x)\right] \tag{9}$$

The capital cost of the power pack comprises a fixed cost, C_{FC}, for the casing, insulation, vent, which cost is considered independent of size over the range of capacities of interest here, plus a variable cost, C_{VP}, which is dependent upon the number and area of cells. The latter cost is split into two parts:

$$C_{VC} = N_C C_{fl} + N_C A C_{el}$$

where C_{fl} = unit combined cost in \$/cell of flanges, gaskets, piping, electrical connections, assembly

C_{el} = unit combined cost in \$/cm^2 of electrolyte and electrodes.

Thus, the principal invested in the fuel cell power pack, P_f, is as follows, based upon the above relations:

$$P_f = C_{FC} + \frac{2V_t(C_{fl} + AC_{el})}{(E^o_{act} - a_p)(2 - x)} \tag{10}$$

If g_o represents the overall fuel cell load factor, the average power output of the pack $\overline{W}$ in watts, may be stated:

$$\overline{W} = g_o p N_C = g_o(E^o_{act} - a_p)V_t Ax/2R_{eff} \tag{11}$$

The corresponding gas cost, in ¢/yr, to operate the power pack at $\overline{W}$ output is:

$$\text{Gas cost} = \frac{(3.415)(8760)(10^{-5})C_g g_o(E^o_{act} - a_p)V_t Ax}{2E_f R_{eff}} \tag{12}$$

where C_g = unit gas cost, ¢/therm

E_f = fuel cell efficiency, fractional

Perhaps 30 or 40% of the gas feed to the cells would be discharged as unreacted methane-plus-steam diluted with oxidation products of the anode reactions. The waste gas would fulfill underfiring requirements for preheating and maintaining the power pack at operating temperature. Since only a fraction of the input energy content of the gas is converted to electrical energy, ample waste heat is available which could be recovered for water heating or other use. If a fraction f_w of the waste heat is so recovered and credited at fuel value against operating costs, then the amount of credit in ¢/yr may be obtained by multiplying Equation 12 by the factor $f_w(1 - E_f)$.

An estimate of the fuel cell efficiency is required here since it bears directly upon the gas cost and waste heat credit. A relation is obtained by considering that the actual efficiency is the theoretical value diminished in proportion to the fraction of unreacted gas and in proportion to polarization and ohmic losses. We may write:

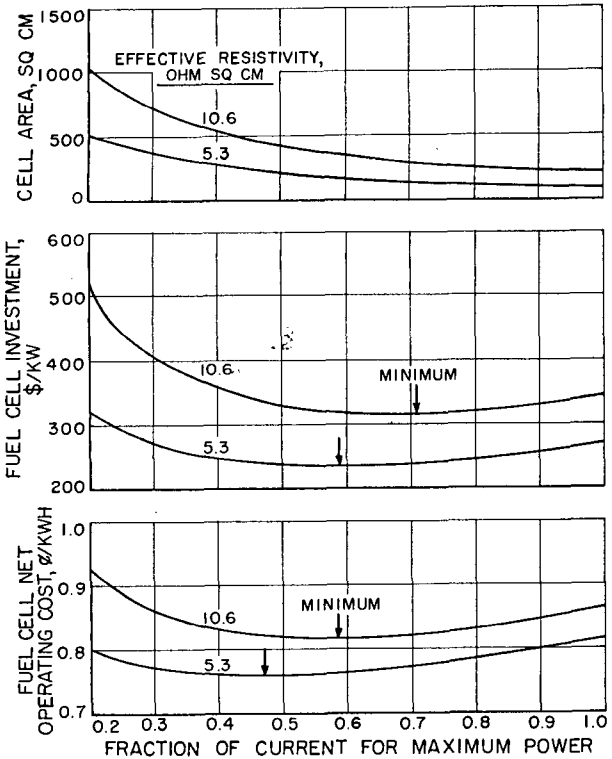

Figure 5. Costs of a methane fuel cell of 1 kw average power output at 90% load factor, with 90% waste heat credit, decrease significantly if the effective cell resistivity can be reduced by 50%

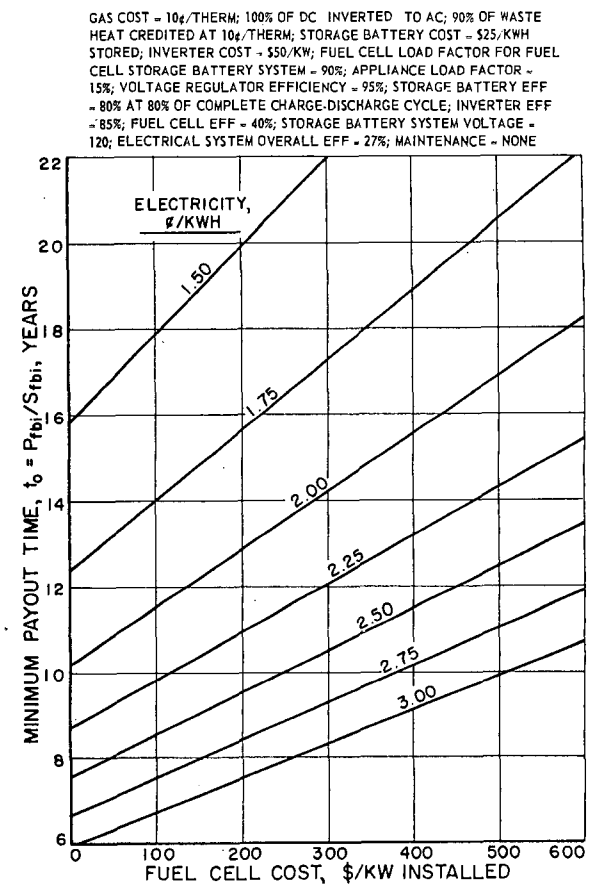

Figure 6. Effect of fuel cell cost and electric cost on payout time of fuel cell-storage battery-dc to ac converter system with 90% waste heat credit, batteries costing $25/kwh storage capacity, and inverter costing $50/kw

$$E_f = E_{theo}E'V/E^o = E_{theo}E'(E^o_{act} - a_p)(2 - x)/2E^o \qquad (13)$$

where E_{theo} = theoretical efficiency or ratio of free energy change to enthalpy change, $\Delta F/\Delta H$, at reaction temperature and concentration conditions.

E' = correction factor for unreacted fuel discharged in waste gas and for additional fuel which may be needed for underfiring.

E^o = theoretical open circuit voltage as given by the Nernst Equation, about 1 volt at 750°C. for products of methane reforming.

Fuel cell maintenance, an additional operating cost, is represented as a fixed part, M_f in $/KW capacity per year, plus a variable portion, m_f in ¢/KWH. Since the fuel cell capacity is $\overline{W}/1000\ g_o$, and the yearly kilowatts output is $8.76\ \overline{W}$, the relationship obtains:

$$\text{Maintenance, ¢/yr} = \frac{(E^o_{act} - a_p)V_t Ax}{2R_{eff}}\left[\frac{M_f}{10} + 8.76\ g_o m_f\right] \qquad (14)$$

The total operating cost in ¢/yr of a power pack which has an arbitrary cell area A comprises the sum of interest on principal, gas cost, and maintenance less waste heat credit as given in the above relations. Dividing this sum by $8.76\ \overline{W}$ yields operating cost in ¢/KWH. Inspection of this relation shows that an optimum value of fraction of current for maximum power, x, exists such that the cost per KWH reaches a minimum.

In addition to the set of calculations which can be made for constant cell area A, it is logical also to compute on the basis of constant average power output $\overline{W}$ as parameter. To accomplish this, Equation 11 is solved for A and this result substituted into all the pertinent cost relations. In these terms, we get from Equation 10:

$$P_f = C_{FC} + \frac{2V_t C_{fl}}{(E^o_{act} - a_p)(2 - x)} + \frac{4\overline{W}R_{eff}C_{el}}{g_o(E^o_{act} - a_p)^2(2 - x)x} \qquad (15)$$

and the net operating cost, with j = interest rate, %, becomes:

$$¢/KWH = jP_f + (0.295)C_g\overline{W}\left[f_w + (1 - f_w)/E_f\right] + \overline{W}(M_f/10\ g_o + 8.76\ m_f) \qquad (16)$$

In both of these relations, the dependence on x is such that a minimum is reached. This can be computed by setting the derivatives to zero.

Calculate Results

Figs. 1 to 5 give typical indications of the manner in which molten carbonate cell performance and cost factors depend upon the operating variables for various optimistic assumptions concerning certain of the cost parameters as indicated in the captions. For all cases where the average load factor of the power pack is held at 90%, the product $E_{theo}E'$ in the fuel cell efficiency calculation is estimated at 0.65; for 15% average load factor $E_{theo}E'$ is estimated at 0.55. The unit costs C_{FC} = $30, C_{fl} = $0.75/cell and C_{el} = $0.003/sq cm are considered rock bottom minima under mass production conditions.

Fig. 1 distinguishes between three average power outputs, 0.5, 1.0 and 2.0 KW at 90% load factor, indicating a rapid decrease in operating cost and investment per KW in going from 0.5 to 1.0 KW, and a less rapid decrease in going from 1.0 to 2.0 K.W. This is a result of the fact that at a fixed current, the number of cells is fixed for 120 volt output, but the power output and electrode-electrolyte costs increase proportionately with cell area, while other fixed costs per cell have been assumed to remain the same. A power pack of 1.0 KW output at 90% load factor would be sufficient for the average home. Under the assumptions made here, the investment for this size unit reaches a minimum of $355/KW, and fuel cell net operating cost a minimum of 0.82¢/KWH, but the minima do not occur at the same value of the operating current.

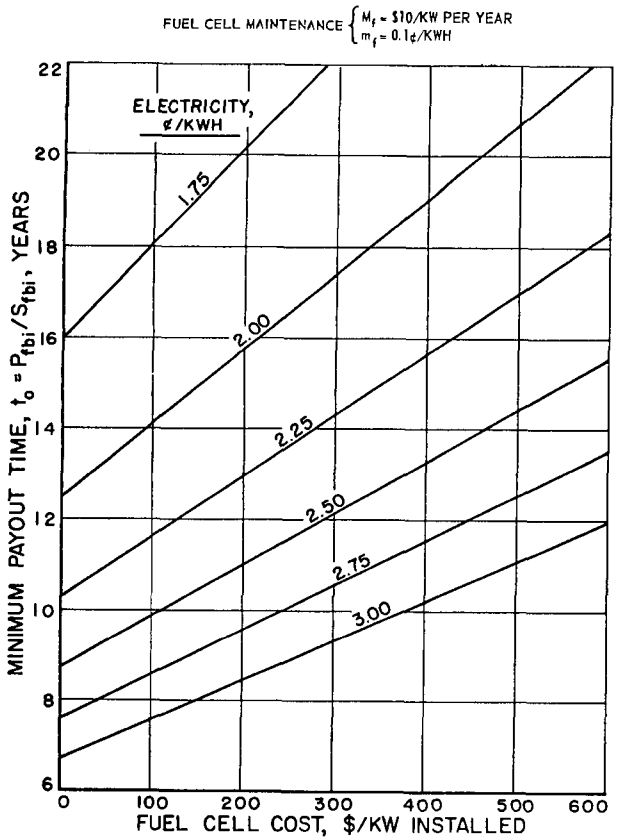

Figure 7. Effect of fuel cell cost, electric cost, and assumed fuel cell maintenance on payout time of fuel cell-storage battery-dc to ac inverter system with 90% waste heat credit, batteries costing $25/kwh storage capacity, and inverter costing $50/kw

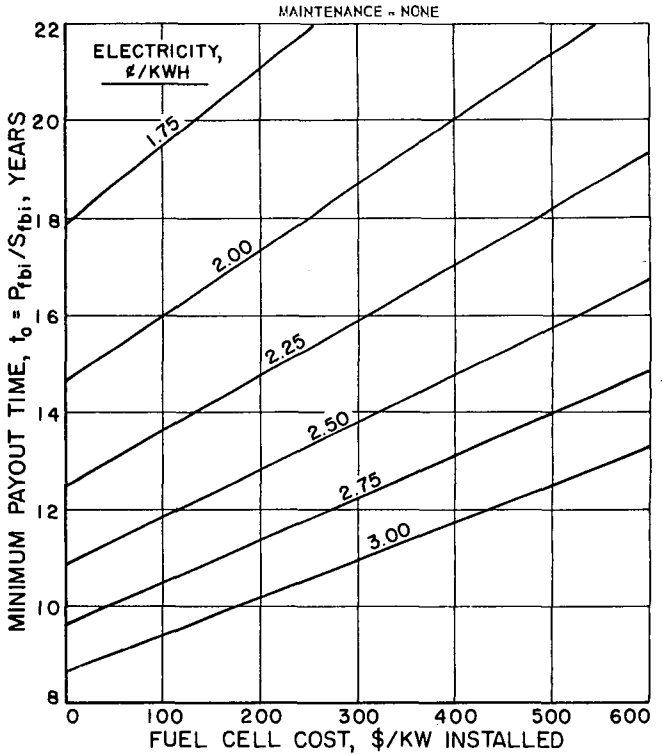

Figure 8. Effect of fuel cell cost and electric cost on payout time of fuel cell-storage battery-dc to ac inverter system with 90% waste heat credit, batteries costing $40/kwh storage capacity, and inverter costing $50/kw

The position of the minima shifts to the right with increasing capacity. Under present technology, cell areas are limited to a maximum of about 100 sq in or slightly over 600 sq cm. Fig. 2 gives a cumulative breakdown of operating costs for the 1 KW case of Fig. 1. The importance of the waste heat credit is stressed here because this can bring operating costs below 1¢/KWH.

The effects of varying the load factor between 15 and 90% and waste heat credit between 0 and 90% for the 1 KW case are explored in Fig. 3. The operating costs at 15% load factor approach or exceed the cost of purchased electricity, 2 to 3¢/KWH.

Since a particular f 1 cell design would have a fixed cell area, a more realistic comparison is given in Figure 4, based on constant cell areas. All the assumptions listed in caption of Fig. 1 apply here. For a fixed cell area, the power pack investment per KW is a minimum at the current corresponding to maximum power, while the operating cost approaches a minimum at a current between 75 and 85% of maximum power for the three areas shown. The number of cells, cell voltage and estimated fuel cell efficiency are the same as in Fig. 1. The power output at 120 volts increases linearly with the current, of course. For the 232 sq cm case, the average power output at 90% load factor is 0.93 KW at x = 0.84, the point of minimum operating cost. If points of constant power output are marked on the cost curves of Fig. 4, the envelope of these points defines the curves of Fig. 1. An area of significant improvement lies in reducing the effective cell resistivity. If a 50% reduction can be achieved, the investment cost may be lowered by as much as 25% and operating costs by 5 to 10%, as shown in Figure 5.

FUEL CELL SYSTEM PAYOUT TIME

Considering the potential savings in operating costs over purchased electric power, the minimum payout time, t_o in years, that the fuel cell-storage battery-dc inverter system can have is given by the general relation:

$$t_o = P_{fbi}/S_{fbi} \qquad (17)$$

$$= \frac{\left[I_f + 24 I_b g_2/DV_b\right]\left[1 + f_i(1 - E_i)/E_i\right] + E_r\left[g_1 + g_2 E_b\right] f_i I_i/g_i}{B\left[\frac{C_e - C'_e}{f} + C'_e + \frac{C_g\left[(1 - E_f)f_w - 1\right]}{29.33\ E_o} - m_f - (1-g')m_b\right] - \frac{24 g_2 M_b}{V_b} - M_f}$$

where $B = 87.6\ E_r(g_1 + g_2 E_b)$

P_{fbi} = total principal invested in fuel cell-storage battery-dc inverter system

S_{fbi} = annual saving in operating cost of fuel cell system over purchased power

I_f = fuel cell investment cost, $/KW installed capacity

I_b = storage battery investment cost, $/kiloamp-hr capacity at a particular voltage

I_i = dc inverter investment cost, $/KW installed capacity
g_1 = g'g''
g_2 = go - g'g''
g' = applicance load factory, fractional
g'' = fuel cell load factor during period of storage battery discharge. Here g'' $\cong$ 1.0.
go = overall fuel cell load factor when combined battery storage, fractional
g_i = dc inverter load factor, here equal to appliance load factor.
E_r = voltage regulator efficiency, fractional.
E_b = storage battery electrical efficiency, fractional.
E_f = fuel cell thermal efficiency, fractional.
E_i = dc inverter electrical efficiency, fractional.

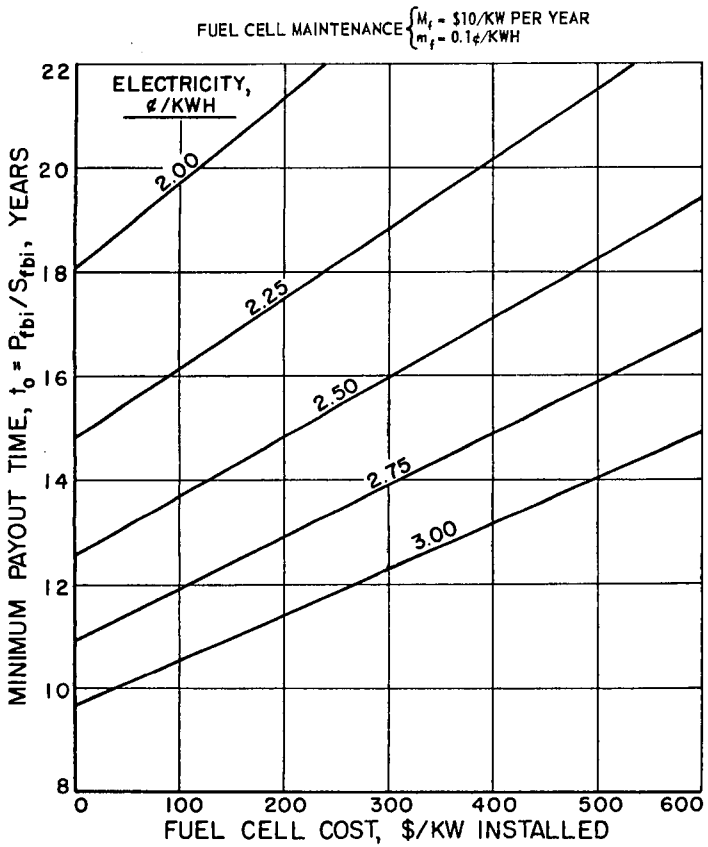

Figure 9. Effect of fuel cell cost, electric cost and assumed fuel cell maintenance on payout time of fuel cell-storage battery-dc to ac inverter system with 90% waste heat credit, batteries costing $40/kwh storage capacity, and inverter costing $50/kw

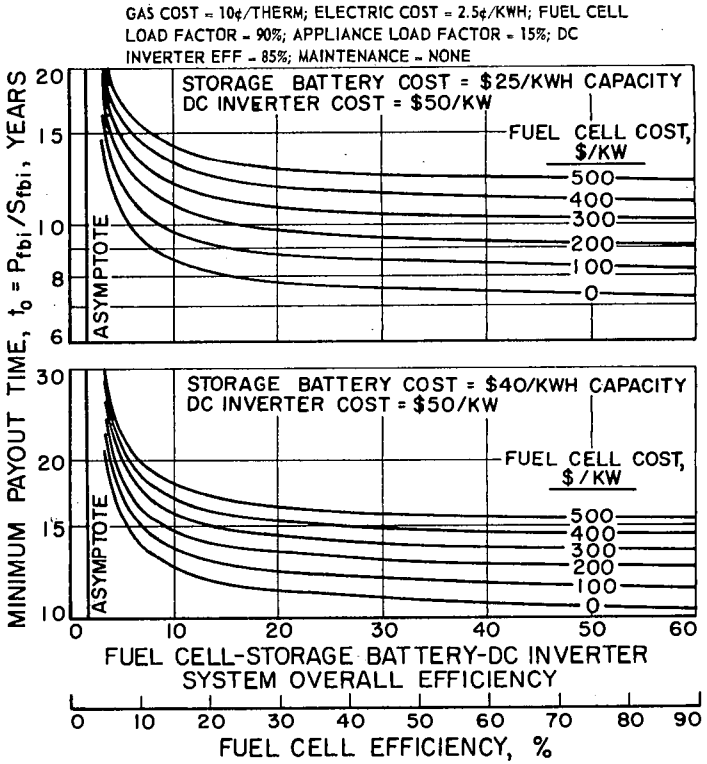

Figure 10. Effect of fuel cell system overall efficiency and fuel cell cost on payout time for fixed gas, electric, storage battery and dc inverter unit costs and with 90% waste heat credit

E_o = $E_r E_f \left[g' + (1 - g')E_b \right] \left[1 - f_i(1 - E_i) \right]$ = overall thermal efficiency of fuel cell system.

C_e = unit cost of purchased electricity prior to fuel cell installation, ¢/KWH.

C_e' = unit cost of portion of electric energy not supplied by the fuel cell, ¢/KWH.

C_g = gas cost, ¢/therm

f = fraction of total yearly electric load supplied by fuel cell.

f_w = fraction of fuel cell waste heat which is utilized in other appliances and credited to fuel cell at fuel value.

f_i = fraction of dc power inverted to ac.

D = fraction discharge of storage batteries; i.e., 1.0 = full discharge during cycle.

V_b = storage battery voltage.

m_f = variable maintenance cost of fuel cell, ¢/KWH output.

M_f = fixed maintenance cost of fuel cell, $/year per KW installed capacity.

m_b = variable maintenance cost of storage battery, ¢/KWH delivered through battery.

M_b = fixed maintenance cost of storage battery, ¢/year per kiloamp-hr installed capacity.

24 = factor which arises because a 24-hr discharge-charge cycle of the storage batteries is assumed.

The payout time in the above relation is the minimum time because interest on the invested capital is not included. If intereat at j% is considered, the corrected payout time, t, increases in accordance with the following expression based on differential compounding:

$$t = - \left[\frac{100}{j} \right] \ln (1.0 - jt_o/100) \tag{18}$$

Equation 17 contains about all of the tangible parameters that can be written into the fuel cell system. This relationship is quite flexible since it permits calculation of any combination such as fuel cell with inverter alone without waste heat recovery or fuel cell-storage battery without inverter by assigning zero values to the appropriate parameters.

In deriving Equation 17, certain intermediate results are of interest. The ratio of total investment of the fuel cell-storage battery system P_{fb} to total investment of the fuel cell alone P_f is given by:

$$\frac{P_{fb}}{P_f} = \left[\frac{g'}{g_1 + g_2 E_b} \right] \left[1 + \frac{24 g_2 I_b}{D V_b I_f} \right] \tag{19}$$

In most cases at low applicance load factors and fuel cell investments of $300/KW or higher, this ratio is less than unity, depending, of course, upon the other parameters. The total principal invested in the fuel cell-storage battery-dc inverter system may be written in the form:

$$P_{fbi} = C_f I_f + C_b I_b + C_i I_i \tag{20}$$

where C_f, C_i = capacity of fuel cell power pack and inverter, respectively, KW

C_b = capacity of storage batteries, kiloamp-hr at system voltage

If L denotes the yearly electric load, KWH, then in terms of parameters already defined:

$$C_f = \frac{Lf \left[1 + f_i(1 - E_i)/E_i \right]}{8760 E_r (g_1 + g_2 E_b)} \tag{21}$$

$$C_b = \frac{Lf\left[1 + f_i(1 - E_i)/E_i\right]}{365DV_bE_r(E_b + g_1/g_2)} \qquad (22)$$

$$C_i = \frac{Lf\, f_i}{8760g_i} \qquad (23)$$

Without storage batteris and inverter, the fuel cell capacity increases to:

$$C_f = \frac{Lf}{8760E_r g'}$$

As an example, if L = 5000 KWH, f = 1.0, f_i = 1.0, D = 0.80, V_b = 120, E_r = 0.95, E_b = 0.80, E_i = 0.85, g' = 0.15, g_1 = 0.15, g_2 = 0.90 - 0.15 or 0.75, then C_b = 0.177 kiloamp-hr at 120 volts for a 15% applicance load factor. This is equivalent to a total electrical storage of 21 KWH. In comparison, the storage capacity of a 6 or 12-volt good grade automobile battery is about 0.75 - 0.85 KWH. This gives an indication of the bulk volume since 21 KWH is equal to about 26 automobile batteries. In this same example C_f = 0.94 KW with storage batteries or 4.0 KW without storage batteries and inverter, indicating a greater than four-fold reduction in power pack capacity by virtue of electrical storage.

Computed minimum payout times for the fuel cell-storage battery-dc inverter system are shown in Figs. 6 to 11 for various assumptions of the cost and operating parameters as indicated in the captions. Certain of these assumptions are admittedly optimistic, particularly 80% electrical efficiency of storage batteries discharged to a depth of 80% and $50/KW for dc inverters. If the battery discharge depth were limited to 60% with electrical efficiency less than 80%, the payout times would increase significantly. In general, if waste heat were not recovered, the payout times would increase by 25 to 35% over the results shown here. If a dc inverter were not used, the payout times would be reduced by 30 to 40% of the values shown.

With storage batteries at a minimum cost of $25/KWH storage capacity and no fuel cell or battery maintenance, we have a minimum payout time of 10 years if purchased power costs 2.5¢/KWH and fuel cell investment cost is $300/KW (Figure 6). This payout time increases to 12 years with the fuel cell maintenance cost assumed in Fig. 7. With higher priced storage batteries, $40/KWH, (Figs. 8 and 9) and electricity at 2.5¢/KWH, a minimum payout time of 10 years cannot be achieved no matter what the fuel cell investment cost.

Figures 10 and 11 explore the effects of overall system efficiency on the payout times for a fixed purchased power cost of 2.5¢/KWH. As is evident, the payout time decreases sharply at system overall efficiencies up to 20%. The slope of the curves becomes nearly horizontal at higher efficiencies, indicating that, with waste heat recovery, the effect of efficiency in going from a fuel cell efficiency of 30% to 60% is not of great significance, except insofar as this determines the amount of waste heat available. At fuel cell efficiencies much below 20%, the quantity of waste heat becomes excessive.

CONCLUSIONS

Relationships have been presented which enable one to judge the conditions under which fuel cells would be economically attractive in a domestic application. With certain experimentally evaluated constants, these relations were applied to the high-temperature molten carbonate cell to arrive at estimates of capital and operating costs. It appeared that these could be sufficiently low that the saving against purchased power should eventually pay out the investment. In a more general manner, the payout time was set up in relation with unit investment costs and operating parameters of fuel cell, storage batteries and inverter. With representative assumptions, a payout time of 10 years for the system is attainable only under the best conditions.

GAS COST = 10¢/THERM; ELECTRIC COST = 2.5¢/KWH; FUEL CELL LOAD FACTOR = 90%; APPLIANCE LOAD FACTOR = 15%; DC INVERTER EFF = 85%;

FUEL CELL MAINTENANCE $\begin{cases} M_f = \$10/KW \text{ PER YEAR} \\ m_f = 0.1¢/KWH \end{cases}$

STORAGE BATTERY AND INVERTER MAINTENANCE = NONE

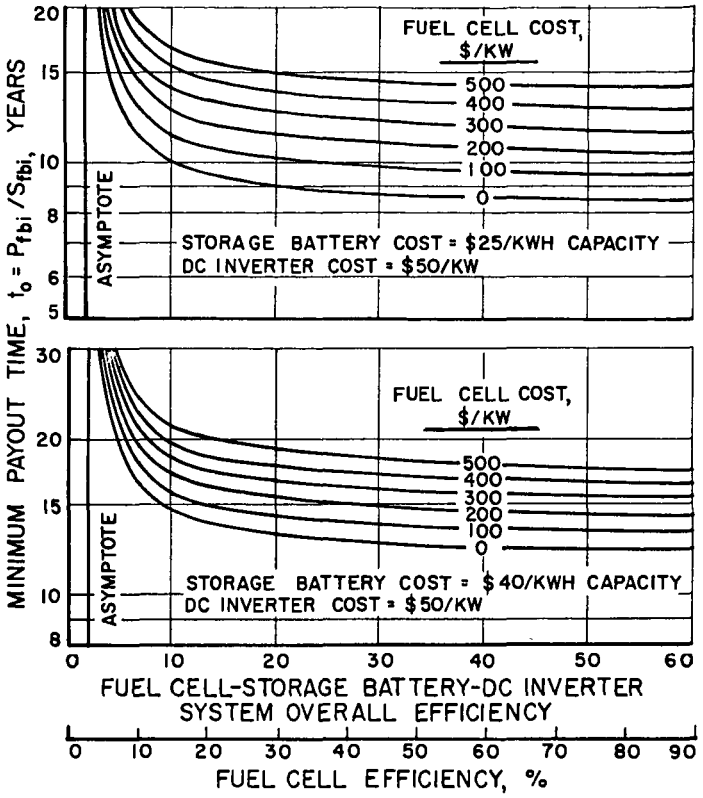

Figure 11. Effect of fuel cell system overall efficiency, fuel cell cost and assumed fuel cell maintenance, on payout time for fixed gas, electric, storage battery and dc inverter unit costs, and with 90% waste heat credit

LITERATURE CITED

(1) Austin, L. G., "Electrode Kinetics of Low-Temperature Hydrogen-Oxygen Fuel Cells", in Young, C. J., ed, "Fuel Cells", 34-50. New York: Reinhold 1960; condensed as "Electrode Kinetics", in Ind. Eng. Chem. 52, 300-01 (1960) April.

(2) Shultz, E. B., Jr., Vorres, K. S., Marianowski, L. G., and Linden, H. R., "High-Temperature Methane Fuel Cells", Paper to be presented at ACS Meeting, Sept. 3-8, 1961, Chicago, Ill.

(3) "Silicon-Controlled Rectifiers Get Ready for Industry", Power 105, 83 (1961) May.

SYMPOSIUM ON FUEL CELLS
PRESENTED BEFORE THE DIVISION OF PETROLEUM CHEMISTRY
AMERICAN CHEMICAL SOCIETY
CHICAGO MEETING, September 3-8, 1961

THE PRELIMINARY APPRAISAL OF THE AMMONIA FUEL CELL SYSTEM

By

R. A. Wynveen
Research Division, Allis-Chalmers Manufacturing Company
Milwaukee 1, Wisconsin

INTRODUCTION

During the past five to ten years there has been a decided increase in fuel cell research. The result has been the development of several prototype fuel cell systems which fall into two types. In one type, hydrogen-oxygen for example, both the fuel and oxidant are gases. The second type uses a liquid fuel and gaseous oxidant and can be exemplified by the methanol-oxygen system.

The oxidant most generally employed has been pure oxygen or air. The fuel, however, has been picked from a wide range of compounds and prototypes have been operated on such gaseous fuels as hydrogen, carbon monoxide, and hydrocarbons. The liuqid fuels most commonly used have been partially oxygenated hydrocarbons, such as alcohols or aldehydes, and special fuels, such as sodium amalgam.

In this preliminary report attention has been centered upon ammonia as a fuel with minor emphasis on the complete ammonia-oxygen system. The material presented covers two areas. First, a discussion of ammonia and some of its characteristics, and second, a report of some of the typical data obtained on several preliminary, but very impractical, ammonia-oxygen fuel cells.

APPLICATION METHODS

Several methods are available for employing ammonia as a fuel for fuel cell consumption. They are:

1. Decomposition of ammonia into its elements and (a) separate the pure hydrogen, or (b) use the nitrogen-hydrogen mixture directly.
2. Direct consumption of ammonia: (a) as a gas, or (b) dissolved in the electrolyte.

Simple equipment has been designed for cracking ammonia. This reversts it to the 75-25 mixture of hydrogen and nitrogen, respectively. This represents a convenient way of securing supplies of hydrogen, one cylinder of ammonia being the equivalent of nine or ten cylinders of hydrogen. Pure hydrogen generating units have been reported (1) which yield hydrogen of 99.995 per cent purity, the nitrogen being removed by liquification. The cost is quoted at less than pure cylinder gas and no more than the "impure" electrolytic grade.

The scope of this report will be limited to the study of the direct use of ammonia as a fuel since cracked ammonia is essentially a hydrogen-oxygen fuel cell and both the cracking and the hydrogen-oxygen fuel cell have already been developed.

When one uses ammonia as an anodic reactant in electrochemical system, two properties should be kept in mind. The first is that the nitrogen-hydrogen bond energy of 118 kcal/mole in the ammonia molecule indicates stability and that the bonds are not readily broken in electrochemical oxidation. Thus, one can anticipate that at room temperature, difficulty will be experienced in the cleavage of the nitrogen-hydrogen bond. As will be shown later, in this report this was found to be the case even under open circuit conditions.

The second important property is the high solubility of ammonia in all conventional electrolyte solutions, both aqueous and non-aqueous. This means that ammonia can readily be supplied to the electrode-solution interface, at the anode, through either the gas or the solution phases. This high solubility, however, has the disadvantage that

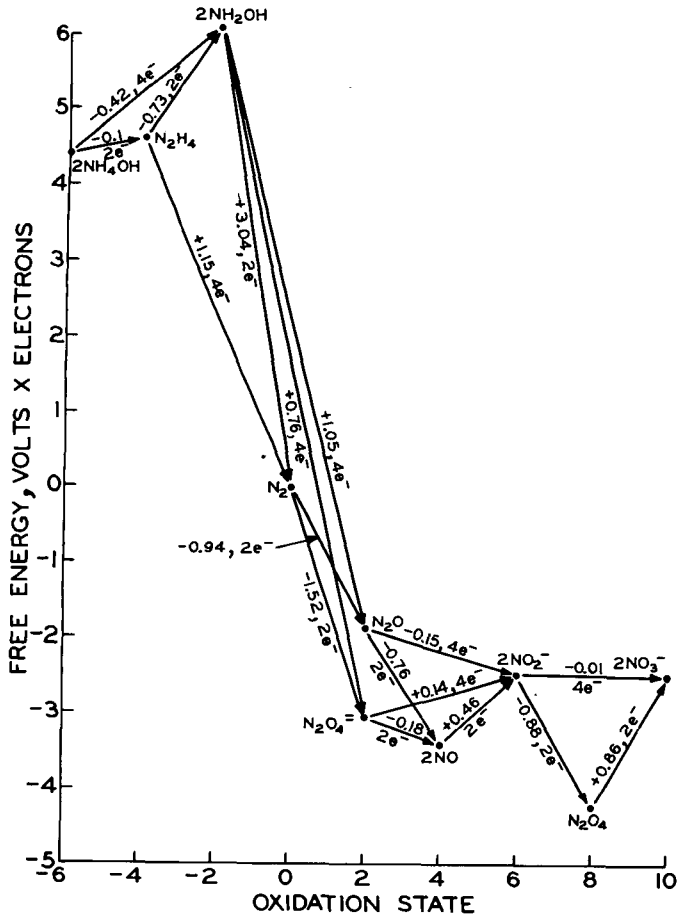

Figure 1. Free Energy of the Nitrogen System In Alkaline Solution at 25° C.

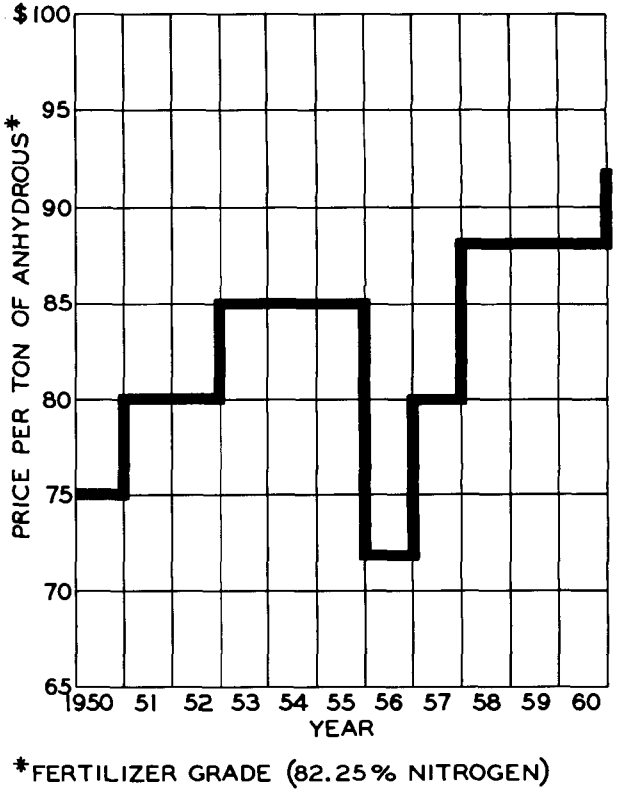

Figure 2. Cost of Anhydrous Ammonia for the Period 1950-1960.

ammonia transport from the anode, through the solution phase, to the cathode is not negligible unless proper operating precautions are taken. High pressure operation will further increase the solubility of ammonia in the electrolyte solution. Thus, ammonia can be introduced through the rear of a porous electrode resulting in a gas-gas fuel cell or through the solution phase giving a "liquid"-gas fuel cell, similar to the methanol-oxygen cell mentioned earlier.

The discussion and experimental results to follow are limited to the use of gaseous ammonia as the fuel.

THERMODYNAMICS AND ELECTRODE REACTIONS

In order to understand the ammonia fuel cell, it is important to establish what chemical reactions are occurring during discharge of the cell. The reactions occurring at the cathode, when using an alkaline electrolyte and oxygen as the oxidant, have been characterized and reported by others. (2-4)

In figure 1 are plotted the free energies and potential relationships for the various oxidation states associated with nitrogen in an alkaline solution at 25°C. These results were tabulated from data reported by Latimer. (5) One can obtain the standard free energy change, ΔF°_{298}, for a half-reaction by multiplying the corresponding values by the Faraday constant, 23.06 kcal/volt/gm. equivalent. Also included are the values of the standard oxidation potentials, E°_{298}, and the number of electrons released for the reactions indicated in the direction of the arrows.

The anode reaction was characterized by first analyzing for the reaction products. As will be pointed out later, the principle products were found to be nitrogen and water. Assuming the half-cell reaction

$$NH_3(g) + 3OH^-(aq) = 1/2\ N_2(g) + 3H_2O(liq) + 3e \qquad (1)$$

a value of 0.77 volts can be calculated for E°_{298}, using the expression relating potential values to free energies,

$$\Delta F^{\circ}_{298} = -nFE^{\circ}_{298} \qquad (2)$$

where the symbols mean,

ΔF°_{298} - change in the standard free energy at 25°C. with all reacting substances at unit activity.
n - number of electrons in the reaction.
F - Faraday's constant, 23.06 kcal/volt/gm. equivalent.
E°_{298} - standard oxidation potential at 25°C.

The American sign convention has been used, i.e., the electrons are on the right-hand side of the equation and therefore a positive value for E°_{298} means that the reduced form of the couple is a better reducing agent than hydrogen. All the potentials are referred to the standard hydrogen electrode.

Coupled with the anodic reaction is an oxygen electrode process. Assuming a very active peroxide decomposing catalyst on the cathode surface greatly simplifies the cathodic process and the two electron process changes to an apparent four electron mechanism. Thus for the half reaction

$$O_2 + 2H_2O + 4e = 4OH^- \qquad (3)$$

the value of E°_{298} is 0.40 volts. Coupling the two half reactions, equation (1) and (3), one obtains for the overall fuel cell reaction

$$4NH_3(g) + 3\ O_2(g) = 2N_2(g) + 6H_2O\ (liq) \qquad (4)$$

and an E°_{298} value of 1.17 volts. As will be apparent later, the actual conditions employed during operation of the ammonia-oxygen cell varied considerably from the standard conditions assumed. Therefore, this value, although accurate for the conditions assumed in its calculation, represents only a first approximation of the theoretical value for the experimental conditions employed. Since the open circuit potential of the fuel cell is related to the change in the thermodynamic functions of free energy, enthalpy and entropy, the calculated effect of temperature and pressure changes could, in principle, be obtained through standard thermodynamic calculations. However, care must be exercised in making these calculations due to such typical factors as:

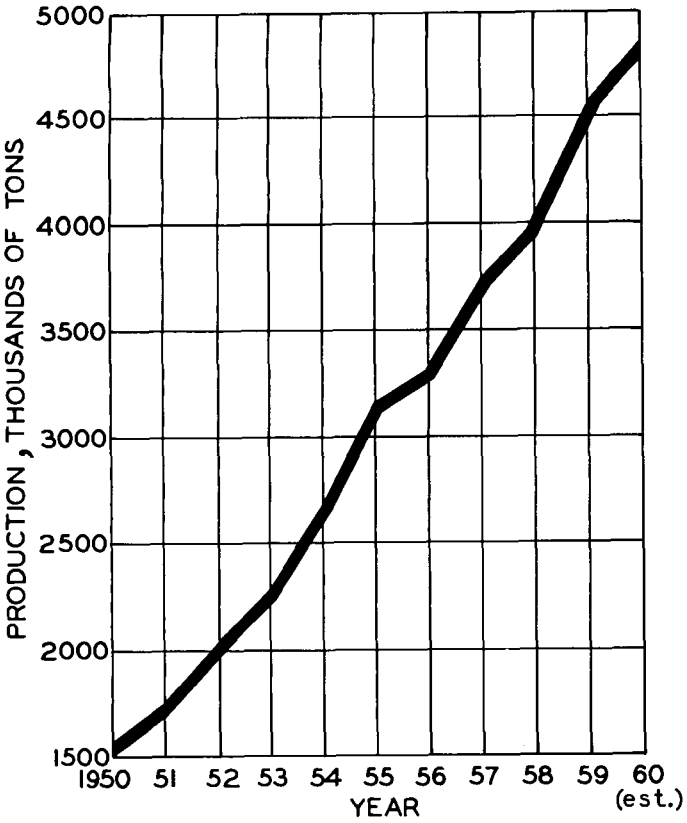

Figure 3. Volume Output of Anhydrous Ammonia for the Period 1950-1960.

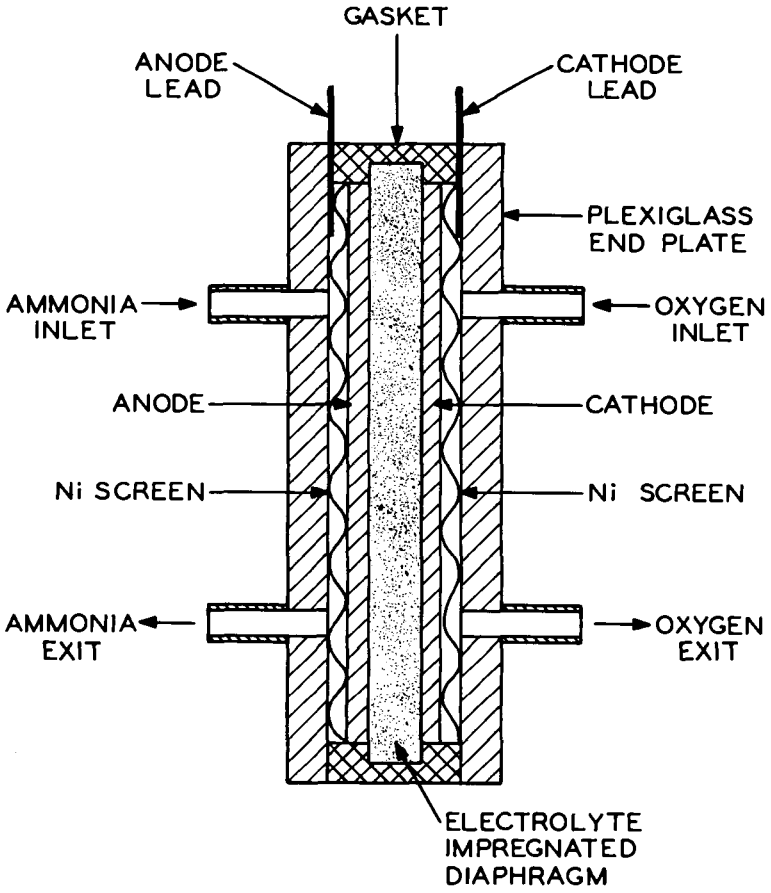

Figure 4. Cross Sectional Diagram of the Experimental Ammonia-Oxygen Fuel Cell.

1. Practical cells are operated in a highly alkaline solution and therefore the activities of the hydroxyl ion and water are not unity.

2. Although activity coefficients can be employed, they should be for individual ionic species, but experimentally only mean activity coefficients can be determined.

3. Several electrons are involved in the electrochemical steps and therefore, mixed electrode potentials might be obtained experimentally which would be difficult to compensate for in the calculations.

CRITERIA

Many criteria have been proposed for evaluating fuel cells and the fuels used in them. To date little can be said concerning how the ammonia-oxygen fuel cells meets these general criteria such as ultimate current density, cell efficiency, power per unit weight or volume, etc. These factors can only be appraised after sufficient scaling-up has been done and an engineering investigation and feasibility study has been made. Nevertheless, from a preliminary appraisal, the ammonia-oxygen fuel cell has many advantages which center around the use of ammonia as the fuel.

Ammonia is economical. The present cost is 4.6 cents per pound, based upon ton quantities. (5) It is produced from readily available raw materials and has a wide increasing range of applications. This serves to guarantee the stability of its market. As figure 2 points out, the cost of anhydrous ammonia only varied over a very narrow range during the period from 1950 to 1960. It should be remembered, however, that as the quantity required decreases, the cost increases rapidly. This is exemplified in Table I where, in addition to various size and weight factors, the cost of ammonia is listed as a function of volume or quantity purchased. It is also obvious that as the required purity of the ammonia increases so does the cost.

TABLE I
GROSS SIZE, WEIGHT AND COST OF ANHYDROUS AMMONIA
AS A FUNCTION OF AMOUNT DESIRED

Cylinder Dimensions,(1) Inches	Gross Weight, lbs.	Ammonia Content, lbs.	Cost	
			Cents per lb.(2)	Cents per Mole(2)
Ton Quantities (Carload Lots)			4.6(3)	
14 x 59	340	150	20	0.8
8 x 53	112	40	25	0.9
8 x 25	52	15	52	2.0
5 x 24	28	5	87	3.3
4 x 14	17	2	165	6.2
2 x 15	4	0.4	400	15.0

(1) Diameter x height.
(2) 99.99 percent purity.
(3) Fertilizer grade.

Ammonia production is already a large tonnage item. From the data presented in figure 3, it can be seen that the output has tripled since 1950. Presently, this rise in production stems from the increased use of ammonia as a fertilizer. (6) This leads one to conclude that in view of the large quantity of ammonia produced one can assume that in the future the price of ammonia should remain relatively constant regardless of any demand caused by fuel cells.

Ammonia is a gas which can readily be liquified. Thus high pressure tanks are not required for its storage. In spite of this, however, the storage facilities needed to stock ammonia is a large cost factor. It has been reported (5) that amortization costs

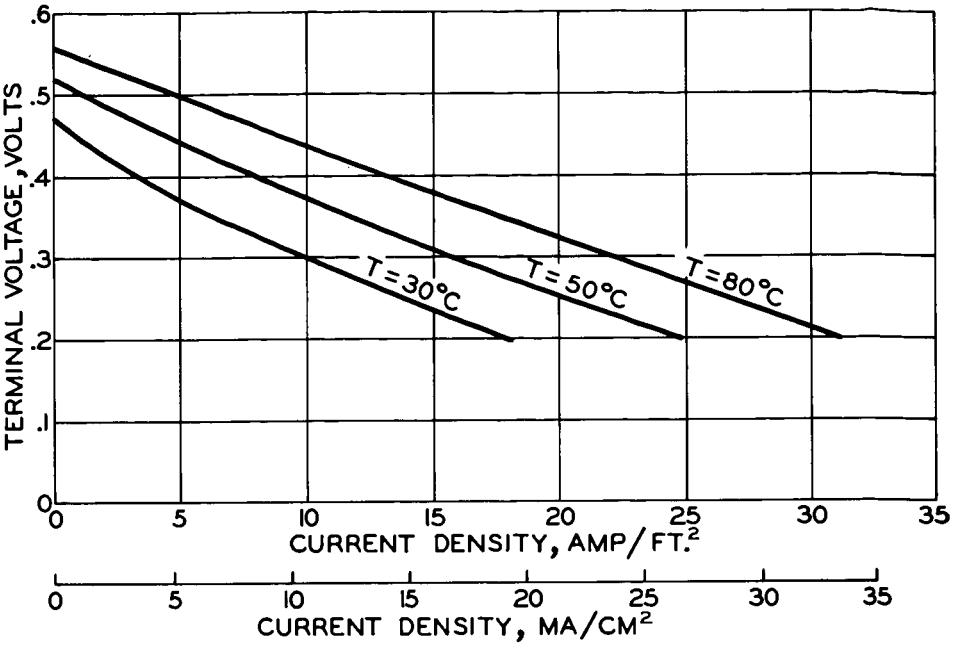

Figure 5. Typical Performance Curves Obtained for the Ammonia-Oxygen Fuel Cell at 30, 50 and 80° C., Atmospheric Pressure and Flowrates of Three Times That Needed to Maintain Reaction.

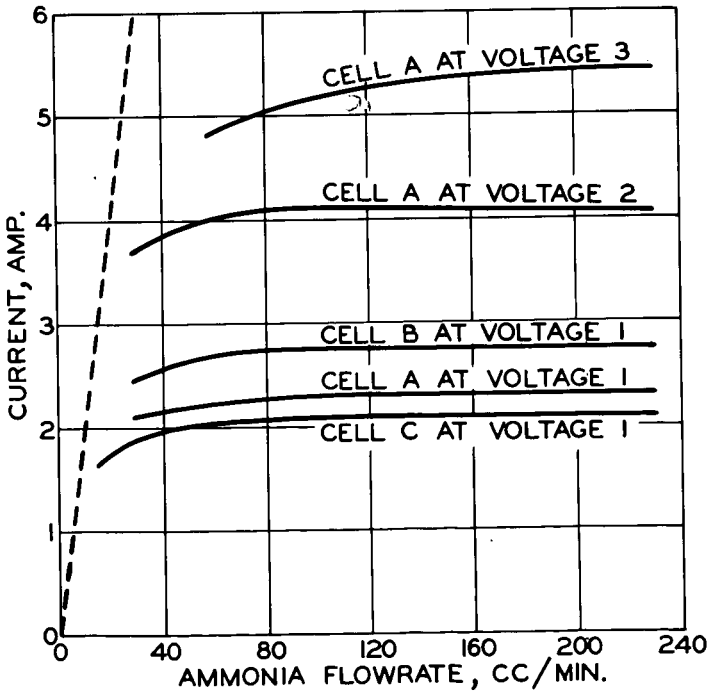

Figure 6. Cell Current As a Function of Ammonia Flow Rate (Atmospheric Pressure, Constant Oxygen Flow Rate, 25° C).

for anhydrous ammonia storage facilities run between 15 to 20 dollars per ton a year. A Horton sphere, of 2500 ton capacity, costs about $275,000. A new technique for storing refrigerated ammonia at atmospheric pressure, rather than in pressurized tanks, has been reported (7) to cut the storage cost in half. The low storage temperature is obtained by surface evaporation of the ammonia. The vapor is recompressed and circulated back into the storage unit.

Ammonia can be handled easily on a wide-scale. The practicality of wise-scale usage of ammonia might be questioned from a safety standpoint. The limits of inflammability, as reported by Lewis and von Elbe (8), are found in Table II. Such mixtures can be ignited by a spark and would explode if confined to a closed space. Higher temperatures increase the danger of combustion or explosion. The dangers that exist, however, are less than those found with hydrogen.

TABLE II
LIMITS OF INFLAMMABILITY OF AMMONIA IN AIR AND OXYGEN
AT ROOM TEMPERATURE AND ATMOSPHERIC PRESSURE

	Percentage-by-Volume Basis	
	Lower	Upper
Air	15.50	27.00
Oxygen	13.50	79.0

Ammonia is toxic, but its pungent odor provides amply warning of its presence. It can be detected in air at concentrations as low as 20 parts per million by volume. In air concentrations of 200 p.p.m. are dangerous and may prove lethal. (9) The American Conference of Governmental Industrial Hygienists has recommended that the maximum allowable concentration for an eight hour daily exposure should be 100 p.p.m. (10) Ammonia solutions produce caustic burns on the skin, a 3 per cent concentration being the maximum that can be tolerated for more than a few seconds.

In conclusion, ammonia is an economical gas which can readily be condensed. It is produced from nonstrategic elements in large volume. Although it is inflammable and toxic, its characteristic odor serves as a warning of its presence.

EXPERIMENTAL

The construction of a laboratory type ammonia-oxygen fuel cell is illustrated diagrammatically in figure 4. The design was chosen as one of convenience in testing various fuel cell components.

Fuel and oxidant were supplied to the cell in such a manner as to permit the gas flow to be controlled. The gas-diffusion electrodes were made of a commercially available porous carbon. Only a preliminary effort was made to use electrodes of controlled pore size distribution. The electrode porosity was 48 per cent. A wire screen was used to manifold the gas and to improve the contact between the electrode and the external circuit. The two electrodes had the same geometric area and were spaced about 0.2 cm. apart. The untreated carbon electrodes were not able to activate the ammonia and for this reason a catalyst was deposited onto the electrode. It was found experimentally that platinum black was suitable, to a limited extent, and was the catalyst employed in this preliminary study. Platinum black also served as the catalyst at the oxygen electrode.

The ammonia and oxygen diffused through the carbon electrodes to the electrolyte interface where electrochemical reaction occurred. The electrolyte employed was a very concentrated potassium hydroxide solution which helped to prevent the transport of fuel to the cathode. In order to minimize flooding of the porous electrodes the electrolyte was held in a porous diaphragm and the electrodes pressed into the surface of the diaphragm.

Performance Characteristics

Figure 5 shows typical voltage-amperage curves for the ammonia-oxygen fuel cell operating at temperatures of 30, 50 and 80°C. The ammonia flow rate was three times that required to sustain the reaction. Because of the exploratory nature of these experiments the commutator technique (11) was not used in making the measurements.

It can be seen that the higher temperatures yield the expected higher outputs. However, the increase in open circuit voltage cannot be accounted for by the theoretical effect of temperature on the cell e. m. f. A more probable reason is a decrease in ammonia transport from the anode to the cathode with the increase in temperature. Open circuit voltages of 0. 70 volts have been reported (12) when platinum and silver oxide catalysts were employed at the ammonia and oxygen electrodes, respectively.

Due to the observed variation of cell output with temperature, it was essential to control the cell temperature. This was accomplished with an air thermostat which held the working temperature constant to $\pm$ 0. 5°C. The use of an air thermostat was chosen because of the ease with which the cells could be manipulated. However, a longer time was required to bring the cells to the proper operating temperature. The cell and thermostat temperatures were continuously recorded through separate, suitably positioned, thermocouples. Once the cell attained the operating temperature, there was very little temperature fluctuation.

In addition to careful control of the cell temperature, it is essential that close attention be given to the gas flow rate employed. Figures 6 and 7 serve to illustrate this point. The cells used for these experiments were all identically constructed according to the procedure described previously. The individual cells were designated as A, B. . . . G, to indicate that seven separate cells were used. An important point to note is that for each curve the cell voltage was held constant. The actual value of this voltage is not essential in illustrating the effect of flow rate on cell output, but does serve to indicate the type of reproducibility obtained (see cells A, B, and C at voltage 1).

Cells A, B, and C were all operated at voltage 1 (actually, 0. 39 volt). In addition, cell A was operated at two other power levels, voltage 2 and 3 (0. 31 and 0. 25 volt, respectively). At the lower current levels it can be seen that the current remains essentially constant until the slower flow rates are approached when the current begins to drop relatively rapidly. The drop off occurs more readily when higher current levels are being maintained, e. g., cell A, voltage 3.

In figure 7 the current outputs of the four remaining cells are given at the lower flow rates, approaching those required to sustain the output. In this case the effect of flow rates on current delivered is very pronounced.

An exact analysis of this effect was not attempted because of its complex nature and the preliminary nature of this investigation. As long as the current remains independent of flow rate, the fuel cell is being limited by some other process than the ammonia flow rate. As the flow rate is decreased a point is reached when the current becomes dependent upon ammonia flow rate or some factor which is a function of the flow rate.

The dashed curves in figures 6 and 7 represent the ammonia flow rate required to just supply the electrode with sufficient fuel to maintain the current being delivered. For cells B, A and C a flow rate of 220 cc/min. represents a flow rate of about 16, 18 and 20 times that required, respectively. In the case of cell A at voltages of 2 and 3, a 220 cc/min. flow rate is 10 to 8 times that required, respectively. The increase in flow rate means an increase in ammonia concentration at the three phase reaction zone. A physical picture of the effect is very complicated since the result depends not only upon an electrochemical reaction, a three phase reaction zone which extends into the solution phase because of the solubility of the ammonia in the electrolyte and an electrode pore network, but also the geometrical shape of the fuel compartment adjacent to the electrode.

The important point stressed here is not the apparent explanation of the observed effect, rather that the consistency and correlation of fuel cell results is strongly tied in with environmental controls. This was further illustrated during a study of the importance of the nitrogen build-up, as reaction proceeds, on the operation of an ammonia fuel cell. A series of runs were carried out to determine the magnitude of this effect. The cell current was followed as a function of the percentage-by-volume of ammonia in a fuel mixture of ammonia and nitrogen. This problem is similar to that found in the use of air instead of pure oxygen. From the results obtained it was observed that the effect of nitrogen content was irregular unless the flow rate was also held constant. For example, figure 8 illustrates the results obtained as the ammonia percentage in the fuel stream was decreased when the total flow through the cell was held constant at 230 cc/min. From these results it can be concluded that the effect of nitrogen build-up is slight until over 50 percent of the fuel gas stream was nitrogen. As expected, the

effect of nitrogen percentage being more pronounced when heavier currents were being drawn. It was also observed that if a lower constant flow rate (less than 230 cc/min.) was used the current fall off appeared at greater ammonia percentages (i.e., with a lower percentage of nitrogen present). This serves to illustrate that the effect of the decreased partial pressure of ammonia is also a function of total flow rate.

One of the initial measurements made on the fuel cell unit was a qualitative determination of the chemical reaction occurring at the anode. This work is still in progress and a more complete quantitative stoichiometric balance will be published later. A sample of ammonia was passed back and forth through the anode compartment of a cell operating at 80°C. With the circuit closed, the current flowing was recorded as a function of time. After observing a total of 14,000 to 20,000 coulombs; the fuel gas was collected and analyzed with a gas chromatograph. The components found were ammonia, nitrogen, and water vapor. No hydrogen was detected. A calculation of the number of coulombs was then obtained from the nitrogen volume observed and the assumption that a three electron process, reaction (1), was occurring. This value was then correlated with the coulombs obtained by integrating the area under the current-time curve. The results of this correlation varied over a range of 0.2 to 5 per cent. This corresponds to a current efficiency of 99.8 to 95 per cent, where the current efficiency, η_i, is defined as

$$\eta_i = \frac{\text{Observed Current} \times 100}{\text{Calculated Current}} \qquad (6)$$

Although the experimental accuracy of these initial coulometric measurements was not as high as desired, they do serve to indicate that the major reaction is that represented by equation (1).

Of the many causes for the low voltages observed, two are of major importance. One being the inherent irreversibility of the oxidation resulting from the transfer of three electrons and the large bond energy associated with the molecule and two, the inadequacy of the catalyst to enhance the reaction rate and minimize the free energy losses.

At the present time an appraisal of the attainable power density, start-up time, attendant corrosion problems, necessary auxiliary equipment, construction materials, side reactions, and reliability have not been made. The low temperature and low pressure operation, however, is characteristic of rapid start-up, less rapid corrosion problems, minimum in auxiliary equipment and cheaper construction materials. The side reactions will be the subject of later studies. Experimental ammonia-oxygen units have not been in service for any long periods of time. It is, therefore, impossible to make any statement concerning the stability or reliability of the system.

SUMMARY

Attention has been centered on ammonia as a fuel with minor emphasis on the ammonia-oxygen system. Of the many ways in which ammonia can be used as a fuel, its application as a gas was studied. The open circuit voltage expected is about 1.1 to 1.2 volts depending upon conditions. The experimentally observed values were about one-half of this.

Criteria used to appraise final fuel cell systems are not applicable to preliminary experimental cells. Ammonia is manufactured from readily available raw materials in large tonnages. Ammonia is low in cost when purchased in large quantities. Although it is inflammable and toxic within certain defined limits, it has an easily detectable odor which warns of its presence. A major advantage in the use of ammonia results from its being an easily condensed gas and hence not difficult to store or transport.

The experimental results were very much dependent upon cell temperature and gas flow rate. The reaction products were found to be nitrogen and water. No attempt was made in the work reported to obtain significant power outputs. Ammonia represents, in many ways, an ideal fuel cell fuel.

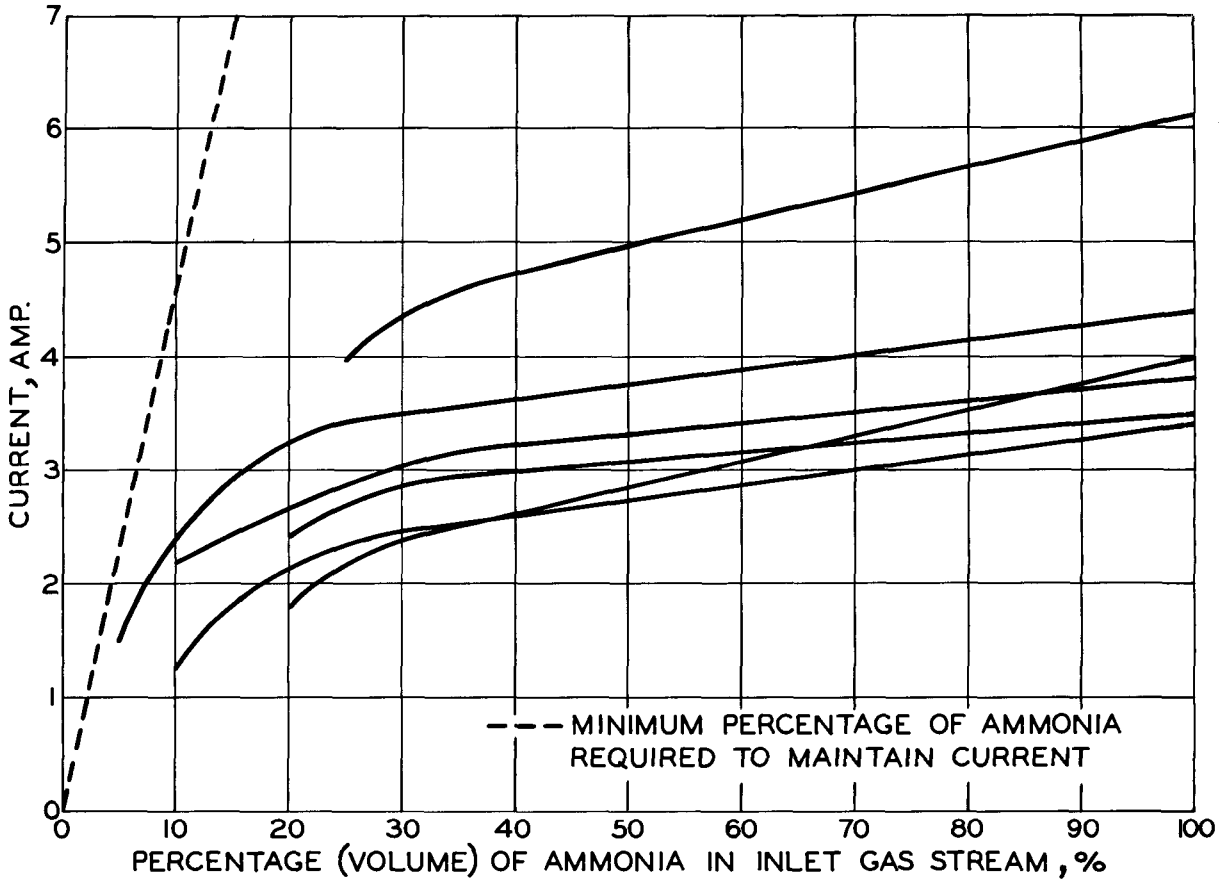

Figure 8. Cell Current as a Function of Ammonia Percentage In An Ammonia-Nitrogen Fuel Mixture (Atmospheric Pressure, Constant Oxygen Flow Rate, Constant Voltage). Flow Rate of Ammonia Plus Nitrogen Held Constant at 230 cc/min.

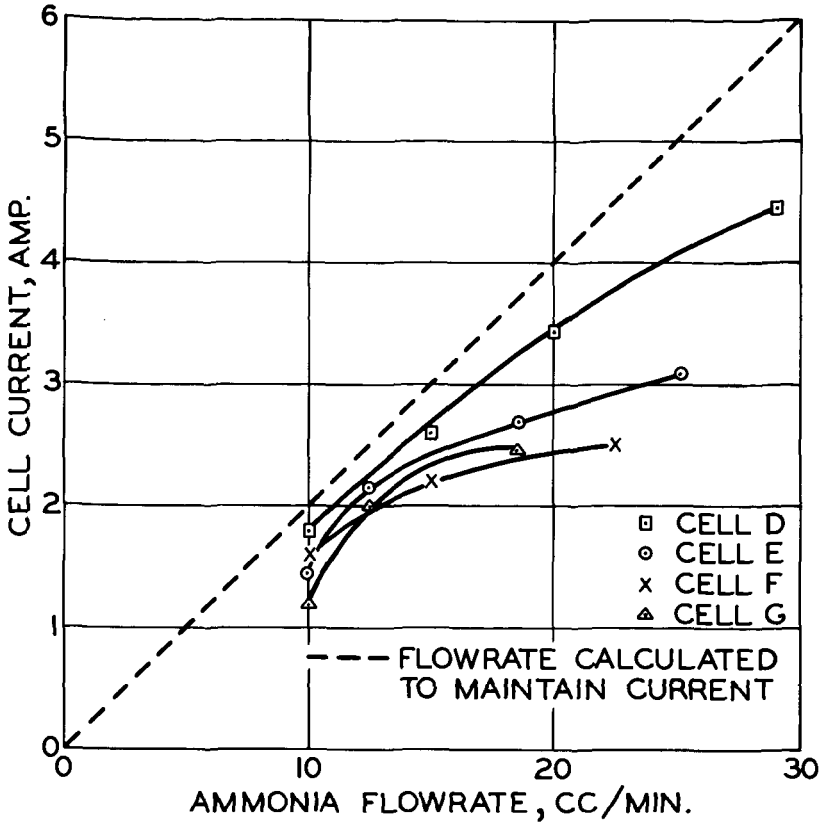

Figure 7. Cell Current As a Function of Ammonia Flow Rate, (Atmospheric Pressure, Constant Oxygen Flow Rate, Constant Voltage, 25° C.)

LITERATURE CITED

(1) U. S. Chemical News, November, 1960.

(2) Berl, W. G., Trans. Far. Soc., 83, 253 (1943).

(3) Witherspoon, R., Urbach, H., Yeager, E., and Hovorka, F., Tech. Report No. 4, Office of Naval Research, Contract Nonr 58100, Western Reserve University (1954).

(4) Davies, M. O., Clark, M., Yeager, E., and Hovorka, F., J. Electrochem. Soc., 106, 56 (1959).

(5) Latimer, W. M., "The Oxidation States of the Elements and Their Potentials in Aqueous Solution", 2nd Edition, Prentice Hall Company, New York, p. 104 (1952).

(6) Chemical and Engineering News, 38, (27), 35, July, (1960).

(7) Chemical and Engineering News, 38, 46, August, (1960).

(8) Lewis, B., and von Elbe, G., "Combustion, Flames, and Explosions Gases", Academic Press, New York, (1951).

(9) Silverman, L., Whittenberger, J. L., and Muller, J., J. Ind. Hyg. Toxicol. 31, 74-8 (1949).

(10) "Anhydrous Ammonia", Compressed Gas Association, Inc., New York, New York, Pamphlet G-2.

(11) Pollnow, G. F., and Kay, R. M., Research Division, Allis-Chalmers Mfg. Company, "A 60 c. p. s. Sine Wave Commutator for Resistance and Potential Measurements", to be published.

(12) Stein, B. R., and Cohn, E. M., Status Report on Fuel Cells (ARO Report No. 2): U. S. Department of Commerce, Office of Technical Services, PB-171-155.

SYMPOSIUM ON FUEL CELLS
PRESENTED BEFORE THE DIVISION OF PETROLEUM CHEMISTRY
AMERICAN CHEMICAL SOCIETY
CHICAGO MEETING, September 3-8, 1961

RADIATION ACTIVATION OF OXYGEN ELECTRODES IN A FUEL CELL

By

K. Schwabe

Experiments by G. Anders and W. Burk
Central Institute for Atomic Physics, Rossendorf, Areas of Radiochemistry,
and the Institute for Electrochemistry and Physical Chemistry of the
Dresden Institute of Technology

INTRODUCTION

Present efforts of increasing the activity and capacity of the oxygen electrode in a fuel cell at low and medium temperatures substantially aim at increasing, as much as possible, the contact zones between the gas, the electrolyte, and the electrode (1); and at accelerating the reduction of oxygen to water by catalytically active electrode material or by suitable additives (2). The present paper represents the first portion of an investigation concerning the activation of electrode processes by ionizing radiation, and deals with the influence of β- and γ-emitters, which are deposited on the electrode, upon the oxygen electrode and its capacity.

It is known that the yield in homogeneous processes, which have been activated by radiation chemistry, is low in respect to the radiation energy absorbed (G values in the order of magnitude of 0.5-5), in the absence of a chain mechanism. A number of investigations have been conducted on the other hand, wherein it was shown that heterogeneous catalytic reactions are accelerated by ionizing radiation. Permanent increases in activation have been achieved particularly by radiation in semiconductor catalysts, although these results are not entirely without contradiction (3). V. I. Spizyn et al (4) were able to find noteworthy activation increases with catalysts, when the catalyst itself is rendered radioactive, evidently because this substantially increases the absorbed dosage of rays, and the catalyst structure is changed.

EXPERIMENTAL PROCEDURE

Our experiments, up to this time, dealt with the addition of β- and γ-emitters to the electrode, which was contacted with 0_2. No clear effect, so far, has been shown by orientation measurements concerning the influence of external X-ray radiation upon the velocity of achieving the oxygen potential and its change during load; so that they shall not be discussed here. The preliminary electrode material was platinum or nickel in the form of sheets, sieves, or cylinders, on which the radioactive elements Ru 106, Ir 192, Tl 204, and Po 210 were precipitated electrolytically. The element was coated with platinum if a risk existed that the element would participate directly in the electrode process, such as in the case of Tl 204 and Po 210. The radiation source was situated in a platinum capsule, when a dense, solid isolation was not possible. The capsule was introduced into the cylindrical electrode of platinum wire mesh. The distance between the radiation source and the electrode was about 0.5 mm, and the interspace was filled with gaseous 0_2 during the measurement. Accordingly, it is not a question here of a direct activation of the electrode, but of radiation (see below). Table 1 shows the radionuclei used so far, showing their half life, decomposition process, energies of the emitted particles and the γ-radiation, as well as the distribution of the radiation energy in question. The Pt-, Ir-, and Au-isotopes were produced by irradiating inactive electrodes in a reactor.

The electrolyte generally was 1 m KOH. The measurements were performed in a cell as shown in Figure 1, and the greatest emphasis was placed upon comparable experimental conditions. A constant current was imparted to the oxygen electrode during capacity measurements, with the aid of an external voltage source of 100 volts and a suitably high resistance. Its potential change as a function of time was measured against a reference saturated calomel electrode.

Table 1

Isotope	Half Life	Type of Decomposition	Particle	% Frequency	Quant. MeV	% Distribution
P-32	14, 3 d	β^- (100%)	1.701	100	-	-
Ru-106	1, 0 a	β^- (100%)	0.0392	100	-	-
Rh-106	30 sec.	β^- (100%)	3.53	68	0.513	11
			3.1	11	0.624	5.8
			2.44	12	0.87	0.3
					1.045	0.9
			2.0	3	1.55	0.3
					2.41	0.1
Ir-192	74, 37 d	β^- (95,5%)	0.675	48	0.201	0.4
		β^- (10^{-4}%)	0.535	41	0.206	3.5
			0.257	7	0.283	0.5
		K (4, 5%)	0.100	< 0.5	0.295	32
					0.308	31
					0.316	89
					0.375	1.7
					0.416	1.4
					0.468	57
					0.485	3.5
					0.588	6.3
					0.604	12.5
					0.613	7.5
					0.885	0.4
Pt-193^m	4, 33 d	K (100%)	-		0.135	
		Isom. (100%)			0.2	
					1.5	
Pt-195^m	3.5 d	K (100%)	-		0.029	
					0.097	
					0.126	
					0.129	
Pt-197	18 h	β^- (100%)	0.670	88.5	0.077	99
			0.479	10.6	0.191	10.6
			0.468	0.9	0.279	0.9
Au-199	3.15 d	β^- (100%)	0.460	4	0.050	3.5
			0.297	73	0.159	77
			0.250	23	0.209	19
Tl-204	4.02 a	($\sim$ 97%)	0.766	$\sim$ 97	0.380	3
	2.50 a	K ($\sim$ 3%)				
Po-210	138.4 d	α (100%)	5.298	100	0.803	10^{-3}
			4.511	$\sim 10^{-3}$		

RESULTS

Only orientation tests have been performed with the radiation sources of Table 1 at this time. Accordingly, this report will deal only with the results achieved with Tl 204 and with Ru 106, especially since these two radiation nuclei probably deserve the most practical interest, owing to their relatively great half life.

It was examined first whether the radiation source has an influence upon the velocity, with which a stationary oxygen potential is established. Figure 2 represents the potential time curve of 5 platinized platinum electrodes, which were contacted with oxygen. It can be seen that the electrodes behave differently, but that a stationary end value is achieved after about 20 minutes. This end value is 200-250 mV below the reversible value. Figure 3 shows the potential time curves for 4 electrodes, which are completely identical with those in Figure 2, after about 3 mC Tl 204/cm^2 had been deposited upon them, and they had been coated again with Pt. These electrodes show a more uniform behavior, establish a stationary value in about 10 minutes, and this value is only about 150-180 mV below the reversible oxygen potential. Figure 4 shows the potential course of these electrodes with an increase in load; the dotted line represents the average course of the electrodes, which were activated with Tl 204, while the full curve shows the average course of the platinized platinum electrodes. It can be seen clearly that the radiation of Tl 204 produces a higher stability of the stationary potential during load, in spite of considerable dispersion. These results were checked by measurements at constant current and the potential course was monitored. Figures 5 and 6 show that the electrodes, which have not been activated, show a more irregular behavior and a faster potential drop (Figure 5) than the activated electrodes (Figure 6), where the potential course is uniform, corresponding to the load and, particularly at 3 ma/cm^2, is much less.

Constant current measurements likewise were performed for Pt electrodes, on which various quantities of Ru 106 had been deposited, and which then again had been platinized. These measurements are represented in Figure 7. The curves designated as No. 1 relate to inactive electrodes, while those designated as No. 2 relate to electrodes, which were activated with 110 mC Ru 106/cm^2. Although activity per cm^2 is substantially greater than the Tl 204, the effect regarding the stabilization of the potential during load is not so clear. Measurements with electrodes, which contained 28 mC/cm^2 of Ru 106, showed approximately the same behavior.

In additional experiments, 45 mC of Ru 106 were placed in a capsule, which was separate from the electrodes, so that it was possible to investigate the same electrode with and without the β-radiation effect of Ru 106. Figure 8 shows that the potential drop of the irradiated electrode during load is not quite so steep as without irradiation, but the difference is slight and requires checking under constant current conditions. The orientation measurements with electrodes, which contained other radionuclei, showed substantially the same differences in comparison with inactive electrodes.

DISCUSSION

Present measurements show that the action of ionizing radiation upon the oxygen electrode accelerates the approach to the stationary potential and the potential value reached is closer to the reversible potential, if the radiation source is situated on the electrode itself. Accordingly, a lower potential drop also occurs during load. It can be assumed, therefore, that the radiation effect accelerates the reduction of 0_2 to H_20_2 or H_20 at the electrode surface. No definite statements can be made now concerning the mechanism of this effect, but it definitely is not probable that the β- or γ-energy influences directly the activation process. Rather, it must be assumed that it increases the activity of the electrode surface and thereby facilitates the reduction process. The present results show that Tl 204 has a greater effect than Ru 106 at a lower level of radioactivity per cm^2; this can be because of its greater β-energy. This, however, requires a thorough investigation, as our measurements in general represent only a beginning. Present tests concern particularly an investigation of the activation of coals by radionuclei.

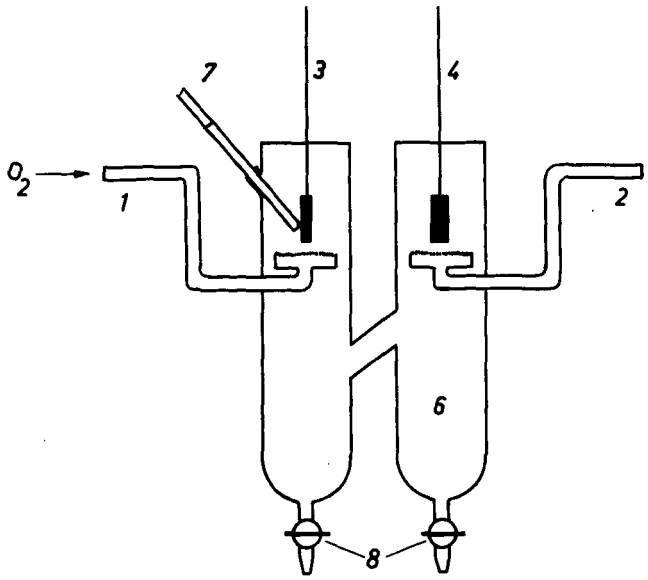

FIGURE 1

1. O_2-Einleitung
2. H_2-Einleitung
3. Kathode
4. Anode
5. Diaphragma
6. Elektrolyt
7. zur Bezugselektrode
8. Hähne zur Entnahme des Elektrolyten

FIGURE 2

Potential-Zeit-Diagramme von unbelasteten inaktiven Elektroden in 1 n KOH
reversibles O_2-Potential + 0,16 V

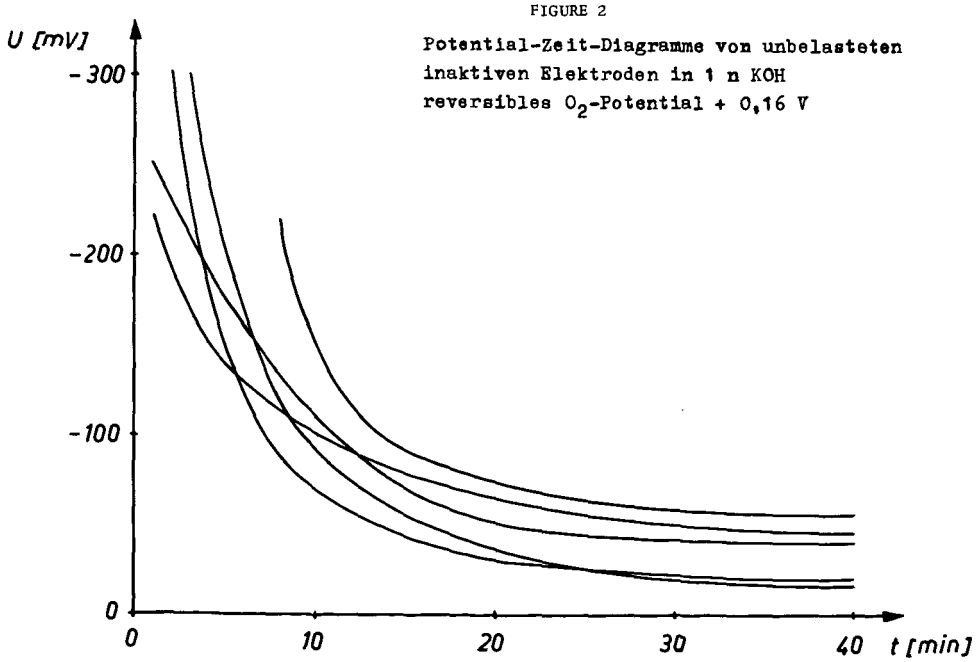

LITERATURE CITED

(1) Schmidt, A., Die Diffusionselektrode, Stuttgart 1923, E. Justi u. Mitarbeiter, Verlag der Akad. d. Wiss. Mainz 1959, Justi, E., Scheibe, W., Winsel, A., D. B. P. 1019361 (23. X. 1954).

(2) Kordesch, K., Marko, A., Österr. Chemikerzeitz. 52 (1951) 125, Kordesch, K., I. /E. C. 52 (1960) 296, Bacon, F. T., E. P. 725661 (16. I. 1953).

(3) Turkevich, I., 2 Konf. UN. friedl. Verw. Genf 1958 P/934, Andersen, H. C., Rylander, P. N., Keith, C. D., AECU-4733 (1960), Kosiba, W. L., Dienes, G. I., Advances in Catalysis 9 (1957) 398, Haissinsky, M. M., Pujo, A. M., Compt. rend. 240 (1955) 2530, Haissinsky, M. M., Duflo, M., 2. Genf. Konf. 1958 P/1233, Haissinsky, M. M., Siejka, J., J. chim. Phys. 56 (1959) 702, Haissinsky, M. M., C. R. Akad. Sci. 216 (1958) 1026, Verselovsky, V. I., 1. Genf. Konf. 7 (1955) 678, Preve, I. u. Montarnal, R., C. R. Acad. Sci. 249 (1959) 1667, Journ. Chim. Phys. 1961, 402.

(4) Spizyn, V. I., Gromov, V. V., Radiochimia 1 (1959) 181; Balandin, A. A., Spizyn, V. I., Dobroselskaja, N. P., Michajlenko, J. E., Dokl. Akad. Nauk SSSR 121 (1958) 495; Spizyn, V. I., Isv. Akad. Nauk, Otdel. Chim. Nauk 1960, 1325; Spizyn, V. I., Tortschenkova, E. A., Dokl. Akad. Nauk SSSR, 132 (1960) 643; Spizyn, V. I., Tortschenkova, E. A., Glaskova, J. N., Dokl. Akad. Nauk SSSR, 133 (1960) 1111.

FIGURE 3

Potential-Zeit-Diagramme von unbelasteten aktiven Elektroden (Aktivität ca. 3 mC Tl 204/ cm^2) in 1 n KOH

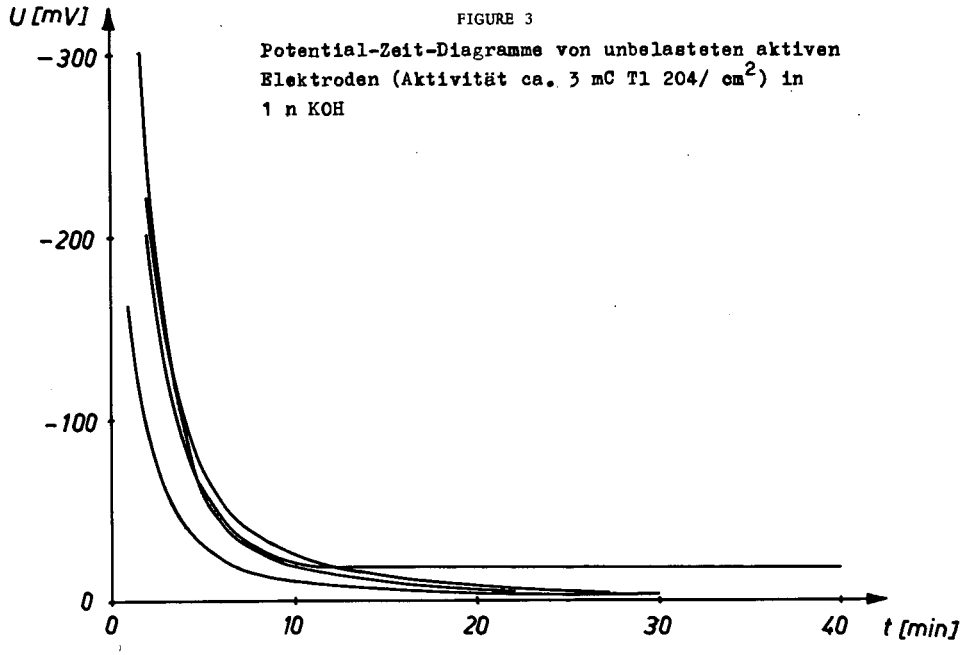

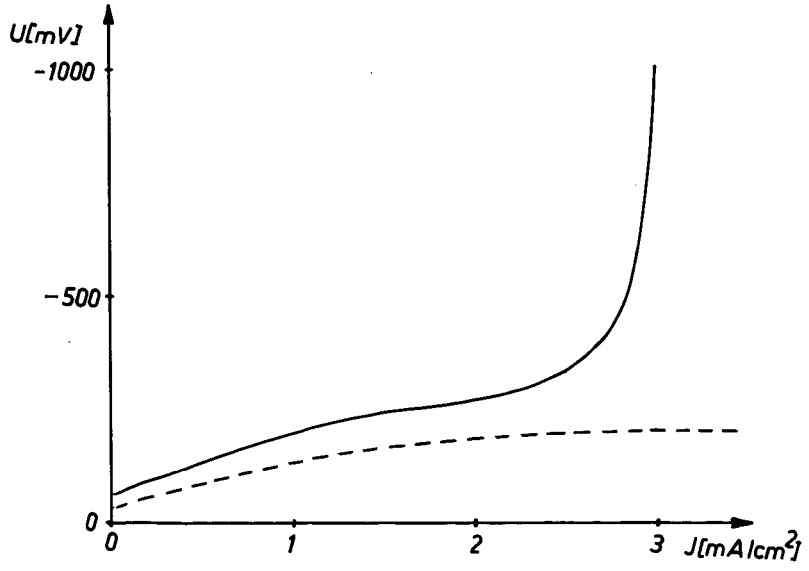

FIGURE 4

Potential-Stromdichte-Diagramme aktiver —— (Tl 204) und inaktiver ___ Elektroden. (Mittelwerte aus 5 Meßreihen)

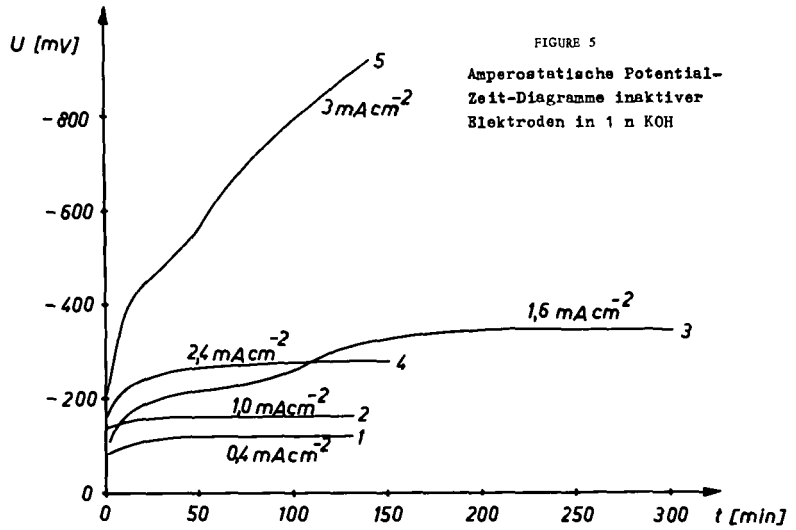

FIGURE 5

Amperostatische Potential-Zeit-Diagramme inaktiver Elektroden in 1 n KOH

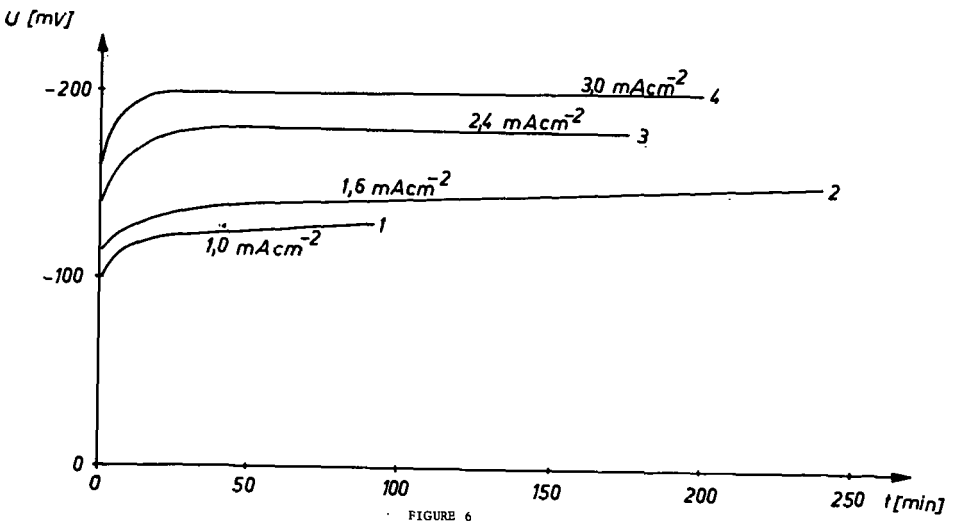

FIGURE 6

Amperostatische Potential-Zeit-Diagramme aktiver Elektroden in 1 n KOH, Aktivität der Elektroden 3 mC Tl 204/ cm^2

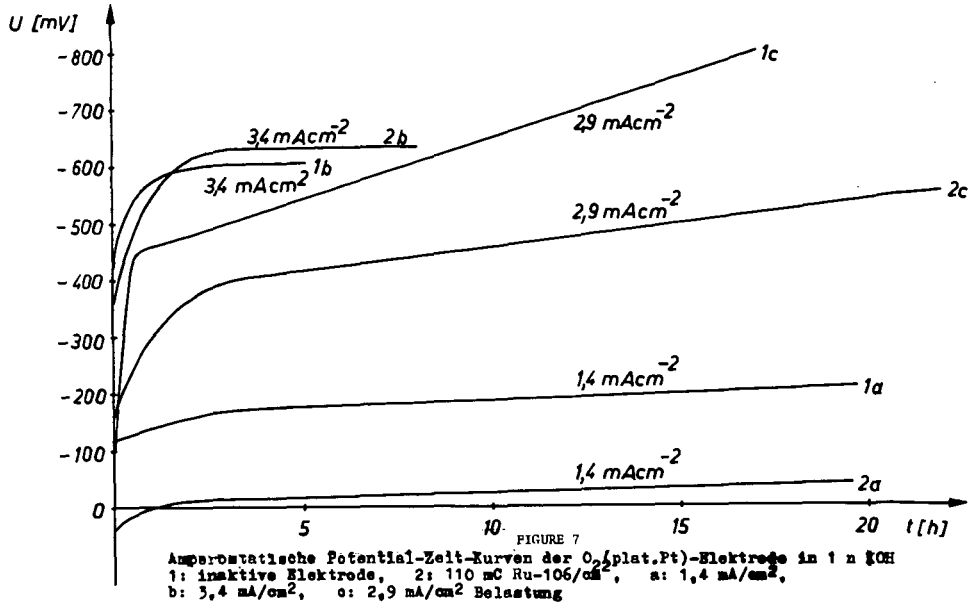

FIGURE 7

Amperostatische Potential-Zeit-Kurven der O_2(plat.Pt)-Elektrode in 1 n KOH
1: inaktive Elektrode, 2: 110 mC Ru-106/cm², a: 1,4 mA/cm²,
b: 3,4 mA/cm², c: 2,9 mA/cm² Belastung

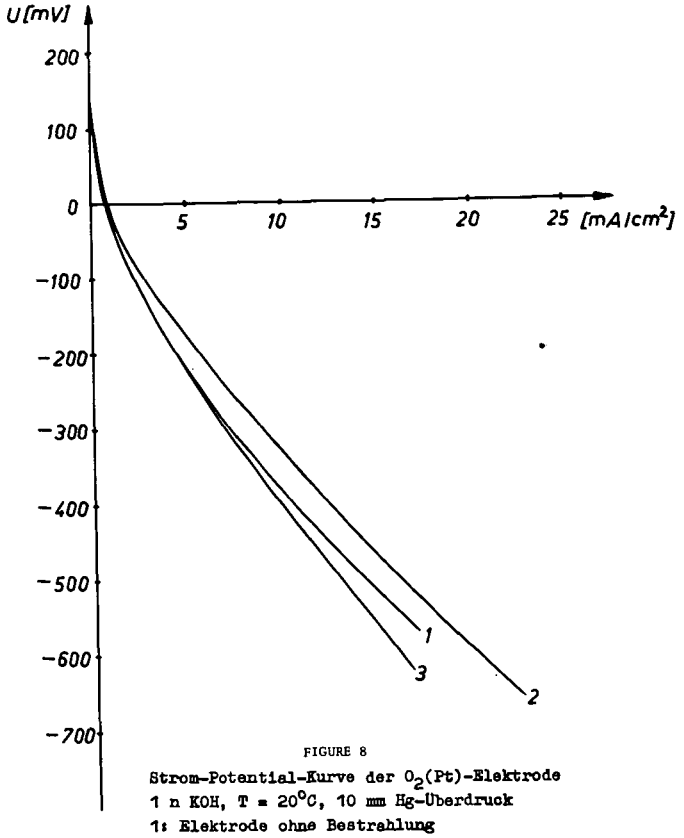

FIGURE 8

Strom-Potential-Kurve der O_2(Pt)-Elektrode
1 n KOH, T = 20°C, 10 mm Hg-Überdruck
1: Elektrode ohne Bestrahlung
2: Elektrode mit 45 mC Ru-106 bestrahlt
3: Elektrode nach Entfernung der Strahlenquelle

SYMPOSIUM ON FUEL CELLS
PRESENTED BEFORE THE DIVISION OF PETROLEUM CHEMISTRY
AMERICAN CHEMICAL SOCIETY
CHICAGO MEETING, September 3-8, 1961

ION-EXCHANGE MEMBRANES IN HYDROGEN-OXYGEN FUEL CELLS

By

Robert M. Lurie, Carl Berger, and Ralph J. Shuman
Ionics, Incorporated, Cambridge, Massachusetts

1. GENERAL

In fuel cell technology, simplicity of form and construction are desired engineering features. In conventional fuel cell systems for instance, electrodes must have uniform porosity to insure an even distribution of gas. Construction flaws and other imperfections cause gas accumulation in the electrolyte and mixing of gases when slight gas pressure difference occurs. In addition sintered metal electrodes are fragile and porous carbon electrodes are both fragile and bulky. The production of these items, in addition, is time consuming and almost amounts to a custom manufacturing operation. It is because of these drawbacks, that the ion membrane fuel cell has attracted so much attention. Essentially it consists of an ion-exchange membrane, cationic or anionic in form, and two "catalytic" electrodes held against each side of the membrane. Reactant gases are brought to either side of the membrane, electron exchange occurs at the catalyst-membrane interface and current flows. The positive advantages of the ion-membrane cell are:

(1) Electrolyte remains non-diluted by water formed as a result of reaction.
(2) The membrane serves as a gas impervious barrier.
(3) The cell is relatively insensitive to gas pressure variation which would cause gas accumulation in the electrolyte of an ordinary liquid electrolyte fuel cell.
(4) Electrode flooding is minimized.

In practice the ion-membrane fuel cell has fallen far short of the expectations and indeed none, to the best of our knowledge, has ever been able to sustain satisfactory power level for a reasonable length of time, e.g., 0.5 - 0.6 volts at 30 - 40 milliampere per square centimeter for three to six months.

A reflection of these operating difficulties can be obtained by comparing the performance of an ion-membrane fuel cell operating on pure hydrogen and oxygen and incorporating platinum catalysts on graphite cloth electrodes in an ionics Fuelox type fuel cell. The comparison is illustrated in Figure 1 and indicates that polarization occurs much more rapidly than for the "non-dry" fuel cell.

2. SOME FACTORS RELATED TO EFFICIENT ION-MEMBRANE FUEL CELL PERFORMANCE

An examination of polarization curves and other data indicate that the hydrogen-oxygen ion-membrane cell has some serious disadvantages which must be overcome in order to attain satisfactory operating conditions. Some of these are:

A. Cell polarization resistance.
B. Drying of membranes.
C. Carbonate formation from carbon containing fuels.

A. Membrane Resistance

The ion exchange membrane is used as the electrolyte component in the fuel cell and while having structural advantages inherent in a solid material it does suffer from the disadvantage that the ionic conduction of leached hydroxyl form anion membrane will be roughly about 1/20 that of a comparable volume of concentrated KOH. 6N KOH in a layer the thickness of our membrane (0.06 cm) has a resistance of .11 ohm-cm^2. Thus the membrane resistance will be one or two ohm-cm^2.

FIGURE 1

HYDROGEN-OXYGEN FUEL CELL
COMPARED WITH FUELOX CELL

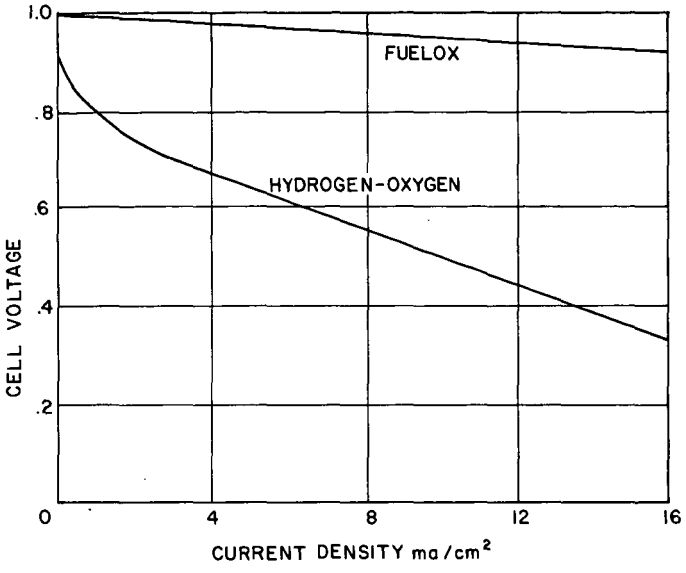

FIGURE 2

MEMBRANE RESISTANCE

ANION MEMBRANE COMPLETELY IMMERSED IN KOH
DIRECT CURRENT

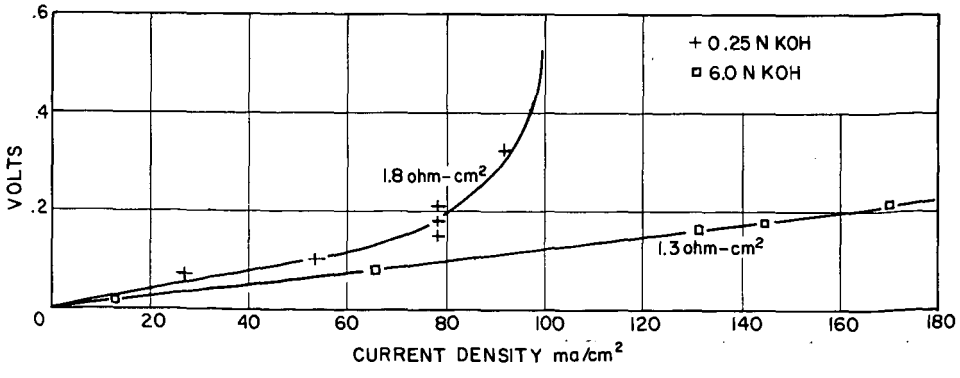

The result of the resistance characteristics of such membranes as well as electrode and concentration polarizations is shown in Figure 1. The hydrogen-oxygen cell is constructed with an anion membrane that was equilibrated in 6N KOH. The slope of the linear position of the curve is 34 ohm-cm^2. One of the objectives of our study was the determination of the source of this high voltage loss, since the membrane resistance alone obviously cannot account for the observed drop.

We first measured the membrane resistance. An investigation of membrane resistance calls for reliable technique under operating conditions approximating those found in actual performance. In routine work membrane resistance is essentially determined by placing platinum tipped probes on either side of a membrane and utilizing a Wheatstone Bridge circuit to determine the desired membrane resistance. Results, although reliable for industrial type uses are semi-quantitative and are not obtained under operating conditions comparable to those found in fuel cells, i.e., alternating current is used. The technique used consists of placing the membrane vertically in KOH (for the anion type) or HCl (for the cation type). Calomel electrodes with capillary salt bridges were placed on opposite sides of the membrane with the tips of the salt bridges touching the membrane. A current was passed through the solution by means of a battery and platinum electrodes placed well away from the membrane. The voltage differential between the calomel electrodes was measured with a Beckman Model G millivoltmeter as a function of current. Figure 2 shows the results of an anion membrane in 0.25N KOH and 6N KOH. The resistance of the former is about 2 ohm-cm^2 and the latter 1.3 ohm-cm^2. It may be noted that in the dilute solution a rapid voltage rise occurs at 90 ma/cm^2. This will be commented on later.

In an effort to separate the hydrogen and oxygen electrode polarizations, half cell studies were undertaken. In this technique (Figure 3) a gas electrode is placed on one side of the membrane while solution is on the other side. A salt bridge-calomel cell is placed against the membrane on the solution side. A current is driven with a battery between the gas electrode and a platinum electrode in the solution. The voltage between the gas electrode and the calomel is measured.

Figure 4 shows the results of hydrogen generation and hydrogen utilization with an anion membrane and 6N KOH solution. The former gives a voltage loss equivalent to 6.1 ohm-cm^2 and the latter 7.7 ohm-cm^2. The difference may be due to hydrogen concentration polarization.

Figure 5 shows the same experiments except that oxygen evolution and utilization are carried out. The irreversible voltage loss usually ascribed to a peroxide decomposition mechanism is apparent. In addition a pronounced voltage drop at low current densities is also observed in agreement with other workers.

Another technique was also used to study the hydrogen electrode. In principle, the technique involves imposing a potential across a membrane supported between two hydrogen electrodes one of which utilizes hydrogen and the other of which generates hydrogen. Both chambers are filled with hydrogen at atmospheric pressure and a battery is used to drive the reaction. A diagram of the experimental approaches is shown in Figure 6. Since the hydrogen electrode is fairly reversible one could examine different hydrogen electrodes (utilizing hydrogen) with a standard electrode evolving hydrogen. Figure 7 illustrates the result of such an experiment using an anion membrane equilibrated in 6N KOH. The slope indicates a total loss of 52 ohm-cm^2. At this point we humidified the hydrogen gas going into each compartment by bubbling the gas through water at 70°C. and excess gas was passed through the cells. The voltage-current density curve changes appreciably down to 16 ohm-cm^2. It may be noted that the two half cells with hydrogen utilization and hydrogen evolution gave 7.7 and 6 ohm-cm^2, respectively, so that the humidified hydrogen-hydrogen dry cell approximates quite well the sum of two half cells.

B. Dehydration

The original hydrogen-oxygen cell yielded a 34 ohm-cm^2 slope as mentioned in the beginning of the paper.

This cell was operated again, but with humidification. Figure 8 illustrates the voltage-current density curves of hydrogen and oxygen half cells, the difference between them, and the actual humidified hydrogen-oxygen cell. The latter has a slope of 22 ohm-cm^2 and is quite close to that predicated with the half cells. From these data it is seen that drying in the vicinity of the electrode area increases greatly the contact resistance at the membrane catalyst interface. Membranes are approximately

FIGURE 3
HALF-CELL TEST EQUIPMENT

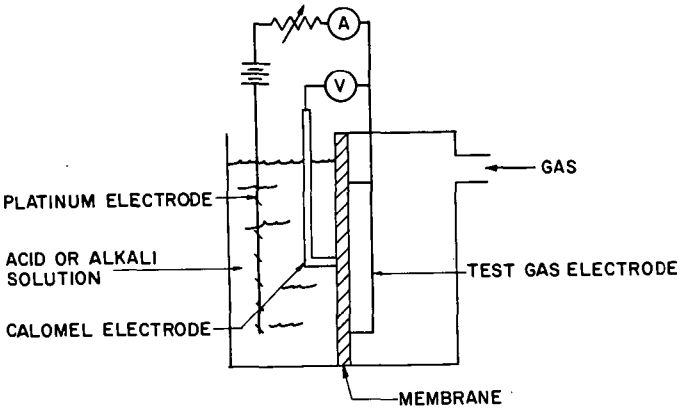

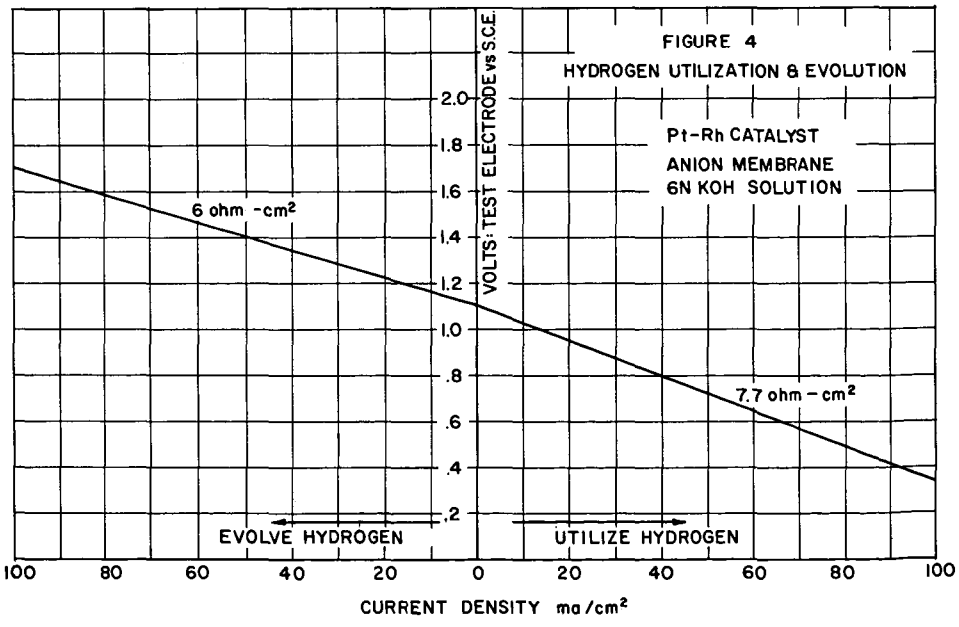

60% water and it can be seen that variations in water content at such surface areas could result in significant changes in ion diffusion rates and more importantly, conductivity of the desiccated portions. Desiccation in all liklihood occurs as a result of the relatively dry fuel gases increasing the rate of evaporation from the surface of the membranes. A number of mechanical arrangements for providing rehumidification have been attempted but it has been found that such approaches are merely stop gas measures which at higher current densities fail to provide solutions to the drying problem.

Ionics has experimented with more "intrinsic" solutions to the problem; one of them mentioned earlier in the paper is the use of semi-dry cell such as the Fuelox cell where the cathode compartment contains aqueous solution of reactants and thereby keeps the cation membrane sufficiently moist even at current densities as high as 50 amp/ft^2. Cells of this type have run for 1000 hours on half hour charge-discharge cycles at about 20 ma/cm^2.

Another approach to this problem involves the "dual membrane" concept (1) which not only eliminates the humidification problem but decreases the conductivity of the membrane components of the fuel cell assembly.

C. Carbonate Formation

In the last analysis the efficient and economical use of the ion membrane fuel cell will rest heavily on the performance of carbonate producing fuels in such power producing devices. Because of its importance it was deemed advisable to determine the effect of carbonate production on the operating characteristics and performance of an ion-membrane cell. A fuel cell using carbon monoxide and oxygen as fuels and a 6 mm thick anion membrane with two waterproofed platinum on graphite electrodes was tested. Figure 9 depicts the performance of this cell. The recorded open circuit voltage is 0.80 - 0.86 volts. After operating for eleven hours the cell was taken apart. The electrode and membrane were found to contain a considerable quantity of solid carbonate.

Alternate tests with membranes soaked in acid were comparatively poor. The maximum open circuit voltage 0.37, the maximum current being about 1 ma/cm^2 at 0.2 volts for a short time.

3. DISCUSSION

1. High Cell Resistances

These resistances are the limiting factor in obtaining high current densities in ion-membrane fuel cells. Possible solution to these problems lies primarily in the area of improved catalyst membrane contact.

2. Drying Out of Membranes

This is a most serious engineering problem and can be solved by:

(a) Using a membrane where desiccation problems are not as serious due to low water content. This will also tend to avoid the rapid se in voltage which was observed to occur when membrane resistances were measured in 0.25N KOH. Thus during cell operation a salt concentration gradient forms in the free water phase in the membrane, as well as in any free water between the catalyst and the membrane. With low water content membranes these gradients should be minimized.

(b) Mechanical "wicking" arrangements have been used, but have not provided a satisfactory means for attaining high current density. Of course, humidification of the fuel gases is a possibility but does involve increased weight and cost penalties.

(c) The best technique found to date is essentially the constant humidification of the membrane as mentioned previously in the Fuelox type cell or the dual membrane cell. An added advantage of this system is that water of formation due to hydrogen-oxygen reaction can be removed by use of dry gases and thereby does not cause undue dilution of the electrolyte being used.

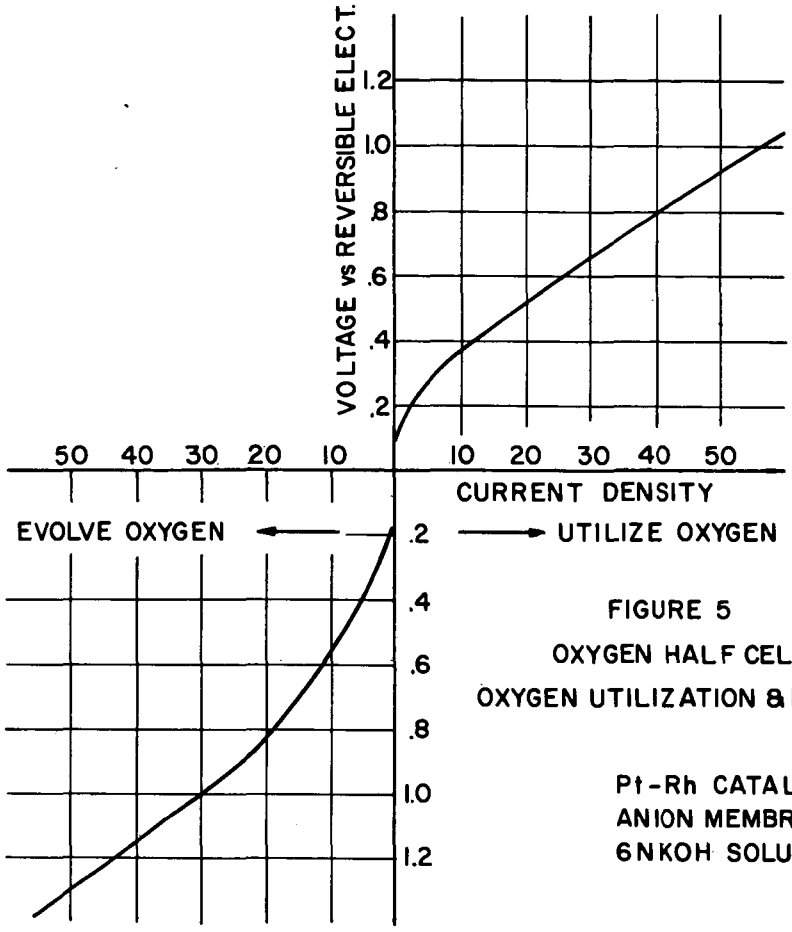

FIGURE 5

OXYGEN HALF CELL

OXYGEN UTILIZATION & EVOLUTION

Pt-Rh CATALYST
ANION MEMBRANE
6 N KOH SOLUTION

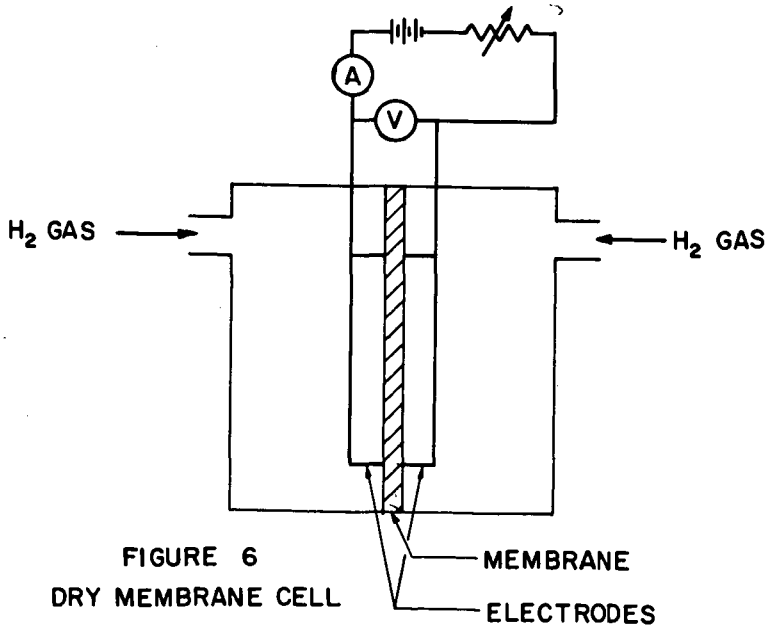

FIGURE 6

DRY MEMBRANE CELL

3. Carbonate Formation

Finally, the problem of carbonate formation remains a serious one. The data on the use of carbon monoxide as a fuel gas indicate, substantially, that the formation of carbonate at the electrode membrane interface essentially degrades operation within a short period of time. Some approaches worthy of mention for avoiding this problem are:

(a) Use of acid type membranes with subsequent venting of carbon dioxide. This, of course, has the formidable barrier of a satisfactory operation of fuel electrode in acid solution.

(b) Continuous regeneration techniques for membranes, i.e., the continuous removal of $CO_3^=$ ion from the reaction interface may be effected by driving the cell in reverse and moving the carbonate ions electrically away from the carbon monoxide electrode.

LITERATURE CITED

(1) Juda, W., Tirrell, C. E., and Lurie, R. M., "Fuel Cells with Ion Exchange Membranes", Energy Conversion for Space Power, Academic Press, New York (1961).

FIGURE 7
MEMBRANE CELL

HYDROGEN UTILIZATION / HYDROGEN EVOLUTION

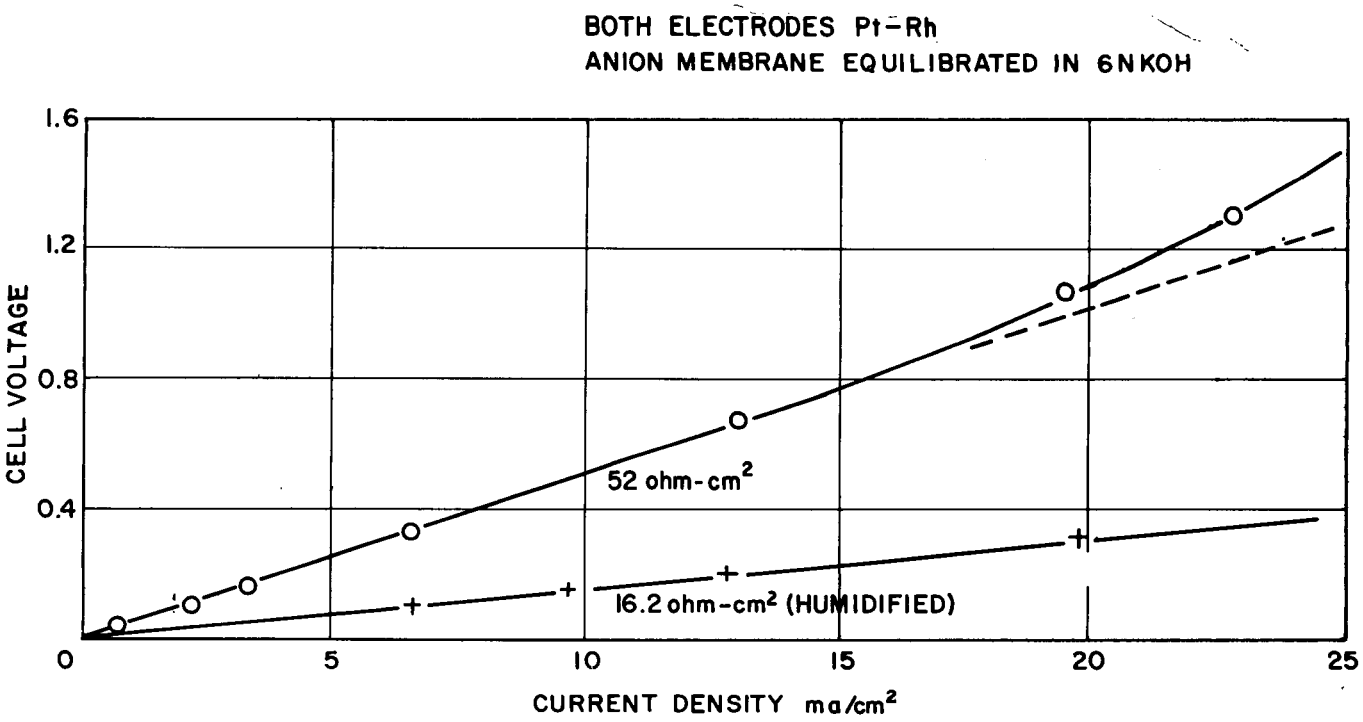

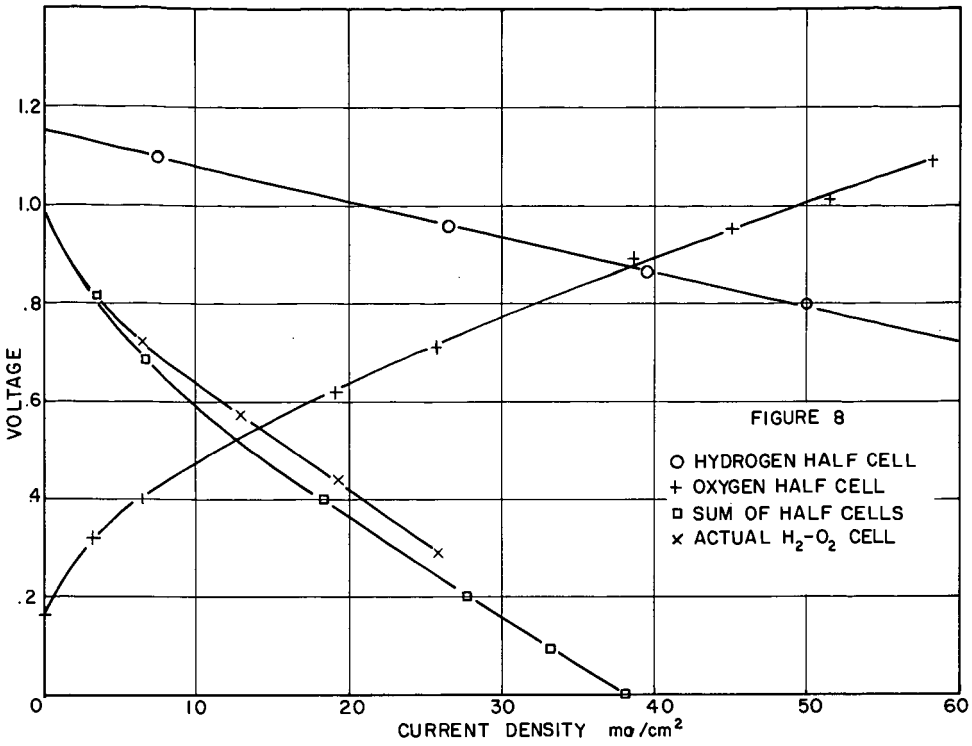

FIGURE 9

$CO-O_2$ DRY CELL

BOTH ELECTRODES – Pt ON GRAPHITE
ANION MEMBRANE – EQUILIBRATED IN 6N KOH

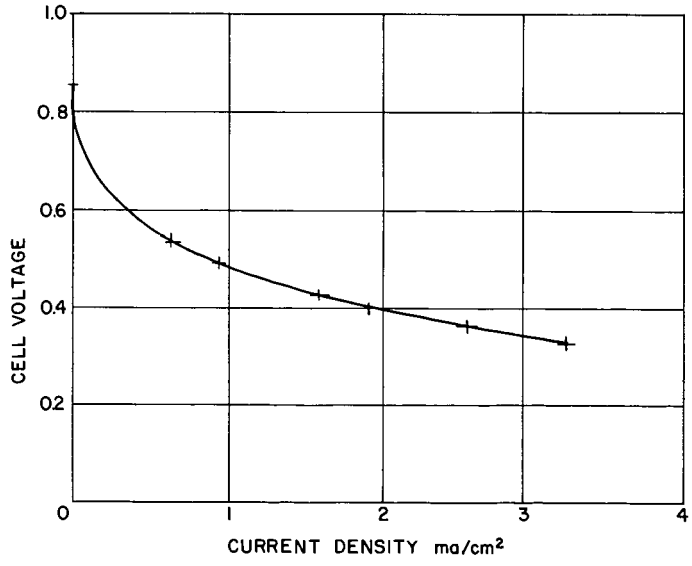

SYMPOSIUM ON FUEL CELLS
PRESENTED BEFORE THE DIVISION OF PETROLEUM CHEMISTRY
AMERICAN CHEMICAL SOCIETY
CHICAGO MEETING, September 3-8, 1961

DESCRIPTION OF A FUEL-CELL POWER-PACK OPERATING ON HYDROGEN AND AMBIENT AIR

By

E. A. Oster and L. E. Chapman
Aircraft Accessory Turbine Department, General Electric Company

INTRODUCTION

Over the past two years, the General Electric Company at Lynn, Massachusetts, has been developing a complete two-hundred-watt power-supply based on the ion-exchange-membrane fuel-cell. This development work which followed the earlier work at the Company Research Laboratory was performed under contract with the Navy Bureau of Ships and the Army Signal Corps. The complete unit is shown in Figure 1. This paper will describe the construction and operation of the unit.

A schematic of the G. E. cationic-membrane fuel-cell operating on hydrogen is shown in Figure 2. The current cells used in battery stacks are about six-tenths of a millimeter thick including the two catalytic electrodes. The hydrogen gas is fed into a dead-ended chamber on one side of the membrane where it is adsorbed on the catalytic anode and is stripped of one electron per hydrogen atom. The resultant hydrogen ions diffuse through the ion-exchange electrolyte while the freed electrons flow along the electrically-conducting catalyst to the current collector contact point, thus producing the negative (-) terminal of the cell. On the other side of the membrane, the oxygen from the air moving over the cell is adsorbed in the cathode. In the region of this catalytic electrode, an overall three-way reaction takes place between the transported hydrogen ions, some form of the adsorbed oxygen, and the electrons which have passed through the external electrical load to form water as the final reaction product. The water, thus formed, may be removed by evaporation or drawn off through a valve at the bottom of the cell casing. About 35 cells of this type, each having an electrode size of approximately 85 square inches, are used in a battery contained in a portable 200-watt fuel-cell system.

CELL PERFORMANCE

The cation-exchange electrolyte is contained in a polymer system reinforced with cloth. The cloth provides the membrane with the structural strength necessary to survive the dimensional changes associated with the differential dehydration occurring during cell operation. The presence of the cloth embedded in the resin impedes the transport of the hydrogen ions through the membrane and thus increases the electrical resistance through the membrane. Therefore, development programs were conducted to decrease the weight ratio of cloth to resin. These have increased performance by approximately 60 percent, from 6.1 watts per square foot to 9.7 watts per square foot.

The effect of reductions in the cell resistance can be observed in Figure 3. The voltage drop from the theoretical open circuit value of 1.23 volts to approximately 0.9 volt is believed to represent irreversibility losses at the oxygen electrode. The remainder of the slope of the polarization curve is strictly a function of the IR drop caused by internal resistance of the cell. Efforts toward reducing these losses result in an increase of cell efficiency and correspondingly a reduction of the heat produced in the cell. Thus, reducing the cell resistance offers a two-fold advantage at a particular power density; first, an increase in fuel efficiency and secondly, a reduction in the dehydration tendencies of the cell.

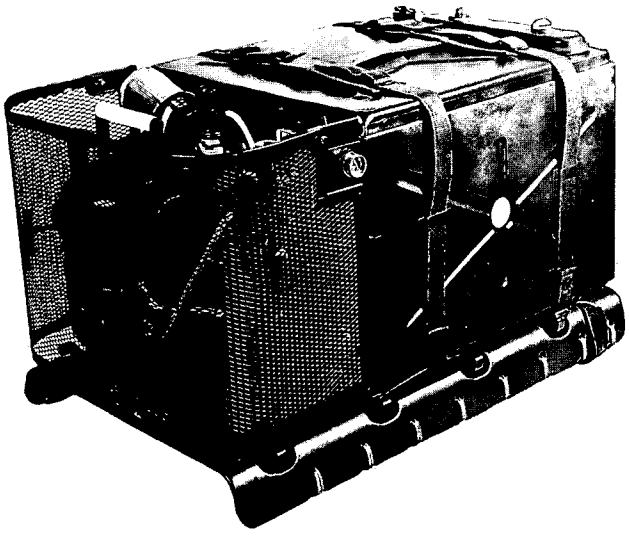

FIGURE 1
THE G. E. 200-WATT POWER-PACK SYSTEM BASED ON A CATIONIC-MEMBRANE FUEL CELL BATTERY STACK

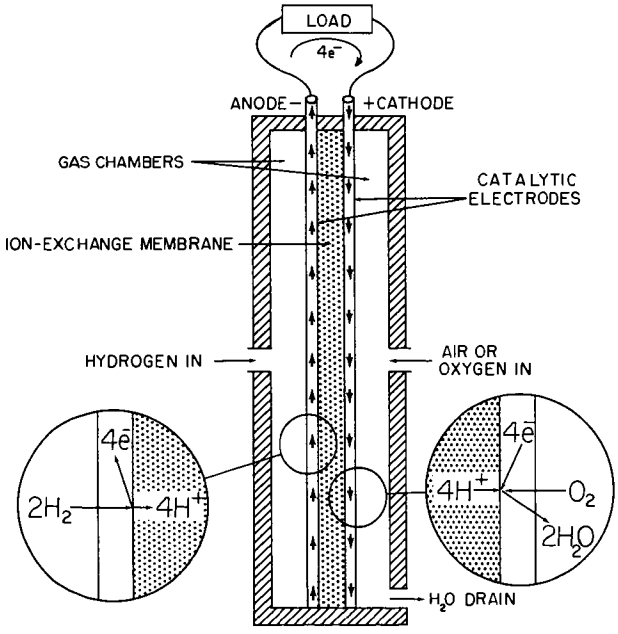

CHEMICAL REACTIONS

ANODE	OVERALL	CATHODE
$2H_2 \rightarrow 4H^+ + 4e^-$	$2H_2 + O_2 \rightarrow 2H_2O$	$4e^- + 4H^+ + O_2 \rightarrow 2H_2O$

FIGURE 2
SCHEMATIC OF G. E. ION-EXCHANGE FUEL-CELL OPERATION

CELL ASSEMBLY CONFIGURATION

Figure 4 shows the air side of a cell assembly for the 200-watt Power Pack. The current collector is formed from two pieces of titanium sheet-stock. The inner piece is .0015 inches thick and is in contact with the catalyst-electrode. Its small channels conduct air over the membrane to provide oxygen for the electrochemical process. The outer perforated piece is .003 inches thick. Its larger channels carry additional air for cooling the air side of this cell and the hydrogen side of the adjacent cell in a stack.

Figure 5 reveals the internal construction of a single cell. The membrane is bonded to a plastic frame that is molded around the anode current collector (hydrogen side). This forms a gas-tight chamber for the hydrogen. The hydrogen supply is attached to the inlet at the top of the cell where it emerges through a series of holes and distributes itself throughout the chamber. A manifold molded into the opposite side of the frame is used for the occasional purging of accumulated inert gases.

Since the hydrogen side of the cell forms a sealed and dead-ended chamber the only gas flow is that necessary to make up for the hydrogen consumed in the reaction. Therefore, the frequency of purging is a function of hydrogen purity.

Ambient air, used both as a coolant and a cell depolarizing reactant, is forced under the battery by a small inlet fan powered from the fuel-cell. From this plenum, the air, flowing up through each cell, is split into reactant air flow and cooling air flow. This design of splitting the air flow is to remove from the battery across water-impermeable barriers as much heat as possible. As shown in Figure 5, a network of wicks covers the air side of the membrane. These are fed from distributor wicks at the base of each cell. Legs extend from the bottom of the cell frame to hold the distributor wicks in the water reservoir. This system of wicks in contact with the membrane is a characteristic of the evaporatively cooled air-breathing fuel cell. It supplies water to make up evaporative losses within the air-breathing cell and to maintain the proper moisture content in the membrane for optimum ion transport and dimensional stability.

HEAT AND MASS TRANSPORT

Several factors contribute to the necessity of cells giving off water to reject heat in some ambients. In air-operating cells, voltages are such that more heat is generated that the product water formed can solely absorb in its evaporation. Thus, what heat is not conducted away will require extra water to evaporate. This latter situation is often true in multi-cell stack operation in various ambients. In multi-cell air operation with some liquid electrolytes this may manifest itself in precipitation in the oxygen electrode pores. In hydrated ion-exchange fuel cells, water can come from the gel structure with a resultant loss in ionic conductivity of the membrane and a desire on its part to change dimension to some degree depending on the gel. Note that increasing convective heat transfer by reasonable higher air velocities will not generally help because in air-water systems the weighted mass-transfer coefficient is intrinsically favored over the heat transfer coefficient. Effects can be made by changing driving forces available for heat and mass transfer.

As previously mentioned in this paper, the General Electric Company has done two things to solve this simultaneous heat and mass transfer problem for ion-exchange fuel cells operating on air in light-weight multi-cell stacks. First, is the forementioned splitting of the flowing air into two parts to effect an internal-stack, air-cooled condenser in close proximity to the two reactive electrodes. In fact, in the present 200-watt design, the distance of the condenser surfaces from the electrode is of the order of 1 or 2 mm. and set only to avoid water droplet bridging. Secondly, when necessary the forementioned make-up water, is supplied by a system of wicks. These approaches prevent a membrane dehydration condition and allow the satisfactory control of membrane temperature - rise.

Heat and mass transfer performance has been estimated for a range of inlet temperatures and humidities at a constant air flow, and is shown in Figure 6.

It can be observed that the total amount of water evaporated by the air passing over the cell is greater than the product water for all conditions except at low temperatures. Therefore, the wicks must make up the difference to maintain a stable system. The wicking system used in these cells is the result of extensive testing and evaluation of types of material, purity of material, number of strands, and number of wicks per channel.

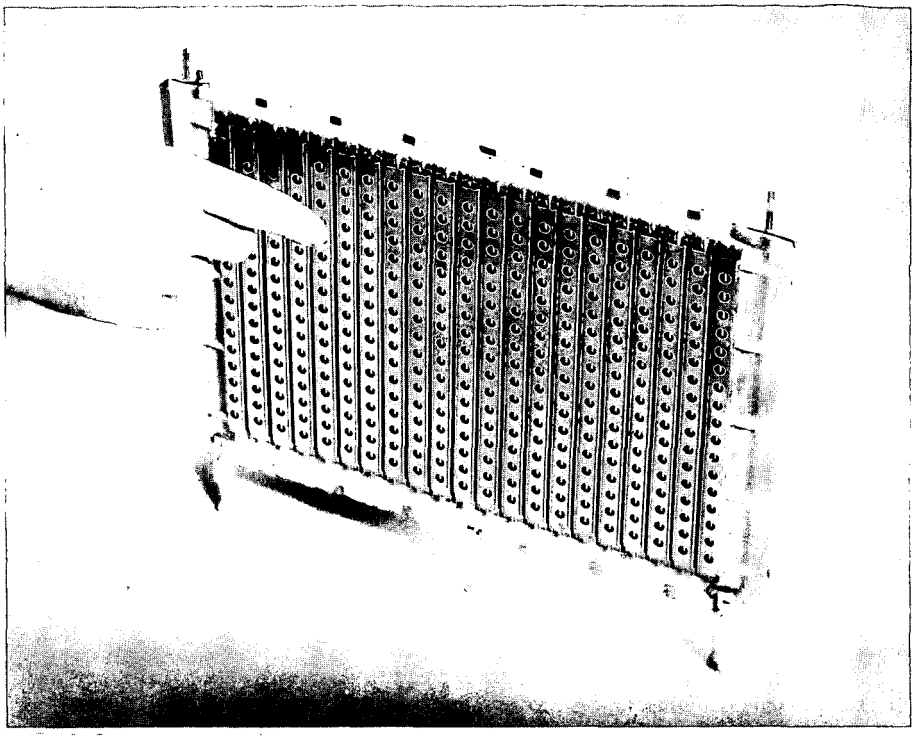

FIGURE 4
SINGLE CELL ASSEMBLY READY FOR BATTERY STACK

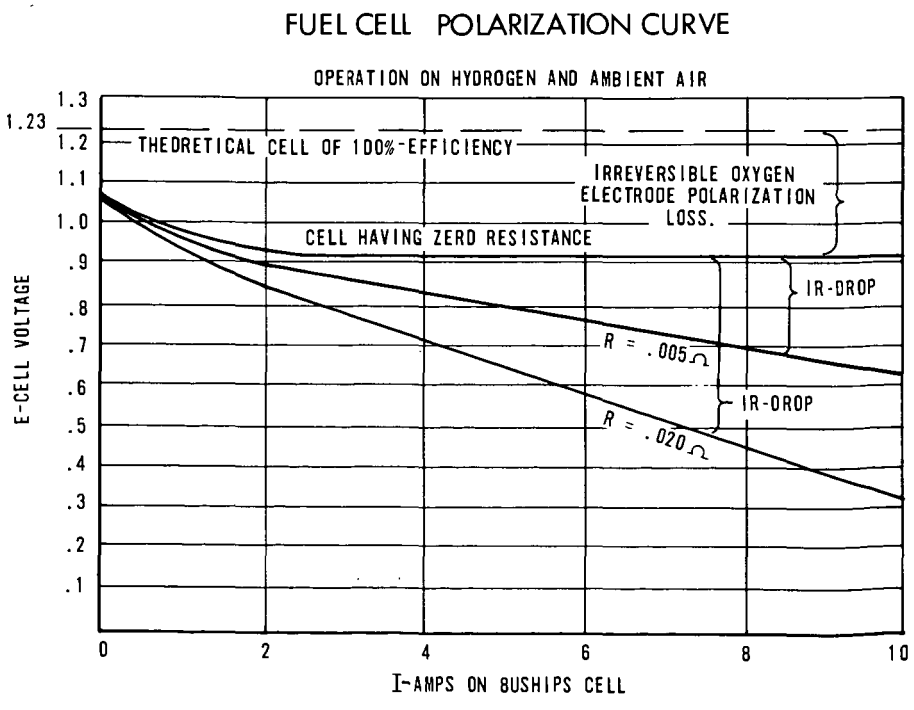

FIGURE 3

Automatic water control is provided by a wicking system that:

1. Has been designed and proven adequate for the conditions of high temperature and low humidity, where the maximum water transport is required.

2. Will transport only the required makeup water to maintain a stable system under any less severe operating condition. Since the wicks work from the bottom, there is no flooding problem because they can only lift water to areas that become less than saturated.

Figure 6 also indicates that at the lower ambient temperatures product water can be generated faster than it can be evaporated. Under these conditions it becomes necessary to reduce the air flow to prevent drowning of the catalyst. A reduction in air flow reduces the convective cooling, thus allowing the membrane temperature to rise. The air passing through the cell also takes a larger temperature rise and thus can evaporate the excess product water from the cells.

The required air flow has been determined experimentally and proven over a considerable number of operating hours at ambient conditions of 40°F. and 100 percent relative humidity.

Thus multi-cell stack operation of fuel-cells on air required detailed consideration of the heat and mass transfer problem which can only be defined experimentally in multi-cell stocks great enough to give a few cells operating in a condition free from end effects or the presence of heavy-weight testing fixtures. Sometime hours are involved in reaching steady state so transients must be considered in the analysis.

BATTERY DESIGN

Figure 7 is a schematic view of the fuel cell battery and its container, showing the cells stacked in series. A single strap clamps them together with the oxygen current of one cell in contact with the hydrogen collector of the next cell. The ribs on the air-side current collector are designed to act as springs, assuring equal pressure distribution to all points of contact with the electrode surface. The end plates are honeycombed epoxy assemblies contoured to distribute the loading uniformly across the current collectors of each cell.

The ambient air is drawn into the unit through a dry mechanical filter by a small fan powered from the fuel cell battery. The air then passes through a calibrated inlet control valve that is manually adjustable to match the air flow to the ambient temperature. The entering air is ducted to the bottom of the battery, flows up through each individual cell, and then out the exhaust.

The makeup water is introduced through a fitting in the cover. Since metal ions will contaminate the membrane, a water purification bed is included as part of the unit. This contains an ion-exchange resin bed that filters and deionizes sufficiently any potable water for use in the fuel cell.

Figure 8 is a translation of the single cell polarization curve showing voltage regulation versus output power. This indicates that inherent voltage regulation of the fuel cell power source is possible between the specification limits of 21 to 28 volts D. C. for loads between 50 and 115 percent.

Observed from the two curves in Figure 8 is a slight performance drop during an operating cycle. This amounts to approximately an 8 percent drop in output voltage. Following a half-hour rest period at open circuit conditions, the performance will recover to its original lever. This phenomenon suggests a tendency toward a concentration polarization effect typical of the presence of small amounts of free electrolyte anions in the cell.

FUEL SUPPLY

Two interchangeable fuel supply systems have been developed for the power pack, each of which will operate the 200 watt unit for approximately seven hours per charge.

In Figure 9, the unit is shown with the guard raised to reveal the bottled hydrogen system. Here, the gas is stored in a steel cylinder at 5000 psig., and is fed to the cells through a two-stage pressure regulator, reducing and regulating the pressure to 1 psig.

The hardware in Figure 10 shows the hydrogen generation system developed to utilize the reaction of sodium-borohydride and a sulfuric acid solution. The system

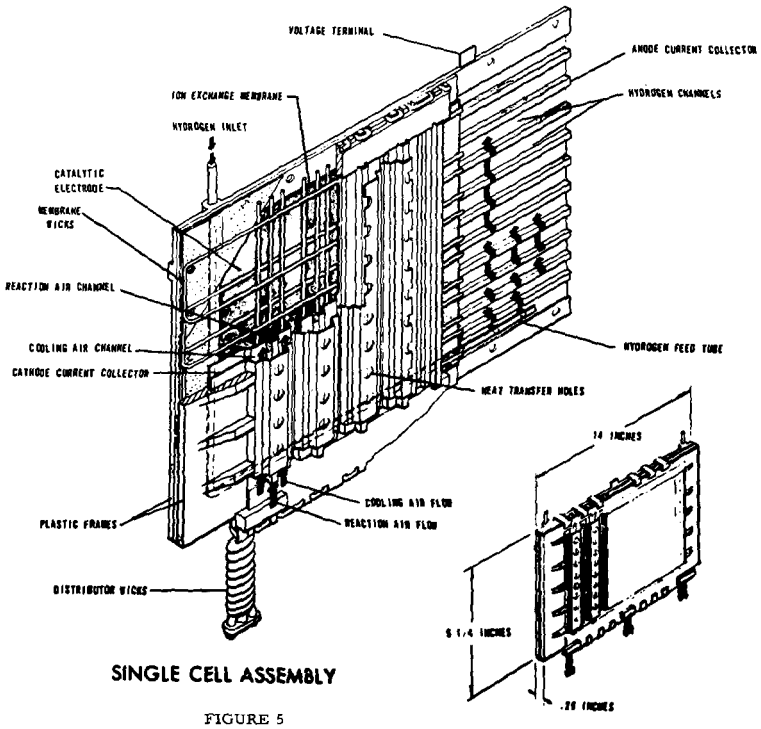

FIGURE 5
DETAILED SCHEMATIC OF SINGLE CELL ASSEMBLY

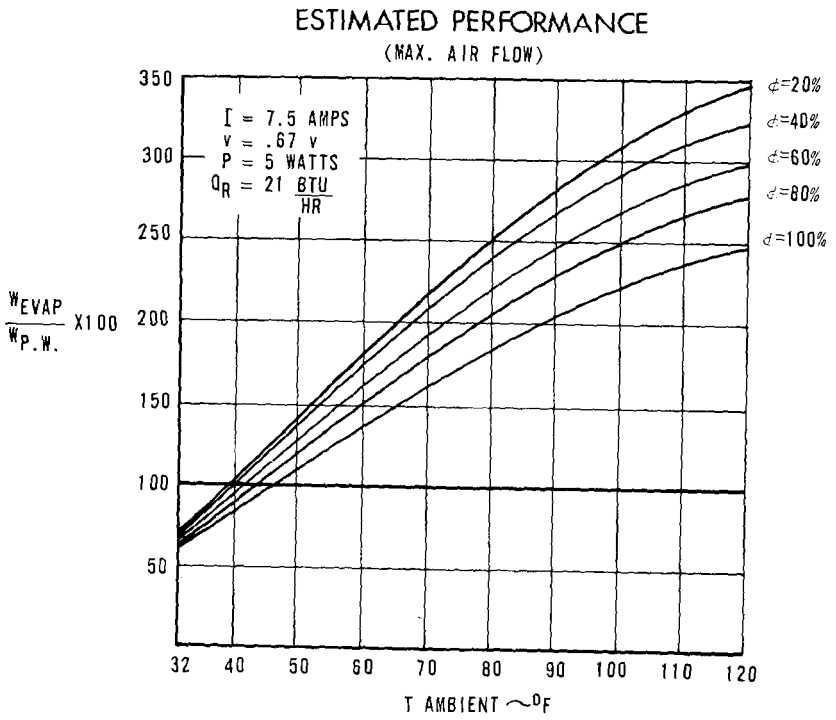

FIGURE 6
ESTIMATED EFFECT OF AMBIENT INLET AIR HUMIDITY AND TEMPERATURE ON MAKE-UP WATER REQUIREMENTS

consists of a two-part tank or canister containing the sodium borohydride in pellet form in the top section and the acid solution in the bottom. The surge tank is also made in two parts.

Gas generation is started by stroking the primer assembly to force the first charge of acid into the borohydride. The gas is accumulated in the surge tank and fills up the displacement volume. Once the system is started, a reference pressure is maintained through a regulator to the acid chamber. As the gas is consumed by the cells, and the pressure in the top half of the system drops below the reference pressure in the bottom half, a quantity of acid will be forced into the chemical. The generation of gas will build up the pressure again, closing the check valve until the next demand signal.

This boot-strap pressurized system generates hydrogen only upon demand, and operates at pressures sufficient to produce good acid distribution to the chemical and to prevent internal components from clogging. The principal purpose for using an acid solution is to depress the liquid freezing point to -65°F. The chemical canister is equipped with a hand-operated blow-down valve and quick disconnect fittings for easy replacement of spent canisters.

Currently, a 700 gram charge of sodium borohydride and a 1300 cc charge of sulfuric acid is consistently producing 50 cubic feet (S. T. P.) of hydrogen gas. This performance represents approximately an 85 percent utilization of the sodium borohydride with 155 percent of the theoretical acid solution requirements. The purity of the hydrogen gas generated has been measured as 99.8 percent with water vapor as the remaining constituent.

LIFE AND RELIABILITY

Life and reliability testing has produced encouraging results and has also contributed a great deal of information toward the better understanding of the elements affecting cell life. At this time, a number of the small 1.8 square inch area cells are running after two years of continuous operation. Several stacks of the large air-breathing cells have operated for 500, 650, and 750 hours. Many cells have also been operated for some 60 hours without failure at ambients of 120°F. and 15 percent relative humidity.

As will happen in the evolution of any new product or process, problems have been encountered during the process of cell development and evaluation. Examples of the problems that have been encountered and solved include:

1. Metal corrosion and ion contamination of the membrane.
2. Bonding of the membrane to the plastic frames.
3. Uniform hydrogen distribution throughout the cell.
4. Wicking configuration and wicking materials.

Currently underway is an extensive program of life and reliability testing that will provide greater understanding of the effects of current density and temperature on the life of the cells. Concurrently, an evaluation test of a complete power source is being run.

FUTURE IMPROVEMENTS

Before summarizing this paper, a few comments concerning recent laboratory work with improved electrochemical cells are in order. These improved large cells possess the higher performance curves of volts versus amps shown in Figure 3.

Usually, such curves as shown in Figure 3 are split into an ohmic polarization loss and the two electrode polarization losses. With a nearly reversible hydrogen electrode, almost all the electrode losses occur on the oxygen or air side. At low current densities, the oxygen and air electrode losses are nearly the same for these catalytic electrodes having a thickness of only 50 microns. At higher current densities the presence of nitrogen in the case of air begins to be noticed. But in contrast, the better electrode polarization curves for oxygen operation continue in a nearly flat slope up to current densities over 100 ma. /cm^2 at values just over 0.9 volts with respect to a hydrogen (N. H. E.) reference. Thus for air or oxygen operation in the range of present interest, these ion-exchange fuel-cells are being run in a region where internal ohmic resistance controls the power density obtainable at any selected fuel-utilization efficiency or output voltage.

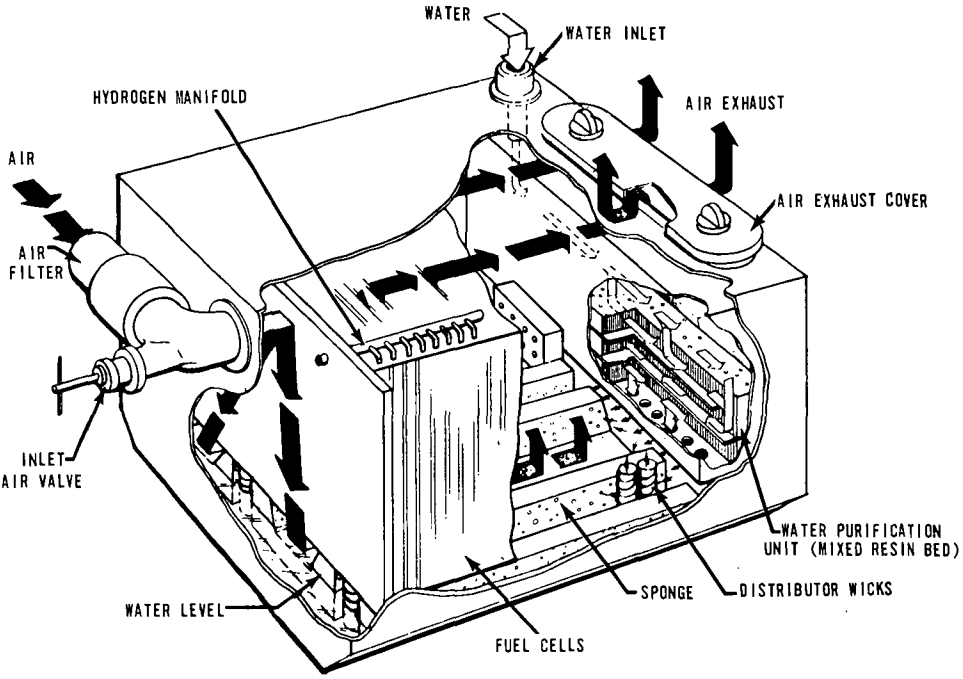

FIGURE 7
SCHMATIC OF POWER-PACK BATTERY-STACK OPERATION ON AMBIENT AIR

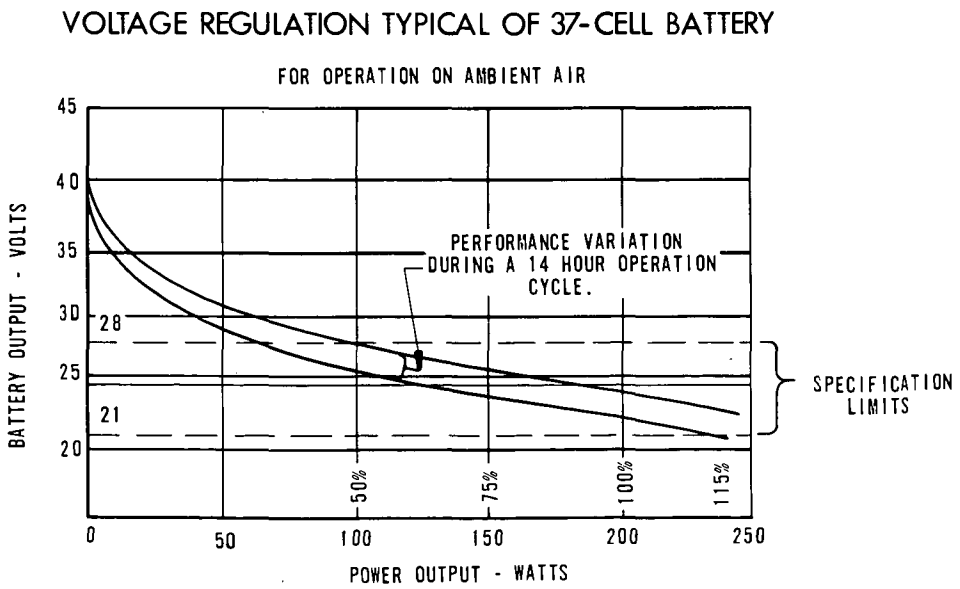

FIGURE 8

During the past year, straight-forward developments in membrane construction have cut our first air-operating cell-resistance by a factor of four. This difference has been demonstrated on several hundred cells of both types made in our laboratory pilot plant. This favorable decrease in resistance has resulted in an increase in performance which may be taken advantage of in two ways. One way would be to increase power output by a factor of two at the same fuel efficiency; the other being to decrease heat rejection by just over 25% at the same power density. Actually, it is usually decided to operate at a point between these two extremes.

Present laboratory programs show on some small cells that we have been able to nearly halve this internal resistance again while obtaining better physical properties.

SUMMARY

The complete 200 watt power source in the present development stage contains 37 cells, measures 12 x 15 x 24 inches and weighs 60 pounds. Included is the 13.5 pound hydrogen generation system that will operate the unit at full load for seven hours.

The feasibility of a small, portable, air-breathing fuel cell power source with an integral hydrogen generation system has been demonstrated in General Electric's 200 watt development program. This program has shown that the ion-exchange membrane fuel cell has the potential for long life air-breathing operation with satisfactory operation at ambient temperatures from 32 to 120°F. and relative humidity from 15 to 100 percent.

We recognize that some further development work is indicated to develop this unit into a piece of practical field hardware. Additional effort is required to evaluate and develop the capabilities of the power supply system to satisfy the requirements of low temperature operation and the appropriate handling, storage, and environmental conditions. Further analysis and evaluation will be required to develop a greater understanding of the heat and mass transfer characteristics of an evaporatively cooled air-breathing fuel cell. Additional life testing of small stacks and 200 watt fuel cell batteries must be run to develop further statistical life and reliability data.

Currently in laboratory development are some new polymer systems showing considerable promise toward superior physical properties, lower internal resistances, and long term stability. It is projected that current desnities may be doubled with the use of the new polymer systems, resulting possibly in a 200 watt air-breathing power source weighing 42 pounds and operating for about 12 hours on one charge of chemical in the hydrogen generator.

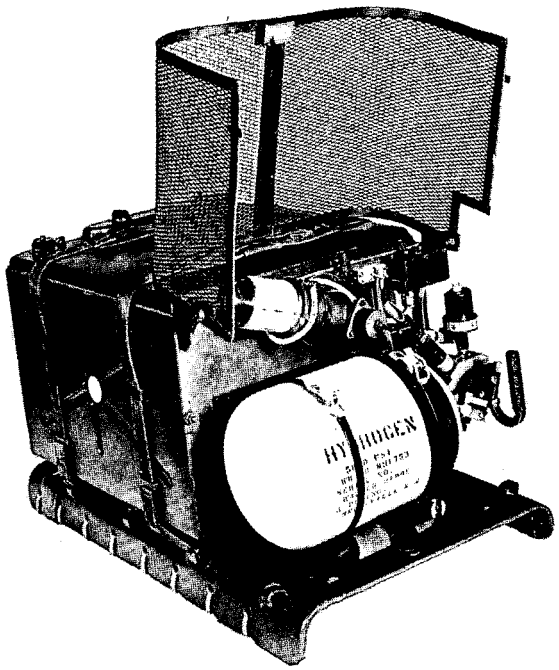

FIGURE 9
END VIEW OF POWER-PACK SHOWING HYDROGEN PRESSURE-BOTTLE GAS SUPPLY

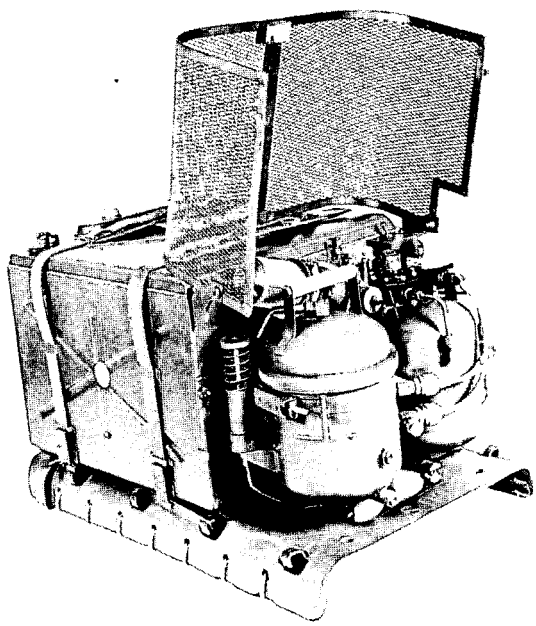

FIGURE 10
END VIEW OF POWER-PACK SHOWING HYDROGEN CHEMICAL-GENERATOR WITH RENEWABLE CANISTER AT LEFT CORNER

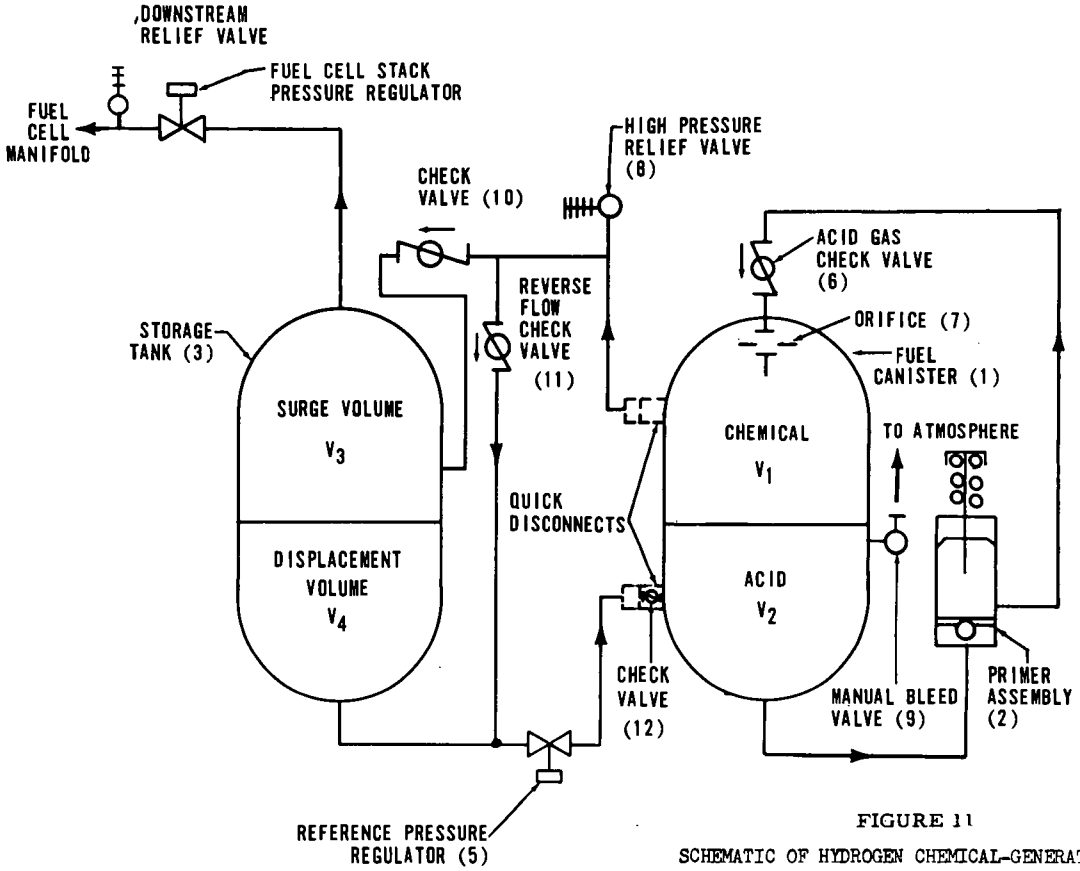

FIGURE 11

SCHEMATIC OF HYDROGEN CHEMICAL-GENERATION SYSTEM

SYMPOSIUM ON FUEL CELLS
PRESENTED BEFORE THE DIVISION OF PETROLEUM CHEMISTRY
AMERICAN CHEMICAL SOCIETY
CHICAGO MEETING, September 3-8, 1961

POLARIZATION AT DIFFUSION ELECTRODES

By

L. G. Austin
Fuel Technology Department, Pennsylvania State University
University Park, Pennsylvania

INTRODUCTION

The theory of electrochemical kinetics at solid electrodes has been well developed and, in particular, the hydrogen evolution reaction has received much study (1). Many fuel cells, however, use porous diffusion electrodes and it is found that the polarization-current curves for fuel cell half-cells do not always correspond to the theory for solid electrodes. Gorin and Recht (2) have considered electrode processes on screen electrodes in molten salts, assuming a well-defined geometry of the metal-gas-electrolyte interface. For low-temperature porous electrodes in aqueous solution, some degree of electrolyte penetration into the porous system is to be expected and concentration gradients in the electrolyte are possible. This paper examines the effect of penetration and also discusses several other relevant features of fuel cell electrode processes.

PROPOSED PHYSICAL MODELS

The general assumption is made that a porous diffusion electrode consists of a highly interlinked porous system. The pores may vary in radius over a wide range but if they are highly interlinked the system can be considered as one pore of very irregular area and cross-section. Consequently, penetration of electrolyte and concentration profiles within the electrode can be considered uniform at a given depth within the electrode (3).

The theory developed below might be expected to apply rather well for a redox system reacting in a porous electrode. In this case the reactant in the electrolyte must diffuse into the electrode and the product, also in the electrolyte, must diffuse back out. Due to mass transport effects, the concentration of reactant within the electrode would fall towards the center of the electrode, while the concentration of product would increase in order to establish sufficient diffusion gradient to remove the product. The theory might also apply for gas evolution on a porous electrode. For example, electrolysis to produce hydrogen would force hydrogen onto the internal surface covered by electrolyte. This hydrogen would diffuse to nucleation sites, probably by diffusion along grain-boundaries and surface irregularities, and be given off as bubbles. Providing the mass transport of gas was not rate restricting and providing the bubbling did not too much disturb the system, the theoretical voltage-current curves developed below might be expected to apply at steady state conditions.

For the case of a gas-diffusion fuel cell electrode it appears unlikely that the electrode would behave exactly like electrolysis in reverse. On the other hand, it is difficult to believe that the reaction area is located only at the conjunction of the gas-solid-liquid meniscus. It seems more reasonable to suppose that gases can diffuse along the surface underneath the bulk of the electrolyte in a pore. A "feeder" system of surface diffusion paths can be visualized, with the geometry of the paths being so small as to maintain gas equilibrium with an appreciable amount of the surface under the electrolyte. The extent of this surface or gas penetration might be small, perhaps being limited to the length of a single crystallite within the metal or carbon. In theory, it should be possible to compare the effective surface utilization during fuel-cell usage with that during electrolysis (gas driven off at the fuel electrode instead of consumed) by comparing the exchange currents for the two cases. In practice, when voltage is applied to a hydrogen fuel cell electrode so that hydrogen is evolved, the current-voltage relation is initially unsteady with time, with appreciable current being passed

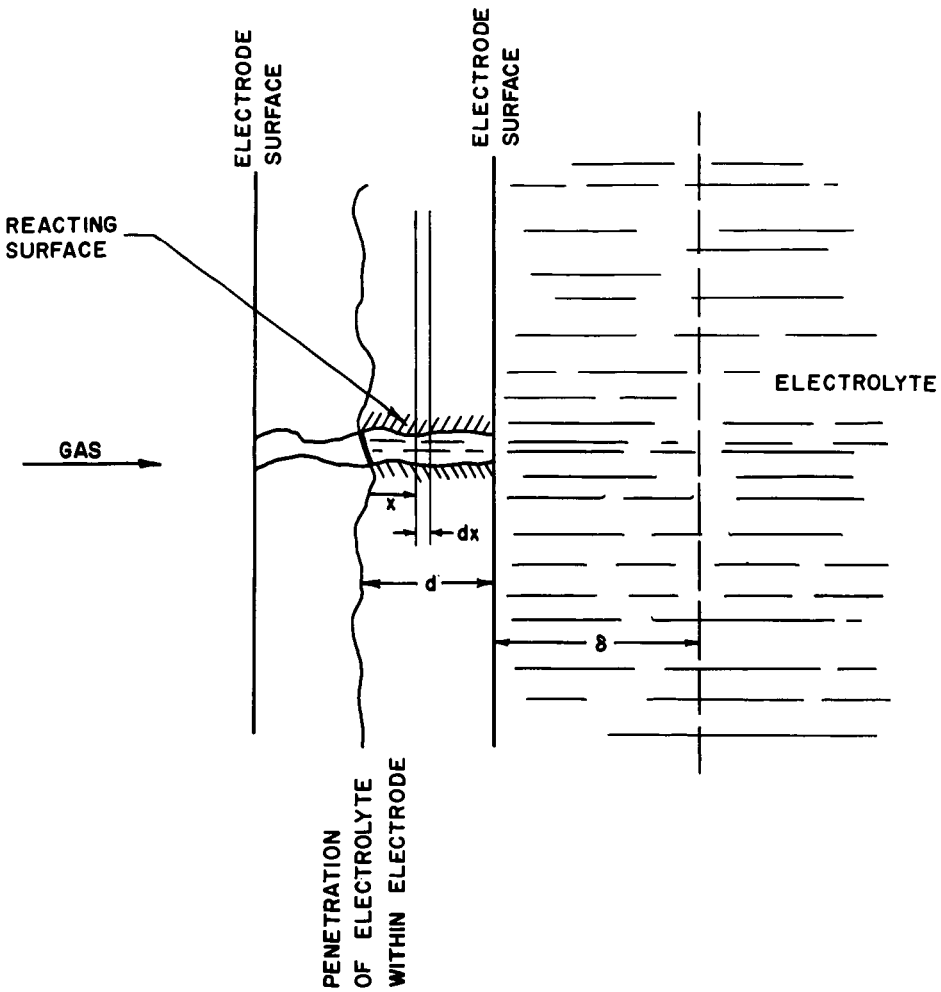

FIGURE I. ILLUSTRATION OF SYSTEM CONSIDERED.

at overvoltages lower than those expected. Presumably this is due to hydrogen being formed on a greater amount of electrolyte-covered surface. Only when this new reacting surface is saturated with the equilibrium quantity of hydrogen will vigorous hydrogen evolution occur. A stable, normal over-voltage/current curve can then be obtained.

The following theory has been derived on the basis of mass transport in the electrolyte as the factor causing polarization. It is possible that mass transport of gas within the "feeder" system is the polarizing factor. The theory would apply equally well to such a system with gas instead of liquid mass transport factors. For electrolyte concentration polarization the limiting current for a given electrode should be dependent on the concentration of electrolyte and independent of the surface catalyst. For gas concentration polarization the limiting current will be a function of gas pressure and if a "feeder" system exists, different surface catalysts might give widely different mass transport coefficients.

EFFECT OF INTERNAL MASS TRANSPORT

Let us consider a system as illustrated in Figure 1. A reactant molecule or ion A in the electrolyte reacts with the surface to give a product B. A must diffuse into the porous system to reach the surface and B must diffuse out of the porous system. The current density at an electrode potential of V is (4)

$$i = kN_s A_e (a_p)^{\alpha} (a_r)^{1-\alpha} \left(e^{-\Delta F_o^*/RT} e^{\alpha \Delta F_o/RT} \left(e^{\alpha n \mathcal{F} \eta/RT} - e^{-(1-\alpha) n \mathcal{F} \eta/RT} \right) \right) \quad (1)$$

where the symbols have the meaning given in the list of nomenclature. Combining factors which are constant for a given system and putting $\eta = E_r - V$, where E_r is the reversible potential,

$$i = K_1 A_e (B)^{\alpha} (A)^{1-\alpha} \left(e^{\alpha n \mathcal{F}(E_r - V)/RT} - e^{-(1-\alpha) n \mathcal{F}(E_r - V)/RT} \right) \quad (2)$$

(A), (B) are the activities of diffusing reactant and product respectively. If (a) is the required function of activities left after removing (A) and (B)

$$K_1 = kN_s (a) e^{-\Delta F_o^*/RT} e^{\alpha \Delta F_o/RT} \quad (3)$$

Consider the case where the reverse reaction represented by the right hand term in the parenthesis in equation 2 is negligible (4). Then

$$i = K_1 A_e (B)^{\alpha} (A)^{1-\alpha} e^{\alpha n \mathcal{F}(E_r - V)/RT} \quad (4)$$

Let S be the area per cm^3 of the porous system in the electrode. Then, at a section dx in the electrolyte/electrode corresponding to x (see Figure 1),

reaction in element dx, per sq cm of geometric area of electrode

$$= K_1 S (B)^{\alpha} (A)^{1-\alpha} e^{\alpha n \mathcal{F} E_r/RT} e^{-\alpha n \mathcal{F} V/RT} dx$$

$$= D(d^2A/dx^2) dx$$

for steady state conditions (assuming activity coefficients to be either unity or constant.) Thus

$$d^2A/dx^2 = K_1 (S/D) e^{-\alpha n \mathcal{F} V/RT} (B)^{\alpha} (A)^{(1-\alpha)} e^{\alpha n \mathcal{F} E_r/RT} \quad (5)$$

If the ohmic resistance within the pores and the electrode is neglected, V must be a constant for the electrode. However, E_r will vary with penetration according to

$$E_r = E_o + (RT/n\mathcal{F}) \ln(A/B) \quad (6)$$

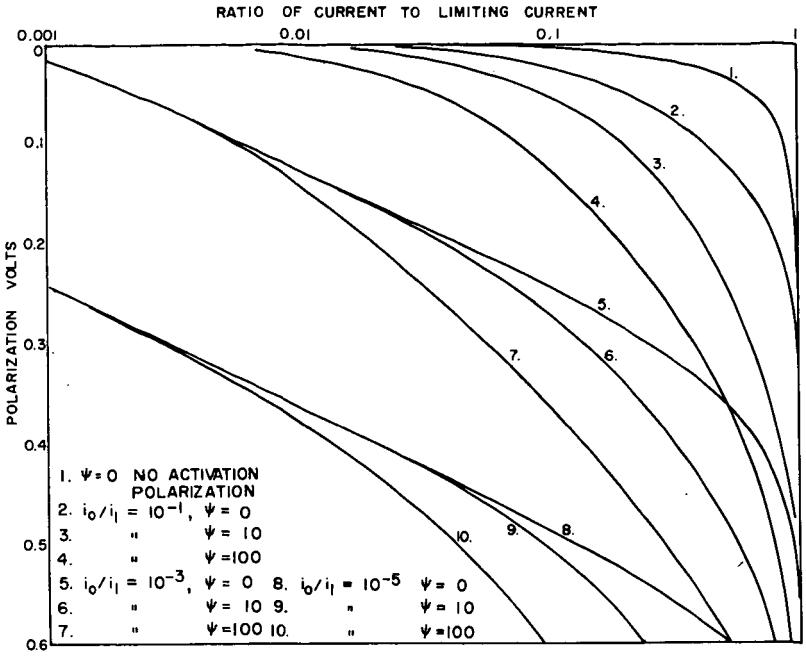

FIGURE 2. RELATION BETWEEN CURRENT, POLARIZATION, EXCHANGE CURRENT, AND Ψ.

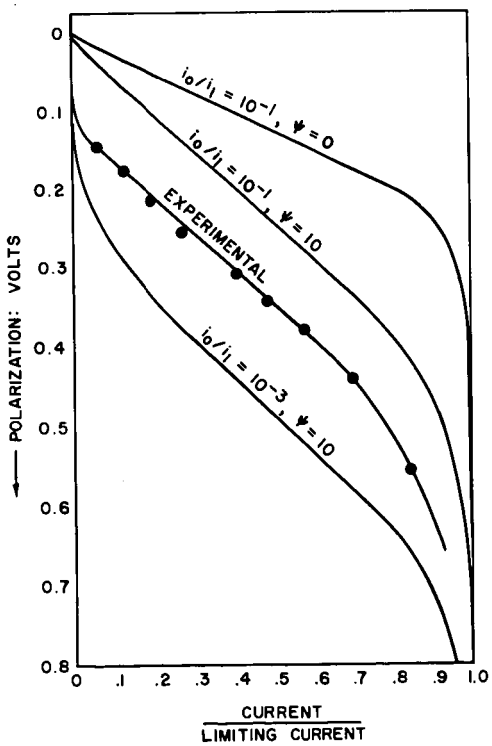

FIGURE 3. COMPARISON OF EXPERIMENTAL AND THEORETICAL POLARIZATION CURVES FOR A POROUS-CARBON H_2 ELECTRODE

Therefore equation (5) can be written as

$$d^2A/dx^2 = K_2(B)^{\alpha}(A)^{1-\alpha}(A)^{\alpha}(B)^{-\alpha} \quad (7)$$

where

$$K_2 = K_1(S/D)e^{-\alpha n\mathcal{F}V/RT}e^{\alpha n\mathcal{F}E_o/RT} \quad (8)$$

Thus

$$d^2A/dx^2 = K_2(A) \quad (9)$$

The solution of this equation for boundary conditions of $A = A_s$ at $x = d$ and $dA/dx = 0$ at $x = 0$ is

$$A = A_s(e^{\sqrt{K_2}x} + e^{-\sqrt{K_2}x})/(e^{\sqrt{K_2}d} + e^{-\sqrt{K_2}d}) \quad (10)$$

The steady state current density (based on the geometric area of electrode) is given by

$$i = D(dA/dx)_{x=d} \quad (11)$$

That is

$$i = DA\sqrt{K_2}\tanh(d\sqrt{K_2}) \quad (12)$$

Let

$$d\sqrt{K_2} = \beta \quad (13)$$

Then

$$i = (D/d)A_s\beta\tanh\beta \quad (14)$$

For a fixed system β is a function of V only.

The effect of concentration polarization in the "stagnant film" on the exterior of the electrode is given by (5)

$$i = (\Delta/\delta)(A_b - A_s) \quad (15)$$

where δ, the thickness of the stagnant film, is defined by equation 15* and Δ is the effective diffusion coefficient (in appropriate units) of A in the electrolyte. The interface concentration A_s is, in general, unknown. Eliminating A_s from equations (14) and (15) gives

$$i = (D/d)A_b\beta^2/(\beta/\tanh\beta + \beta^2/\psi) \quad (16)$$

where

$$\psi = (\Delta/\delta)(d/D) = \frac{\text{ease of mass transport at exterior}}{\text{ease of mass transport in interior}} \quad (17)$$

Now if there were no concentration polarization effects inside or outside of the electrode the current would be the "ideal" current where

$$i_{ideal} = dSK_1(B_b)^{\alpha}(A_b)^{1-\alpha}e^{\alpha n\mathcal{F}(E_{rb}-V)/RT}$$

$$= dSK_1(A_b)e^{\alpha n\mathcal{F}E_o/RT}e^{-\alpha n\mathcal{F}V/RT}$$

From equation 8

$$i_{ideal} = dD\,K_2(A_b)$$

and from equation 13

$$i_{ideal} = (D/d)(A_b)\beta^2 \quad (18)$$

Therefore, from equations (16) and (18)

$$i = \frac{i_{ideal}}{\beta/\tanh\beta + \beta^2/\psi} \quad (19)$$

*The δ concept is retained for convenience as it allows a direct comparison of D with Δ.

In equation (19) the term

$$\frac{1}{\beta/\tanh\beta + \beta^2/\psi} \qquad (20)$$

represents an effectiveness factor for the utilization of the electrode. At low currents it will tend to 1, but at currents approaching the limiting current it will tend to zero. The limiting current is given by

$$i_l = (\Delta/\delta)(A_b) \qquad (21)$$

Therefore

$$(d/DA_b) = \psi/i_l$$

Since $i_{ideal} = i_o e^{\alpha n \mathcal{F}\eta/RT}$ where i_o is the exchange current per unit geometrical area of electrode

$$\beta^2 = \psi(i_o/i_l)e^{\alpha n \mathcal{F}\eta/RT}$$

Thus equation (19) can be expressed as

$$i/i_l = \frac{(i_o/i_l)e^{\alpha n \mathcal{F}\eta/RT}}{\sqrt{\psi(i_o/i_l)e^{\alpha n \mathcal{F}\eta/RT}}/\tanh\sqrt{\psi(i_o/i_l)e^{\alpha n \mathcal{F}\eta/RT}} + (i_o/i_l)e^{\alpha n \mathcal{F}\eta/RT}} \qquad (22)$$

FOUR ZONES OF POLARIZATION VERSUS CURRENT

We can now describe four zones in the polarization current relation. Firstly, at low currents where no mass transport polarization exists and the reverse reaction is appreciable, the polarization versus current relation is

Zone I $$i = i_o(e^{\alpha n \mathcal{F}\eta/RT} - e^{-(1-\alpha)n\mathcal{F}\eta/RT}) \qquad (23)$$

At higher currents the normal Tafel region is reached. In this case, if concentration polarization is negligible the required relation is

Zone II $$i = i_o e^{\alpha n \mathcal{F}\eta/RT}$$

or $$\eta = (2.3RT/\alpha n \mathcal{F}) \log i - (2.3RT/\alpha n \mathcal{F}) \log i_o$$

$$= a + b \log i \qquad (24)$$

The slope of the $\eta/\log i$ curve is b. This can be obtained from equation (19) by noting that at small values of β, $\beta/\tanh\beta$ is one and $\beta^2 \to 0$.

When concentration polarization within the pores of the electrode comes into force and if ψ is large, equation (19) can be simplified to (since $\beta/\tanh\beta$ for $\beta > 2$ is very nearly β),

Zone III $$i = i_{ideal}/\beta$$

$$= \sqrt{(D/d)(A_b)}\, i_o e^{\alpha n \mathcal{F}\eta/2RT}$$

or $$\eta = a^1 + 2b \log i \qquad (25)$$

The slope of the polarization/current curve is now twice the normal Tafel slope.

At higher currents where mass transport in the stagnant film becomes important, $\beta^2/\psi \gg \beta$ and

Zone IV

$$i \rightarrow i_o e^{\alpha n \mathfrak{f} \eta / RT} / (i_o/i_l) e^{\alpha n \mathfrak{f} \eta / RT} \qquad (26)$$

$$\rightarrow i_l$$

Calculated Polarization Versus Current Curves

In practice, the four zones will probably not often occur in discrete recognizable form. For instance, if the penetration of the electrolyte into the electrode is zero then Zone III disappears completely. Furthermore, the transition zones between the various may be quite extended, and the zones themselves relatively short. Figure 2 illustrates the effect of ψ on the polarization-current curve. The representative values of ψ were chosen as follows. The theory of diffusion through porous media (6) indicates that

$$D = \Delta\theta/q \qquad (27)$$

where θ is the porosity and q is a tortuosity factor. Taking θ as 0.3 and q as $\sqrt{2}$ (6)

$$\psi = 5d/\delta$$

δ is of the order (5) of 0.05 cms for unstirred electrolytes, to 0.001 cms for high rates of flow past the electrode. d is possibly in the range of 0 to 0.1 cms. Therefore ψ can quite reasonably range from zero to 500. For unstirred electrolytes a value of ψ of 10 seems reasonable. Therefore, values of ψ of 0, 10 and 100 were used in the calculations.

It is convenient to plot the current in the form given by equation (22), that is, in the dimensionless form i/i_l. The unknown variables in the current-voltage relation are then ψ, i_o/i_l and αn. Figure 2 shows a series of curves, on a logarithmic current basis, calculated from equation (22). The value of αn chosen was 1/2* and the calculations performed for room temperature conditions: the value of b in the Tafel equation is thus approximately 0.12 volts per logarithmic current increment.

Use of Curves

It can be noted from Figure 2 that although there are three adjustable parameters, the curves for values of ψ between 10 and 100 vary in position more than in shape. Change in αn changes the scale of the voltage ordinate, but again the shape of the curves at different values of ψ is fairly definite. Therefore the curves do not represent a theory which can be forced to fit any given set of data.

Figure 3 shows a linear plot of the curves compared with a typical hydrogen half-cell curve for an activated porous carbon electrode (with negligible ir loss to the reference electrode).

Where only the normal concentration polarization in the exterior "stagnant" film is applicable, that is $\psi = 0$, the straight line portion of the curve has a slope of about 2b. Therefore, the cell behaves as if it had an extra ohmic resistance of

$$r = 2b/i_l \qquad (28a)$$

At values of ψ between 10 and 100, the slope is about 3.9b and

$$r = 3.9b/i_l \qquad (28b)$$

Interfering Factors

A number of factors can change the shape of the polarization-current curve in ways not predicted by the theory. Some of these are as follows.

In solving equation 7 it was assumed that the activity of the reactant occurred in first order form. However, if the equation is solved for zero or second order it is found that the final result is the same as equation 22.

It has been assumed that concentrations giving mass transport are proportional to activity gradients giving polarization. The effects of deviations from this assumption are probably fairly small.

*For different values of αn or b, the voltage scale must be adjusted accordingly.

Where more than one reaction path is possible the total current at a certain voltage is the sum of the reaction currents. One current will normally out-weigh the other in the polarization-current relation. However, if the Tafel b coefficient is higher for the predominating reaction at near open-circuit conditions than for another possible reaction, the second reaction may come to be predominating at higher current drains (7). In addition, when the limiting current for a given reaction is reached it is often observed that another more highly polarized reaction can occur to give extra current. This sometimes has the effect of making the limiting current ill-defined.

When consecutive reactions or processes are involved, the polarization at a given current is the interacting sum of the two polarization effects (7). This is so for an electrochemical reaction in series with a mass transport process, or an electrochemical reaction in series with another reaction such as chemisorption or desorption. At low currents the polarization due to one reaction may be negligible but it may become an added polarization at higher currents.

OPEN-CIRCUIT POLARIZATION

Equation 22 was derived on the assumption that the reactions were far from equilibrium and the reverse current negligible (see equation 4). At low currents when the system is near equilibrium this assumption is clearly not true. However, there are a number of factors which make measurements at or near open circuit conditions difficult to interpret. Consequently, this region is sometimes of less importance than the higher current density regions considered. Some of the factors which affect low current density results are as follows.

At low current densities, the currents produced by secondary reactions due to impurities, electrode corrosion, or depolarization by diffusion or leakage of gas to the opposite electrode may be sufficient to interfere with the reaction under investigation. For example, where these reactions have free energies differing from the basic reaction, all of the reactions cannot be at equilibrium at a certain open-circuit potential. The electrode thus tends to assume a mixed open-circuit potential. For precise electrochemical measurements it is necessary to rigorously purify the components to minimize secondary reactions (8), but this is sometimes impossible or undesirable in practical fuel cells.

For high temperature systems it is possible that oxides form on an electrode faster than they can be reduced by the fuel. In this case, the apparent open-circuit potential will be a potential between that corresponding to the fuel pressure and that corresponding to the hypothetical fuel pressure in equilibrium with the oxide. Again, the fuel may be irreversibly cracked at the electrode and the potential will then correspond to the free energy of the active constituent in the fuel gas and not the total free energy of the fuel.

CONCENTRATION POLARIZATION AT LOW CURRENTS

Under certain circumstances, concentration polarization may occur at low currents. Let us consider concentration polarization at conditions where activation polarization is negligible. If the reversible potential corresponding to the bulk activities of the reactants and products is E_b, the actual reversible potential is, for first order reactions,

$$E_r = E_b - (RT/n\mathcal{F}) \ln(R_b P/R P_b)$$

where R, P are the actual activities of reactant and product and R_b, P_b are the bulk activities. Putting

$$\eta = E_b - E_r,$$

$$\eta = (RT/n\mathcal{F}) \ln(R_b P/R P_b) \qquad (29)$$

Now

$$i = k_1(R_b - R) = k_2(P - P_b) \qquad (30)$$

where k_1, k_2 are appropriate mass transport factors in units corresponding to current. Combining equations 29 and 30 to eliminate the unknowns R and P,

$$\eta = (RT/n\mathcal{F}) \ln[(1 + i/P_b k_2)/(1 - i/R_b k_1)] \qquad (31)$$

In normal circumstances R_b, P_b are large quantities and η is negligible at small values of i. However, where a product of reaction is present in only very small bulk concentration, $i/P_b k_2$ may be significant at very low currents. Then

$$i = k_2 P_b (e^{n\mathcal{F}\eta/RT} - 1) \qquad (32)$$

This has the form

$$i = I(e^{\alpha n\mathcal{F}\eta/RT} - e^{-(1-\alpha)n\mathcal{F}\eta/RT})$$

with $\alpha = 1$, and I an apparent exchange current. For appreciable values of η

$$i = P_b k_2 e^{n\mathcal{F}\eta/RT} \qquad (33)$$

For example, consider the formation of peroxide ion in oxygen-alkaline half-cells according to $O_2 + H_2O + 2e \rightarrow OH^- + HO_2^-$.

If the value of the activity of HO_2^- is the equilibrium value of $HO_2^- \rightleftarrows \frac{1}{2}O_2 + OH^-$

then the reversible half-cell voltage corresponds to the reaction $\frac{1}{2}O_2 + H_2O + 2e \rightarrow 2OH^-$.

However, the equilibrium concentration of peroxide ion in the bulk of the solution is of the order of 10^{-16} gm-ions per liter. The mass transport factor is of the order of 25 milliamps per sq cm per gm-ion per liter for unstirred electrolyte. In order to diffuse away peroxide ion the concentration of peroxide ion at the electrode must increase considerably and, since the equilibrium concentration is so small, the increase produces a large deviation from the expected open-circuit value of the

$$\frac{1}{2}O_2 + H_2O + 2e \rightarrow 2OH^-$$

reaction. Substituting values into equation 33 gives

$$i = (25)(10^{-16}) \text{ antilog } (\eta/0.03)$$

This gives a polarization of 0.36 volts at the small current of 2.5 microamps per sq cm and a polarization of 0.51 volts at 250 milliamps per sq cm, for an uncatalyzed electrode.

If a catalyst is added to the surface of the electrode to bring about decomposition of the peroxide according to $HO_2^- \rightarrow OH^- + \frac{1}{2}O_2$,

then polarization is much reduced. Mass transport polarization effects of the OH^- ion are small due to the large bulk concentration of the ion already present. Let us assume that the catalyst causes a first-order decomposition of peroxide at the electrode surface, of the form

$$\text{rate} = k_3 P \qquad (34)$$

where k_3 is a rate constant in amps per sq cm of electrode per gm-ion liter^{-1} of peroxide. Then

$$i = k_2(P - P_b) + k_3 P \qquad (35)$$

and

$$\eta = (RT/n\mathcal{F}) \ln[(i + k_2 P_b)/(k_2 + k_3)P_b]$$

or

$$i = (k_2 + k_3)P_b[e^{n\mathcal{F}\eta/RT} - k_2/(k_2 + k_3)] \qquad (36)$$

For an appreciable value of η

$$i = (k_2 + k_3)P_b e^{n\mathcal{F}\eta/RT} \qquad (37)$$

Comparing equation (37) with equation (33) it is seen that the effect of the catalyst, which increases k_3, is to increase the apparent exchange current. Thus a greater current is required to produce a given amount of polarization.

A more general treatment which combines the effects of activation polarization with the mass transport and catalytic decomposition effects given above is as follows.

The following equations are combined:

$$E_r = E_b - (RT/n\mathcal{F})\ln(P/P_b)$$

$$i = k_2(P-P_b) + k_3P$$

$$i = kN_sA_e(R_b)^{1-\alpha}(P)^{\alpha}(e^{\alpha n\mathcal{F}(E_r-V)/RT} - e^{-(1-\alpha)n\mathcal{F}(E_r-V)/RT})$$

$$= I(P/P_b)^{\alpha}(e^{\alpha n\mathcal{F}(E_r-V)/RT} - e^{-(1-\alpha)n\mathcal{F}(E_r-V)/RT})$$

$$\eta = E_b - V$$

These give

$$i = I\left\{e^{\alpha n\mathcal{F}\eta/RT} - e^{-(1-\alpha)n\mathcal{F}\eta/RT}[(i + k_2P_b)/(k_2 + k_3)P_b]\right\}$$

Then, if i is appreciable and, if P_b is very small,

$$i/P_b \gg k_2$$

Therefore

$$i = \frac{I\, e^{\alpha n\mathcal{F}\eta/RT}}{1 + (I/k_2 + k_3)P_b e^{-(1-\alpha)n\mathcal{F}\eta/RT}} \qquad (38)$$

When $I/(k_2 + k_3)P_b$ is large and at moderate values of η, equation 38 reduces to equation 37. At large values of η, the equation reduces to the normal equation

$$i = Ie^{\alpha n\mathcal{F}\eta/RT}.$$

It should be noted that since I contains a term $(P_b)^{\alpha}$, (see equation 4), then values of I will be about $\sqrt{P_b}$ smaller than the usual exchange currents for unit activities. However, k_3 must still have large values to overcome the influence of the small value of P_b. For any appreciable amount of catalysis k_2 is probably much smaller than k_3 and the equation which is most likely to apply is

$$i = k_3P_be^{n\mathcal{F}\eta/RT} \qquad (39)$$

Of course, many assumptions have been made in the above analysis, but it does serve to show that the current-voltage relation may be almost entirely dependent on the effectiveness of the peroxide decomposing catalyst.

CONCLUSIONS

Very little precise information on the mechanisms and causes of polarization in fuel cells has appeared up to the present. Possibly this is partly due to the previous lack of theories to explain the shape of the polarization-current curves in the range of currents of practical use (9). Stender and Ksenzhek (10) have considered theoretically and experimentally the case where concentration gradients in the electrode are negligible, but appreciable ohmic resistance occurs within the pores. For practical fuel cells, the opposite case considered in this paper is perhaps more generally applicable since high concentrations of strongly conducting electrolytes are used.

Even with the application of the theory developed herein, results of polarization investigations of both gas usage and gas evolution are still sometimes difficult to interpret. For the hydrogen half-cell using porous electrodes, for instance, our experimental work indicates that dual consecutive and simultaneous reaction mechanisms are present with some catalyst materials and electrolytes.

ACKNOWLEDGMENTS

I wish to thank the Office of the Chief of Ordnance, Diamond Ordnance Fuze Laboratories, Washington, and the Ordnance Research Laboratory of the Pennsylvania State University for financial assistance for the fuel cell program of The Pennsylvania State University.

SYMBOLS

a	Tafel constant $(2.3RT/\alpha n\mathcal{F})\log(i/i_o)$.
a^1	Pseudo Tafel constant defined by equation 25.
(a_p)	The product of the activities of reaction products, each raised to the appropriate power necessary to satisfy the Nernst equation for the reaction considered.
(a_r)	As for (a_p), but for the reactants involved.
A	Activity or concentration of the mass transport limited reactant.
A_b	The value of A in the bulk of the electrolyte (or gas phase).
A_e	The effective reaction area per unit geometric area of the electrode.
A_s	The value of A at the external surface of the electrode.
B	The activity or concentration of the product of reaction.
B_b	The value of B in the bulk of the electrolyte.
d	The thickness of the effective reaction penetration in the electrode (see Figure 1).
D	The effective diffusion coefficient of A in the electrode pores.
E_o	The reversible open-circuit potential at unit activity.
E_r	The reversible potential for the concentrations A,B.
E_{rb}	The reversible potential for the concentrations A_b,B_b.
$\mathcal{F}$	Faraday
ΔF_o	Standard state free energy change.
ΔF_o^*	Standard state free energy of activation.
i	Current density.
i_l	Limiting current density.
i_o	Exchange current.
I	An apparent exchange current (equation 32) or, the exchange current for unit activity of P (equation 38).
k	Pre-exponential rate constant in units of current density.
k_1	Mass transport factor defined by equation 30.
k_2	Mass transport factor defined by equation 30.
k_3	Decomposition rate defined by equation 34.
K_1	Constant defined by equation 3.
K_2	Constant defined by equation 8.
K_3	Constant defined by equation A4.
n	Number of electrons in the Nernst equation.
N_s	Number of active sites per unit effective area.
P	Activity or concentration of reaction product at low currents.
P_b	The value of P in the bulk of the electrolyte.
q	Tortuosity factor for pores in the electrode.
r	Apparent ohmic resistance.
S	Surface area of electrode per unit volume.
V	Voltage of electrode.
α	The fraction of polarization aiding the reaction in the direction considered.
β	Parameter defined by equation 13.
δ	Effective thickness of stagnant film.
Δ	Effective diffusion coefficient of reactant in electrolyte.
η	Polarization.
ψ	Parameter defined by equation 17.
θ	Effective cross-sectional area, per unit area, of electrode for mass transport $\simeq$ porosity.

LITERATURE CITED

(1) Parsons, R., "Handbook of Electrochemical Constants", p. 95, Academic Press, Inc., New York, 1959.

(2) Gorin, E., and Recht, H. L., Chapter 8 in "Fuel Cells", Ed. G. Young, Reinhold Pub. Corp., New York, 1960.

(3) Austin, L. G., "Effect of Mass Transport on the Carbon-Carbon Dioxide Reaction", p. 65, Doctoral Thesis, Pennsylvania State University, 1961.

(4) Austin, L. G., Chapter 4 in "Fuel Cells", Ed. G. Young, Reinhold Pub. Corp., New York, 1960.

(5) Kortum, G., and Bockris, J. O'M., "Textbook of Electrochemistry", p. 400, Vol. II, Elsevier Pub. Co., New York, 1951.

(6) Carman, P. C., "Flow of Gases Through Porous Media", p. 46, Academic Press, Inc., New York, 1956.

(7) Parsons, R., Trans. Faraday Soc., (London), 54, 1053 (1958).

(8) Bockris, J. O'M., "Modern Aspects of Electrochemistry", p. 212, Butterworth's Scientific Publications (London), 1954.

(9) Yeager, E., Technical Report 13, "The Measurement of Polarization", p. 17, Office of Naval Research Contract Nonr 2391(00), Project NR359-277, (1960).

(10) Stender, V., and Ksenzhek, O., Zhur. priklad. Khim., 32 III, 121 (1957). Quoted in reference 9 above, p. 18.

APPENDIX

DERIVATION OF THE INTERNAL MASS-TRANSPORT-AFFECTED POLARIZATION RELATION FOR NEAR REVERSIBLE CONDITIONS

Instead of making the assumption involved in equation 4, let us use the full equation

$$i = k_1 A_e (B)^{\alpha} (A)^{1-\alpha} (e^{\alpha n \mathcal{F} (E_r - V)/RT} - e^{-(1-\alpha) n \mathcal{F} (E_r - V)/RT}) \qquad (A1)$$

Substituting for E_r from

$$E_r = E_o + (RT/n\mathcal{F}) \ln(A/B)$$

$$i = K_1 A_e (Ae^{\alpha n \mathcal{F} (E_o - V)/RT} - Be^{-(1-\alpha) n \mathcal{F} (E_o - V)/RT}) \qquad (A2)$$

As before, a differential equation relating concentration and distance is obtained, this time of the form

$$d^2A/dx^2 = K_1 (S/D)(Ae^{\alpha n \mathcal{F} (E_o - V)/RT} - Be^{-(1-\alpha) n \mathcal{F} (E_o - V)/RT}) \qquad (A3)$$

This can be put as

$$d^2A/dx^2 = K_2 A - K_3 B \qquad (A4)$$

where K_2, K_3 are constants. For equimolar counter-diffusion of A and B

$$A + B = A_b + B_b = \text{constant}$$

This assumes that concentration gradients external to the electrode are negligible, that is, we are dealing with the low current range.
Equation A4 can now be expressed as

$$d^2A/dx^2 = (K_2 + K_3) [A - K_3 (A_b + B_b)/(K_2 + K_3)] \qquad (A5)$$

The solution of this equation is similar to that given before, with the end result,

$$i = D[A_b - K_3(A_b + B_b)/(K_2 + K_3)]\sqrt{K_2 + K_3}\ \text{tanhd}\sqrt{K_2 + K_3}$$

$$= D[(A_bK_2 - B_bK_3)/\sqrt{K_2 + K_3}]\text{tanhd}\sqrt{K_2 + K_3} \qquad (A6)$$

Now

$$i_{ideal} = dSK_1(A_be^{\alpha n\mathcal{F}(E_o-V)/RT} - B_be^{-(1-\alpha)n\mathcal{F}(E_o-V)/RT}) \qquad (A7)$$

Therefore

$$A_bK_2 - B_bK_3 = A_bK_1(S/D)e^{\alpha n\mathcal{F}(E_o-V)/RT} - B_bK_1(S/D)e^{-(1-\alpha)n\mathcal{F}(E_o-V)/RT}$$

$$= i_{ideal}/dD$$

and

$$i = \frac{i_{ideal}}{d\sqrt{K_2 + K_3}}\ \text{tanhd}\sqrt{K_2 + K_3} \qquad (A8)$$

When $A_b \simeq B_b$ and if the reaction is near equilibrium, $K_2 \simeq K_3$ and

$$K_2 + K_3 \simeq 2K_2$$

$$\simeq \frac{2\, i_o e^{\alpha n\mathcal{F}\eta/RT}}{dDA} \qquad (A9)$$

Since $d/DA_b = \psi/i_l$,

$$i = \frac{i_{ideal}}{\sqrt{2}\sqrt{\psi i_o/i_l}e^{\alpha n\ \eta/RT}}\ \tanh(\sqrt{2}\sqrt{\psi i_o/i_l}e^{\alpha n\mathcal{F}\eta/RT}) \qquad (A10)$$

This is of the same form as obtained before, except for the numerical factor $\sqrt{2}$, but the i_{ideal} is in this case the complete form

$$i_{ideal} = i_o(e^{\alpha n\mathcal{F}\eta/RT} - e^{-(1-\alpha)n\mathcal{F}\eta/RT})$$

SYMPOSIUM ON FUEL CELLS
PRESENTED BEFORE THE DIVISION OF PETROLEUM CHEMISTRY
AMERICAN CHEMICAL SOCIETY
CHICAGO MEETING, September 3-8, 1961

THEORY OF POLARIZATION OF POROUS GASEOUS-DIFFUSION ELECTRODES

By

H. B. Urbach
Research Laboratories, United Aircraft Corporation
East Hartford, Connecticut

INTRODUCTION

The decay of polarization at the interface between a flat-plate electrode and the adjacent electrolyte has been treated analytically by Grahame (1) and Scott (2). These authors have pointed out that formidable computational difficulties are involved in the determination of kinetic parameters from experimental data because of concentration changes which occur at the interface. However, Grahame (1) has shown that approximate solutions which reveal the major characteristics of the problem can be obtained with the aid of certain simplifying assumptions. The polarization-time curve for the limiting case in which the concentration polarization is zero has been calculated by Grahame, but his results show an extremely rapid decay of the polarization which is not verified by experimental observations of systems in which concentration polarization occurs.

The problems associated with a theoretical treatment of the porous gaseous-diffusion electrode can be expected to be even more complex than those for the flat plate due to the greater geometrical irregularity which results in an increase in concentration polarization. In addition, intensive studies of the porous electrode have revealed additional experimental characteristics that are controversial. For example, Yeager and co-workers (3), using the interrupter technique, have observed polarization vs. current relationships during experiments on the oxygen-fed porous carbon electrode which show that the polarization depends on the resistance of the electrolyte. However, the accepted theory for the interrupter technique indicates that the resistive component of polarization should not be observable with this technique. This paper presents a theory for the porous electrode which includes the resistance of the electrolyte within the pores as well as concentration and activation polarization. The numerical results obtained with this theory are compared with experimental results.

THEORETICAL MODEL

The porous gaseous-diffusion electrode is analogous to a bundle of tubes of uniform radius and length. (4) In the actual porous electrode the tubes or pores are quite tortuous and nonuniform in structure and diameter. In addition they are interconnected. The small pores are flooded and only regions of large diameter have a sufficiently low capillary pressure to be maintained free of electrolyte at the prevailing differential pressure. It is proposed that the pore may be visualized in terms of a constricted tube as depicted in Figure 1. The reaction of the active gas occurs on the wall of the tube in the region of the thin meniscus where the electrolyte and gas are in contact. This active electrochemical area, called the diffuse three-phase zone, is small relative to the total surface of the pore. Electrolytic conduction exists through the length of the pore. In regions where the pore is constricted, there will be considerable current density and, consequently, an appreciable ohmic potential loss may occur. In this model, the pore region in the pore region in the part of the flooded porous structure adjacent to the main body of the electrolyte will be referred to as the mouth. The pore region in the part of the flooded porous structure adjacent to the gas phase will be referred to as the interior region. The constriction in the pore is assumed to separate the interior region and the mouth of the pore. All the resistance of all constrictions which become flooded when the differential gas pressure decreases is lumped into a single resistance, ρ, per unit area of electrode.

Fig. 1

IDEALIZED MODEL OF ELECTRODE PORE

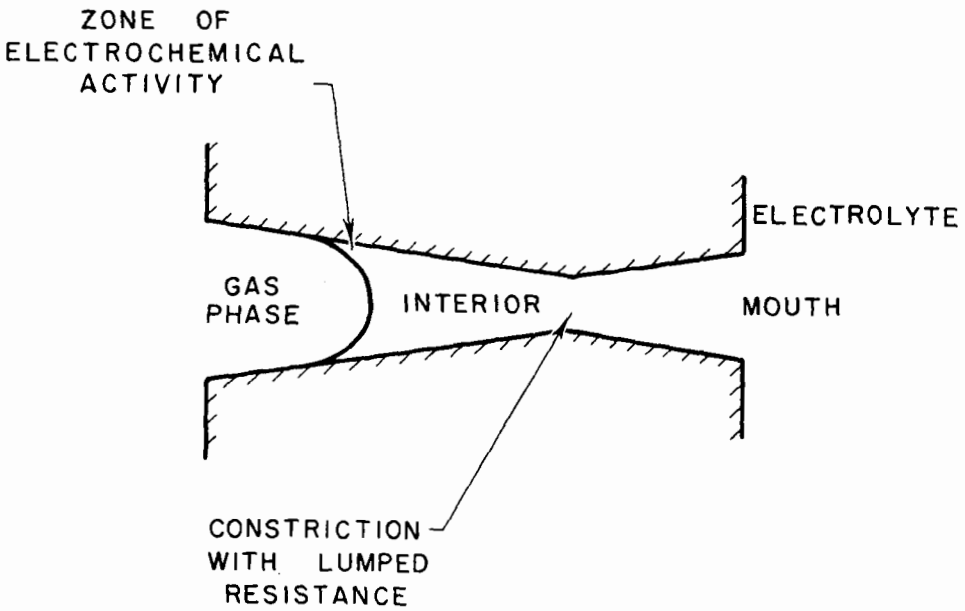

Fig. 2

LOCATION OF ELECTRICAL ANALOGUES IN PORE

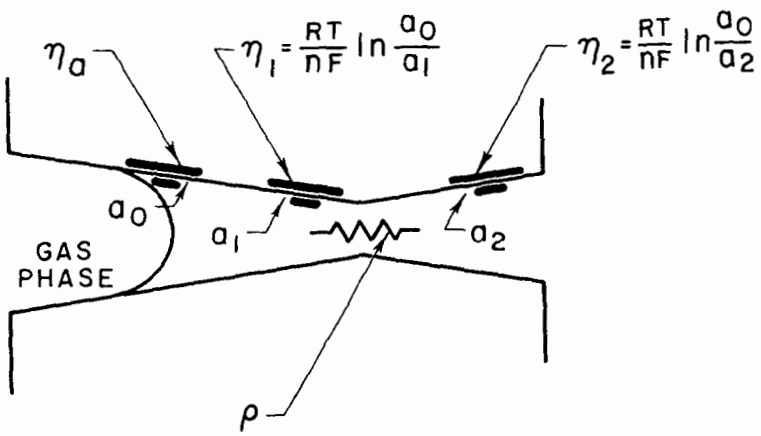

Normally, under open-circuit conditions, the area of the electrode wetted with electrolyte is uniformly covered with a layer of active gas. When a current is drawn which exceeds the flow rate of gas to the mouth, the active electrochemical area degenerates to the diffuse three-phase zone. Where loads are so small that diffusion and convection mechanisms are sufficiently rapid to replace the adsorbed gas which is discharged, the flat-plate model of the electrode becomes adequate. We are concerned here only with loads which result in an active electrochemical area restricted to the diffuse three-phase zone. Under such conditions, there will be a high concentration of active gas in this zone. It is assumed that the electrode is operated in a current range where the gas adsorbed on the surface in the diffuse three-phase zone is approximately in equilibrium with the gas phase. In this area a fixed activity, a_0, of gas is assumed. In the flooded interior of the pore, the equivalent gas-phase activity of the gas at the surface is a_1, while in the mouth of the pore the gas activity is a_2. With these activities, the following concentration potentials exist:

$$\eta_1 = \frac{RT}{nF} \ln \frac{a_0}{a_1} \tag{1a}$$

$$\eta_2 = \frac{RT}{nF} \ln \frac{a_0}{a_2} \tag{1b}$$

where η_1 is the concentration polarization existing in the interior of the pore,
η_2 is the concentration polarization in the mouth of the pore,
R is the gas constant,
T is the absolute temperature,
n is the number of electrons involved in the electrochemical process and
F is the charge equivalent of a gram-mole of electrons.

The discussion below may be generally applied to any gaseous electrode but lte us consider, in particular, the hydrogen electrode in concentrated caustic. The value of the reatios of hydrogen activity may be as high as 10^6 for observed polarization values of 200 mv. Long periods of anodic operation of the hydrogen electrode result in the formation of an activity gradient due to the water formed. Because of the greater volume of space accessible to the water, the water activity ratio never becomes as significant as that of the hydrogen. For a 100% increase in water activity, a 10 mv change can be expected at 90°C. Since water is present in macroscopic quantities compared to surface concentrations of the gas, the decay of water concentration polarization would require much more time (other parameters being equal). For the following discussion we will assume that water concentration polarization is negligible.

When an external load is suddenly removed, the concentration potentials begin to discharge through the long pore. The concentration gradients may relax through normal diffusion of matter, but in fine capillary pores this process is extremely slow compared with electrochemical transport. For this discussion, relaxation of concentration gradients by diffusion is assumed to be insignificant. The discharge of the concentration gradients in the mouth of the pore is limited by resistance and activivation polarization, whereas discharge in the interior of the pore is limited only by the activation polarization. The activation polarization is considered negligible in regions remote from the diffuse three-phase zone because the area is relatively large and the current density is extremely low. The equivalent electrical analog of the discharging process in the pore is shown in Figures 2 and 3. Although potential sources exist everywhere along the interface, for this discussion it is assumed that the potential sources are localized as in Figure 2. The activation polarization is represented by ηa and the capacitances of the double layer (assumed constant) are C_1 and C_2 associated with the interior and mouth portions of the pore, respectively. The equations of potential balance are

$$\eta_a = \eta_1 \tag{2}$$

$$\eta_a = \eta_2 - i_2 \rho \tag{3}$$

where i_2, the current in the resistive leg, is defined as the sum of the faradaic current through the potential source η_2 and the capacitative current discharging from C_2.

Fig. 3

SCHEMATIC DIAGRAM OF ELECTRICAL ANALOGUE OF PORE

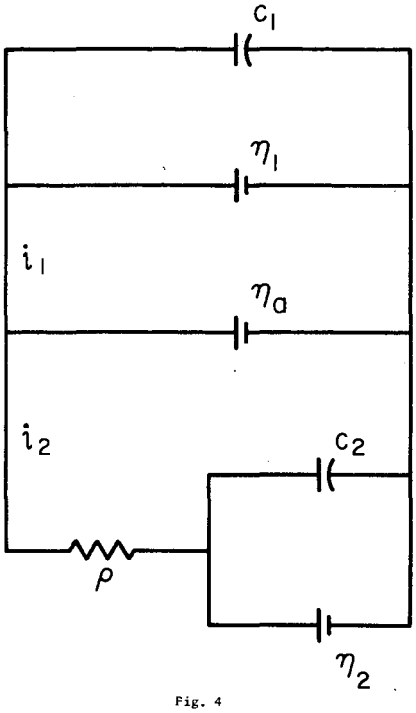

Fig. 4

EFFECT OF C ON POLARIZATION

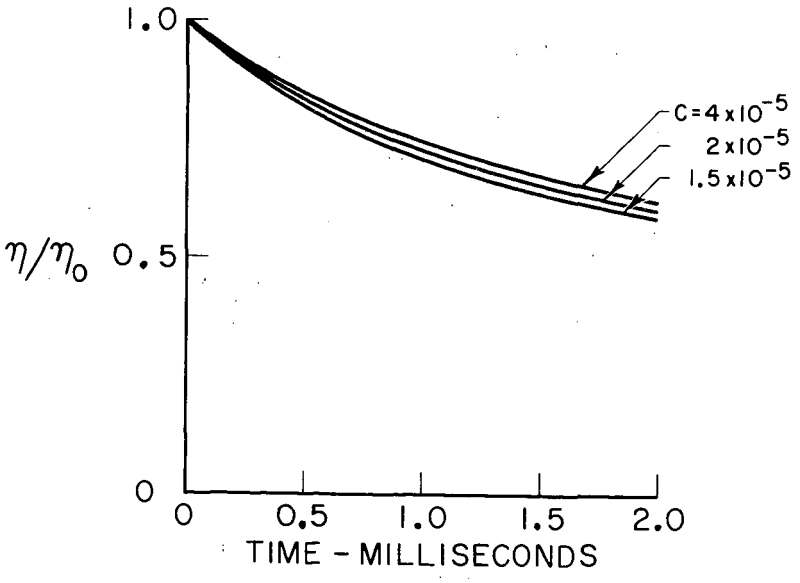

The current i_1 is similarly defined, as the sum of the faradaic current through η_1 and the current discharging from C_1.

$$i_1 = nF \frac{d(V_1 a_1)}{dt} - C_1 \frac{d\eta_1}{dt} \qquad (4a)$$

$$i_2 = nF \frac{d(V_2 a_2)}{dt} - C_2 \frac{d\eta_2}{dt} \cdot \qquad (4b)$$

where V_1 and V_2, the equivalent volumes of gas per cm^2 of surface area, represent the capacity of the surfaces in the interior and mouth of the pore for adsorption of the gas. In the case of discharge of hydrogen ions on a severely oxidized metal lattice, the equivalent volume may be very large. It is assumed that the activity of hydrogen in the mass of the solid heterogeneous oxide changes homogeneously and continuously. In numerical calculation, these volumes can be assumed to include both the equivalent volume of adsorbed gas and the volume of dissolved gas in the electrolyte contained in the appropriate region of the pore.

If the transmission coefficient is 1/2, the equation relating activation polarization and current may be written

$$i_1 + i_2 = 2 i_0 \sinh \frac{nF\eta_0}{2RT} \qquad (5)$$

where i_0 is the exchange current. Equations (1) through (5) can be combined (see Appendix) to yield the following simultaneous, first-order, nonlinear, differential equations.

$$\frac{d\eta_2}{dt} = - \frac{\left(\frac{\eta_2 - \eta_1}{\rho}\right)}{C_2 + \frac{V a_0 n^2 F^2}{RT} e^{-\frac{nF\eta_2}{RT}}} \qquad (6)$$

$$\frac{d\eta_2}{dt} = - \frac{2 i_0 \sinh \frac{nF\eta_1}{2RT} + \frac{\eta_1 - \eta_2}{\rho}}{C_1 + \frac{V a_0 n^2 F^2}{RT} e^{-\frac{nF\eta_1}{RT}}} \qquad (7)$$

These equations are in a form suitable for solution on an analogue computer.

RESULTS OF ANALOGUE COMPUTER CALCULATIONS

Equations (6) and (7) from the preceding section were used to determine the variation of polarization with time for various values of the parameters C, $V a_0$, i_0, and ρ occuring in these equations. The equations were solved using a Berkeley EASE Model 1032 analogue computer at the UAC Research Laboratories.

The values of parameters incorporated into the analogue computer program are listed below.

n = 2 electrons/mole for the case of hydrogen

F = 96,500 coulombs/gram-equivalent of electrons

R = 8.314 joules/degree mole

T = 460 deg K

$C_1 = C_2$ = 1.5×10^{-5} to 4×10^{-5} farad/cm^2

a_0 = 4.46×10^{-5} moles/cm^3 at STP conditions

Fig. 5

EFFECT OF Va_0 ON POLARIZATION

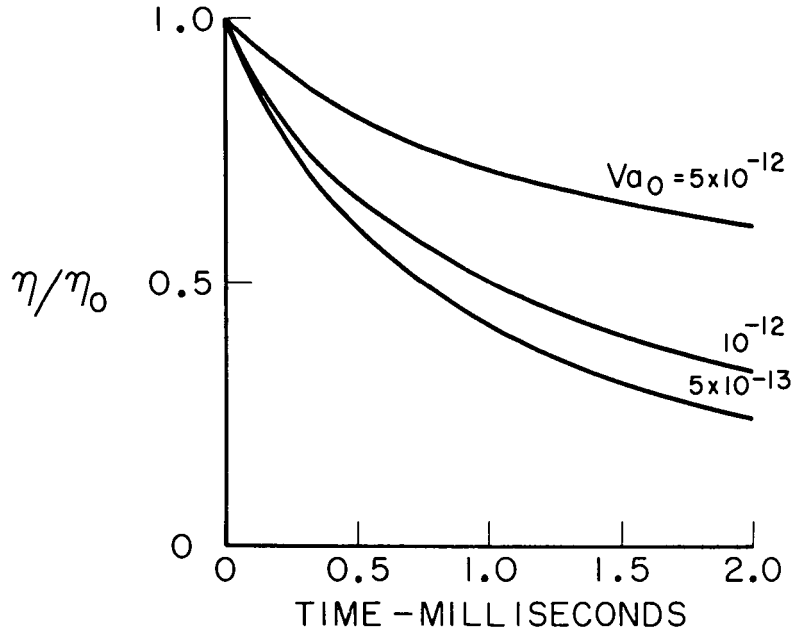

Fig. 6

EFFECT OF i_0 ON POLARIZATION

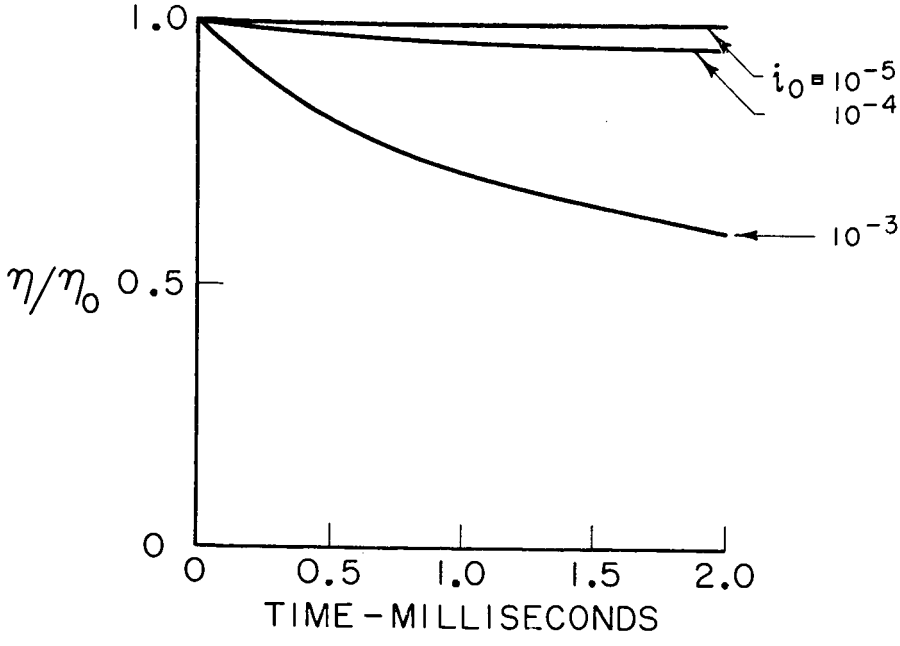

$$\rho = 5 \text{ to } 20 \text{ ohms}$$

$$i_o = 10^{-3} \text{ to } 10^{-5} \text{ amp/cm}^2$$

$$V_1 \text{ to } V_2 = 10^{-8} \text{ to } 10^{-7} \text{ cm}^3/\text{cm}^2 \text{ at STP conditions}$$

$$V_{a_o} = 5 \times 10^{-13} \text{ to } 5 \times 10^{-12} \text{ moles/cm}^2$$

The quantity, V , has units of length since it is volume per unit of area. It represents the effective thickness of the hydrogen-depleted zone to which hydrogen activity is being returned. If the zone is a bare metallic unoxidized surface, the length in question has dimensions of the hydrogen atom, namely 10^{-8} cm. However, this length must be corrected by the molar volume ratio appropriate to the gaseous state which at atmospheric pressure is 10^{-3} to 10^{-2} times as dense as the adsorbed state. In addition, the surface coverage (5) by hydrogen in competition with an electrolyte such as KOH is only about 1% or less so that an additional factor of 10^{-2} or less may be required. The resultant over-all V_o factor is 4.46×10^{-13} or less for the case of pure hydrogen adsorbed on an oxide-free surface. If, however, the surface is in a state of oxidation involving one to 10^4 oxide layers, then the oxide layer may be up to 10^{-4} cm in thickness and the resultant over-all V_{a_o} factor may range from 4.46×10^{-6} to 4.46 to 10^{-12} moles/cm^2 or less. The values used in the computer program are representative of the moderately low range, namely 5×10^{-13} to 5×10^{-12}.

The variation of polarization for various values of the parameters C, V_{a_o}, i_o, and ρ is shown in Figures 4 through 7. The effects of C and V_{a_o} are closely interrelated because of their simultaneous occurrence in the denominators of Equations (6) and (7). If the exponential term is large relative to the initial value of C there is negligible effect until C approaches the magnitude of the exponential. For the value of the variables used in these calculations, the effect of increasing C is to decrease the initial slope and reduce the curvature as shown in Figure 4.

The effect of the magnitude of V_{a_o} is influenced by the rapidly changing exponential factor. At low polarization values and high values of V_{a_o} the capacitance term becomes negligible and the exponential term decreases the slope and increases the flatness of the long time decay portion of the curve as shown in Figure 5.

For a given polarization, increasing i_o causes the slope of the initial portion of the polarization decay curve to increase. This variation is shown in Figure 6. This may also be seen analytically: when C is large compared to the exponential term, Equations (6) and (7) can be combined to give

$$\frac{d\eta_2}{dt} + \frac{d\eta_1}{dt} \cong - \frac{2\, i_o \sinh \frac{nF\eta_1}{2RT}}{C + \frac{V_{a_o} n^2 F^2}{RT} e^{-\frac{nF\eta_1}{2RT}}} \qquad (8)$$

The effect of increasing ρ is similar to the effect of increasing C and V_{a_o} simultaneously. Figure 7 shows the calculated family of curves obtained by varying ρ.

In general, the calculated decay curves shown in Figures 4 through 7 fall off slowly and at a given time the values of polarization are substantially above the values predicted by Grahame (1) for his highly simplified model (see Figure 8). For the case where i_o is 10^{-3} amp/cm^2, C is 2×10^{-5} farad/cm^2, V_{a_o} is 10^{-12} moles/cm^2 and ρ is 10 ohms, the theory presented herein predicts a 50% decay in polarization during the first millisecond. For the same i_o, and C, Grahame's results which neglect concentration changes predicts a 90% decay in polarization after one millisecond.

DISCUSSION

A quantitative comparison of the theory developed in this paper with results obtained experimentally is extremely difficult because of the problems that arise in precise evaluation of such parameters as C and V_{a_o} in an experimental electrode. However, the qualitative comparison of theoretical and experimental results is not difficult. Experimental data for a hydrogen electrode in a KOH cell operating at temperatures of approximately 190°C. were obtained at the UAC Research Laboratories.

Fig. 7

EFFECT OF ρ ON POLARIZATION

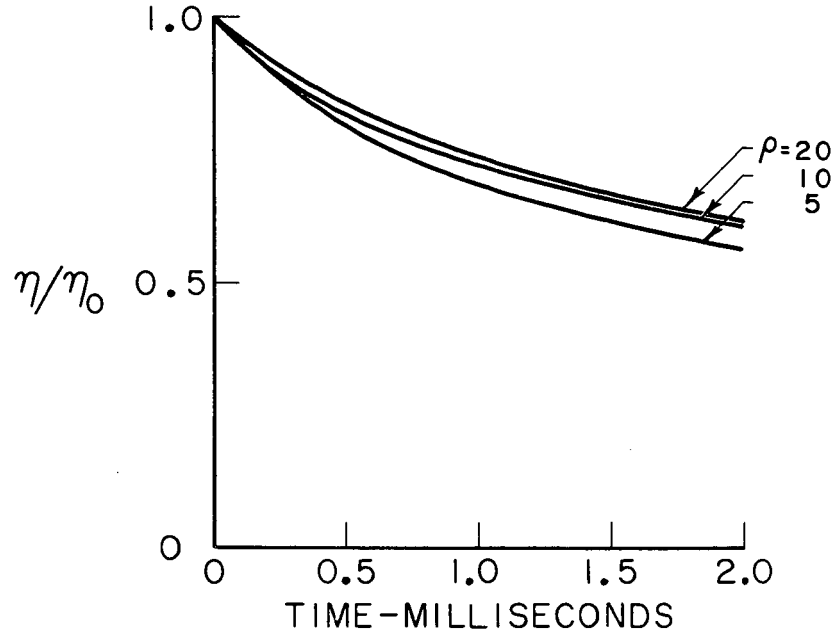

Fig. 8

THEORETICAL DECAY OF POLARIZATION FOR FLAT PLATE WITH NO CONCENTRATION CHANGE

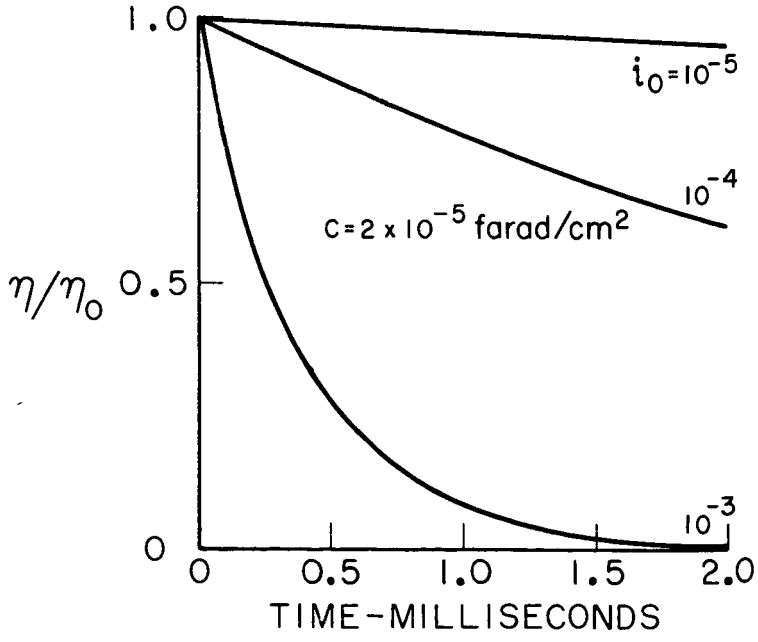

Representative decay curves from these experiments are shown in Figure 9. The shape of these curves is similar to that of the experimental results reported in Reference 6. The most significant feature of these curves is their relatively slow decay (less than 25% for times less than 1 millisecond). This feature is reporduced qualitatively by the theory presented herein as indicated by the theoretical curve shown in Figure 9 which is plotted for a value of i_o equal to 10^{-3} amps/cm^2. The values of i_o for the experimental data were estimated by combining the values of i_2 and η_2 observed experimentally with an experimental value of ρ (of the order of 5 ohms) in Equations (3) and (5). The value of i_o for the limiting case of zero resistance (corresponding to $\eta_2 = \eta_1$) was also calculated. In all cases the estimated values of i_o were found to be between 10^{-2} and 10^{-3} amps/cm^2. The values calculated using the theory proposed in this paper are obviously in better agreement with the experimental data than are those of Grahame. (If the theoretical curve for $i_o = 10^{-2}$ amps/cm^2. had been plotted instead, the agreement with the present theory would not have been as good but the agreement with results calculated from Grahame's theory would have been much worse). Although the theory presented herein is in reasonable agreement with the experimental results, it is obvious that the shape of the experimental curve is not satisfactorily reproduced. The major point of difference between the theoretical and experimental curves is in the relatively fast initial decay coupled with an abrupt change in slope during the first 0.1 millisecond for the experimental case. This abrupt change indicates that two decay processes are operative initially and that one relaxation process is relieved in a short time. It is believed that this process can be accounted for in the theory by removing the assumption that a_o is constant. By considering the relaxation time for a_o to recover to its equilibrium value, closer agreement between theory and experiment should result.

The Resistivity Effect - The shift of the polarization decay curve with change in resistivity of the electrolyte, as indicated in Figure 7, shows that the proposed theoretical model is able to predict a resistivity effect of the type suggested in Reference 3. Further insight into the implication of Equation (3), which is derived from the model, may be obtained if this equation is rearranged in the form

$$\eta_2 = \eta_o + i_2 \rho \qquad (3a)$$

In this form, Equation (3a) can be interpreted as indicating that the observed polarization is a simple addition of a pure activation polarization and a pure ohmic potential loss in the manner of Figure 10. The possibility that such a relation might exist was originally suggested by Yeager. (3) The experimental data of Urbach and Witherspoon (7) lend support to this hypothesis. Figure 11 taken from Reference 7 shows that the cathodic polarization curves of oxygen on carbon electrodes in solutions of potassium hydroxide of varying concentration go through a minimum at 5M KOH at which concentration the conductivity is a maximum. Figure 12 from the same reference shows the different cathodic polarizations for oxygen on carbon electrodes in equal concentrations of sodium and potassium hydroxide. In the potassium hydroxide solution, which is the better conductor, the polarization is lower.

In view of the theory presented here, it is seen that the interrupter technique can reveal an ohmic component of the polarization drop when the external current path is broken because an internal current through the pore continues to flow until the polarization has completely decayed and the ohmic loss must therefore become a component of the observed polarization as shown by Equation (3a). A rough quantitative check on the validity of Equation (3a) can be obtained by examining the polarization vs current curves of Figure 12 for large values of the cell current. The ratio of slopes under these conditions should approximate the resistivities of the electrolytes since, for large values of current

$$\frac{\eta_2}{i_2} = \frac{\eta_o}{i_2} + \rho \cong \rho \qquad (9)$$

In the experimental data of Figure 12, the ratio of slopes for high current densities is 1.3 whereas the ratio of resistivities of sodium and potassium hydroxide is 1.55. The relationship between the ratio of slopes and the ratio of resistivities is good since the ratio of the slopes should be on the low side except in the limit, as indicated by the expression

Fig.9

EXPERIMENTAL POLARIZATION DECAY VS TIME

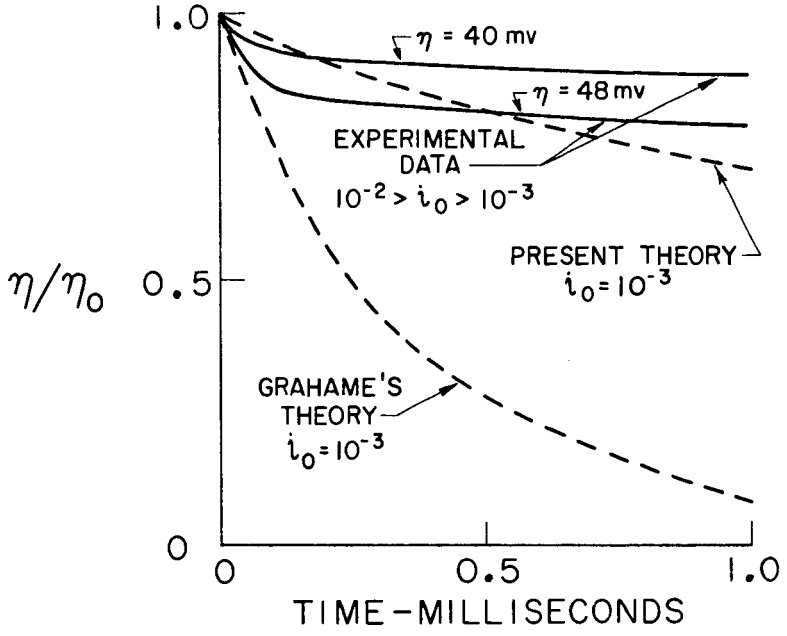

Fig. 10

COMPONENTS OF OBSERVED POLARIZATION IN POROUS ELECTRODE

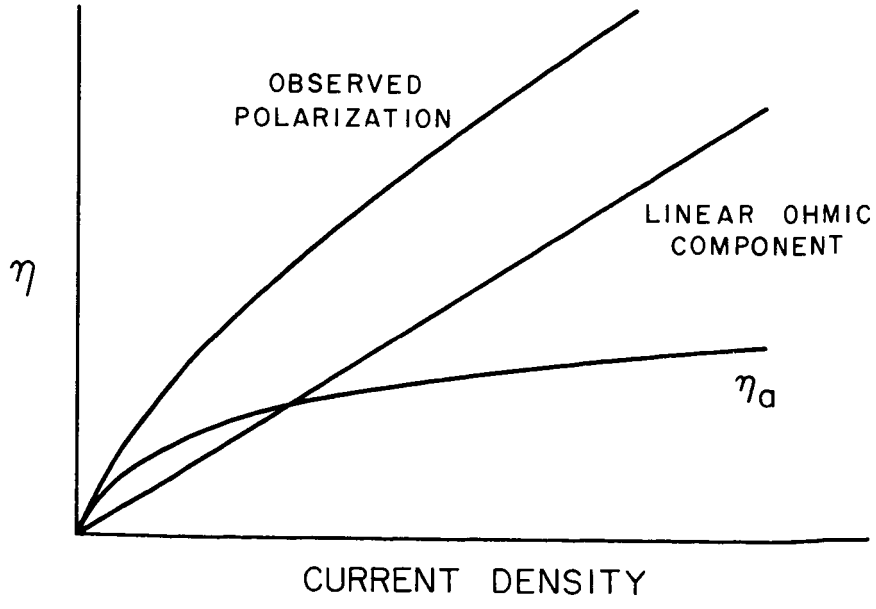

$$\frac{\frac{\eta_a}{i} + \rho_{NaOH}}{\frac{\eta_a}{i} + \rho_{KOH}} < \frac{\rho_{NaOH}}{\rho_{KOH}} \qquad (10)$$

The resistivity effect permits one to write the concentration polarization as the sum of a pure activation polarization and a pure ohmic potential loss factor. This relation is possible only for a concentration polarization within the pore. Concentration polarization outside the pore must be regarded in the classical manner.

Flat Plate as a Special Case of the Porous Electrode - The equations derived from the model postulated herein can be reduced to those of Grahame (1) in the special case where the resistivity, ρ, of the electrolyte approaches zero. In this case Equation (3) can be written

$$\eta_a = \eta_2 \qquad (11)$$

From Equations (2), (3), (6), and (7), we can therefore deduce (see Appendix)

$$\frac{d\eta}{dt} = -\frac{2 i_o \sinh \frac{nF\eta}{2RT}}{C + \frac{V_{a_o} n^2 F^2}{RT} e^{-\frac{nF\eta}{RT}}} \qquad (12)$$

If, in Equation 12, V_{a_o} is representative of a clean unoxidized surface, then the coefficient of the exponential term is negligibly small and we obtain an equation identical in form with Grahame's (1) expression for the flat plate electrode.

The integration of Equation (12) yields

$$2 V_{a_o} nF \left(e^{-\frac{nF\eta}{2RT}} - e^{-\frac{nF\eta_o}{2RT}} \right) + \left(V_{a_o} nF + \frac{RTC}{nF} \right) \ln \frac{\tanh \frac{nF\eta}{4RT}}{\tanh \frac{nF\eta_o}{4RT}} = -i_o t \qquad (13)$$

The constant η_o is the initial polarization. If the concentration polarization has been negligible V_{a_o} becomes extremely small. Therefore, the exponential term in the denominator of Equation (12) may be neglected and Grahame's integrated form can be obtained (Equation 14).

$$\frac{RTC}{nF} \ln \frac{\tanh \frac{nF\eta}{4RT}}{\tanh \frac{nF\eta_o}{4RT}} = -i_o t \qquad (14)$$

Equation (14) was based on the assumption of unchanging concentrations in Grahame's (1) paper. Equation (13) can be extended to the flat plate case if it is assumed that some areas of the flat plate are more anodic than others so that they suffer a slight drift away from the equilibrium concentration of adsorbed hydrogen when under heavy external loads. The more sluggish areas of the electrode may be presumed to possess the equilibrium concentration of matter. If concentrations change, then the integrated form, Equation (13), may represent the polarization decay where the exponential factor is appreciable.

Effect of Change in the Differential Pressure Across an Electrode - One of the practical problems associated with the development of porous electrodes is the determination of the optimum operating pressure drop across an electrode. Experimentally it has been noted that the polarization increases as the differential pressure across an electrode decreases. This effect is qualitatively explained by the present theory on the grounds that the decrease in pressure increases the flooding of the pores and thereby increases the lumped resistance of the electrolyte. Hunger's (4) theory of electrode current limited by the viscous flow of gas through the pore predicts that the current density should be related to the square of the differential pressure. It would seem that a resistive term might be included in Hunger's (4) theory to account for additional current limitation by the ohmic factor.

Fig. 11

EFFECT OF CONDUCTIVITY ON POLARIZATION

REFERENCE 7

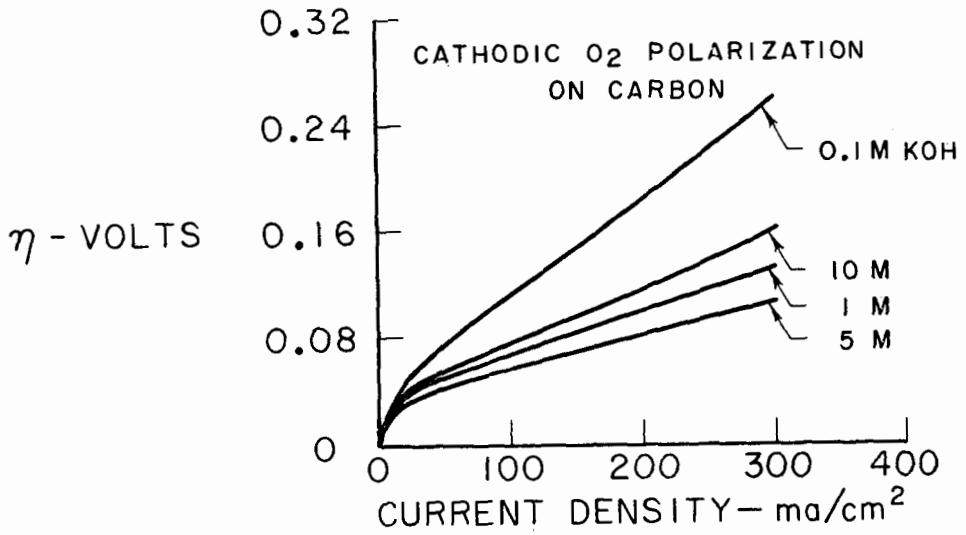

Fig. 12

EFFECT OF CONDUCTIVITY ON POLARIZATION

EQUAL IONIC STRENGTH

REFERENCE 7

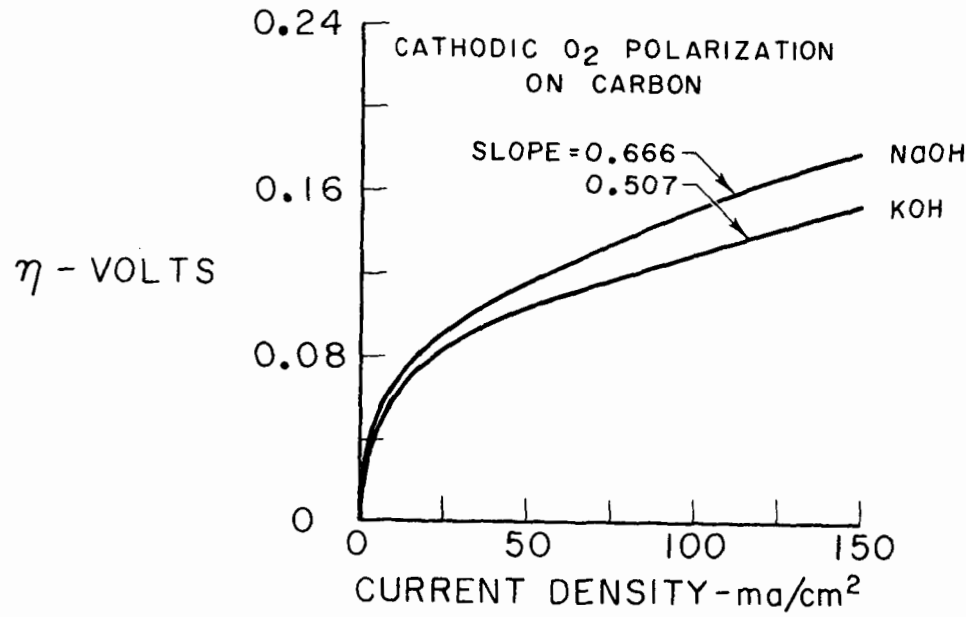

Effect of Increasing the Number of Pores - The present state of porous sintered electrode technology does not permit an unlimited increase of the number of pores within an electrode without concomitant reduction in the diameter of the pores. While the active area may increase with increased numbers of pores, the ohmic-loss factor must also simultaneously increase so that a minimum may be expected in the function relating electrode polarization and pore size.

CONCLUSIONS

A model of the porous electrode has been presented which provides a basis for calculating polarization decay curves for electrodes which have significant amounts of concentration polarization in the pore. Comparison of theoretical and experimental curves shows qualitative agreement between the long-time values of polarization. In particular, the inclusion of concentration polarization eliminates the extremely rapid decay of polarization which was obtained in earlier theoretical studies. (1) The model gives rise to a quantitative relation between the observed polarization and the ohmic potential loss which is in agreement with some experimental data and concepts suggested by Yeager. (3) Finally, the treatment indicates that concentration polarization inside a pore behaves as the sum of a pure ohmic potential loss and a pure activation polarization.

APPENDIX

The basic Equations (1) through (5) lead to the results of Equations (6) and (7) as shown below.

Eliminating η_d from Equations (2) and (3) it follows that

$$i_2 = \frac{\eta_2 - \eta_1}{\rho} \tag{15}$$

Eliminating i_2 from Equations (4b) and (15) it follows that

$$nF \frac{d(V_2 a_2)}{dt} - C_2 \frac{d\eta_2}{dt} = \frac{\eta_2 - \eta_1}{\rho} \tag{16}$$

Equation (1b) can be rearranged and differentiated.

$$\frac{da_2}{dt} = -\frac{a_0 nF}{RT} e^{-\frac{nF\eta_2}{RT}} \frac{d\eta_2}{dt} \tag{17}$$

The volume, V_2, is constant and $\frac{da_2}{dt}$ can be eliminated from Equation (16) with the expression (17).

$$-\left(\frac{V_2 a_0 n^2 F^2}{RT} e^{-\frac{nF\eta_2}{RT}} + C_2 \right) \frac{d\eta_2}{dt} = \frac{\eta_2 - \eta_1}{\rho} \tag{18}$$

Equation (6) is a rearrangement of Equation (18).

Equations (4a) and (4b) may be added to yield that the total current.

$$i_1 + i_2 = nF \frac{d(V_1 a_1)}{dt} + \frac{nFd(V_2 a_2)}{dt} - C_1 \frac{d\eta_1}{dt} - C_2 \frac{d\eta_2}{dt} \tag{19}$$

If Equation (2) is multiplied by $\frac{nF}{2RT}$, and the hyperbolic sine of each member is taken, then using Equation (5) one obtains

$$\frac{i_1 + i_2}{2 i_0} = \sinh \frac{nF\eta_1}{2RT} \tag{20}$$

Using (17) and the analogous equation for i_1 Equation (19) can be written

$$i_1 + i_2 = -\frac{V_1 a_0 n^2 F^2}{RT} e^{-\frac{nF\eta_1}{RT}} \frac{d\eta_1}{dt} - \frac{V_2 a_0 n^2 F^2}{RT} e^{-\frac{nF\eta_2}{RT}} - C_1 \frac{d\eta_1}{dt} - C_2 \frac{d\eta_2}{dt} \qquad (21)$$

Using (21) to eliminate $i_1 - i_2$ Equation (20) can be written

$$-\left(\frac{V_1 a_0 n^2 F^2}{RT} e^{-\frac{nF\eta_1}{RT}} + C_1\right) \frac{d\eta_1}{dt} - \left(\frac{V_2 a_0 n^2 F^2}{RT} e^{-\frac{nF\eta_2}{RT}} + C_2\right) \frac{d\eta_2}{dt} = 2 i_0 \sinh \frac{nF\eta_1}{2RT} \qquad (22)$$

The derivative of η_2 with its coefficient can be eliminated through (18) so that

$$-\left(\frac{V_1 a_0 n^2 F^2}{RT} e^{-\frac{nF\eta_1}{RT}} + C_1\right) \frac{d\eta_1}{dt} + \frac{\eta_2 - \eta_1}{\rho} = 2 i_0 \sinh \frac{nF\eta_1}{2RT} \qquad (23)$$

Equation (23) is a rearrangement of Equation (7).

Equation (11) leads to Equation (12) in the following manner. In Equation (5) we write i for $(i_1 - i_2)$ and using Equation (4a) without subscripts we eliminate the current.

$$nFV \frac{da}{dt} - \frac{C d\eta}{dt} = 2 i_0 \sinh \frac{nF\eta}{2RT} \qquad (24)$$

Using Equation (17) $\cdot \frac{da}{dt}$ can be eliminated to yield (25) which is a form of (12).

$$-\left(\frac{V a_0 n^2 F^2}{RT} e^{-\frac{nF\eta}{RT}} + C\right) \frac{d\eta}{dt} = 2 i_0 \sinh \frac{nF\eta}{2RT} \qquad (25)$$

Equation (12) can be rearranged and integrated to give

$$\int_{\eta_0}^{\eta} \frac{\left(\frac{V a_0 n^2 F^2}{RT} e^{-\frac{nF\eta}{RT}} + C\right)}{\sinh \frac{nF\eta}{2RT}} d\eta = -2 i_0 \int_0^t dt \qquad (26)$$

The exchange current is relatively unaffected by changes in concentration since a_0 was assumed constant. The left member of (26) can be broken into a sum of integrals.

$$C \int \operatorname{csch} \frac{nF\eta}{2RT} d\eta + \frac{V a_0 n^2 F^2}{RT} \left[- \int e^{-\frac{nF\eta}{2RT}} d\eta + \right. \qquad (27)$$

$$\left. \frac{1}{2} \int \frac{e^{-\frac{nF\eta}{2RT}}}{1 + e^{-\frac{nF\eta}{2RT}}} d\eta + \frac{1}{2} \int \frac{e^{-\frac{nF\eta}{2RT}}}{1 - e^{-\frac{nF\eta}{2RT}}} d\eta \right] = -2 i_0 t$$

When the integration is performed the result is Equation (13).

$$2Va_0nF\left(e^{-\frac{nF\eta}{2RT}}-e^{-\frac{nF\eta_0}{2RT}}\right)+\left(Va_0nF+\frac{RTC}{nF}\right)\ln\frac{\tanh\frac{nF\eta}{4RT}}{\tanh\frac{nF\eta_0}{4RT}}=-i_0t \qquad (13)$$

ACKNOWLEDGMENT

The author wishes to express his appreciation to Mr. D. G. McMahon for his helpful criticism and discussion. In addition, he extends his thanks to Mr. Frank Scanlon for his assistance in the analogue computation.

LITERATURE CITED

(1) Grahame, D. G., J. Phys. Chem., 57, 757 (1953).
(2) Scott, T., J. Chem. Phys., 23, 1936 (1955).
(3) Urbach, H. B., Witherspoon, R. R., and Yeager, E., Abstracts of the Spring Meeting of the American Chemical Society, New York, N. Y., April, 1953.
(4) Hunger, H., USASRDL Technical Report 2001, AD-219732, December 15, 1958.
(5) Schuldiner, S., J. Electrochem. Soc., 106, 891 (1959).
(6) Armstrong, G., and Butler, J. A. V., Trans Faraday Soc., 29, 1261 (1933).
(7) Urbach, H., and Witherspoon, R. R., Thesis, "Kinetics of the Oxygen Electrode". Western Reserve University, Cleveland, Ohio, October 1953.

SYMPOSIUM ON JET FUELS
PRESENTED BEFORE THE DIVISION OF PETROLEUM CHEMISTRY
AMERICAN CHEMICAL SOCIETY
CHICAGO MEETING, September 3-8, 1961

POTENTIAL DISTRIBUTION AND INTERNAL RESISTANCE IN ELECTROCHEMICAL MATRIX CELLS WITH DISCONTINUOUS CONTACTS

By

M. Eisenberg and L. Fick
Lockheed Missiles & Space Division, Sunnyvale, California

I. INTRODUCTION

Recent advances in the field of electrochemical fuel cells have brought about renewed interest in cells employing either solid electrolytes or solid matrices holding electrolytes. Thus interest stems from a tendency to avoid the difficulties resulting from the use of fluid electrolytes, such as "flooding" of the electrode and other problems in the maintenance of a 3-phase equilibrium at a gaseous electrode. These difficulties are readily avoided when a solid-matrix electrolyte is employed, such as found in ion-exchange membrane cells or the Ketelaar-type high temperature fuel cells. On the other hand, the use of such electrolytes involves two other possible difficulties.

One is the practical problem of assurance that the electrode material makes a uniform contact with the electrolyte matrix throughout the area; and the other, the more fundamental problem of an increased effective cell resistance, resulting from the necessity of employing discontinuous contact electrodes to assure satisfactory access of the gaseous reactant. It is the latter problem that this paper is concerned with.

In practice, the contact electrodes are in the form of either a screen pressed against the electrolyte matrix or membrane by means of backup plates or in the form of perforated metal sheets. The interesting question is then, how does the resistance of such a cell compare to that of a cell of identical dimensions which would employ solid continuous electrodes? A mathematical treatment of this problem requires idealization of geometry. Thus, for the case of screens, one can assume that the contact points are in the shape of either squares or circles located on square centers; for the case of perforated plates, the contact area may be that left after the punching of square or round holes on square centers in a continuous sheet.

The problem of square contacts was first considered by Gorin and Recht (1). Their solution, basically correct, was found, however, to be slowly convergent (2), necessitating at least a 100 term computation for the summation terms. For very thin electrolyte layers and screens with a low ratio of contact area to total area, it was found, for instance, that computation of only 10 terms would lead to an error, in the resistance value, of the order of 100%.

This paper restates the solution for the case of square contacts and solves three other cases, namely circular contacts and contact electrodes with square holes and round holes on square centers. Two important aspects must be borne in mind. One is that the solution inquires only about the primary potential (or current) distribution. It does not deal with the more complex problem resulting from polarization contributions (i.e., with the secondary distribution problem). The other point is of a practical nature arising from the fact that the contact geometry is idealized for the sake of the mathematical models, amenable to an exact solution of the Laplace equation. In practice, however, metal powder or other catalysts are employed together with the screens or contact plates so that the actual cell resistance may be different. Still, however, information obtained from such computations is desirable for a first order estimate of the resistivity of the cells with discontinuous contact electrodes.

In order to bring the solutions of the four cases into the realm of practical interest, numerical computations of the exact solutions were performed, employing ranges of geometric parameters corresponding to those of practically available screens and plates.

TABLE I

RESULTS OF RESISTANCE RATIO CALCULATIONS

Electrolyte Thickness h (inches)	Dimension C (inches)	% Area Contact	RESISTANCE RATIO R_{eff}/R			
			Square Contacts	Circular Contacts	Square Holes	Circular Holes
0.040"	0.004"	1	21.0170	16.7620		
		2	10.4728	9.4411		
		5	4.3832	4.3512	1.3549	
		10	2.4672	2.5215	1.2747	
		15	1.8644	1.9014	1.2302	
		25	1.4132	1.4222	1.1759	1.2215
		40	1.1836	1.1776	1.1276	1.1203
		50	1.1146	1.1052	1.1047	1.0861
		60				1.0624
		75	1.0332		1.0603	1.0372
0.040"	0.008"	1	40.8890	32.5241		
		2	19.9456	17.8824		
		5	7.7666	7.7024	1.7098	
		10	3.9345	4.0431	1.5494	
		15	3.2886	2.8029	1.4604	
		25	1.8264	1.8440	1.3519	1.4431
		40	1.3672	1.3552	1.2373	1.2406
		50	1.2293	1.2103	1.2094	1.1721
		60				1.1248
		75	1.0821		1.1207	1.0744
0.040"	0.010"	1	50.8612	40.4051		
		2	24.6819	22.1031		
		5	9.4583	9.3781	1.8873	
		10	4.6682	4.7848	1.6868	
		15	3.1611	3.2536	1.5755	
		25	2.0330	2.0555	1.4399	1.5539
		40	1.4590	1.4440	1.3191	1.3008
		50	1.2866	1.2629	1.2618	1.2152
		60				1.1560
		75	1.0831		1.1508	1.0929
0.040"	0.012"	1	60.8334	48.2862		
		2	29.4187	26.3237		
		5	11.1500	11.0537	2.0648	
		10	5.4018	5.5647	1.8241	
		15	3.5932	3.7043	1.6906	
		25	2.2396	2.2666	1.5278	1.6646
		40	1.5508	1.5328	1.3829	1.3610
		50	1.3439	1.3155	1.3142	1.2582
		60				1.1872
		75	1.0997		1.1810	1.1115
0.040"	0.016"	1	80.7779	64.0482		
		2	38.8915	34.7649		
		5	14.5332	14.4049	2.4197	
		10	6.8691	7.0862	2.0988	
		15	4.4577	4.6057	1.9214	
		25	2.6528	2.6888	1.7038	1.8862
		40	1.7344	1.7105	1.5106	1.4813
		50	1.4586	1.4207	1.4189	1.3443
		60				1.2496
		75	1.1330		1.2413	1.1487

II. MATHEMATICAL FORMULATION

(1) General

The effective internal resistance of the flat galvanic cell, illustrated in cross-section in Figure 1, may be computed from the potential distribution obtained from the solution of the Laplace equation:

$$\nabla^2 V = 0 \qquad (1)$$

relating the potential V to the position in the electrolyte under steady state conditions. From the general solution for the potential, the cell resistance can be obtained by calculating the potential difference between the electrode-electrolyte interfaces (at positions $\frac{h}{2}$ and $-\frac{h}{2}$ in Figure 1). The effect of the cell and electrode geometry is best expressed as the ratio of the effective resistance (Reff) to the resistance (R) of a cell consisting of two solid continuous plane electrodes.

When A_c (see nomenclature) represents the conducting portion of the area element of size 2d x 2d, then the boundary condition at the contacts with the electrolyte is (see Figures 1 and 2):

$$\left.\frac{\partial V}{\partial z}\right]_{z = \pm \frac{h}{2}} = \frac{i\,S}{Ac/4d^2} = K \qquad (2)$$

over the contact area Ac (with periodicity in the x and y directions) and

$$\left.\frac{\partial V}{\partial z}\right]_{z = \pm \frac{h}{2}} = 0$$

elsewhere on the electrode plane.

It should be noted that (see nomenclature and Figure 2) for screen electrodes (square and circular contacts) $A_c = A$; for perforated plates $A_c = 4d^2 - A$.

Due to the periodicity in the x and y directions, the general form of the potential, V, is assumed to be:

$$V = \sum_{n=1}^{\infty} \sum_{m=1}^{\infty} a_{nm}(z) \cos \frac{n\pi x}{d} \cos \frac{m\pi y}{d} + C_0 + C_1 \qquad (3)$$

where n, m = 0, 1, 2, 3, ... in the x and y directions respectively. Substitution into equation (1) gives:

$$\nabla^2 V = \sum_{n=1}^{\infty} \sum_{m=1}^{\infty} \left[\frac{\partial^2 a_{nm}}{\partial z^2} - \frac{(n^2+m^2)\pi^2}{d^2} a_{nm}\right] \cdot \qquad (4)$$

$$\cdot \cos\left(\frac{n\pi x}{d}\right) \cos\left(\frac{m\pi y}{d}\right) = 0$$

The above indicates that the Fourier coefficient a_{nm} is of the form:

$$a_{nm} = b_{nm} \sinh\left(\frac{\pi z \sqrt{n^2+m^2}}{d}\right) \qquad (5)$$

the sinh (rather than cosh) being chosen because of the necessity for an even function to express the relationship. Substituting (5) into (3) and taking the partial derivative with respect to z one obtains:

$$\left.\frac{\partial V}{\partial z}\right]_{z = \pm \frac{h}{2}} = C_1 + \frac{\pi}{d} \sum_{n=1}^{\infty} \sum_{m=1}^{\infty} b_{nm} \sqrt{n^2+m^2} \cos \frac{n\pi x}{d} \qquad (6)$$

$$\cdot \cos \frac{m\pi y}{d} \cosh \frac{\pi h \sqrt{n^2+m^2}}{2d}$$

Electrolyte Thickness h (inches)	Dimension C (inches)	% Area Contact	RESISTANCE RATIO R_{eff}/R			
			Square Contacts	Circular Contacts	Square Holes	Circular Holes
0.080"	0.016"	1	40.8890	32.5241		
		2	19.9456	17.8824		
		5	7.7666	7.7024		
		10	3.9345	4.0431		
		15	3.2886	2.8029		
		25	1.8264	1.8440		1.4431
		40	1.3672	1.3552		1.2406
		50	1.2293	1.2103		1.1721
		60				1.1248
		75	1.0821			1.0744
0.080"	0.020"	1	50.8612	40.4051		
		2	24.6819	22.1031		
		5	9.4583	9.3781		
		10	4.6682	4.7848		
		15	2.3550	3.2536		
		25	2.0330	2.0555		1.5539
		40	1.4590	1.4440		1.3008
		50	1.2866	1.2629		1.2152
		60				1.1560
		75	1.0831			1.0929
0.120"	0.004"	1	7.5817	6.2013		
		2	4.1260	3.7856		
		5	2.1164	2.1059	1.1171	
		10	1.4842	1.5021	1.0907	
		15	1.2852	1.2975	1.0760	
		25	1.1363	1.1393	1.0581	1.0731
		40	1.0606	1.0586	1.0421	1.0397
		50	1.0378	1.0347	1.0346	1.0284
		60				1.0206
		75	1.0110		1.0199	1.0123
0.120"	0.008"	1	14.1633	11.4028		
		2	7.2519	6.5711		
		5	3.2329	3.2118	1.2343	
		10	1.9683	2.0004	1.1813	
		15	1.5705	1.5949	1.1519	
		25	1.2727	1.2786	1.1161	1.1462
		40	1.1212	1.1172	1.0842	1.0794
		50	1.0756	1.0694	1.0691	1.0568
		60				1.0412
		75	1.0219		1.0398	1.0245
0.120"	0.010"	1	17.5539	14.0824		
		2	8.8624	8.0062		
		5	3.5928	3.7815	1.2946	
		10	2.2178	2.2629	1.2280	
		15	1.7174	1.7482	1.1911	
		25	1.3429	1.3504	1.1460	1.1839
		40	1.5238	1.1553	1.1059	1.0999
		50	1.0951	1.0873	1.0869	1.0714
		60				1.0518
		75	1.0276		1.0501	1.0309

(4) Solution for Circular Contacts

For circular contacts of radius c on 2d centers (see Figure 2C) the expression for C_1 is:

$$C_1 = \frac{\pi}{4} K r^2 \tag{14}$$

and the expression for R_{eff}/R is:

$$\frac{R_{eff}}{R} = 1 + \frac{16d}{\pi^2 rh} \sum_{n=1}^{\infty} \frac{J_1(n\pi r)}{n^2} \tanh \frac{n\pi h}{2d} \tag{15}$$

$$+ \frac{16d}{\pi^2 rh} \sum_{n=1}^{\infty} \sum_{m=1}^{\infty} \frac{J_1(\sqrt{n^2+m^2}\,\pi r)}{n^2 + m^2} \tanh \frac{\sqrt{n^2+m^2}\,\pi h}{2d}$$

Where J_1 is the Bessel function of the first kind of order 1.

(5) Solution for Plane Electrodes with Circular Holes

For this case (see Figure 2D), the expression for K is:

$$K = \frac{i \int}{(1 - \frac{\pi r^2}{4})} \tag{16}$$

since $A_c = 4d^2 - A$

and the expression for R_{eff}/R is:

$$R_{eff}/R = 1 - \frac{4c}{\pi h(1 - \frac{\pi r^2}{4})} \sum_{n=1}^{\infty} (-1)^n \frac{J_1(n\pi r)}{n^2} \cdot \tag{17}$$

$$\cdot \tanh \frac{n\pi h}{2d} - \frac{4c}{\pi h(1 - \frac{\pi r^2}{4})} \sum_{n=1}^{\infty} \sum_{m=1}^{\infty} (-1)^{m+n}$$

$$\cdot \frac{J_1(\sqrt{n^2 + m^2}\,\pi r)}{m^2 + n^2} \tanh \left(\frac{\sqrt{n^2 + m^2}\,\pi h}{2d} \right)$$

III. RESULTS OF COMPUTATIONS

The solutions of the single and double summations in equations (11), (13), (15) and (17), for the four electrode configurations outlined in the preceding section, all exhibit the same convergence characteristics. The value of the sums (both single and double) plotted against the number of terms computed, oscillate about the true solution with decreasing amplitude, and a periodicity which are a direct function of the argument r. Low values of r produce the maximum amplitude and minimum period. High values result in minimum amplitudes and maximum periods. A maximum of 100 terms (100^2 for the double summation) was required to establish the convergence characteristics sufficiently to determine the true solution for the case of very small r - values. Most of the other cases converged with a much lower number of terms. An example of this convergence characteristic is shown in Figure 3.

A computer program for the IBM 7090 was written for the solution of the summation terms involved in each of the four different electrode configurations. For this study, the convergence characteristics were then determined by inspection. The added sophistication of programmed convergence inspection was considered but not deemed worth while for the expected volume of production on the program.

An interesting question is how the distribution of contact positions (expressed by dimension c) per unit cross-sections area of cell would affect the cell resistance for a given fractional contact area. To investigate this point, the resistance ratio was also computed as a function of c for several values of fixed fractional contact areas.

Electrolyte Thickness h (inches)	Dimension C (inches)	% Area Contact	RESISTANCE RATIO $R_{eff/R}$			
			Square Contacts	Circular Contacts	Square Holes	Circular Holes
0.120"	0.012"	1	21.0171	16.7620		
		2	10.4728	9.4411		
		5	4.3832	4.3512		
		10	2.4672	2.5215		
		15	1.8644	1.9014		
		25	1.4132	1.4222		1.2215
		40	1.1836	1.1776		1.1203
		50	1.1146	1.0425		1.0861
		60				1.0624
		75	1.0332			1.0372
0.120"	0.016"	1	27.5262	21.9635		
		2	13.5989	12.2268		
		5	5.6827	5.4571	1.4720	
		10	3.1934	3.0236	1.3654	
		15	2.1497	2.1989	1.3062	
		25	1.5495	1.5615	1.2340	1.2947
		40	1.2442	1.2362	1.1698	1.1600
		50	1.1524	1.1399	1.1393	1.1145
		60				1.0830
		75	1.0442		1.0294	1.0494
0.120"	0.020"	1	34.1078	27.1649		
		2	16.7248	15.0125		
		5	6.6163	6.5630	1.5892	
		10	3.4356	3.5258	1.4560	
		15	2.4349	2.4964	1.3822	
		25	1.6859	1.7008	1.2921	1.3678
		40	1.3048	1.2948	1.2119	1.1997
		50	1.1903	1.1828	1.1738	1.1429
		60				1.1036
		75	1.0552		1.0720	1.0617

TABLE 2

CELL WITH 80 MESH SCREEN ELECTRODES

Wire diameter: 0.0047"; Sieve Opening: 0.0070"

C = 0.00235 in.
T = c/d = 0.401
% Area Contact: 12.1%

Cell Thickness h inches	Resistance Ratio $R_{eff/R}$
.01	3.6913
.02	2.3456
.03	1.8970
.04	1.6728
.05	1.5382
.06	1.4480
.07	1.3844
.08	1.3363
.09	1.2990
.10	1.2691
.11	1.2309
.12	1.2242

Values of the resistance ratio, R_{eff}/R were computed (see Table 1) for the four electrode configurations over the following range for each of the parameters:

Cell thickness, H: 0.040", 0.080" and 0.120"
Electrode dimension, c: 0.004", 0.008", 0.010"
0.012", 0.016", 0.020"
% Area contact for square contacts: 1, 2, 5, 10, 15, 25, 40, 50, 75%
% Contact for circular contacts same as for square (except no 75%)*
% Contact for square holes: 5, 10, 15, 25, 40, 50, 75%
% Contact for circular holes:* 25, 40, 50, 60, 75%

In addition, the circular hole configuration was extended to the range of parameters which approximate a porous plate of interest in fuel cells (see Table 2):

Dimension: $c = 4 \times 10^{-5}$ inches (corresponding to 2 dia pores)
60×10^{-5} inches (corresponding to 30 dia pores)
% contact: 25, 40, 50, 60, 75.

In addition, as a special typical case, a cell with 80 mesh (U. S. series) screen contact electrodes with assumed similar contacts, was calculated in Table 3 for several cell thicknesses.

Figures 4, 5, 6, and 7 show plots of some of the data for demonstrating significant relationships within the parameters involved.

IV. DISCUSSION

Exact solutions of the Laplace equation for the four cases considered were possible. Due to slow convergence, however, it was found desirable to carry out the computations to a 100 terms for some cases. In the solution for the resistance ratio, R_{eff}/R, the oscillation of the first (single) summation term (see for instance equation 11), is larger than for the double summation term and, furthermore, it is considerable for small values of the dimensional parameter $\underline{r}$. Figure 3 shows that even for a relatively large value of $\underline{r}$ ($r = 0.1$), it takes at least 25 terms to compute a reliable value for the single summation term. For a case in which $r = 0.01$, it takes about 100 terms to obtain a dependable value of the sum.

Some selected results of Table 1 are presented in Figure 4 for cells of electrolyte thickness $h = 0.040$" for the four types of electrode contact configurations. From the point of view of access of fuel cell reactants, the percentage area of contact is an important consideration. As seen in Figure 4, the resistance ratio values are reasonably close for either square and circular contacts or for square and circular holes; however, below a 40% area contact, at any given value of fractional area contact, it makes a considerable difference whether the contacts are made with perforated plates or with screens. Thus, for example for the parameters presented in Figure 4, at a 20% area contact, the screens give a resistance ratio of 2.5, while the perforated plate, only 1.5. Such a difference would not normally be intuitively anticipated.

As the cell thickness increases, the resistance ratio for the case of discontinuous contact electrodes becomes smaller, as should be obvious by inspection of the equations. Thus, in Figure 5, for cells twice as thick as those of Figure 4, (i.e., $h = 0.080$"), much smaller resistance ratios are evident. Again here, for the case of perforated holes, the resistance ratio, R_{eff}/R, values are lower than for the case of square or circular contacts (i.e., screen electrodes).

To illustrate the importance of the dimensional parameter "c", its affect on the resistance ratio is shown in Figure 6 for a thin cell ($h = 0.040$") with a deliberately low contact area of only 1%. By reason of physical dimensions (very low mesh screens), this case, of little practical value, serves only to emphasize the point that all things being equal, dimensional parameter "c" should be made, whenever possible, very small. Thus, for a given percentage area contact and given thickness, it is desirable to have as much distributed contact as possible (i.e., small values of dimension "c"). For the more practical case, illustrated in Figure 7, with a 40% area contact and a cell thickness of 0.040", it can be seen that decreasing parameter "c" from 0.020 to 0.010 results in a lowering of the resistance ratio from about 1.9 to about 1.45 for the case of square or round contacts.

*Lower and upper limits set by nature of configuration.

TABLE 3A

CELLS WITH POROUS PLATES

With 2 Micron Dia. Pores (C = 0.00004")

Cell Thickness h, inches	% Area Contact	Resistance Ratio R_{eff}/R
0.040"	25%	1.00387
	40	1.00210
	50	1.00151
	60	1.00109
	75	1.00065
0.080"	25%	1.00111
	40%	1.00060
	50	1.00043
	60	1.00031
	75	1.00018
0.120"	25%	1.00073
	40	1.00039
	50	1.00028
	60	1.00021
	75	1.00012

TABLE 3B

With 30 Micron Dia. Pores (C= 0.00060")

Cell Thickness h, inches	%Area Contact	Resistance Ratio R_{eff}/R
0.040"	25%	1.03322
	40	1.01804
	50	1.01290
	60	1.00935
	75	1.00557
0.080"	25%	1.01661
	40	1.00902
	50	1.00645
	60	1.00468
	75	1.00279
0.120"	25%	1.01107
	40	1.00608
	50	1.00430
	60	1.00312
	75	1.00185

To bring the results of these computations closer to the realm of practical applications, resistance ratio values have been computed for cells of various thicknesses, employing 80 mesh (U. S. series) screen electrodes. From the data for such screens, it can be calculated that the percentage area contact is 12.10%. Table 2 gives the results of these computations. The results indicate that for a cell thickness of 0.040", the effective resistance is 67% higher due to the screen electrodes as compared with solid contact electrodes. And even for a cell three times as thick (h = 0.120"), the resistance penalty is still more than 22%. Thus, the consideration of the geometric parameters in a matrix electrolyte cell are indeed important.

Finally, it was of some interest to consider an idealized form of a porous electrode. Porous electrodes are now commonly employed in fuel cell technology. Contacts with the electrolyte are usually made with plates having pore diameter either in the range of 1-4 microns or in the range of 20-40 microns. If for simplicity, the porous plate can be treated as one perforated with uniform round holes located on square centers, then equation (17) can be employed. Results of these computations are given in Tables 3A and 3B for 2 micron and 30 micron pore diameter plates, respectively. The variations of cell thickness and percent area contact in the range of 25 - 75% are also included. The immediately obvious conclusion is that the cell resistance with porous plates is significantly lower than for any perforated plates or screens considered in this study. The highest value of 1.033 is shown in Table 3B for the coarse plate and the smallest value of cell thickness and percent area contact. This indicates that at least from the point of view of primary current distribution and resistance ratio, the use of even coarse porous plates is advantageous over other discontinuous contact electrodes. The consequences of such considerations in the basic design of electrochemical fuel cells is fairly obvious. In the final analysis, however, such considerations must be linked with the mass transport aspects of the reactants and products to and from the contact zone between electrode and electrolyte.

ACKNOWLEDGMENTS

The assistance of Dr. J. V. Breakwell with the mathematical treatment is gratefully acknowledged. This study was supported by the General Research Program of the Lockheed Missiles and Space Division.

V. NOMENCLATURE

A	- General area portion (conducting or hole) of the electrode area element 2d x 2d (see Figure 2).
A_c	- Conducting portion of area element 2d x 2d.
c	- Half of diameter or side of contact or hole area portion A.
d	- Half of the center distance between conducting portions.
h	- Thickness of electrolyte matrix, cm or in.
i	- Current density, amp/cm^2
K	- $i\rho/(A/4d^2)$
R	- Total resistance of a cell with solid continuous electrodes, ohms.
R_{eff}	- Total resistance of a cell with discontinuous electrodes, ohms.
r	- c/d
V	- Potential, volts.
x, y, z	- Cartesian coordinates in electrolyte matrix geometry.
ρ	- Specific resistivity of electrolyte matrix, ohm - cm.

VI. LITERATURE CITED

(1) Gorin, E., and Recht, H. L., Chem. Eng. Prog. 55, 51 (Aug. 1959).
(2) Fick, L., and Eisenberg, M., Chem. Eng. Prog. 61 (to be published).

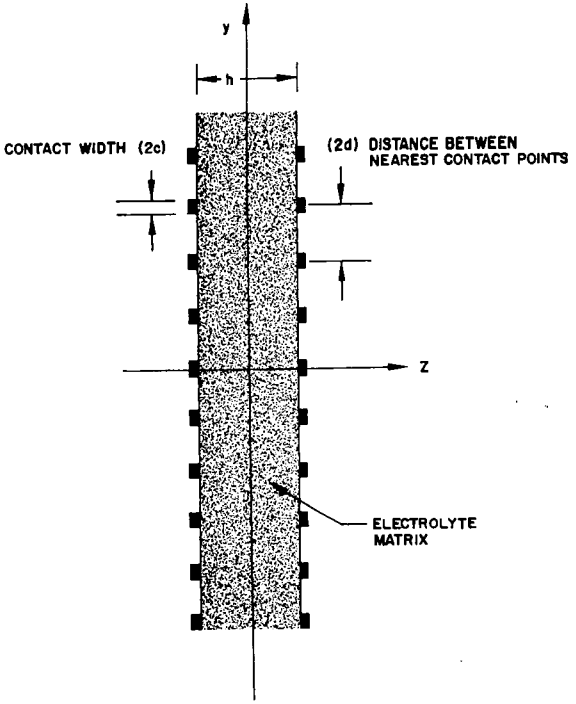

DIMENSIONS c AND d ARE THE SAME IN THE X-DIRECTION

FIG. 1 CROSSECTION OF A MATRIX CELL WITH DISCONTINUOUS ELECTRODE CONTACTS

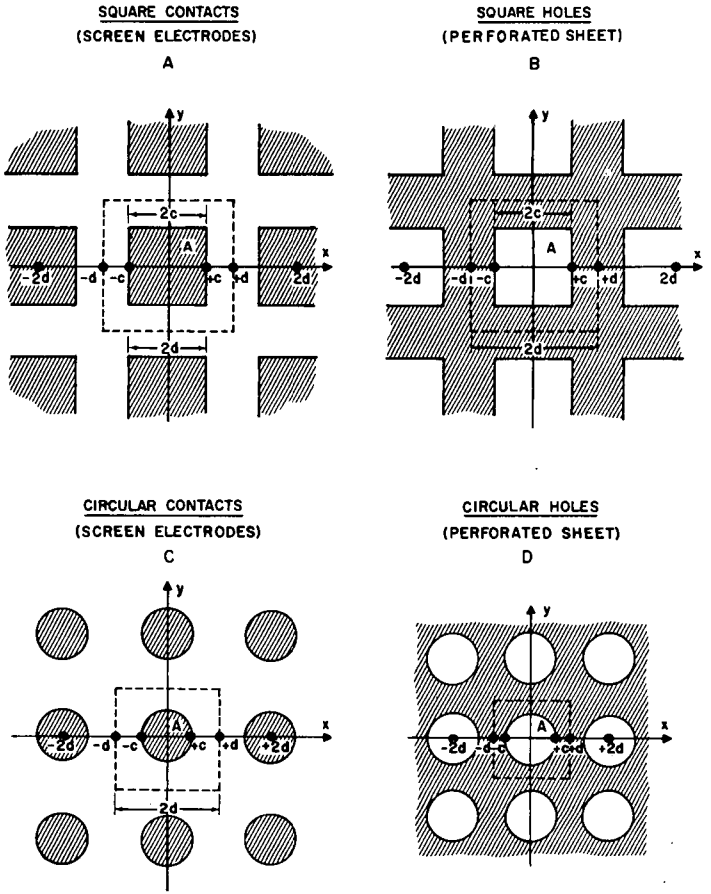

FIG. 2 PRESENTATION OF CONDUCTING OR HOLE AREA PORTION "A" WITHIN SQUARE 2d x 2d.

VII. APPENDIX

Detailed derivation for the expression for resistance ratio R_{eff}/R for the square contact case is included in this section. The derivation of this ratio for the other three cases was arrived at in a similar fashion.

From the previous section:

$$C_1 = \frac{Kc^2}{d^2} \tag{10}$$

The result of integrating the right hand side of equation (8) is:

$$Kc\,\frac{d}{n\pi}\sin\frac{n\pi c}{d}\ ;\ \text{or}\ Kc\,\frac{d}{m\pi}\sin\frac{m\pi c}{d}$$

The result of integrating the right hand side of equation (9) is:

$$K\,\frac{d^2}{nm\pi^2}\sin\frac{n\pi c}{d}\sin\frac{m\pi c}{d}$$

and substitution of equations (5), (8), (9), and (10) into equation (3) yields the general solution for the potential distribution for either square holes or square contacts:

$$V = C_0 + K\left\{\frac{c^2}{d^2} + \frac{2c}{\pi^2}\sum_{n=1}^{\infty}\sin\frac{n\pi c}{d}\cos\frac{n\pi x}{d}\right.$$

$$\cdot\ \sinh\frac{n\pi z}{d}\Big/n^2\cosh\frac{n\pi h}{2d} + \frac{2c}{\pi^2}\sum_{m=1}^{\infty}\sin\frac{m\pi c}{d}$$

$$\cdot\ \cos\frac{m\pi y}{d}\sinh\frac{m\pi z}{d}\Big/m^2\cosh\frac{m\pi h}{2d}$$

$$+\ \frac{4d}{\pi^3}\sum_{n=1}^{\infty}\sum_{m=1}^{\infty}\sin\frac{n\pi c}{d}\sin\frac{m\pi c}{d}\cos\frac{n\pi x}{d}\cos\frac{m\pi y}{d}$$

$$\left.\sinh\frac{\sqrt{n^2+m^2}\,\pi z}{d}\Big/\left(nm\sqrt{n^2+m^2}\cosh\frac{\sqrt{n^2+m^2}\,\pi h}{2d}\right)\right. \tag{10a}$$

For squares, the value of K in equation (2) is given by:

$$K = \frac{i\rho}{r^2} \tag{10b}$$

and substituting for K into equation (10a)

$$V = C_0 + i\rho z + \frac{2i\rho d}{\pi^2 r}\sum_{n=1}^{\infty}\frac{\sin n\pi r\,\sinh\left(\frac{n\pi z}{d}\right)}{n^2\cosh\left(\frac{n\pi h}{2d}\right)}$$

$$\cdot\ \cos\frac{n\pi x}{d} + \frac{2i\rho d}{\pi^2 r}\sum_{m=1}^{\infty}\frac{\sin m\pi r\,\sinh\left(\frac{n\pi z}{d}\right)\cos\frac{m\pi y}{d}}{m^2\cosh\left(\frac{m\pi h}{2d}\right)}$$

$$+\ \frac{4i\rho d}{\pi^3 r^2}\sum_{n=1}^{\infty}\sum_{m=1}^{\infty}\frac{\sin n\pi r\,\sin m\pi r\,\sinh\left(\frac{\sqrt{n^2+m^2}\,\pi z}{d}\right)}{nm\sqrt{n^2+m^2}\cosh\left(\frac{\sqrt{n^2+m^2}\,\pi h}{2d}\right)} \tag{10c}$$

$$\cdot\ \cos\frac{n\pi x}{d}\cos\frac{m\pi y}{d}$$

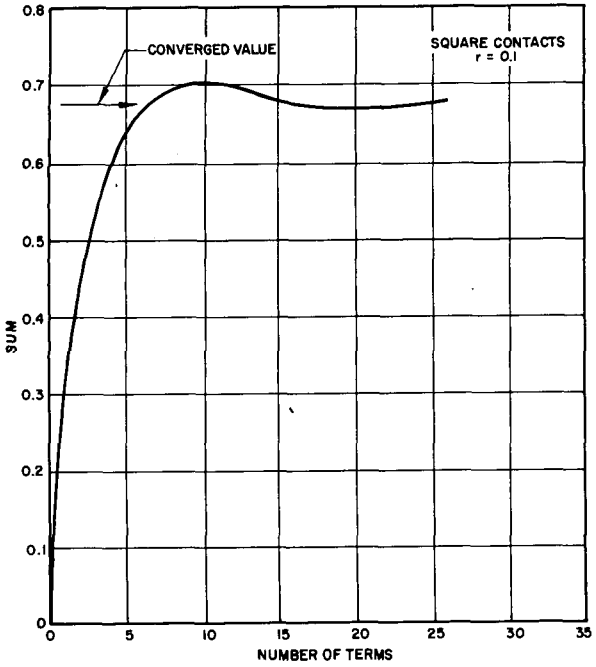

FIG 3. CONVERGENCE CHARACTERISTICS FOR SINGLE SUMMATION TERM IN EQUATION (11)

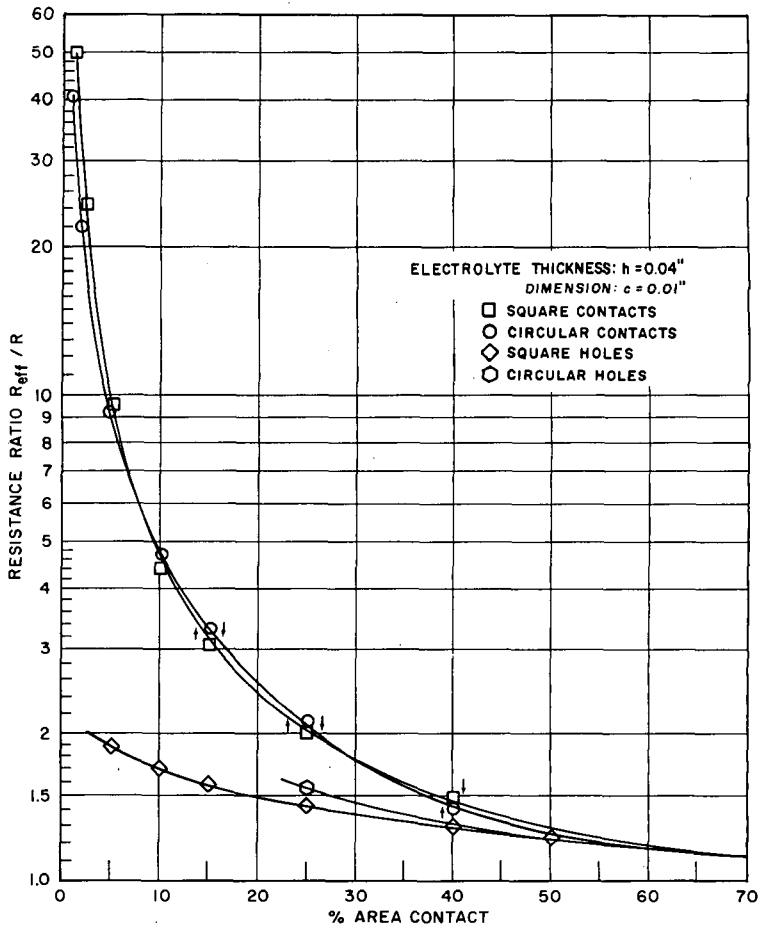

FIG. 4 RESISTANCE RATIOS AS FUNCTION OF PERCENTAGE CONTACT AREA FOR VARIOUS ELECTRODE CONFIGURATIONS

Using this expression for V, the ratio of the resistance of an electrode pair consisting of square contacts to that of a pair of plane electrodes is given by:

$$\frac{R_{eff}}{R} = \frac{V(x=0,\ y=0,\ z=\frac{h}{2}) - V(x=0,\ y=0,\ z=\frac{-h}{2})}{i\,\rho\,h}$$

$$= \frac{i\,\rho\,h}{i\,\rho\,h} + \frac{8d}{\pi^2 h r} \sum_{n=1}^{\infty} \frac{\sin n\pi r}{n^2} \tanh \frac{n\pi h}{2d} \qquad (11)$$

$$+ \frac{8d}{\pi^3 r^2 h} \sum_{n=1}^{\infty} \sum_{m=1}^{\infty} \frac{\sin m\pi r \sin n\pi r}{n\,m\,\sqrt{n^2+m^2}} \tanh \frac{\sqrt{n^2+m^2}\,\pi h}{2d}$$

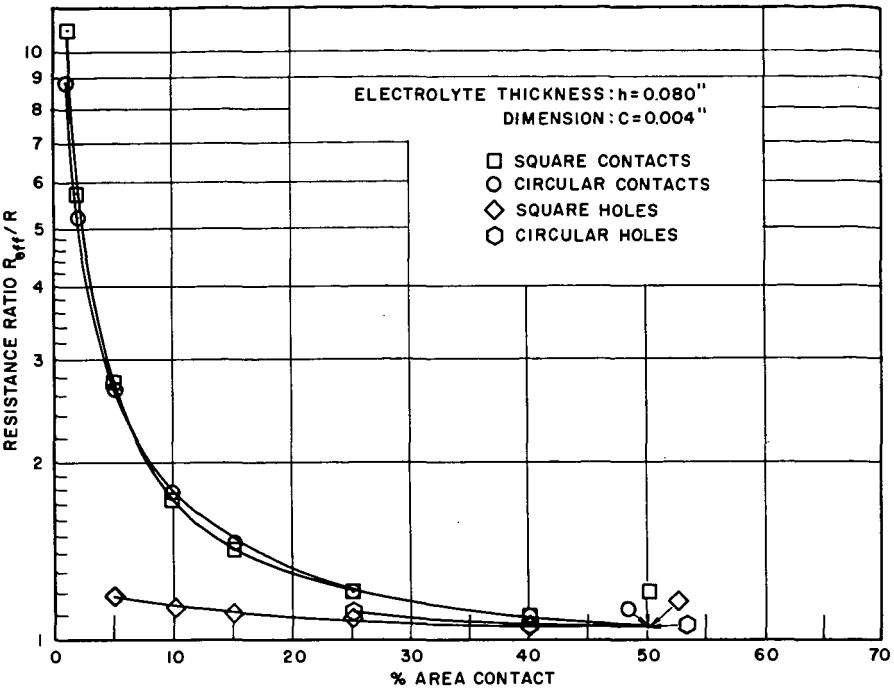

FIG. 5 THE EFFECT OF PERCENT AREA CONTACT ON THE RESISTANCE RATIO R_{eff}/R

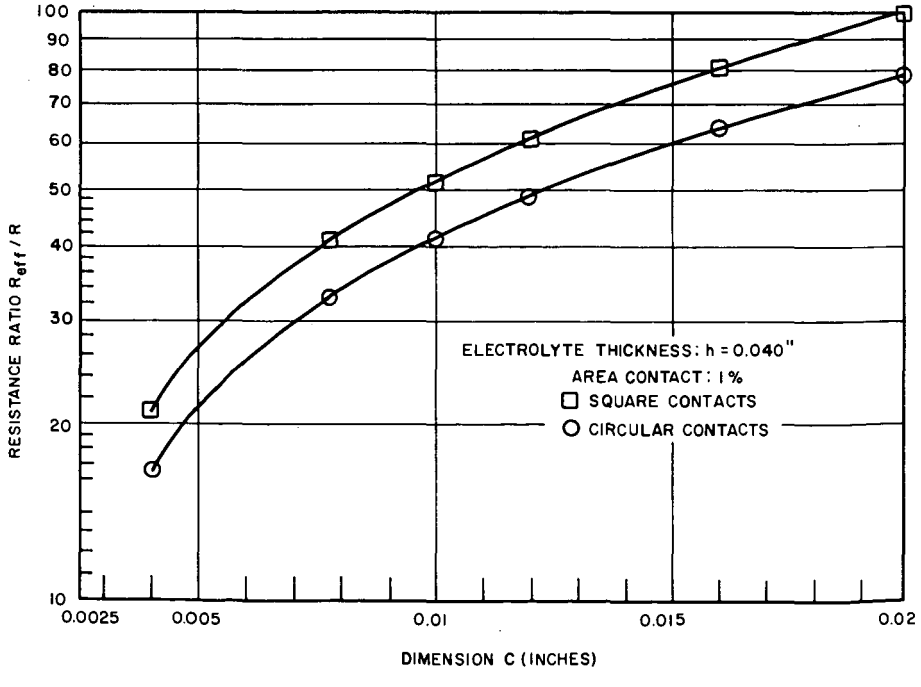

FIG. 6 THE EFFECT OF THE DIMENSION "C" ON THE RESISTANCE RATIO R_{eff}/R AT 1% AREA CONTACT

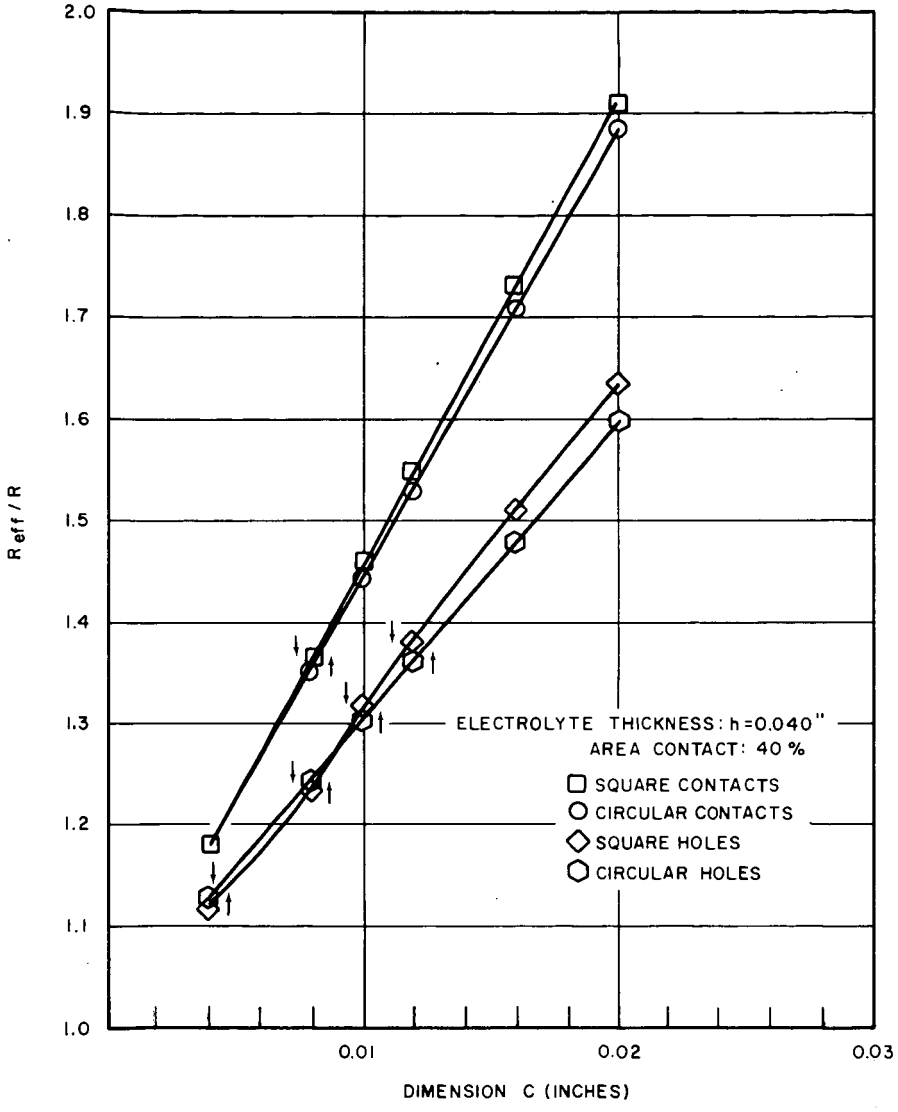

FIG. 7 THE EFFECT OF THE DIMENSION "C" ON THE RESISTANCE RATIO R_{eff}/R AT 40% AREA CONTACT

SYMPOSIUM ON FUEL CELLS
PRESENTED BEFORE THE DIVISION OF PETROLEUM CHEMISTRY
AMERICAN CHEMICAL SOCIETY
CHICAGO MEETING, September 3-8, 1961

DSK - ELECTRODES FOR THE CATHODIC REDUCTION OF OXYGEN

By

Heiner M. Dittmann, Edward W. Justi and August W. Winsel
Institute of Technical Physics
Braunschweig Institute of Technology, Braunschweig, Germany

1. INTRODUCTION

At the Spring Meeting of the Electrochemical Society in Indianapolis this year, Justi and Winsel (1) reported on their DSK-system (2) and its application to fuel cell technology. Previously, (in the monograph "High-drain hydrogen-diffusion-electrodes operating at ambient temperature and low pressure") Justi, Pilkuhn, Scheibe, and Winsel (3) had described in detail the method employed in preparing the DSK-hydrogen electrode, using nickel as the basic material, as well as its electro-chemical properties. To complete the picture of these fuel cells, this paper will deal with the DSK-oxygen-electrode. We trust that we may be allowed to present only a brief description of how DSK-electrodes are made, confining ourselves to the specific properties of the oxygen-electrodes.

2. THE METHOD BY WHICH THE DSK-OXYGEN-ELECTRODE IS PREPARED

It is characteristic of the DSK-electrode that it contains a Raney catalyst in an electronic conducting supporting matrix. (4) To make a DSK-electrode, the powered Raney alloy is mixed with the supporting matrix powder, the resulting mixture formed into an electrode under pressure and then sintered. The non-noble components of the Raney alloy (Al, Zn, Si) are then leached out while the Raney metal is retained in the pores of the electrode as a highly effective catalyst. Instead of first pressing the electrode and then sintering it, the hot-pressing technique permits preparation in one process. (5) The DSK-oxygen-electrode contains Raney silver as the catalyst. For many years it has been known that silver possesses good properties as an oxygen-carrier and as a decomposition catalyst for H_2O_2. (6, 7)

These same properties are reinforced in the Raney silver owing to its larger specific surface area. (8) The Raney silver is formed in the pores of a supporting matrix which 1) possesses good sintering properties, 2) has good electrical conductivity, and 3) is not attacked by the activating solvent and the fuel cell electrolyte at the oxygen potential. These conditions reduce considerably the number of substances which can be considered. We should like to mention that the noble metals, including silver, are too expensive to be used in great amounts. However, nickel and nickel alloys, which passivate in alkaline solution, and finally carbon can be employed. At first we used a silver supporting matrix and later a nickel one. The many difficulties which arose in the development of oxygen-electrodes described here have been eliminated largely by K.-H. Friese (9) in our laboratories. They originated for the most part in the Raney alloy.

2.1 The Raney Silver-Alloy

The first condition which must be fulfilled by a Raney alloy for use in DSK electrodes is its ready malleability. The Raney alloy should therefore be as brittle as possible. In the most often used Raney nickel alloys of the Ni/Al system this condition is ideally fulfilled; however, this is not the case for the Raney silver alloys in the Ag/Al systems. The latter alloys as normally produced are so thoroughly ductile that when placed under a press flattening into wide sheets rather than fracturing occurs. When placed in a ball mill thin plates result which are not at all suitable for sintering.

Friese, Justi and Winsel (4) managed to increase considerably the brittleness and also improve the electrochemical properties of the oxygen electrode by adding a small quantity of manganese (less than 0.3 weight percent). Later it turned out that this method was inferior when compared with a thermal treatment of controlled melting.

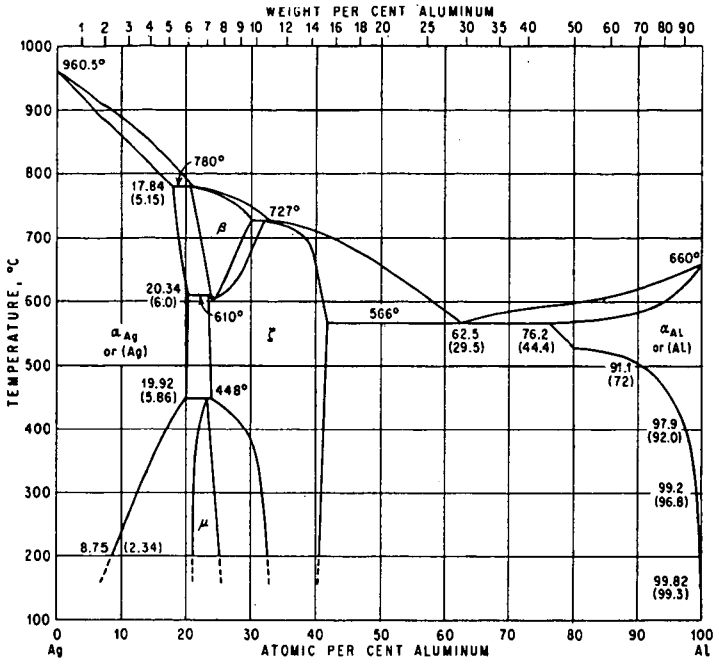

Fig. 1 Ag-Al

Fig. 1 - Phase Diagram of the Binary System Ag/Al.

Fig. 2 - DSK Oxygen electrode with plexiglas attachment, used for the present experiments. The pipe serves both as gas inlet and as conductive lead.

Under a calcium chloride protective melt 65% by weight of silver is melted with 35% by weight of aluminum in a carbon crucible. As can be seen in the Ag/Al phase diagram (Fig. 1) a solid melt appears as a crystalline mass from the ζ and α_{Az} phases slightly above the eutectic temperature of 566°C. (10). Both phases are attacked by potassium hydroxide, yielding chiefly the sought-after Raney silver from the ζ phase.

If one can produce a melt of this composition and quenches it from 800° to less than 100°C., a brittle regulus is obtained which shows strong texture formation at the fractured surfaces. According to Friese one can obtin a good malleable Raney alloy for DSK electrodes by means of this treatment.

The second condition which a Raney alloy must fulfill is the capacity to be formed into a stable electrode element when mixed with the supporting matrix powder. Our experience has taught us that this condition is not easily met. A supporting matrix made of nickel requires a sintering temperature of at least 600°C. However, at this temperature according to the phase diagram the liquid α_{Az} phase in the alloy 65% Ag, 35% Al is already present. This liquid phase reacts spontaneously with the nickel supporting matrix in KOH solution to yield the non-attackable intermetallic compound AlNi. The result is a very homogeneous product from which no Al can be dissolved, therefore permitting no Raney silver to be obtained. The product is therefore not suitable for oxygen electrodes. The only possible way to prepare DSK electrodes with Raney Ag as a catalyst on a supporting nickel matrix is the hot pressing method. (5) By the use of the latter it is possible to make use of the increased reactivity of metals in the plastic flow state. (11) Applying temperatures between 300 and 500°C. and pressures to one ton/cm^2 the individual powder grains are welded together. As a consequence of this treatment the composition of the grains in the interior regions does not change. Potassium hydroxide solution is then able to activate the electrode element which remains mechanically stable.

By means of this hot pressing technique we were able, with Dr. Friese's aid, to produce single layer electrodes which yielded current densitites over 500 ma/cm^2 below 100°C. - though at the cost of rather high gas losses. (8, 9)

2.2 Double Layer Electrodes

To avoid a situation whereby gas bubbles escape through large pores into the electrolyte without reacting we have prepared, as did Bacon (12) electrodes consisting of two layers. (13) The fine-pore protective layer is made from carbonyl nickel alone, or with the addition of a fine-grained Raney alloy which yields Raney silver upon activation. The large-pore operating layer is produced likewise from carbonyl nickel and Raney alloy powder. The porosity is influenced both by the particle size of the alloy and through the addition of KCl powder as filler. After hot pressing the filler is easily dissolved. (14)

In many cases electrodes were prepared in our laboratory with an additional gas conducting layer to increase the mechanical rigidity. This third layer contains no silver but consists of porous nickel.

All of the following electrochemical properties of our DSK oxygen electrodes are the results of experiments on multilayered electrodes which permitted no gas bubbles to escape unreacted into the electrolyte.

3. THE ELECTROCHEMICAL PROPERTIES OF AG-DSK-ELECTRODES USED FOR THE CATHODIC REDUCTION OF OXYGEN

3.1 The Experimental Procedure

Disk shaped electrodes about 2 mm thick and 40 mm in diameter were pressed into plexiglass, the borders made gastight, leaving a 10 cm^2 surface area to yield current, see Fig. 2. Nickel foil was employed chiefly as the counter electrode on which oxygen was envolved. The polarization was measured with the aid of a saturated calomel electrode employed as reference electrode. In addition the siphon of the electrode was fitted with a Luggin capillary for use as a potential measuring device and placed directly on the surface of the oxygen electrode. In this manner the resistance polarization is for the most part excluded, except for that which unavoidably originates within the pores. (3, 15) A D. C. voltage amplifier with a high threshold resistance (Knick-Berlin) was used to measure the potential while a milliampere meter of the 0.2 class recorded the current.

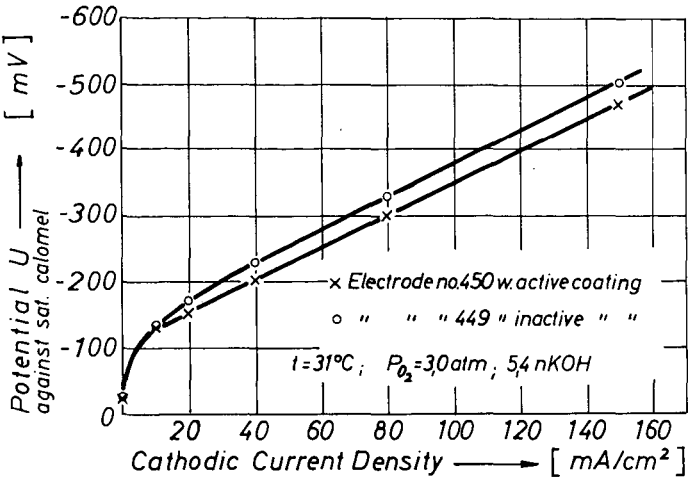

Fig. 3. Comparison between the performances of two electrodes, the upper having an active, the lower an inactive protecting layer. Electrolyte: 5.4 n KOH; temperature: 31°C; p=30 atm.

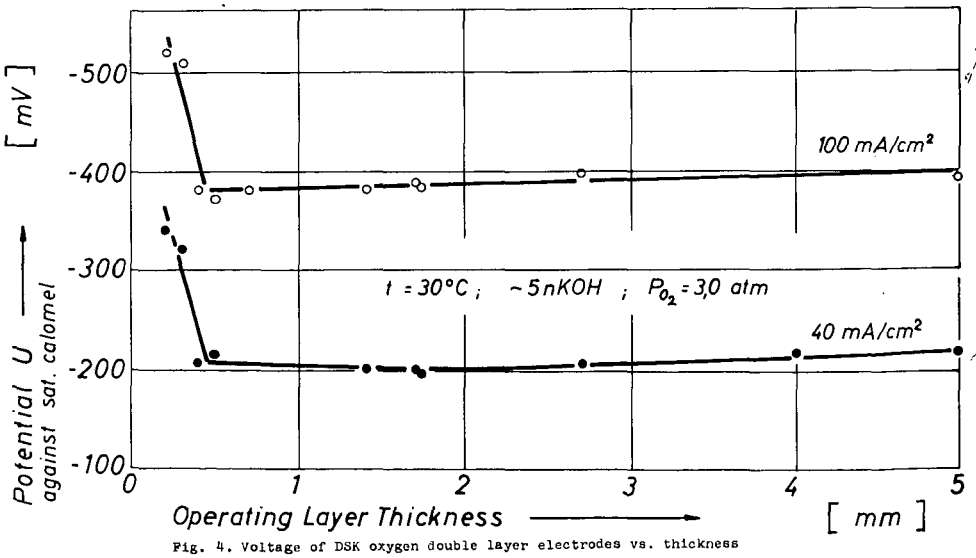

Fig. 4. Voltage of DSK oxygen double layer electrodes vs. thickness of operating layer. Parameter: operating current densities. Electrolyte: 5 n KOH; temperature: 30°C; p=3.0 atm.

3.2 The Influence of the Protective and Operating Layers

The significance of the individual layers during the cathodic reduction of oxygen was investigated in two series of measurements. In this manner we hoped to determine where the silver, as the active as well as most expensive electrode component, could be most suitably placed.

3.21 The Protective Layer

The significance of the protective layer during the polarization of an electrode is completely clear when it is limited to the voltage drop which occurs in the electrolyte located within the pores. However, it is not clear whether the protective layer itself also participates directly in the cathodic oxygen reaction. The latter might be expected if, or example, the diffusion of oxygen molecules into the electrolyte-filled protective layer was of a comparable order of magnitude to the current yielding ability of the electrodes. It might also have been the case if, within the scope of the Berl reaction, (16) hydrogen peroxide were formed which then diffused into the protective layer where it could be electrochemically reacted.

These questions are most simply resolved by employing similar electrodes, once with and once without Raney silver in the protective layer. In Fig. 3 the comparison is shown. The current density - polarization curves of electrodes with and without Raney silver in the protective layer differ only by a few hundredths of a volt. This difference can probably be ascribed to the somewhat increased broadening resistance in the inactive protective layer which is due to a lesser porosity. In no case, however, is there a characteristic co-functioning of the protective silver layer on the oxygen reduction.

3.22 The Operating Layer

In answer to the question how thick should one make the operating layer of the DSK-silver-electrode, we have plotted, in Fig. 4, the polarization as a function of operating layer thickness of otherwise similar electrodes for two different current densities. Here one sees that approximately 0.5 millimeter thick layers yield the largest effects with the smallest amount of material. Increasing layer thickness does not improve the electrode performance; however, thicknesses below 0.5 mm show a strong performance deterioration. One may then conclude that the reaction zone of the electrochemical oxygen reduction penetrates approximately 0.5 mm. into the working layer.

In Figure 5 the silver content of the working layer has been changed, the latter being limited due to demands of mechanical rigidity. As would be expected the electrode with the largest silver content reveals the least polarization at equal current densities in the pressure range of 1 to 4 atmospheres.

Considering these facts we have been able to reduce the amount of silver for optimal electrodes to 0.05 g/cm^2 electrode surface by using a gas conduction layer with increased mechanical rigidity. This amount is insignificant with respect to the price of the electrode.

3.3 The Influence of Operating Conditions

3.31 The Oxygen Pressure

The influence of oxygen pressure on the electrochemical properties of the oxygen electrode can be seen in Fig. 5. At a certain pressure at which the operating layer is pressed free, the electrode commences to function. At constant current density the polarization diminishes with increasing pressure. However, in the region of approximately 2 to 4 atmospheres it becomes almost pressure independent. A further increase in pressure causes the protective layer to be pressed free permitting the gas to escape unreacted into the electrolyte as fine bubbles.

3.32 The Electrolyte Concentration

On account of its nickel supporting matrix our DSK electrode functions only in alkaline solution. It has been tested at various concentrations of potassium hydroxide whose conductivity maximum lies at about six normal. In Figure 6 the cathodic current density for varying degrees of polarization is plotted as a function of the concentration of potassium hydroxide. Between three and four normal all curves show a maximum which is shifted to lower concentrations with increasing polarization. The resistance minimum of the electrode can be explained as follows:

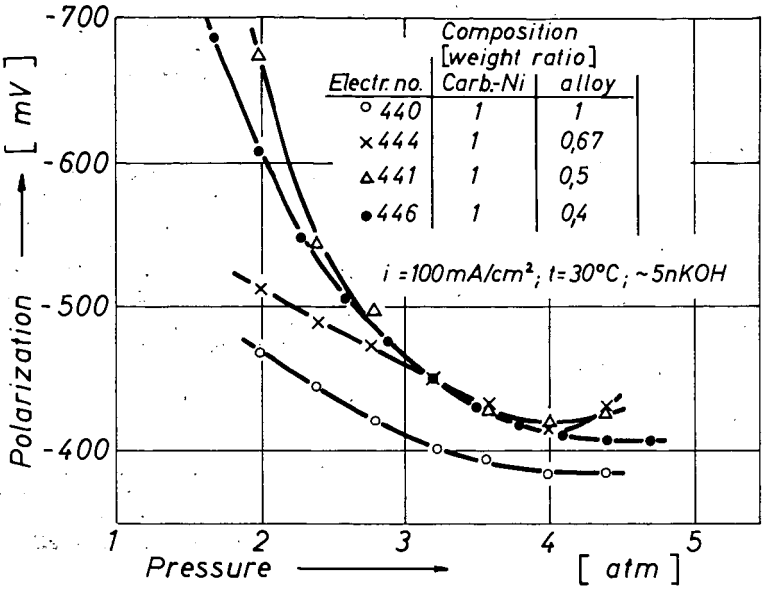

Fig. 5. Voltage of different DSK oxygen double layer electrodes against sat. calomel vs. operating oxygen pressure. Constant current density i = 100 ma/cm^2; electrolyte 5 n KOH; t=30°C.

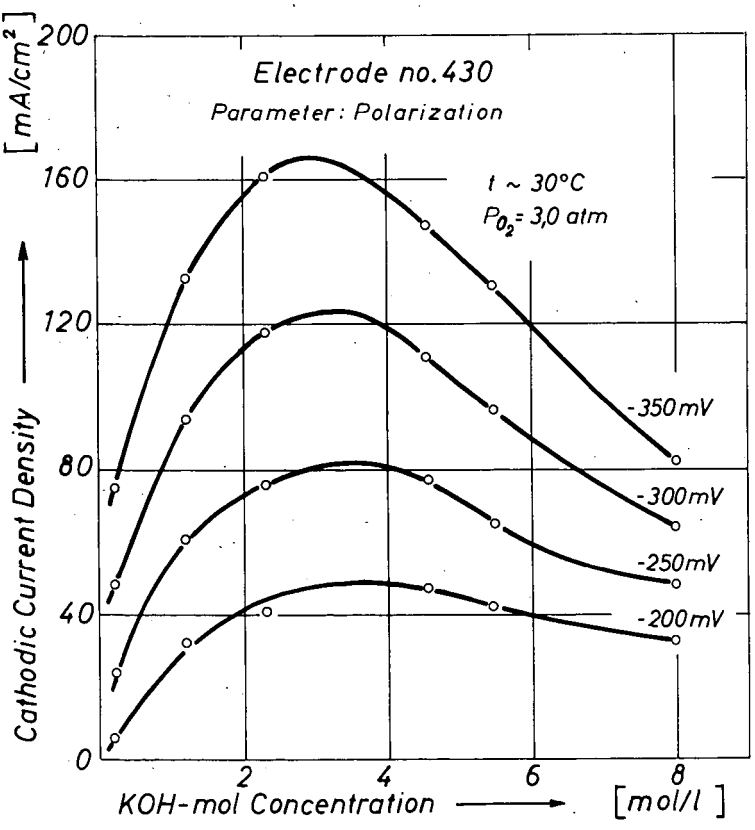

Fig. 6. Current density i vs. KOH concentration at t=30°C and p=3.0 atm. Parameter: polarization.

During cathodic current flow the KOH concentration increases within the pores as compared to that in the bulk electrolyte. The electrolyte resistance minimum is then reached when the alkali in the pores attains the optimal concentration. The greater the polarization is this will be the case the lower the concentration is.

3.4 The Stability of the Catalyst

In order to determine if Raney silver ages with time an oxygen electrode has been exposed to alternating loads since December 1959. Since March 23, 1960, it has been placed in an hydrogen-oxygen cell which operates during the day at 50 ma/cm^2 and overnight at 30 ma/cm^2. During this period (15 months) the electrode did not change. (17)

3.5 The Gas Efficiency

The current yield is, of course, important in judging the economic efficiency of an electrode. For example, if one admits one mole of oxygen to an oxygen electrode, then one can obtain maximally 4 x 96,500 Ampere-secs. as the electrical change. Deviations from this may be caused by gas bubbles which have escaped into the electrolyte electrochemically unreacted, by back diffusion of oxygen molecules into the electrolyte, and also by the fact that the electron yield of the electrochemical elementary process is not complete. If the reduction of the oxygen molecule is carried to H_2O four electrons per oxygen molecule are liberated. But if the reduction is carried only as far as H_2O_2 then only two electrons are released. (16) Between these ideal cases many intermediate values are conceivable. These occur as a result of the electron yield obtained by the catalytic or electrochemical decomposition of the H_2O_2 formed in the Berl reaction. (18)

The current yield of our DSK electrodes was determined by measuring at the electrodes the current flow of the flowing gas streams. The left diagram in Figure 7 shows the gas flow to the stationary loaded hydrogen electrode, the right diagram to the stationary loaded hydrogen electrode, the right diagram to the oxygen electrode. The drawn-in thick lines are calibration curves of the flowmeter which correspond to a complete gas utilization. The experimental points determined at three different temperatures confirm the almost 100 per cent electrochemical reaction of the admitted gases. (17)

In the right diagram the standard calibration plot for the Berl process is seen on the dashed curve. Apparently within the scope of our measuring accuracy the true electron yield of the single process is four. From this we should like to conclude that perhaps the H_2O_2 formed in accordance with the Berl mechanism occurs as a short-lived intermediate product.

4. CONCLUSION

This report has been presented as a review of the technology as well as the capacity of our DSK electrodes. It would not be complete if nothing were said about the future development. We believe that through further improvements, especially of the technology of the protective layers, the polarization characteristics of our electrodes may be improved. Allied with this our efforts are primarily concerned with the further technical development of hydrogen-oxygen cells and other fuel cells for carbon monoxide (3) and with liquid fuel-electrolyte (19) mixtures.

ACKNOWLEDGMENTS

The authors express their grateful appreciation to their sponsoring firms, the Ruhrchemie AG at Oberhausen and the Steinkohlen Elektrizitat AG at Essen for support of this work and publishing permit. The authors are also indebted to Dr. K.-H. Friese for many stimulating discussions and to Dr. Bernard R. Stein, ARO, Frankfurt, Germany, for the skillful translation.

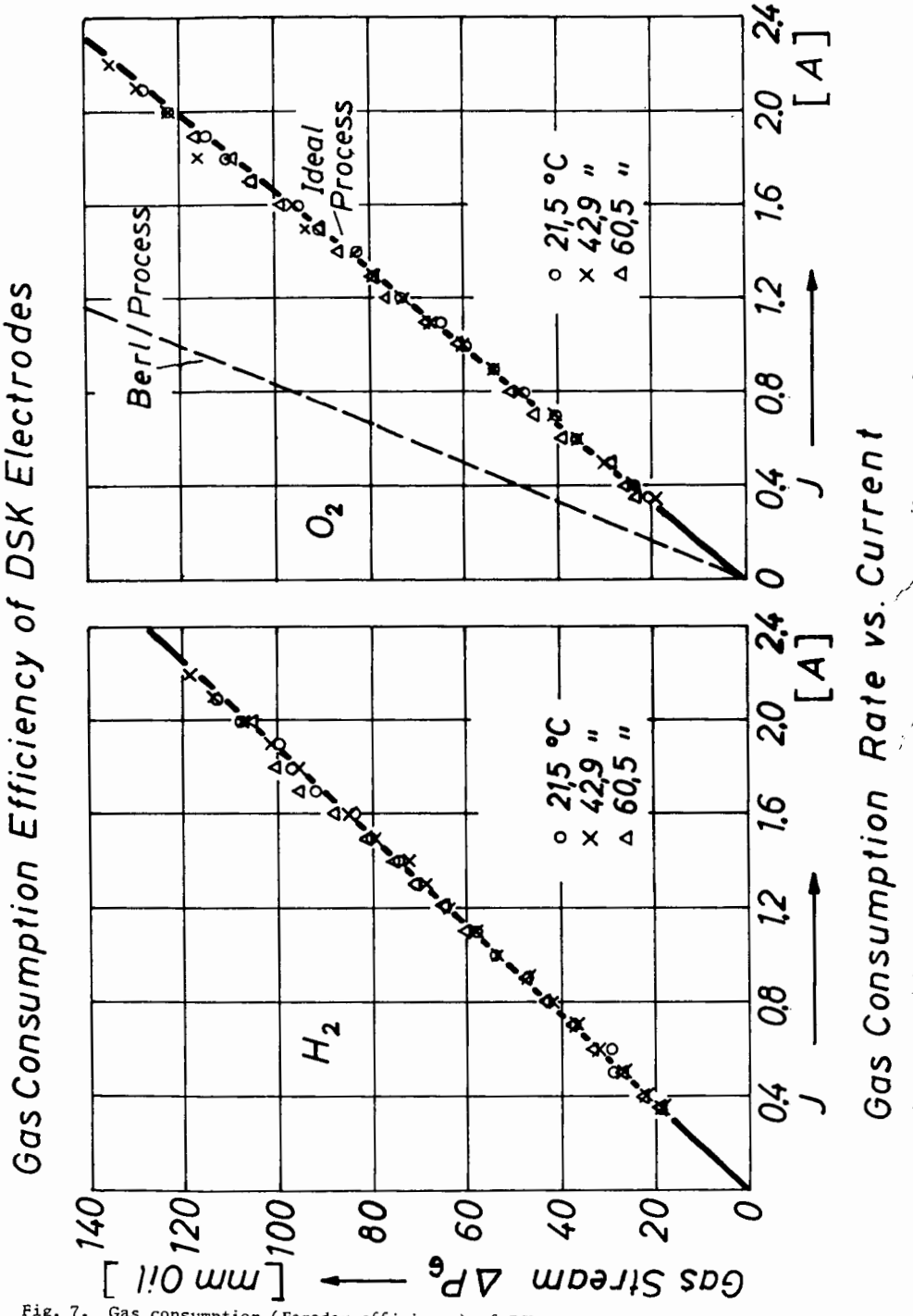

Fig. 7. Gas consumption (Faraday efficiency) of DSK double layer electrodes with hydrogen (left) and oxygen (right) vs. current. The thick lines are calibrating lines for the flow-meters, indicating complete electrochemical reaction of the gases according to $H_2 + \frac{1}{2}O_2 = H_2O$. The dotted line (right) applies to the Berl reaction $H_2+O_2 = H_2O_2$.

LITERATURE CITED

(1) Justi, E., and Winsel, A., 119th Meeting of the Electrochemical Society, Indianapolis (1961); J. electrochem. Soc., to be published; Naturwiss. 47, 298 (1960).

(2) Winsel, A., Dissertation, Braunschweig, T. H., (1957), Justi, E., Scheibe, W., and Winsel, A., DBP 1 019 361 (1954); USA pat. 2 928 891; Brit. pat. 806 644; French pat. 1 132 762; Scheibe, W., Dissertation, Braunschweig, T. H. (1959).

(3) Justi, E., Pilkuhn, M., Scheibe, W., and Winsel, A., "High Drain Hydrogen-Diffusion-Electrodes Operating at Ambient Temperature and Low Pressure", Abh. d. Math. -Nat. Kl. d. Akad. d. Wiss. u. d. Lit. Mainz, No. 8, Komm. Verlag Steiner, Wiesbaden, 1959.

(4) Friese, K. -H., Justi, E., and Winsel, A., Austrian pat. 207 429 (1957).

(5) Friese, K. -H., Justi, E., and Winsel, A., Austrian pat. 205 089 (1958).

(6) Kordesch, K., and Marko, A., Osterr. Chem. Ztg. 52, 125 (1951).

(7) Witherspoon, R. R., Urbach, H., Yeager, E., and Hovorka, F., Tchn. Report No. 4, Navy Research (1954).

(8) Friese, K. -H., Diplomarbeit, Braunschweig, T. H. (1956).

(9) Friese, K. -H., Dissertation, Braunschweig, T. H. (1959).

(10) Hansen, M., "Constitution of Binary Alloys", McGraw-Hill Book Co., New York, 1958.

(11) Sully, A. H., "Metallic Creep and Creep Resistant Alloys", London, 1949.

(12) Bacon, F. T., Brit. pats. 667 298 (1952) and 725 661 (1955); USA pat. 2 716 670 (1955).

(13) Dittmann, H., Diplomarbeit, Braunschweig, T. H. (1961).

(14) Heuer, W., Diplomarbeit, Braunschweig, T. H. (1959).

(15) Winsel, A., Z. Elektrochem. To be published.

(16) Berl, W. G., Trans. Electrochem. Soc. 83, 253 (1943).

(17) Winsel, A., Z. Elektrochem. To be published.

(18) Vielstich, W., Z. physik. Chem. (N. F.) 15, 409 (1958).

(19) Justi, E., and Winsel, A., USA pat. 2 925 454; Brit. pat. 821 688; French pat. 1 148 012; DAS 1 071 175 (1955).

SYMPOSIUM ON FUEL CELLS
PRESENTED BEFORE THE DIVISION OF PETROLEUM CHEMISTRY
AMERICAN CHEMICAL SOCIETY
CHICAGO MEETING, September 3-8, 1961

FUEL CELL INTERMEDIATES AND PRODUCTS

By

Maurice J. Schlatter
California Research Corporation, Richmond, California

I. INTRODUCTION

Studies of fuel cell intermediates and products were carried out with two different objectives. The first work, supported by California Research Corporation, was initiated in December 1958. It consisted of an exploratory evaluation of fuel cells as reactors for producing chemicals. Concurrently, pilot studies aimed at utilizing hydrocarbons or petroleum-derived fuels in power fuel cells were initiated. Early in 1960, this latter phase was expanded as a fundamental program supported by Army Ordnance and under the general direction of Diamond Ordnance Fuze Laboratories. Initial objectives of this project include the determination of the kinetics and detailed reaction mechanisms of low temperature oxidations of hydrocarbons and hydrocarbon oxidation intermediates at fuel cell anodes. The methanol product studies reported here are a part of this continuing program.

When our work was initiated, there were few reported product data for fuel cells or for low voltage anodic oxidations in the potential range obtainable at fuel cell anodes. Scarcely more information was available on the low temperature fuel cell performance of fuels other than hydrogen. Therefore, it was necessary for us to screen many compounds in order to select some that were sufficiently active in fuel cells for initial product studies. Results of these experiments are also of interest in the interpretation of product data and are included in this report.

II. APPARATUS

A. Fuel Cell Electrodes

Electrodes were our most important apparatus problem. We were not concerned with preparing the best possible electrodes for a particular fuel cell reaction but rather with making versatile, reproducible electrodes for comparative screening tests and electrodes capable of producing sufficient reaction to allow isolation and identification or analysis of the reaction products.

Electrode forms used in most of the later product work are shown in Figure 1. These hollow, cylindrical, porous carbon electrodes are suitable for use in acidic or in basic electrolytes. They can be used as noncatalytic electrodes or impregnated or plated with catalytic materials. They are equally useful with gases, with liquid reactants insoluble in the electrolyte, and with soluble reactants. Stackpole Porous Carbon No. 139* was the most satisfactory of the porous carbon supports which we tested. This material came to our attention through the electrode studies of Anthony and Humphrey. (1)

Platinized electrodes were used as fuel anodes in most of the work reported here. They were also used as oxygen cathodes in acidic and sometimes in basic electrolytes. They were prepared by plating porous carbon electrodes for 20 minutes at a current density of 40 ma/cm^2 of geometric area and an initial temperature of 25°C. The plating electrolyte contained 10 grams of platinum per liter and was prepared by dissolving pure chloroplatinic acid in 0.12 N hydrochloric acid. It was contained in a cylindrical "Karbate"** impervious graphite cup which served as anode. After allowing the electrode to stand in the electrolyte for 10 minutes, current was passed through the system and electrolyte was drawn into the electrode and forced out again every two minutes. Equally active electrodes were sometimes obtained with less platinum. However, this was not always the case; and the longer plating time which did give reproducible results was adopted as standard.

*Stackpole Carbon Company
**National Carbon Company

Table I

Relative Reactivities of "Reductants" in Basic Electrolyte Fuel Cell

Group	Potential Relative to H_2-O_2 Fuel Cell,[a] %	Reductant	Group	Potential Relative to H_2-O_2 Fuel Cell, %	Reductant
A	85	Hydrazine Formaldehyde	E	(50-65)[b]	n-Octanol n-Decanol Ethylamine
B	50-75	Ethanol Benzyl alcohol[c] 2-Aminoethanol Isopropanol n-Propanol Ethylene glycol Methanol Glycerol Sorbitol			Acetone Ethylene[c] Propane[c] Acetylene[c] Butadiene[c] n-Dodecanol
			F	(25-35)[b]	n-Tetradecanol
		Glucose Isobutanol sec-Butanol n-Butanol	G	(1-6)[b]	Soluble Starch Cumene p-Xylene Toluene
C	20-40	Sodium formate Sodium glycolate n-Pentanol Hydroxylamine Benzaldehyde[c] Ammonia Sodium tartarate n-Hexanol Allyl alcohol	H[d]	Inactive	t-Butanol Sodium acetate Sodium maleate Sodium succinate Sodium citrate Potassium oxalate Ethyl ether Dioxane Potassium m-toluate
D	2-5 (65-70)[b]	Sucrose n-Heptanol			

a Percentages relative to hydrogen compared at current densities corresponding to H_2-O_2 potential of 0.7 volt in the cell used for the comparison.

b Figures in parentheses are based on comparison made at current density corresponding to 0.9 volt H_2-O_2 potential.

c Assignment of relative position may be subject to considerable error.

d Compounds in this group may have slight activities.

Table II

Relative Reactivities of "Reductants" in Basic and Acidic Fuel Cells According to Pavela[3]

Group	Electrolyte	
	1 N NaOH	1 N H_2SO_4
Good reactivity	Methanol Ethanol Ethylene glycol	Methanol Ethanol Formic acid
Fair reactivity	Benzyl alcohol Propylene glycol Sodium formate Isopropanol sec-Butanol	
Bad reactivity	n-Propanol n-Butanol α-Phenylethyl alcohol	
No effect	t-Butanol Phenol Ethyl ether	Acetic acid Benzoic acid

Silver-silver oxide catalyzed oxygen cathodes were generally used with basic electrolytes. These were prepared by plating at 25°C. in 10% silver nitrate solution using a concentric, cylindrical silver anode. Silver was deposited in three one-minute intervals at a cathode current density of 10 ma/cm^2. Between platings, the elctrode was rinsed with distilled water and loose silver removed by wiping with filter paper. The electrode was activated by electrolytic oxidation at 20 ma/cm^2 using a cylindrical "Karbate" cup as cathode. Three per cent sodium hydroxide was drawn through the electrode during the 10-minute electrolysis.

B. Test Procedures

The electrodes were used in various ways. In many screening experiments in basic electrolytes, a platinized porous carbon anode was used with a cathode of silver-silver oxide on porous carbon. The fuel or reductant* under test was dissolved in the electrolyte. Oxygen was passed through the porous cathode. With this arrangement, fuel cell activity is observed when the reductant reacts selectively at the platinized anode and does not combine rapidly with oxygen at the cathode.** Some reductants insoluble in the electrolyte were screened by drying the electrode under helium and then saturating with the compound under test. Other materials were passed through the electrode as gas or vapor or sometimes in an inert carrier gas. The "fuel cell" consisted of anode and cathode immersed in electrolyte contained in a beaker or in a "U" tube.

Some compounds, such as hydroquinone, sulfides, and mercaptides, when dissolved in basic electrolyte will react at an uncatalyzed porous carbon anode and will also react directly with oxygen at the cathode. To test these materials in basic electrolyte, a three-compartment fuel cell (Figure 2) was used with Nalfilm-2*** cation exchange membrane separations. These separators are effective in retarding the diffusion of reactants and products from the anolyte to the catholyte.

Cathodes consisting of silver-silver oxide on porous carbon were unsatisfactory in acidic electrolytes. However, platinized porous carbon electrodes were effective in acid and were used for oxygen cathodes as well as for fuel anodes. When soluble reductants were studied, it was necessary to separate anolyte and catholyte. This was done using the three-compartment fuel cell and Nalfilm-1 anion exchange membrane separators.

Product studies, too, were ordinarily carried out in the three-compartment cell.

Over-all cell voltages were recorded. Cell currents were held constant with an automatically controlled, variable load resistance. Individual electrode potentials were measured against a Beckman saturated calomel electrode using a Luggin capillary bridge containing cell electrolyte. Potentials were measured with a Beckman Model G pH meter.

III. RELATIVE REACTIVITIES OF REDUCTANTS IN BASIC ELECTROLYTE FUEL CELLS

Relative reactivities reported in this section were obtained from screening experiments. The electrolyte was usually 15 weight per cent sodium hydroxide and the temperature 50°C., though some series were run at 25°C. and 80°C.

These experiments were carried out during the period when different electrode designs and variables were being studied. Because of this, several sets of data involving different compounds were obtained. Typical data plots are shown in Figures 3 and 4. In these, as well as in many similar plots, only directly comparable data obtained in similar systems using the same or similar electrodes are included in each figure.

---

* "Reductant" is used in some cases in reference to the fuel or compound oxidized at the anode, especially where partial oxidation to give useful chemical products is being considered.

** Justi and coworkers (2) have also used fuels dissolved in an electrolyte which contacts dissimilar electrodes.

***National Aluminate Company. Manufacture of these materials has been discontinued. Alternative materials are being considered.

Table III

Carbon Dioxide Formed from Fuel Cell Oxidation of Propane and Ethylene

Hydrocarbon	Gas Rate, ml/hr	Time, hr	Charge Transferred, amp hr	CO_2	
				Found, mg	% of Theory*
Propane	50	5.63	0.326	80.0	99.5
Ethylene	50	12.63	0.632	160.3	92.7
	44	9.18	0.459	115.0	91.6
	800	4.83	0.242	64.8	97.7
	800	15.28	0.764	200.6	98.5

* Theory: $C_3H_8 + 5O_2 \longrightarrow 3CO_2 + 4\ H_2O$ (20-electron change)

3/20 CO_2 per Faraday = 246.5 mg CO_2 per ampere hour

$C_2H_4 + 3O_2 \longrightarrow 2CO_2 + 2H_2O$ (12-electron change)

1/6 CO_2 per Faraday = 274 mg CO_2 per ampere hour

Table IV

Comparison of Relative Fuel Cell Reactivities of Propane, Ethylene, and Acetylene on Different Electrodes

	Platinized Porous Carbon	Palladized Porous Nickel
1.	Ethylene > Acetylene > Propane 35% KOH > 30% K_2CO_3	Propane > Ethylene > Acetylene 25% K_2CO_3 = 27% KOH
2.	Propane > Ethylene > Acetylene 5 N H_2SO_4	
3.	Acetylene 35% KOH > 5 N H_2SO_4	
4.	Propane, Ethylene 5 N H_2SO_4 > 35% KOH	

Often, different time schedules were used in testing reductants which were later compared. On the figures, the data obtained at each current setting are shown as two points connected by a vertical line. The upper point is the potential one minute after operation at the indicated current density. The lower point is the potential just before the current was increased to the next higher value. The intervening time, in minutes, is shown by the small figures adjacent to this point. For comparison purposes, some adjustments were made in drawing the polarization curves in order to compensate for differences in the test schedules.

"Relative reductant reactivities" were established by comparing the over-all voltages produced by reductant-oxygen fuel cells under equivalent conditions. Compensation for different electrode activities was achieved by relating the reactivity of each compound in a particular test series to hydrogen. For reactive materials, the comparisons were made at the current density which gave 0.7 volt output from a hydrogen-oxygen cell included in each test series. With less reactive reductants, which did not give sufficient current under these conditions, comparisons were made at the current density corresponding to a hydrogen-oxygen cell potential of 0.9 volt. This is illustrated by the dashed lines on Figure 4. The relative reactivities obtained in this way are approximate. Differences in solubility and molecular weight make comparison of different compounds under exactly the same conditions impossible. In general, only one concentration of a soluble reductant in the electrolyte was run. Experiments with some reductants showed that performance is insensitive to concentration above a minimum value. Although this value may not have been reached for all substances tested, we do not believe that this has seriously affected the reliability of the reactivity order.

A reactivity sequence for the compounds tested on platinized porous carbon electrodes in basic electrolyte fuel cells is shown in Table I. The compounds fall into distinct reactivity groups. Assignments of compounds to these groups are quite certain; but within the groups, some transpositions may have occurred between compounds of similar reactivity.

Pavela (3) has also determined a reactivity sequence, based on the rates of low voltage electrolytic oxidations. This is shown in Table II. It is similar to our sequence except for greater differences in the relative reactivities of the C_1-C_4 alcohols.

Some compounds which do not require catalytic electrodes are not shown in Table I. This group includes hydroquinone, p-aminophenol, mercaptides, and some inorganic sulfur compounds.

IV. FUEL CELL OXIDATION INTERMEDIATES AND PRODUCTS

A. Hydrocarbons

Gaseous hydrocarbon fuel cell activity was studied in cells operating below 100°C. and at atmospheric pressure. Ethylene, acetylene, and propane were active in hydrocarbon-oxygen fuel cells at 80°C. using platinized porous carbon electrodes with 5 N sulfuric acid, 35 weight per cent potassium hydroxide, or 30 weight per cent potassium carbonate electrolytes.

With 5 N sulfuric acid electrolyte, complete or nearly complete oxidation of propane and ethylene to carbon dioxide and water was obtained. Preliminary evidence for aldehydes and ketones formed in the fuel cell oxidation of ethylene has been reported. (4) In our case, however, preliminary mass spectrographic analyses and vapor-liquid chromatography showed no oxidation products other than carbon dioxide and water. Comparison of the weights of carbon dioxide produced in the cells with the theoretical amounts obtainable from the current produced gave nearly quantitative agreement, as shown in Table III.

These results were obtained in the three-compartment fuel cell (Figure 2) with Nalfilm-1 anion exchange membrane separators. The carbon dioxide in the excess hydrocarbon leaving the anode compartment was determined by absorption in Ascarite after removing water with Anhydrone.

Propane gave the best voltage - current density characteristics of the hydrocarbons studied on platinized porous carbon anodes. In one case, an initial potential of 0.5 volt at a current density of 2 ma/cm^2 was obtained. After seven hours of rather erratic operation, 0.5 volt was still obtainable for short periods but at 1.3 ma/cm^2.

Propane, ethylene, and acetylene were also active on platinized and palladized porous nickel electrodes with either aqueous potassium hydroxide or potassium carbonate electrolyte.

Table V

Comparison of Methanol-Oxygen Fuel Cells with Acidic and Basic Electrolytes at 24°C (Cylindrical Platinized-Porous Carbon Electrodes)

	Units	Acidic Electrolyte		Basic Electrolyte	
Oxygen Half-Cell					
Catholyte		2.3 M H_2SO_4		4.5 M NaOH	
Cathode Current Density	ma/cm²	0	1.56	0	1.56
Cathode Potential (E_c)	volt vs SCE	0.825	0.665	-0.060	-0.185
Calculated Oxygen Reference Potential[a] (E_{ref})	volt vs SCE	0.953	0.953	0.140	0.140
$E_{ref} - E_c$	volt	0.128	0.288	0.200	0.325
Methanol Half-Cell					
Anolyte		1.56 M CH_3OH in 2.3 M H_2SO_4		1.56 M CH_3OH in 4.5 M NaOH	
Anode Current Density	ma/cm²	0	1.27	0	1.27
Anode Potential (E_A)	volt vs SCE	0.215	0.372	-0.920	-0.732
Oxygen-Methanol Fuel Cell					
$E_c - E_A$ (Cell Potential[b])	volt	0.610	0.293	0.860	0.547

a Calculated for the ideal cathode reactions: $O_2 + 4H^+ + 4e^- = 2H_2O$ $E_o = 0.987$ v
$O_2 + 2H_2O + 4e^- = 4OH^-$ $E_o = 0.159$ v

b Corrected for electrolyte and separator resistance.

Relative fuel cell reactivities of the hydrocarbon gases studied varied with different catalytic electrodes and with different electrolytes. These differences are summarized in Table IV.

Some of these reactivity relationships may be subject to correction. However, they do serve to show the order of complexity that may be expected in dealing with these reactions.

B. Alcohols

1. Methanol in Basic Electrolyte

Methanol product studies were carried out in a three-compartment fuel cell using platinized porous carbon electrodes at a cell current of 50 ma (anode current density, 1.27 ma/cm^2). The anolyte was 1.56 M methanol in 4.5 M sodium hydroxide. Sodium hydroxide (4.5 M) was used in center and cathode compartments.

Net products formed at 24°C. and 53°C. are plotted in Figures 5 and 6 against ampere-hours produced. As 100 ml of anolyte was used in these experiments, molar product concentrations are approximately 10 times the net moles of product produced. The actual concentrations were slightly less because the net product curves are corrected for analytical samples which were withdrawn at intervals and replaced with equal volumes of a feed stock retain.

Samples from the anode compartment were analyzed for formaldehyde and formate immediately after they were taken from the cell. Formaldehyde was determined by a sensitive colorimetric method using chromotropic acid in sulfuric acid as the colorimetric reagent. (5) Formate was determined by reduction with magnesium and hydrochloric acid, followed by colorimetric determination of the formaldehyde formed. The method used was adapted from a procedure described by Grant. (6) In the formate analysis of these fuel cell products, the amount of formaldehyde was small enough to be neglected.

Formaldehyde was definitely formed in these fuel cells, though the amount which appeared in the electrolyte was very small compared with the quantity of methanol oxidized. The concentration reached by the end of the experiment at 24°C. was only 2.5×10^{-4} M, and 3.5×10^{-4} M at 53°C. By contrast, the amount of formate initially formed corresponded closely to theory assuming that formate is the only product. With time, as the formate concentration increased, more formate was oxidized, presumably to carbonate.

Air oxidation and electrochemical oxidation of methanol in base can both give formaldehyde. Although air was not excluded from the anode in our experiments, it is evident from Figure 7 that most of the formaldehyde found in the basic electrolyte fuel cells came from electrochemical processes. In the experiment which produced the data shown, no current was drawn from the cell for 168 hours. During this period, the formaldehyde concentration increased gradually as the result of air oxidation of the methanol in the basic anolyte. Then the cell was operated intermittently at 50 ma load. Each time current was drawn, the formaldehyde concentration increased rapidly at first, tapering off as the formaldehyde concentration increased.

Apparatus and electrolyte were identical with those used in the methanol fuel cell experiment which gave the data for Figure 5.

Platinized porous carbon electrodes also have the property of catalyzing non-electrochemical reactions of formaldehyde. This too is evident from the data plotted in Figure 7. In addition to the fuel cell which was operated intermittently, a control air oxidation was carried out with 150 ml of the methanol-in-base which was used as anolyte in the fuel cell. This was contained in a 250-ml volumetric flask. During the first 217 hours, samples were drawn for analysis with minimum disturbance of the contents of the flask. In the remainder of the experiment, the flask was shaken vigorously when each sample was withdrawn. The formaldehyde concentrations are shown by a dashed line in Figure 7.

In the first part of the control experiment, formaldehyde was produced by direct air oxidation at a constant rate. Under similar conditions and at null current, the rate of increase of formaldehyde in the fuel cell anode compartment was about half that in the control. Also, when the fuel cell current was interrupted after a period of operation under load, the formaldehyde concentration decreased. The rate of this decrease was greater at higher concentrations.

Table VI

Effect of Chemical Structure on "Reductant" Activity in Basic Electrolyte Fuel Cell

Active	Inactive or Very Slightly Active
Simple Alcohols 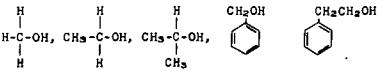 $CH_3(CH_2)_nOH$: Activity decreases as n increases	
Polyols and Dihydric Phenols 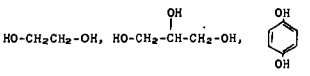 Glucose, Sorbitol ≫ Sucrose ≫ Soluble Starch	
Substituted Alcohols and Phenols 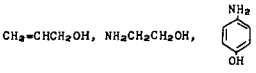	
Hydroxy Acids 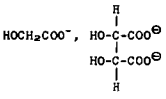	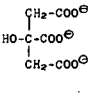
Other Carboxylic Acids 	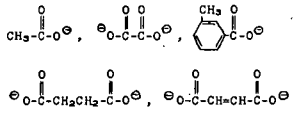
Carbonyl Compounds 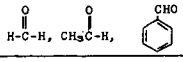	
Ethers	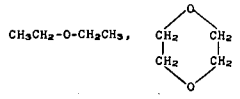
Nitrogen Compounds $NH_2NH_2 \gg NH_3$, $NH_2OH > CH_3CH_2NH_2$	
Sulfur Compounds $HS^\ominus$, $CH_3S^\ominus$, n-$BuS^\ominus$ S° (as polysulfide)	$S_2O_3^\ominus$, $SO_3^\ominus$, $SO_4^\ominus$, CH_3  SO_3H (5 N H_2SO_4 electrolyte)

The forms of the decreasing formaldehyde concentration curves, which were obtained at zero current, were probably determined by the rate at which formaldehyde was produced by air oxidation reduced by the rate of the catalytic conversion of formaldehyde to other products. The ascending curve was determined by these factors together with the rates of electrochemical formation and subsequent electrolytic oxidation of formaldehyde at the electrode and attendant mass transfer effects between electrode and solution.

It is possible that all or part of the decrease in formaldehyde concentration is due to platinum-catalyzed reduction of water by formaldehyde, giving hydrogen and formate as the products.

The decrease in formaldehyde concentration may also be due to disproportionation to give methanol and formate. This occurs slowly in basic solution at room temperature but is known to be accelerated by platinum. (7)

2. Methanol in Acid Electrolyte

Products formed from the fuel cell oxidation of 1.56 M methanol in 2.3 M sulfuric acid at 23°C. are shown in Figure 8. Some data from a 24°C. basic electrolyte experiment (Figure 5) are included for comparison. Formic acid and formaldehyde concentration curves are plotted in addition to net product in order to show the approach to steady state concentrations. The saw-tooth shape of these curves is the result of replacing analytical samples, drawn at intervals, with feed stock to maintain a constant anolyte volume.

Formaldehyde analyses were carried out as described for the basic electrolyte experiments. Formic acid analyses proved to be more difficult. Both sulfuric acid and formaldehyde in appreciable amounts interfere in the formate-formic acid analysis used in the basic electrolyte experiments and, therefore, had to be removed before satisfactory analyses could be obtained. This was accomplished by converting most of the formaldehyde present into the nonvolatile phenylhydrazone. The volatile formic acid, added water, and excess methanol were then distilled at room temperature in vacuo into a Dry Ice-cooled side arm of a special distillation tube. An aliquot of the distillate was analyzed for formic acid as described for the basic electrolyte. Some of the formaldehyde in the original sample is not removed by the phenylhydrazine treatment. Therefore, a second aliquot of the distillate was analyzed for formaldehyde and a suitable correction was applied. The analytical procedure is still far from satisfactory. Our most consistent results were obtained by running analyses in quadruplicate and arbitrarily using the highest value obtained. Standards were treated in a manner as nearly identical with the fuel cell electrolyte as possible. Unexpected difficulty was experienced with large reagent blanks which varied from day to day. The reason for these variations is still not clear. In the experiment shown, the data points obtained fell on a smooth curve; but difficulties in relating this to reproducible standards were such that we can only place the steady state formic acid concentrations between 4.5 and 6.5×10^{-3} M.

In contrast with basic methanol solutions, no formaldehydr was formed by air oxidation of methanol in a retain sample of the acid electrolyte.

The relative amounts of formaldehyde and formic acid produced in fuel cell oxidations of methanol are quite different in acidic compared with basic electrolytes. In acid, the concentration of formaldehyde was several times the highest concentration attained in base. Formic acid was not the principal product, as was the case with formate in base, but reached concentrations of the same order as those of formaldehyde. The total amounts of formaldehyde and formic acid together accounted for only a very small fraction of the methanol oxidized. Carbon dioxide was probably the principal product in acid. Its presence was shown qualitatively, but quantitative data were not obtained.

During the product studies, it was also observed that the potential of the methanol-oxygen fuel cell was significantly lower in acid than in base. This was true at open circuit and also at equivalent loads. The data in Table V show that the oxygen electrode performs as well in acidic as in basic electrolyte at the low current densities used in these experiments. Therefore, the poorer over-all cell performance in acid must be due to the methanol half-cell.

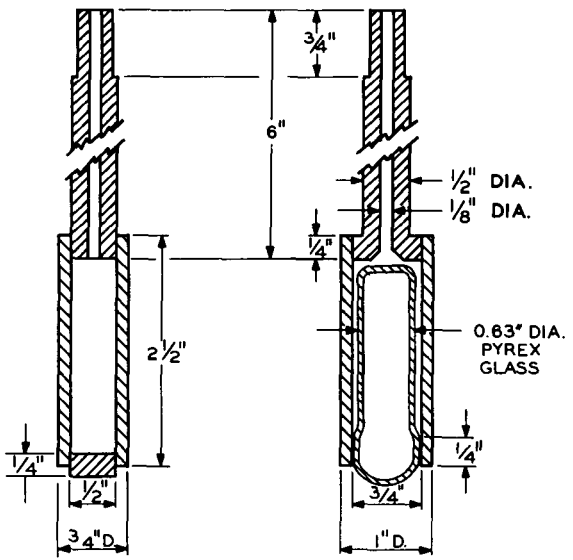

"KARBATE" IMPERVIOUS GRAPHITE (NATIONAL CARBON CO.)

POROUS CARBON NO.139 (STACKPOLE CARBON CO.)

JOINTS SEALED WITH EPON 828-Z RESIN (SHELL CHEMICAL CO.) HEATED 30 MIN. AT 100°C BETWEEN APPLICATIONS, FINISHED FOR 1 HOUR AT 150-160°C.

FIGURE 1. ELECTRODE CONSTRUCTION

FIGURE 2. THREE COMPARTMENT FUEL CELL

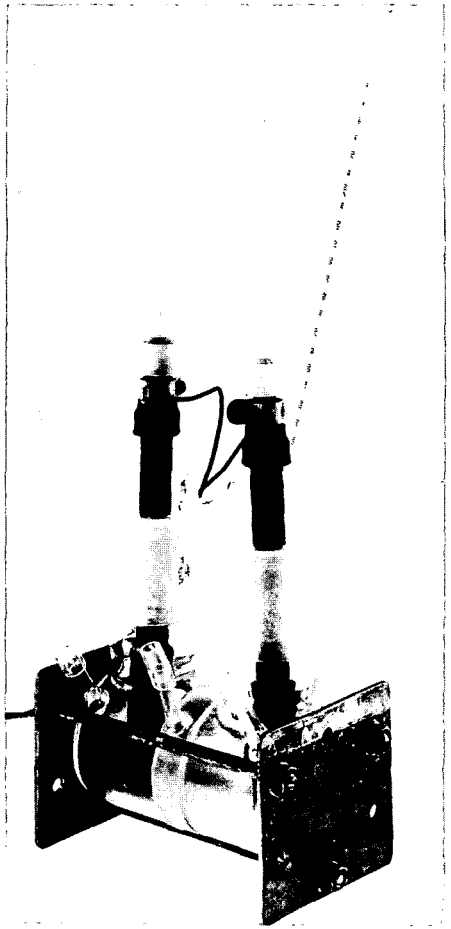

3. Ethanol, Isopropanol, and Benzyl Alcohol in Base Electrolytes

Limited product studies were made with ethanol, isopropanol, and benzyl alcohol. The ethanol data were obtained early in our program. Ethanol (5 volume per cent) was dissolved in 15 weight per cent sodium hydroxide electrolyte. This solution was contained in a small beaker at room temperature. It contacted a 1/4-inch diameter platinized porous carbon anode (6 cm^2 area) and a similar silver-silver oxide on porous carbon cathode. Oxygen was forced through the cathode at a slow rate. Analysis of the electrode after 173 hours of operation at 10 ma current (1.67 ma/cm^2) gave 37% of the theoretical amount of acetic acid based on the amount of electricity produced. No acetaldehyde was detected.

The isopropanol and benzyl alcohol product studies were made in the three-compartment cell.

The isopropanol experiments were carried out at room temperature using 5 volume per cent isopropanol dissolved in 5 weight per cent potassium hydroxide as anolyte. A 10 cm^2 platinized porous carbon anode and a silver-silver oxide on porous carbon oxygen cathode of similar size were used. Rapid deactivation of the anode occurred with isopropanol, and it was necessary to replace anodes several times during 12 hours of fuel cell operation at 20 ma current (2.0 ma/cm^2). Steam distillate from the basic electrolyte contained 14.5% of the theoretical amount of acetone.

The benzyl alcohol experiments were carried out at 50°C. in 35 weight per cent potassium hydroxide electrolyte. Similar 30 cm^2 platinized porous carbon electrodes were used for anode and oxygen cathode. The anode was dried by warming in a test tube while passing helium through the electrode. Air was excluded, and the electrode was saturated with benzyl alcohol. A total of 0.997 ampere-hour was drawn from the cell over a period of 41 hours at currents from 10 to 50 ma (0.3-1.67 ma/cm^2). Pure benzoic acid amounting to 78% of theory was recovered. No benzaldehyde was detected in the excess benzyl alcohol contacting the anode. In a similar experiment, the two Nalfilm-2 diaphragms separating anode, center, and cathode compartments in the product fuel cell ruptured. In this case, some benzaldehyde was found, presumably formed by direct oxidation of benzyl alcohol with oxygen.

4. Discussion of Fuel Cell Oxidations of Oxygen-Containing Compounds

Methanol has been suggested as an "ideal" liquid fuel for fuel cells. Although good current densities have been achieved in such cells, they present problems which must still be solved before practical low temperature methanol fuel cells can be developed. In basic electrolyte, formate is formed which is less reactive than methanol. This limits the performance of the cell. To be practical, either formate must be removed, with attendant loss of more than one-third of the energy of the methanol fuel, or means must be found to accelerate the electrolytic oxidation of formate to carbonate. Furthermore, methods must be developed to remove formate and/or carbonate from the cell electrolyte and to replace or regenerate hydroxide. In acidic electrolytes, on the other hand, complete oxidation of methanol to carbon dioxide and water and the removal of these products an be achieved without difficulty. However, the lower over-all cell potentials obtained from methanol in acid, compared with base, mean lower efficiencies. Higher potentials will have to be obtained before practical acidic electrolyte, methanol fuel cells can be realized.

Gross effects of structure on the fuel cell reactivities of alcohols and related compounds in basic electrolytes are summarized in Table VI. Hydroxy compounds having a hydrogen attached to the carbon which carries the hydroxyl group are active. This is true of simple primary and secondary alcohols, polyols, salts of certain hydroxy acids, 2-aminoethanol, and allyl alcohol. t-Butyl alcohol and citrate, which do not have this kind of a hydrogen atom, are inactive. Ethyl ether and dioxane, which do have hydrogen atoms on the carbon atoms attached to oxygen but which lack hydroxyl hydrogen, are also inactive. Aldehydes and formate, in hydrated form, contain hydroxyl hydrogen and hydrogen attached to the carbon atom which carries the hydroxyl group. These are active; ketones and other unsubstituted carboxylic acids are not.

The following mechanism for the fuel cell oxidation of methanol in basic electrolyte was presented in a previous paper.(8) It is consistent with the structural requirements for fuel cell reactivity which we have just discussed, with product data, and with the results of kinetic and mechanism studies which were carried out using electrochemical techniques.

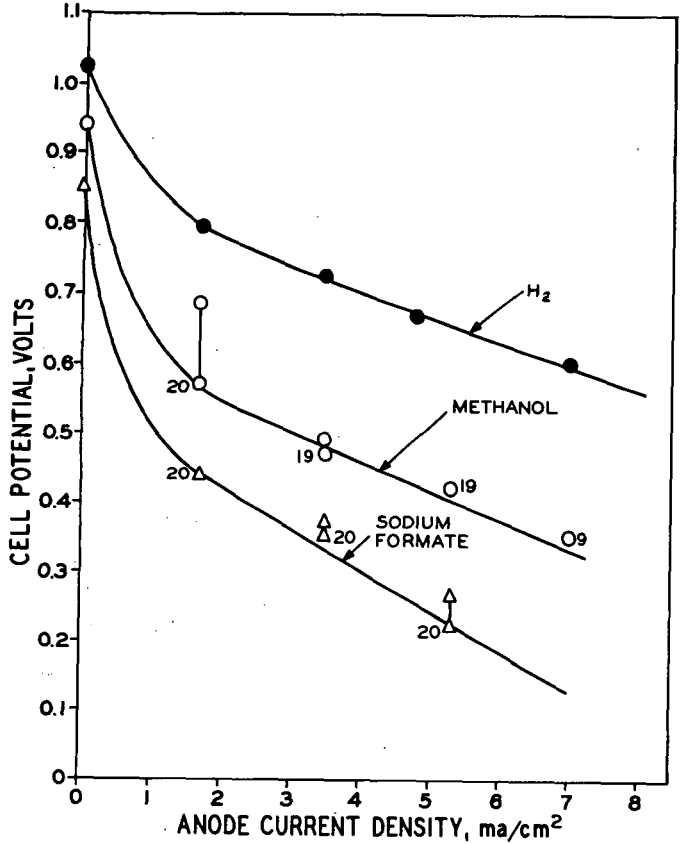

FIGURE 3. FUEL CELL PERFORMANCE OF METHANOL AND SODIUM FORMATE AT 50°C

2 VOLUME PER CENT METHANOL AND 2 WEIGHT PER CENT SODIUM FORMATE IN 15 WEIGHT PER CENT SODIUM HYDROXIDE ELECTROLYTE

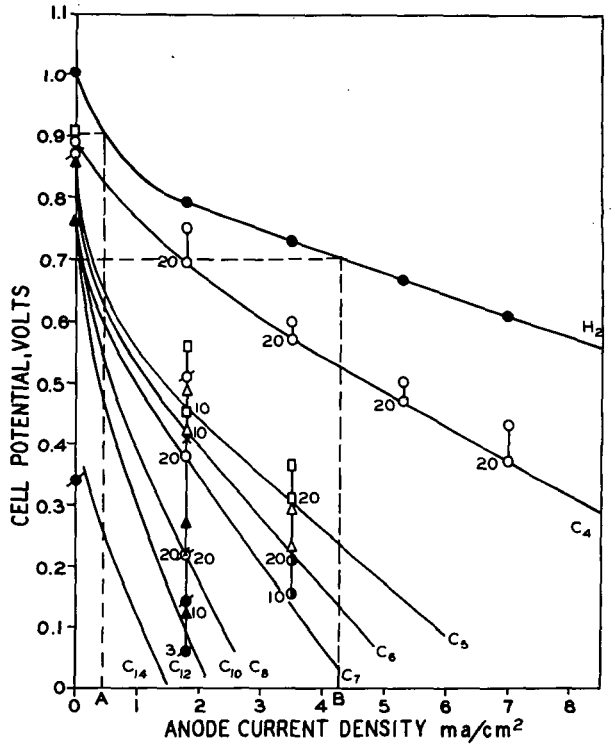

FIGURE 4. PERFORMANCE OF N-C4 TO N-C14 ALCOHOLS IN FUEL CELL AT 50°C

ANODE SATURATED WITH ALCOHOL UNDER TEST, 15 WEIGHT PER CENT SODIUM HYDROXIDE ELECTROLYTE

A. CURRENT DENSITY USED IN COMPARING SUBSTANCES HAVING LOW REACTIVITY

B. CURRENT DENSITY USED IN COMPARING REACTIVE SUBSTANCES

$$CH_3OH + OH^- \underset{k_b}{\overset{k_f}{\rightleftharpoons}} CH_3O^- + H_2O \qquad (1)$$

$$CH_3O^- \xrightarrow[\text{slow}]{Pt} CH_2O^- \text{ (ad)} + H \text{ (ad)} \qquad (2)$$

$$H \text{ (ad)} + OH^- \xrightarrow{\text{fast}} H_2O + e^- \qquad (3)$$

$$CH_2O^- \text{ (ad)} \xrightarrow[k_{s,h}]{\text{slow}} CH_2O + e^- \qquad (4)$$

$$CH_2O + H_2O \xrightarrow{\text{fast}} CH_2(OH)_2 \qquad (5)$$

$$CH_2(OH)_2 + 3OH^- \xrightarrow{\text{fast}} HCOO^- + 3H_2O + 2\,e^- \qquad (6)$$

$$HCOO^- + 3OH^- \xrightarrow{\text{slow}} CO_3^= + 2H_2O + 2\,e^- \qquad (7)$$

The net reactions given by Equations (6) and (7) each occur by a series of steps similar to those detailed for methanol.

The mechanism written for methanol appears to be equally valid when applied by analogy to the fuel cell-reactive hydroxyl compounds discussed above. In these cases, however, the reaction stops when the oxidation product does not satisfy the structural requirements for fuel cell reactivity which we have defined. Thus, we expect ethanol oxidizes to acetate via acetaldehyde, benzyl alcohol to benzoate via benzaldehyde, and isopropanol stops at acetone.

Our exploratory experiments accounted for yields of only 37% acetate from ethanol and 15% acetone from isopropanol. In part, these low yields can be attributed to losses occurring during fuel cell operation and product analysis. In addition, however, the electrode fouling which was particularly noticeable with isopropanol suggests losses by product polymerization at the anode. Similar condensations, giving products which would not have been detected by our analytical method, may have occurred with acetaldehyde formed as an intermediate in the oxidation of ethanol. Yeager (9) reports an acetone yield of greater than 70% from isopropanol. He also notes evidence for acetone condensation products.

Our early experiments also did not rule out the possibility that acetate and acetone formed on an electrode by electrochemical oxidation and not released from the adsorbed state might be more reactive than these same materials tested by the methods used in determining the reactivity sequence. Thus, our low product yields from the oxidation of ethanol and isopropanol might have resulted in part from further oxidation of the expected products. This problem is of great interest in connection with the complete oxidation of fuels in energy fuel cells. It provided a major incentive for the quantitative product studies which we carried out with methanol.

The methanol studies have shown that once a molecule of methanol is attacked on a platinized porous carbon electrode, it need not be completely oxidized to carbonate or even to formate before it is desorbed from the electrode. This is shown conclusively by the escape of some formaldehyde, which is much more reactive than methanol, into the fuel cell electrolyte. It is also clear from comparisons of the amounts of formate in the electrolytes with the amounts theoretically possible assuming complete conversion of methanol to formate (Figures 5 and 6). At the beginning, in these

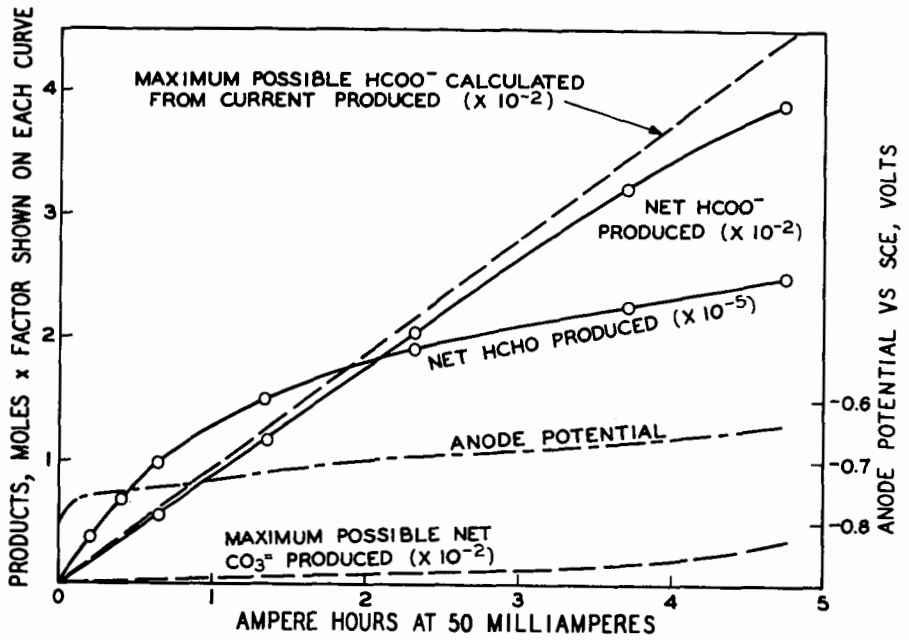

FIGURE 5. FUEL CELL PRODUCTS FROM 1.56 M METHANOL IN 4.5 M SODIUM HYDROXIDE ELECTROLYTE AT 24°C

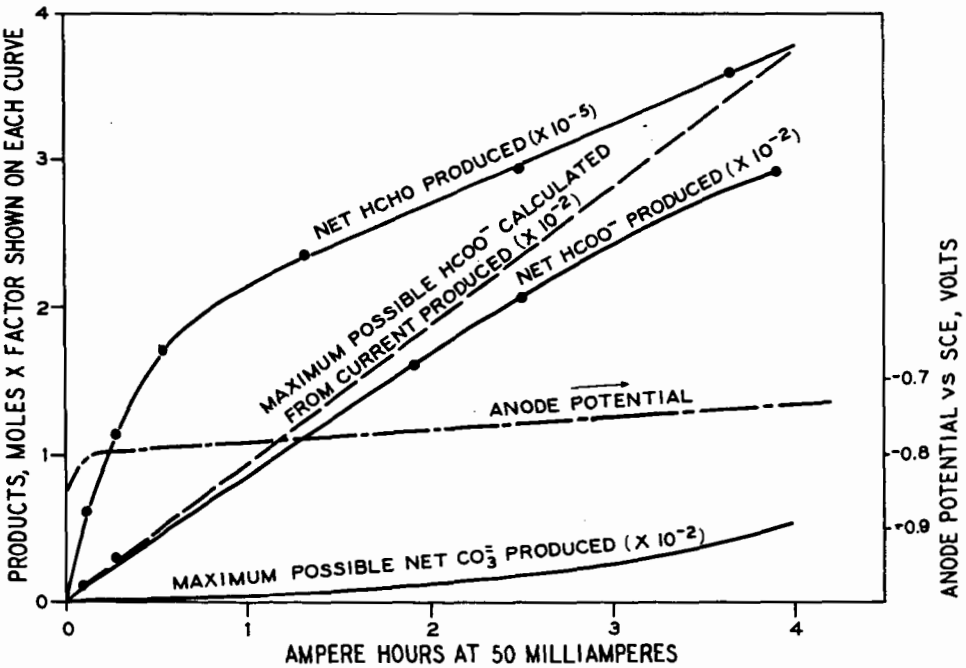

FIGURE 6. FUEL CELL PRODUCTS FROM 1.56 M METHANOL IN 4.5 M SODIUM HYDROXIDE ELECTROLYTE AT 53°C

experiments, very little formate was converted to carbonate; yet later, as the concentrations of formate increased in the electrolyte, more was oxidized further to carbonate. These results are in a sense discouraging. However, they do offer hope for the detection of hydrocarbon oxidation intermediates produced in fuel cells, even when these are much more reactive than the hydrocarbon fuel. Thus, some clues to the complex processes which must occur in the observed complete fuel cell oxidation of hydrocarbons, such as propane, to carbon dioxide and water may be obtainable from analysis of electrolytes and products. Such work is in progress in our laboratories.

In contrast to the compounds discussed above are some reducing agents, such as hydroquinone and p-aminophenol, which do not require catalytic electrodes for electrochemical activity. These compounds exist largely as anions in strongly basic solutions and would appear to be ideally suited for a concerted attack by hydroxyl with the release of two electrons at the anode:

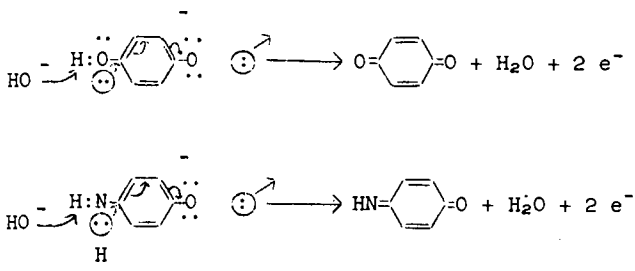

Here, the oxidation probably stops at the stable quinoids.

V. FUEL CELL PRODUCT STUDIES WITH SULFUR-CONTAINING REACTANTS

Some inorganic, as well as organic, sulfur compounds were oxidized in fuel cells using acidic and basic electrolytes. In general, for this group, compounds that gave good fuel cell activity did not require catalytic electrodes but worked as well on porous carbon alone.

A. Mercaptans

Mercaptans oxidized readily to pure disulfides in basic electrolyte:

$$\text{(Anode Reaction)} \quad 2RS^- \longrightarrow R\text{-}S\text{-}S\text{-}R + 2\,e^-$$

Fuel cell performance of methyl mercaptan and of n-butyl mercaptan dissolved in 2 N sodium hydroxide electrolyte at 50°C. is shown in Figure 9. A platinized porous carbon anode was used with the methyl mercaptan, an untreated porous carbon rod with the n-butyl mercaptan. The reactions were carried out in a three-compartment cell. The oxygen cathode was platinized porous carbon. Sodium hydroxide (2 N) was used as catholyte and center compartment electrolyte.

In both experiments, liquid products began to separate after a short period. These were shown by mass spectrographic analysis to be pure methyl and n-butyl disulfides.

Complete analysis of the product was not attempted. Methyl disulfide recovered by simple separation of the organic layer was 30% of theory based on the methyl mercaptan charged.

The yield of n-butyl disulfide, recovered by simple separation of the organic layer in the anode compartment, was 55% based on the amount of energy produced by the cell.

The mechanism of oxidation of mercaptide to disulfide may consist merely in the discharge of the ion at the anode followed by combination of the resulting radicals:

$$RS^- \longrightarrow RS\cdot + e^-$$

$$2RS\cdot \longrightarrow RSSR$$

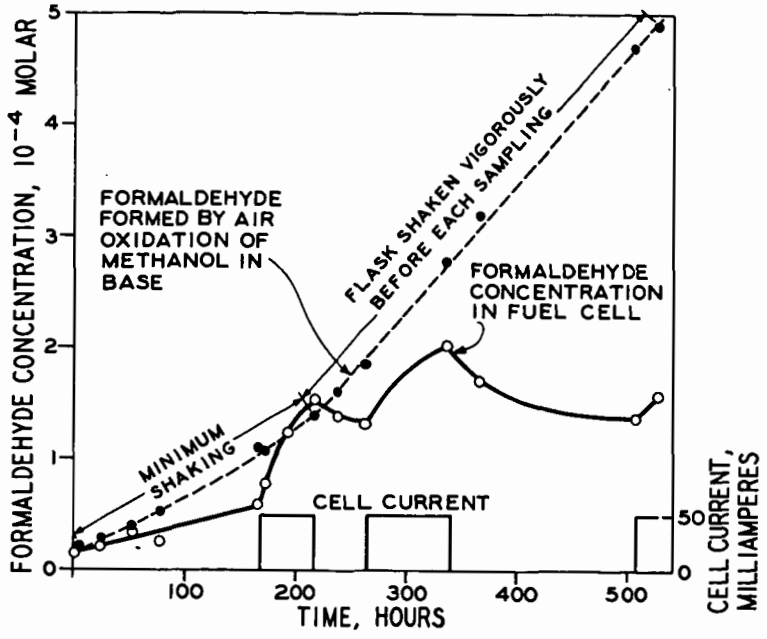

FIGURE 7. CHANGES IN FORMALDEHYDE CONCENTRATION IN A METHANOL FUEL CELL OPERATED INTERMITTENTLY UNDER LOAD AT 24°C

1.56 M. METHANOL IN 4.5 M SODIUM HYDROXIDE ELECTROLYTE

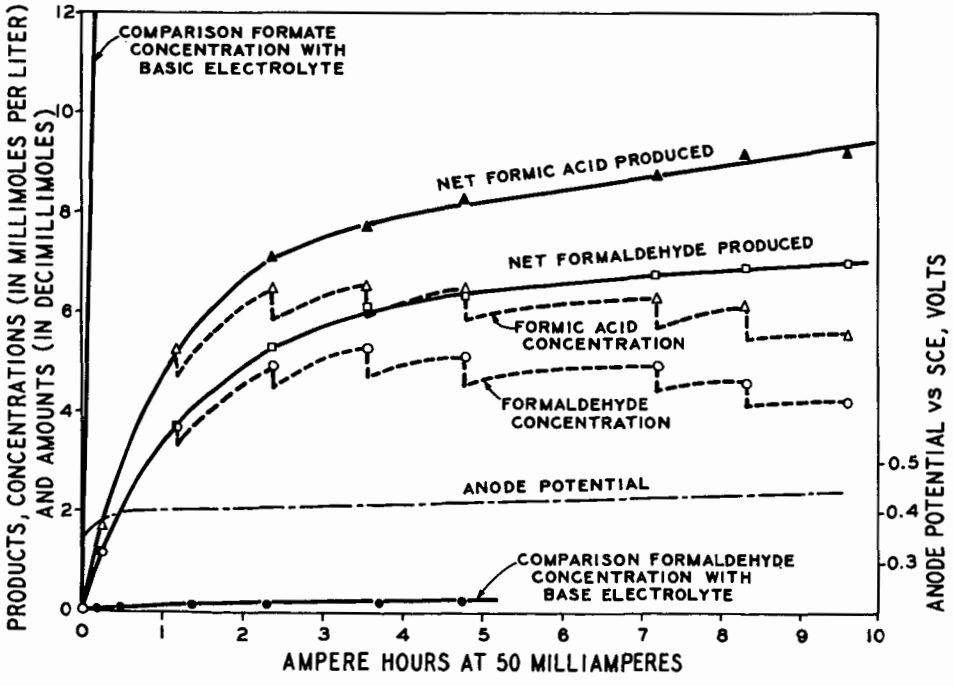

FIGURE 8. FUEL CELL PRODUCTS FROM 1.56 M METHANOL IN 2.3 M SULFURIC ACID ELECTROLYTE AT 23°C

B. Sodium Sulfide

Sodium sulfide is oxidized at the anode of a fuel cell to thiosulfate via polysulfide:

$$S^{=} + H_2O \rightleftharpoons SH^{-} + OH^{-}$$

$$SH^{-} + OH^{-} \longrightarrow (S^{\circ}) \text{ (as polysulfide)} + H_2O + 2\ e^{-}$$

$$2(S^{\circ}) + 6OH^{-} \longrightarrow S_2O_3^{=} + 3H_2O + 4\ e^{-}$$

Porous carbon rod electrodes were nearly as effective as platinized porous carbon for the sulfide half-cell. Sodium sulfide alone or with added base was used in the anode section of a three-compartment fuel cell. The other compartments contained sodium or potassium hydroxide solutions as electrolyte. Platinized porous carbon electrodes were used as oxygen cathodes.

In sustained operation under load, the anolyte turned to a deep orange color which then gradually faded to colorless. This is due to the formation of polysulfide which then reacts further, giving thiosulfate. Figure 10 shows the changes in composition occurring and the cell potential as a function of the total energy produced per mole of sulfur of any form in the system. The amount of sulfite present was negligible at all times. Sulfate, present in small amount initially, increased only slightly in concentration.

C. Hydrogen Sulfide

The possibility of converting hydrogen sulfide to sulfuric acid in a fuel cell using sulfuric acid electrolyte was investigated. Instead of sulfuric acid, elemental sulfur was formed. This collected largely on the surface of the electrode, eventually deactivating it. Extraction with hot xylene and ether followed by heating in boiling water, while passing helium through the electrode, restored most of the original activity. Platinized carbon electrodes were used in these experiments, but later work indicates that porous carbon would work equally well for the hydrogen sulfide anode.

In one experiment, a fuel cell was operated for 23.1 hours at a current of 30 ma (1 ma/cm^2). Hot xylene extraction of the electrode and evaporation of the extracts gave 0.35 gram of sulfur. This corresponds to 84% of theory, based on the following half-cell reaction.

$$H_2S \longrightarrow S + 2H^{+} + 2\ e^{-}$$

D. Sulfur Dioxide

Sulfuric acid production from sulfur dioxide in fuel cells was investigated. Platinized carbon electrodes in 5 N sulfuric acid at 50°C. gave much better performance when separated by Nalfilm-1 anion exchange membranes. In sustained operation at 100 ma cell current (3 ma/cm^2), the potential only decreased from 0.37 to 0.34 volt in five hours and then remained constant for an additional 11 hours. Cutting the diaphragm at this point dropped the potential sharply from 0.35 volt at 100 ma to 0.18 volt at 60 ma. This decreased further in 20 minutes to 0.128 volt.

Concentrated sulfuric acid from the sulfur dioxide-oxygen fuel cell would be desirable, but increasing the sulfuric acid electrolyte concentration seriously decreased performance (Figure 11).

VI. PREPARATION OF ANHYDROUS HYDROGEN BROMIDE IN A BROMINE-HYDROGEN FUEL CELL

Reaction of bromine and hydrogen in a fuel cell to give anhydrous hydrogen bromide and by-product electrical energy was investigated. The 48% hydrobromic acid azeotrope was selected as electrolyte in order to permit hydrobromic acid formed in the cell to be separated in anhydrous form by distillation.

The fuel cell used consisted of three compartments separated by Nalfilm-1 anion exchange membranes. Platinized porous carbon electrodes were used initially for both hydrogen and bromine, but later the cathode in the bromine compartment was replaced with a porous carbon rod with no significant change in performance.

Helium saturated with bromine gave a potential of 0.5 volt at a current density of 5 ma/cm^2 at 50°C. No significant loss of activity occurred in 16 hours of operation.

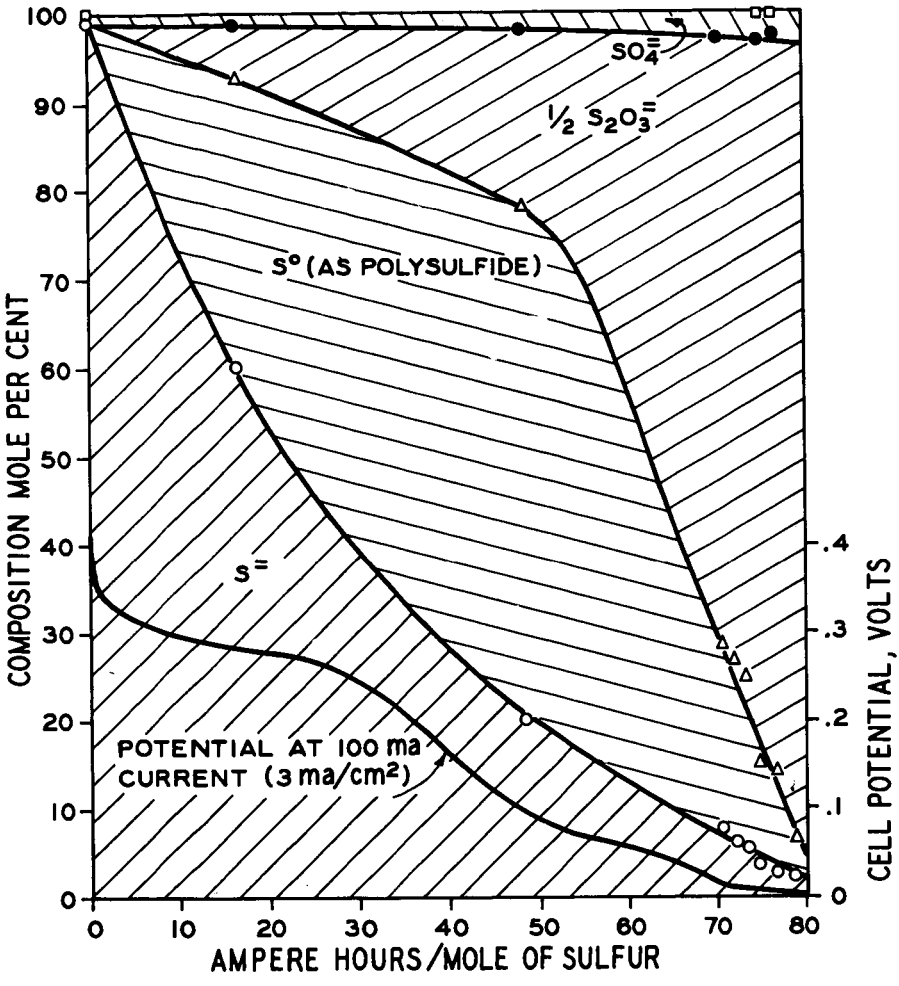

FIGURE 10. CHANGES IN ANOLYTE COMPOSITION IN A BASIC ELECTROLYTE SODIUM SULFIDE-OXYGEN FUEL CELL AT 24°C

□ = NEGLIGIBLE $SO_3^=$ CONCENTRATION

Later, sufficient bromine was added to the cathode compartment to give a second phase and the mixture stirred by rapidly raising and lowering the electrode by means of a motor driven eccentric. Current densities of 14 ma/cm^2 were drawn for six hours under these conditions. The potential remained at 0.28 volt for two and one-half hours and then gradually decreased to 0.17 volt.

A tenfold improvement in current density, which might reasonably be expected from improved electrode and cell design, would give an anhydrous hydrogen bromide production rate of 1 pound per hour per square foot of electrode surface.

VII. ACKNOWLEDGMENT

The author is indebted to Dr. G. H. Denison and Dr. W. G. Toland who were instrumental in initiating and endouraging these fuel cell studies. He also wishes to acknowledge the help of Dr. L. R. Griffith who provided some of the data on the reactivity of hydrocarbons and to thank him with Dr. R. P. Buck and Dr. R. T. Macdonald for helpful discussions and invaluable aid while preparing this paper.

The author also wishes to thank the Army Ordnance Corps for partial financial support and the directors of the Diamond Ordnance Fuze Laboratories and the management of the California Research Corporation for encouraging the publication of the material included in this paper.

VIII. LITERATURE CITED

(1) Anthony, P. O., Masters Thesis (1954), Ph. D. Thesis (1957), Ohio State University.
Humphrey, R. A., Ph. D. Thesis (1955), Ohio State University.

(2) Justi, E., Pilkuhn, M., Scheibe, W., and Winsel, A., Jahrb. Akad. Wiss. Lit. Mainz., 1959, No. 8.

(3) Pavela, T. O., Ann. Acad. Sci. Fennicae, Ser. A., II, No. 59 (1954).

(4) Young, G. J., and Rozelle, R. B., "Fuel Cells", Editor G. J. Yound, Reinhold Publishing Corporation, New York, New York, 1960, p. 23.

(5) Thompsett, S. L., and Smith, D. C., Analyst, 78, 209 (1953).

(6) Grant, W. M., Anal. Chem., 20, 267 (1948).

(7) Geissman, T. A., "Organic Reactions", Vol. II, John Wiley and Sons, New York, New York, 1944, p. 95.

(8) Buck, R. P., Griffith, L. R., Macdonald, R. T., and Schlatter, M. J., Proceedings of the Fifteenth Annual Power Sources Conference, May 1960, Atlantic City. In press.

(9) Yeager, J. F., Electrochemical Society Meeting Abstracts, Indianapolis, Indiana, April 1961, Abstract No. 104.

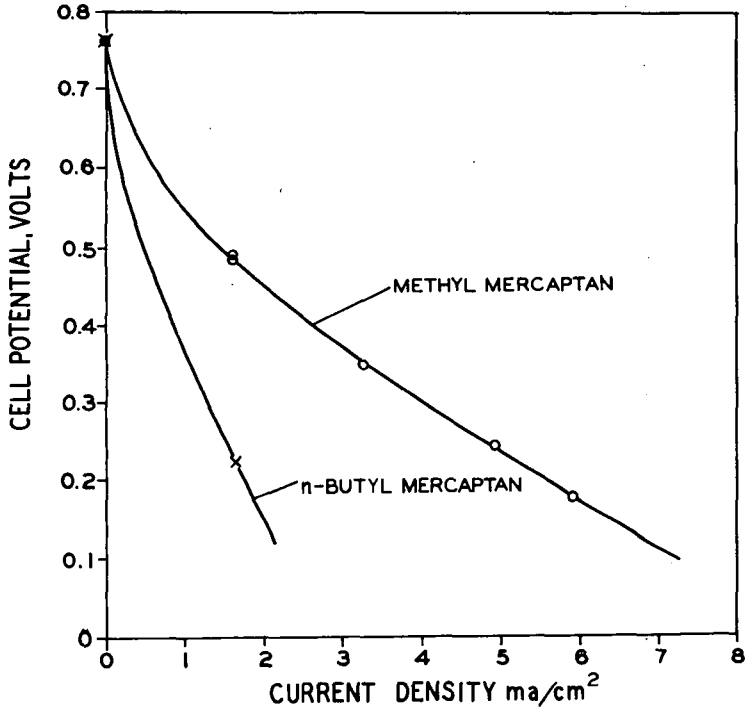

FIGURE 9. PERFORMANCE OF MERCAPTAN-OXYGEN FUEL CELLS AT 50°C

1.19 M METHYL MERCAPTAN AND 0.91 M n-BUTYL MERCAPTAN IN 2M SODIUM HYDROXIDE ELECTROLYTE

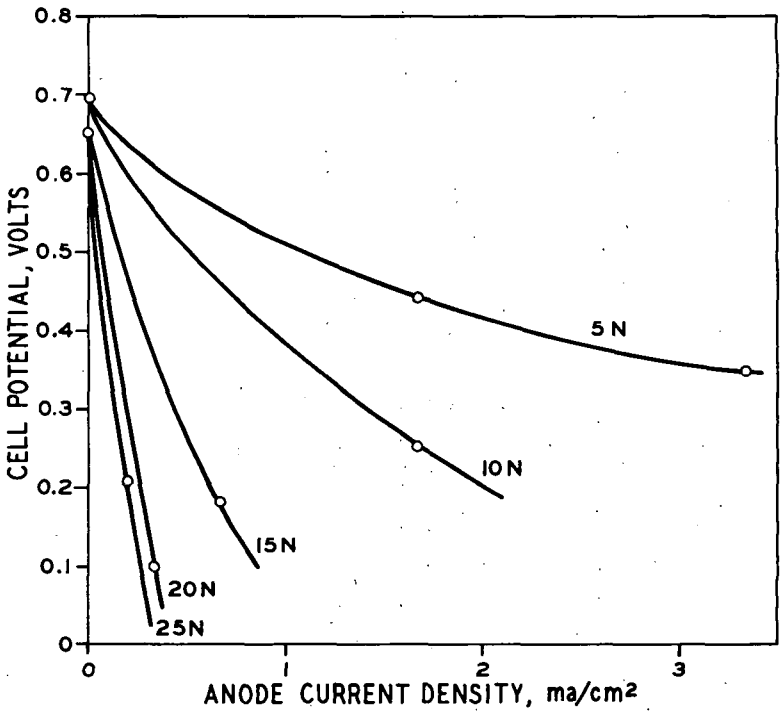

FIGURE 11. EFFECT OF SULFURIC ACID ELECTROLYTE NORMALITY ON SO_2-O_2 FUEL CELL PERFORMANCE AT 50°C